STRUCTURAL DEVELOPMENT, THERMAL EVOLUTION, AND TECTONIC SIGNIFICANCE OF A CORDILLERAN BASEMENT THRUST TERRANE, MARIA FOLD AND THRUST BELT, WEST-CENTRAL ARIZONA

by

James Howard Knapp

B.S. Geology, Stanford University
(1983)

Submitted to the Department of
Earth, Atmospheric, and Planetary Sciences
In Partial Fulfillment of the Requirements for the Degree of

Doctor of Philosophy

at the

Massachusetts Institute of Technology

February, 1989

Signature of Author: _____
Department of Earth, Atmospheric, & Planetary Sciences, MIT
Dec. 19, 1988

Certified by: _____
Dr. B. Clark Burchfiel
Thesis Supervisor

Certified by: _____
Dr. Kip V. Hodges
Thesis Supervisor

Accepted by: _____
Dr. Thomas H. Jordan
Chairman, Departmental Graduate Committee

STRUCTURAL DEVELOPMENT, THERMAL EVOLUTION, AND TECTONIC SIGNIFICANCE OF A CORDILLERAN BASEMENT THRUST TERRAIN, MARIA FOLD AND THRUST BELT, WEST-CENTRAL ARIZONA

by

James H. Knapp

Submitted to the Department of Earth, Atmospheric, and Planetary Sciences
on December 2, 1988 in partial fulfillment of the requirements for the degree of
Doctor of Philosophy

ABSTRACT

West-central Arizona records a geologic history characterized by basement-involved deformation in the Late Cretaceous Maria fold and thrust belt, followed by major crustal extension in mid-Tertiary time in the Whipple-Buckskin-Rawhide detachment system. This area is unique within the Cordillera of the western United States for the nature and style of Mesozoic thrust-related deformation, and contains some of the most highly extended crust within the entire Basin and Range, suggesting a causal link between Mesozoic and Tertiary tectonism. This study addresses aspects of the structural development, thermal evolution, and tectonic significance of the Maria fold and thrust belt in west-central Arizona, focusing on the Mesquite Mountain and Moon Mountains areas of the Colorado River Indian Reservation.

Basement-involved thrusting is evidenced in the southern Moon Mountains by the Valenzuela thrust system, which places Precambrian gneisses and Jurassic intrusive rocks over a deformed and metamorphosed section of lower Mesozoic sedimentary rocks. Thrusting took place at amphibolite facies conditions of metamorphism, and structures and fabrics associated with the Valenzuela thrust appear to indicate both south- and north-directed phases of movement. The age of thrusting is bracketed by U-Pb zircon dating of late Middle Jurassic (160 ± 15 Ma) intrusive rocks which are carried in the hanging wall of the thrust, and garnet-bearing pegmatites (71.1 ± 6.7 Ma) which are syn- to late-kinematic with the youngest, north-directed period of movement. This age marks the first direct dating of deformation in the Maria fold and thrust belt, and is consistent with regional timing constraints. The Valenzuela thrust system is correlated with the Tyson thrust system of the adjoining northern Dome Rock Mountains, implying a regional scale for this structure.

Extensional deformation of middle Tertiary age is recorded both at Mesquite Mountain and in the Moon Mountains. Rocks of the Mesquite Mountain area consist mainly of the migmatitic Mesquite Gneiss, and minor amounts of deformed metasedimentary rocks which are enveloped within the crystalline gneisses. Eight phases of deformation are recognized, documenting a continuous progression from development of ductile, penetrative fabrics to successively more localized, brittle faulting in the footwall of the regional Whipple-Buckskin-Rawhide detachment system. A maximum age for onset of mylonitization is provided by U-Pb zircon dating of granitic injection

associated with migmatization of the Mesquite Gneiss at 67.2 ± 1.4 Ma. Envelopment of metasedimentary rocks along mylonitic shear zones of Tertiary age is a manifestation of footwall incisement during development of the detachment system, and demonstrates that accommodation of extensional strain did not in general take place along pre-existing thrust faults. The Moon Mountain and Copper Peak detachment faults in the northern Moon Mountains constitute the exposed southwestern limit of the Whipple-Buckskin-Rawhide detachment system at this latitude. The presence of Tertiary mylonitic fabrics in the footwalls of these faults indicates that footwall rocks were exhumed from levels deep enough to produce ductile deformation, and implies that the breakaway (surface expression) of the detachment system is not preserved here. A late- to post-kinematic biotite granite in the footwall of the Copper Peak detachment fault yields a U-Pb zircon age of 20.8 ± 3.2 Ma, dating the end of ductile fabric development below this structure.

The thermal history of crystalline nappes from the central segment of the Maria fold and thrust belt, as indicated by $^{40}Ar/^{39}Ar$ thermochronology, is characterized by three phases since Late Cretaceous time. Regional heating of the crust was associated with thrusting and crustal thickening in the early Late Cretaceous (90?-70 Ma), followed by uplift and slow cooling (5-10°C/m.y.) throughout latest Cretaceous and early Tertiary time. Very rapid cooling was associated with uplift and tectonic denudation in the Whipple-Buckskin-Rawhide detachment terrain in late Oligocene to early Miocene time. Hornblende spectra record significant thermal heterogeneity within the region during the Late Cretaceous thermal event, which is thought to reflect differing structural levels within the thrust belt. Data from the Moon Mountains and northern Plomosa Mountains suggest that these areas may have been reheated during the onset of crustal extension in late Oligocene time.

Basement-involved thrusting and crustal thickening in the Maria fold and thrust belt was broadly coeval with arc magmatism associated with subduction of the Farallon Plate in Late Cretaceous time. Thrusting may have been active as early as 80-90 Ma (Reynolds et al., 1986), but appears to have ended by 70 Ma. Arc magmatism made an eastern sweep through the southwestern Cordillera of North America during Cretaceous time, and was probably at the longitude of present-day western Arizona during the Late Cretaceous (Coney and Reynolds, 1977). On a local scale, thrusting does not appear to have been controlled by thermal anomalies due to arc magmatism. Much of the magmatic activity in the Maria fold and thrust belt appears to be syn- to post-kinematic, and may represent a response to crustal thickening. A renewed thermal event, distinct from that associated with the Late Cretaceous, is evidenced both by renewed magmatic activity and the resetting of $^{40}Ar/^{39}Ar$ syetematics in potassium feldspar in western Arizona in late Oligocene time. The discordance between Mesozoic shortening and Cenozoic extension directions in western Arizona may have been strongly influenced by plate reorganization which occurred synchronously with the onset of extension at this latitude (Stock and Molnar, 1988).

Thesis Supervisors:

Dr. B. Clark Burchfiel, Schlumberger Professor of Geology

Dr. Kip V. Hodges, Associate Professor of Geology

"Desert is land stripped to the essentials, freed of superficialities; and living in it can revitalize one's perspective."

Ruth Kirk

ACKNOWLEDGEMENTS

Having spent the last four and a half years engaged in the pursuit of doctoral knowledge, I am now firmly convinced that the completion of a Ph.D. program is no trifling matter. To succeed in such a rigorous and unpredictable endeavor, the aid and support of many people is invaluable. Here I take pause to acknowledge, if only in the smallest way, the numerous people who have helped me.

I turn first to my thesis advisors, Clark Burchfiel and Kip Hodges, who have been a beacon of knowledge for me throughout my tenure at M.I.T., and in the process have taught me a great deal about things geologic. Clark, in his own inimitable way, has perfected the Socratic method of thesis advising, of which I only now understand I have been the lasting beneficiary. And to the irrepressible Dr. Hodges, I owe a tremendous deal of thanks for his insightful mind, critical eye, and unrelenting faith in my ability to bring this thesis to completion.

The Tribal Council of the Colorado River Indian Tribes generously granted me permission to conduct research at Mesquite Mountain and in the Moon Mountains on the Colorado River Indian Reservation. Chuck Lamb, director of the Tribal Museum, was particularly instrumental in negotiating my case to work on the Reservation, and has shared freely with me his vast knowledge of the Mojave Indians and their ancient homeland. Weldon Johnson, Curtiss Martin, and the rest of the Museum staff have been an invaluable source of friendship and logistical support during my trips to the field. It has been my pleasure to work with the people of the Colorado River Indian Tribes, and I hope the information presented herein will be of continuing value to them.

My early ponderings of the geology of the Mojave-Sonoran Desert were irrevocably enhanced by many insightful scientists, including Messrs. Steve Reynolds and Jon Spencer (the Arizona Geological Survey), Keith Howard, Calvin Miller and his COWPIE, Doug Walker, Dave Miller, and Elizabeth Miller. Many complexities of the geology of western Arizona were brought to light by Steve Richard, Steve Laubach, Anna Buising, Bruce Bryant, and Joan Fryxell. Wiki Royden, John Grotzinger, Fred Frey, Roger Burns, and Stan Hart of the faculty at M.I.T. opened my eyes to many new ideas and have made my stay at M.I.T. that much more fruitful.

I will be eternally grateful to those people who assisted me with field work in the deserts of the great Southwest. These courageous men and women braved weeks of isolation with me and my eccentricities, often with only a creosote bush in which to take solace. Carrie Decker and Nathan Estes saw me through days on end of high-speed

geological touring of the Mojave Desert during the early stages of this work, while it was just starting to take form. Tom Knapp, a fine friend and brother, provides lasting good memories of the sibling mapping team. Maureen Noonan and Scott Ritterbush were invaluable assistants during my final two field seasons, and were always at the ready to do what was necessary, even if it meant following me up some cliff they didn't care about at the end of a long day. Special appreciation is expressed to Scott Ritterbush, who doggedly persevered in helping with the collection and crushing of 1,800 lbs. of rock for U-Pb geochronology.

During the course of this thesis research, I have been the recipient of kind hospitality in places far and wide. Terry Naumann took pity on me at an early stage, and many times spared me the ravages of fear and loathing in Las Vegas. While I was processing samples for Ar analysis at SUNY Albany, in New York, Matt Heizler, Suzanne Baldwin, and Pete Copeland kindly took me into their homes without complaint. Nick Rose, Beth Robinson and Alan Leinbach provided friendly accommodations in the San Francisco Bay Area while I transformed hundreds of pounds of rock into dust in search of zircons. My extended visits to Lawrence, Kansas, to work on the U-Pb zircon geochronology could not have been more enjoyable and productive, thanks to the hospitality of Doug Walker and members of the KU geology department.

Financial support for this research didn't come easily in these times of soft money and hard NSF budgets. I am most grateful to Clark Burchfiel for his generous support through his endowed Schlumberger Chair of Geology at M.I.T., which, even when it was "on its back, kicking its legs in the air", miraculously continued to issue forth funds to cover the expenses for my research. Dr. Mark Harrison gave most generously of both moral and material support with the use of his lab at SUNY Albany for the Ar-Ar analyses. The Department of Earth, Atmospheric, and Planetary Sciences at M.I.T. is acknowledged for nine semesters of teaching assistantship support, including my early days as a teaching assistant for Introductory Planetary Science, and for financial support through the Student Research Fund. Technical and secretarial support from Nancy Dallaire, Liz Scorsello, Meredith Smith, and Judith Stein has been much appreciated over the years.

The intellectual stimulation provided by my colleagues at M.I.T. cannot be underestimated. I have been the beneficiary of support from and interactions with my fellow graduate students Liz Schermer, Barbara Sheffels, Laurence Page, Larry McKenna, Joann Stock, Mary Hubbard, Kurt Sternlof, Dan Tormey, Vincent Salters, Tom Juster, Donald Hickmott, David Dinter, Tom Sisson, Sarah Kruse, Carolyn Ruppel, Geoff Abers, Joanne Fredrich, Steve Hickman, Kevin Johnson, and from a different era,

Doug Walker, Dave Klepacki, Peter Tilke, Zhang Pei Zhen, Alan Leinbach, and Peter Wilcock. Larry McKenna deserves special mention for his knowledge of statistics and computers, and his willingness to share it freely. Inhabitants (present and former) of the little red school house up the River, including Bryan Kriens, Phil England, Brian Wernicke, and Zeke Snow, have been a source of lively discussion and entertainment. To these, and many others I've probably neglected to mention, I extend my thanks for your patience and interest.

Special appreciation is offered to my fellow graduate student and friend, Tanya Furman, who saw me through some of my toughest trials at M.I.T. How she managed it is still a mystery to me, but I'm thankful all the same. Her friendship, along with that of many close friends, has been a continuing source of inspiration.

Lastly, but most importantly, I thank my family for the support and encouragement they have given me throughout this endeavor. For all the times I have placed my commitment to this work above all else, I am particularly thankful for the understanding they have shown. My sister Mary has been a pillar of strength during the last months of this campaign, and her efforts will not soon be forgotten. She has brought a great deal of enjoyment to my last year in Boston. And to my parents, I dedicate this thesis, with the hope it will in some small way signify the appreciation, respect, and love I have for them.

TABLE OF CONTENTS

INTRODUCTION

The region of west-central Arizona records a complex history of deformation, metamorphism, and magmatism along the southwestern edge of the North American craton. This area was the site of extensive basement-involved folding and thrusting in the Maria fold and thrust belt during Late Cretaceous time. Episodes of southeast and south-directed folding and thrusting were followed by phases of north-vergent deformation, and syntectonic metamorphism was characterized by greenschist to lower amphibolite facies. Lower crustal levels experienced partial melting due to this crustal thickening, and large volumes of granitic plutons were intruded at higher crustal levels. Subsequently, large portions of middle crustal rocks were exposed in middle Tertiary time as the result of major crustal extension in the regional Whipple-Buckskin-Rawhide detachment terrain. This deformation was typically accompanied by greenschist facies, retrograde metamorphism, basin formation, and both basaltic and granitic magmatism. The superposition of these tectonic regimes in the region of west-central Arizona has led to a very complicated configuration of structural, magmatic and metamorphic elements.

The tectonic significance of the Maria fold and thrust belt of southeastern California and western Arizona is crucial to an understanding of the Mesozoic history of the cratonal edge of the southwestern Cordillera. The involvement of crystalline basement rocks in large-scale folds and thrust nappes of Mesozoic age is unique within the thrust belt from British Columbia, Canada, to Sonora, Mexico. In addition, the orientation and vergence of structures in the Maria fold and thrust belt contrasts markedly with the consistently east-vergent, décollement style of thrusting exhibited in much of the remainder of the Cordillera. The origin of this anomalous segment of the Mesozoic thrust belt has been variably attributed to transpression along the cratonal margin, the lack of a thick stratigraphic cover, and localization of thrusting due to softening of the crust from arc magmatism.

Tertiary extensional deformation was directly superimposed on the region of Mesozoic thrusting and crustal thickening, and resulted in extensive exhumation of mid-crustal crystalline rocks in the Whipple-Buckskin-Rawhide detachment terrain. Metamorphic core complexes, which have been identified as major extensional features within the Cordillera, are spectacularly developed in western Arizona, and record some of the largest magnitudes of Tertiary extension in the entire western United States. The

coincidence of these two tectonic regimes is suggestive of a genetic relation between them, as has been proposed for other areas of the Basin and Range.

The superposition of deformational, metamorphic, and magmatic episodes has hindered a clear understanding of the nature and timing of geologic events in western Arizona. Only in recent years have workers begun to recognize the style and decipher the magnitude and timing of deformation in the Maria fold and thrust belt. Accurate reconstruction of the thrust belt here is still made difficult by disruption and segmentation within the detachment system. In turn, the controls of Mesozoic tectonism on Tertiary extension are difficult to assess given the uncertainties in the pre-Tertiary configuration of the crust in this region.

This study addresses aspects of the structural, thermal, magmatic, and tectonic history of west-central Arizona, concentrating on the Mesquite Mountain and Moon Mountains areas of the Colorado River Indian Reservation. Field mapping, structural and petrographic analysis, $^{40}Ar/^{39}Ar$ thermochronology, and U-Pb geochronology have been integrated to document the geologic history recorded in the rocks exposed in this region. The results from these studies are presented in four separate chapters, due to the diversity of the techniques used and the application of the results.

Each chapter has been developed in a form intended to be suitable for publication. A chapter has been devoted to each of (1) stratigraphy and structure of Mesquite Mountain, (2) stratigraphy and structure of the Moon Mountains, (3) $^{40}Ar/^{39}Ar$ thermochronology of crystalline thrust nappes in the Maria fold and thrust belt, and (4) U-Pb geochronology and tectonic implications of magmatism in west-central Arizona. Some repetition of background material and regional relations is unavoidable, but is kept to a minimum in each of the four chapters.

The Mesquite Mountain area records a continuous progression from penetrative, ductile deformation to brittle faulting in the crystalline rocks of the footwall of the Whipple-Buckskin-Rawhide detachment system. The age of this deformation is constrained to be Tertiary on the basis of field relationships and U-Pb zircon geochronology of migmatitic rocks. These relations provide a genetic link between mid- and upper-crustal deformation in the development of the detachment system, and record progressive incisement of the footwall as mylonitic rocks were carried to higher crustal levels.

Both Mesozoic thrust faulting and Tertiary detachment faulting are documented in the Moon Mountains, and demonstrate that thrust faulting and associated amphibolite facies metamorphism occurred in Late Cretaceous time, based on U-Pb zircon geochronology. Exposures of the Moon Mountain and correlative Copper Peak detachment faults in the northern Moon Mountains constitute the western limit of the Whipple-Buckskin-Rawhide detachment system at this latitude. Ductile Tertiary fabrics below these structures indicate that footwall rocks were exhumed from considerable depths (sufficient to produce mylonitization), and indicate that the actual breakaway for the detachment is not preserved. Granitic rocks from the footwall of the Copper Peak detachment constrain the termination of ductile fabric development to be ~21 Ma.

The thermal history of west-central Arizona is characterized by three phases since Late Cretaceous time. Heating and partial melting were associated with Late Cretaceous crustal thickening, followed by uplift and slow cooling throughout latest Cretaceous and early Tertiary time. Very rapid cooling in mid-Tertiary time resulted from unroofing of mid-crustal rocks in the footwall of the Whipple-Buckskin-Rawhide detachment system. Age spectra from $^{40}Ar/^{39}Ar$ analyses reveal that different structural levels from the Maria fold and thrust belt are preserved, and suggest that a renewed period of heating was associated with the onset of extension.

Igneous rocks from the Mesquite Mountain and Moon Mountains areas are representative of Jurassic, Late Cretaceous, and mid-Tertiary magmatism, and help to constrain the timing and significance of events in the crustal evolution of this region. Significantly, the locus of deformation does not appear to be strongly controlled by the presence of magmatism in the Maria fold and thrust belt. Magmatism is better interpreted as a post-tectonic response to crustal thickening. In addition, the presence of magmatic activity during the early stages of crustal extension implies that heat was being introduced to the crust during this time, and may have been integrally related to the cause of extension.

Field work on the Colorado River Indian Reservation of western Arizona was conducted during four months of field work in three field seasons between mid-October, 1986, and mid-November, 1987. Geologic maps at a scale of 1:24,000 of both Mesquite Mountain and the Moon Mountains make up approximately two 7.5 minute U.S.G.S. topographic quadrangles, and are included (as xerox reduced versions) as Plates 1-1 and 2-1. These constitute the first thorough compilations of the rocks and structures exposed on the Colorado River Indian Reservation, and fill an important gap in the geology of

western Arizona and southeastern California. The $^{40}Ar/^{39}Ar$ analyses were carried out in conjunction with Matthew Heizler in Dr. T.M. Harrison's laboratory at SUNY Albany during the Fall of 1987 and the Spring of 1988. Analyses for U-Pb zircon geochronology were obtained in collaboration with Dr. Douglas Walker at the University of Kansas in Lawrence, Kansas during the Spring and Summer of 1988.

CHAPTER 1

MID-TERTIARY DETACHMENT TECTONICS AT MESQUITE MOUNTAIN, WEST-CENTRAL ARIZONA

James H. Knapp

ABSTRACT

Mesquite Mountain, situated on the Colorado River Indian Reservation of west-central Arizona, records a continuous progression of deformational styles characterized by older, penetrative, ductile fabrics to younger, more localized, brittle structures in the footwall of the regional Whipple-Buckskin-Rawhide detachment system. Rock types consist primarily of deformed migmatitic gneiss, herein termed the Mesquite Gneiss, and minor amounts of deformed intrusive and metasedimentary rocks. Eight phases of deformation are recognized, beginning with D_1 development of gneissic compositional layering and intrafolial folding associated with *in situ* partial melting and injection of the Mesquite Gneiss in Late Cretaceous time. A variably developed, mylonitic fabric (D_2) clearly postdates migmatization, and marks the earliest manifestation of extension. Penetrative mylonitization was associated with development of the Mesquite Mountain (D_3) and Agency (D_4) fault zones, wherein deformed metasedimentary rocks of Paleozoic and/or Mesozoic age are enveloped within mylonitic basement gneisses. High-angle, oblique-normal, ductile faulting was synchronous with development of the Agency fault zone, marking a change to more localized ductile shear. Subsequent phases of faulting were characterized by a transition to brecciation and chloritic alteration along low-angle faults (D_5), followed by three generations of high-angle, brittle faults (D_6-D_8).

Movement on the Mesquite Wash Hills fault (D_8), along the eastern flank of Mesquite Mountain, partly postdates deposition of the upper Miocene to lower Pliocene Bouse Formation, and constitutes some of the youngest faulting documented in the lower Colorado River region. A lower age limit on deformation at Mesquite Mountain is provided by U-Pb zircon dating of migmatization in the Mesquite Gneiss at ~67 Ma, demonstrating that all succeeding fabrics and structures are Tertiary in age. Recognition of strictly Tertiary-age mylonitic fabrics in pre-Tertiary crystalline rocks of the western Arizona extensional terrain contrasts markedly with occurrences of Mesozoic fabrics reported from surrounding ranges.

Deformation at Mesquite Mountain originated in the footwall of the Whipple-Buckskin-Rawhide detachment system. Both gneissic and mylonitic foliation are presently southwest-dipping; mylonitic lineation plunges consistently to the southwest. Shear indicators in mylonitic rocks indicate a predominant top-to-the-northeast asymmetry, consistent with Tertiary mylonitic fabrics observed in the Whipple and Buckskin Mountains to the north and northeast. The Mesquite Mountain and Agency fault zones represent features associated with incisement of the footwall of the detachment system. Envelopment of Phanerozoic metasedimentary rocks within these Tertiary-age structures resulted from localization of shear within the less competent carbonate lithologies. Although these supracrustal rocks were first carried to depth below Mesozoic crystalline thrust nappes of the Maria fold and thrust belt, reactivation of these thrusts was clearly not the primary mechanism for accommodation of large extensional strain. The continuous progression from penetrative, ductile deformation to more localized, brittle faulting records a successively more shallow crustal setting for footwall deformation, and provides a genetic link between mid- and upper-crustal deformation within the detachment system. Seismic reflection data (Hauser et al., 1987) indicate that Mesquite Mountain is presently in the hanging wall of a splay of the detachment, implying that large-scale incisement of crustal blocks has occurred during the development of the Whipple-Buckskin-Rawhide detachment system.

INTRODUCTION

The lower Colorado River region of western Arizona and southeastern California contains some of the most spectacularly displayed examples of metamorphic core complexes in the western United States Cordillera. Extensive work within this region

during the past decade has greatly increased our understanding of continental extensional tectonics; however, many details of the evolution of detachment fault* terrains remain unresolved. Primary among these are the nature and timing of mylonitization (and general deformation of the lower plate) in relation to detachment faulting.

Several studies (e.g., Davis et al., 1980; Davis and Lister, 1988) have argued that mid-crustal mylonite zones exposed in the lower Colorado River extensional corridor were kinematically inactive during detachment faulting. Other workers (Rehrig and Reynolds, 1980; Davis, 1983; Reynolds and Spencer, 1985) envision mylonitization to be synchronous with and integrally related to development of the detachment fault.

Structural relations at Mesquite Mountain reveal a continuous progression from ductile, penetrative fabrics to brittle, detachment-related faulting, and imply that mid-crustal mylonites are genetically related to detachment faulting at upper-crustal levels. In addition, ductile deformation at depth, characterized by zones of distributed shear, appears to pass into splays of the detachment as lower-plate gneisses are successively incorporated into the hanging wall by "incisement" (after Davis and Lister, 1980). Despite pre-existing zones of weakness in the crust produced by deep-seated Mesozoic thrust faults, accommodation of large magnitudes of extensional strain took place along newly generated structures rather than through reactivation of thrust faults.

LOCATION AND GEOLOGIC SETTING

Mesquite Mountain, situated in the Colorado River Trough of west-central Arizona, lies within the southern Basin and Range province of southeastern California and southwestern Arizona. Surrounding mountain ranges include the Whipple and Buckskin Mountains to the north, the Plomosa Mountains to the east, the Moon Mountains to the south, and the Big Maria and Riverside Mountains to the west (Fig. 1.1). The region is characterized by generally elongate mountain ranges surrounded by broad alluvial valleys, with sparse vegetation and excellent exposure typical of the Mojave-Sonoran Desert. Bedrock exposures reveal a complex geologic history for this region that involved repeated episodes of deformation, metamorphism, and igneous activity. Two major tectonic regimes are presently recognized: (1) a Mesozoic

*Use of the term "detachment fault" here follows that of numerous workers in the lower Colorado River extensional terrain (e.g. Davis and Lister, 1988; Reynolds and Spencer, 1985), and refers to a low-angle fault which has significant displacement and is of subregional to regional extent.

compressional regime, characterized by thrusting, large-scale folding, greenschist to amphibolite facies metamorphism, and calc-alkaline magmatism (e.g. Reynolds et al., 1986, 1988), and (2) a Cenozoic extensional regime that involved profound crustal extension, normal faulting, basin formation, greenschist facies metamorphism, and bimodal magmatism (e.g. Davis et al., 1980).

Crystalline basement rocks are extensively involved in Mesozoic-age deformation along a 250-km segment of the Cordilleran thrust belt called the Maria fold and thrust belt. Large-scale crustal extension occurred in late-Oligocene to mid-Miocene time in the Whipple-Buckskin-Rawhide area immediately to the north and northeast of Mesquite Mountain.

Western Arizona and adjoining areas of southeastern California were the locus of large-scale crustal extension in mid-Tertiary time. Large regions of mid-crustal crystalline rocks were exposed as a result of major northeast-southwest-directed extension within the regional Whipple-Buckskin-Rawhide detachment system. Deformation in the footwall of the detachment was characterized by penetrative, ductile deformation, whereas extension in the hanging wall was largely accommodated through displacement and rotation along high-angle normal fault systems. The detachment fault itself is today represented as an irregular, domal surface in several mountain ranges, including the Whipple, Buckskin, Rawhide, and Harcuvar Mountains.

Rock types exposed at Mesquite Mountain consist primarily of polydeformed migmatitic gneiss (the Mesquite Gneiss), minor amounts of deformed intrusive and metasedimentary rocks, and the post-tectonic upper Miocene to Pliocene Bouse Formation. A sequence of eight deformational events is recorded at Mesquite Mountain, documenting a progressively more shallow crustal setting for deformation of these rocks since burial during Mesozoic compressional deformation.

PREVIOUS WORK

Previous work within the mountains of the Colorado River Indian Reservation has been limited. Ross (1923) may have been the first to describe geologic features on the Reservation. He made note of the "lake deposits of the Colorado River Indian Reservation" in a survey of groundwater resources of the area. Wilson et al. (1969) showed only very general geologic relations on the state geologic map, indicating the presence of Mesozoic metamorphic rocks at Mesquite Mountain. Metzger (1968) and

Metzger et al. (1973) developed early ideas on the significance of the Bouse Formation, and included exposures along the western flank of Mesquite Mountain as a reference section for the Bouse Formation. More recently, Buising (1986, 1988) has conducted studies on the Bouse Formation, including the exposures at Mesquite Mountain. The present study constitutes the first thorough description of the rocks and structures at Mesquite Mountain, and relates these features to evolution of footwall deformation in the regional Whipple-Buckskin-Rawhide detachment terrain.

PHYSIOGRAPHY

Mesquite Mountain consists of an elongate, north-northeast-trending, low-lying ridge with two small outliers, situated within the Colorado River Indian Reservation, about 15 km south of Parker, Arizona (Fig. 1.1; Plate 1-1). Elevations are low within the Colorado River area, but topography is rugged, and slopes can be steep. Agency Peak, at 1797 feet (548 m), is the highest point in the area, and the surrounding flood plain of the Colorado River is at an elevation of ~350 ft (107 m). Bouse Wash forms the northern boundary of Mesquite Mountain, and the Colorado River flood plain forms its western boundary. A number of informal names have been introduced for convenience in identifying geologic features of the Mesquite Mountain area. These informal geographic terms are introduced here, and identified on Figure 1.2. Mesquite Hill is the name given to the small outlier to the southwest of Mesquite Mountain proper. The Mesquite Wash Hills form the low-lying topography on the east side of Mesquite Mountain and are separated from the main mountain by the Mesquite Wash Hills fault. Several references are made to peak 1625', located at the south end of Mesquite Mountain. Migmatite Wash is the northwest-trending wash along the southwestern side of peak 1625', and is the informal type locality of the Mesquite Gneiss.

DESCRIPTION OF ROCK UNITS

Rock types exposed at Mesquite Mountain consist largely of polyphase, migmatitic gneiss, herein referred to as the Mesquite Gneiss, and minor amounts of deformed intrusive and metasedimentary rocks. Two generations of basic to intermediate dikes are present: porphyritic tonalite dikes were intruded during mylonitization, whereas quartz diorite to diabase dikes post-date all fabrics and structures in the crystalline rocks. All bedrock exposures are mantled by deposits of the late Miocene to early Pliocene

Bouse Formation and overlying gravels of the Colorado River depositional system. The age of units exposed at Mesquite Mountain ranges from Precambrian to Recent; however this record is incomplete. Multiple phases of deformation, greenschist to lower-amphibolite facies metamorphism, and lack of radiometric age control make reliable interpretation of absolute ages of most rock types difficult. Relative ages of lithologies are deduced from field relations. Detailed descriptions of the units are categorized by metamorphic, sedimentary, and igneous rock types. Within each of these divisions, units are discussed in order of decreasing relative age.

METAMORPHIC ROCKS

Metamorphic rocks at Mesquite Mountain are divided into rocks of the Mesquite Gneiss migmatite complex, and metasedimentary rocks which occur within the Mesquite Mountain and Agency fault zones. These metamorphic rocks predominate the exposed bedrock at Mesquite Mountain, and record at least two phases of metamorphism: an older amphibolite facies event associated with Mesozoic thrust faulting, and a younger, retrograde, greenschist facies event which occurred in conjunction with Tertiary mylonitization and detachment faulting.

MESQUITE GNEISS (Kmg)

The Mesquite Gneiss constitutes the major rock type exposed at Mesquite Mountain, and consists of a well-developed and extensively deformed migmatite complex. Good exposures are found throughout the area, but the unit was first recognized and described from exposures in Migmatite Wash (Fig. 1.2). Compositional layering within the Mesquite Gneiss is defined by thin (< 2 mm) to thick (15-20 cm), fine- to coarse-grained, leucosomatic segregations of quartz + potassium feldspar + plagioclase + biotite ± muscovite alternating with melanosomatic layers which contain the assemblage quartz + plagioclase + biotite ± hornblende (Fig. 11.3). Bands of medium- to coarse-grained amphibolite (hornblende + plagioclase ± epidote ± chlorite) comprise up to 10-15 volume percent of the gneiss. Metamorphic fabrics in these amphibolites are characterized by an aligned mineral lineation defined by dynamically recrystallized hornblende. Development of gneissic layering was associated with amphibolite facies metamorphism and extensive granitic injection. Abundant, medium- to coarse-grained, 10-150 cm thick sills of biotite-bearing granite intrude the Mesquite Gneiss both concordantly and discordantly with respect to the compositional layering. Minor amounts of mylonitic augen gneiss occur within the Mesquite Gneiss, making up 1-2% of the unit.

These augen gneisses occur as relatively coherent bodies, up to several hundred meters in length, that are distributed irregularly within the remainder of the gneiss. The Mesquite Gneiss contains complex internal structures that include intrafolial isoclinal folds and disharmonic, micro- to macro-scale folds (Fig. 1.4). Despite the extensive deformation, the compositional layering dips relatively consistently (40-75°) west- to southwest.

METASEDIMENTARY ROCKS (ms)

A series of highly deformed and metamorphosed sedimentary rocks, including marble, quartzite, and calc-silicate rock, is exposed at Mesquite Mountain. Occurrence of these lithologies is restricted to the Mesquite Mountain and Agency fault zones, and to a complex structural zone at the south end of Mesquite Mountain where the Mesquite Mountain fault zone has been disrupted by later high-angle and low-angle faults. These metasedimentary rocks are characterized by complex internal deformation and, where exposed, they are consistently in sheared contact with the surrounding Mesquite Gneiss and granitic rocks. A total of five different lithologies are recognized: (1) micaceous, calcite marble, (2) cherty, calcite marble, (3) banded calc-silicate rock, (4) quartzite, and (5) coarse-grained, dolomitic marble. The stratigraphic ordering and relative ages of these lithologies is uncertain. These lithologic units occur as thin, fault-bounded slivers within the Mesquite Mountain and Agency fault zones; at the scale of the map (1:24,000), these units cannot be represented individually. All lithologies of this metasedimentary sequence are included on the geologic map and cross sections under the unit "ms" (Plates 1-1, 1-2), which consists roughly of 50% micaceous calcite marble, 35% banded calc-silicate rock, 10% cherty calcite marble, and 5% quartzite and dolomitic marble.

Orange Micaceous Calcite Marble

By far the most distinctive and common lithology of the metasedimentary rocks of the Mesquite Mountain and Agency fault zones consists of a conspicuous, orange-weathering, micaceous calcite marble. Exposures of this unit are resistant, rough-weathering ledges of foliated marble which vary in structural thickness from < 1 to > 20 m. Contacts with the surrounding gneiss are everywhere sheared, and contacts with other metasedimentary units are sheared but may in part reflect an original stratigraphic ordering. This marble unit typically is in contact with the banded calc-silicate unit and the cherty calcite marble.

This unit outcrops as either one- to five-meter thick, discontinuous slivers, or as large, resistant ledges up to 20 m thick, of orange- to light brown-weathering, massive, medium- to coarse-grained, muscovite-rich marble which is tan to greenish brown on a fresh surface. Abundant clots of medium- to coarse-grained tremolite, forming resistant irregular knobs, are typical in the coarser grained portions of the unit.

Cherty Calcite Marble

Numerous exposures of deformed, cherty calcite marble occur within the Mesquite Mountain and Agency Fault Zones, typically as thin (<2 m), discontinuous lenses. Contacts with surrounding units are invariably sheared and typically parallel a penetrative foliation within the marble. This marble occurs as 0.5-2 meter-thick, irregular, resistant ledges of bluish grey- to greyish brown-weathering, cherty marble which is light green to grey with black streaks on a fresh surface. The weathered surface is characterized by resistant, medium to coarse grains of quartz, feldspar, tremolite, and diopside in a recessive matrix of fine- to very fine-grained calcite. Irregular clots and lenses of dark brown- to black-weathering chert and quartz-rich silty material form resistant knobs which vary from 1-30 cm in diameter.

In thin section, this unit contains the minerals calcite + quartz + tremolite + diopside + potassium feldspar + plagioclase ± muscovite. All phases (except calcite) occur as rounded, medium to coarse grains floating in a fine- to very fine-grained matrix of calcite. Many grains are fractured, and tremolite and diopside, which are not in textural equilibrium with the surrounding phases, show reaction along cleavage planes to very fine-grained sericite(?) + calcite(?). A well-developed foliation is defined by trains of broken and smeared calcite grains in the matrix, resembling a ductile flow foliation, and the alignment of the long axes of many porphyroclast grains. This foliation is folded around small-scale intrafolial folds, and floating isoclinal fold hinges are commonly preserved within the chert bands.

Banded Calc-silicate Rocks

A significant portion of the metasedimentary sequence in the Mesquite Mountain and Agency fault zones consists of a distinctive interval of banded calc-silicate rocks. Exposures of this unit form resistant cliffs and ledges of brownish green-weathering, banded rocks which display intrafolial folding and complex internal structure. These rocks contain the mineralogy quartz + potassium feldspar + biotite + calcite + chlorite ±

epidote , and probably were derived from interbedded calcareous sandstone and siltstone. Correlation of these rocks with known stratigraphy is made difficult by the lack of primary features in the rock, and the degree of metamorphism and deformation recorded in the unit. This unit was not studied in detail, and is deserving of more careful study in order to clarify stratigraphic and structural relations with the surrounding units of the metasedimentary rocks.

Quartzite

Pure, milky-white quartzite is locally present at Mesquite Mountain. The most significant exposure consists of a rubbly outcrop of massive, blocky-weathering quartzite at the base of the western flank of peak 1625' at the south end of Mesquite Mountain. Structural thickness of this unit is less than 3 m. Contacts with surrounding units are obscured by slope wash and talus, but exposures of Mesquite Gneiss are present below the quartzite, and the contact between the quartzite and the underlying gneiss is inferred to be a fault. The upper contact of the quartzite is not exposed, but is likewise inferred to be a fault, based on the projection of structurally higher, west-dipping, low-angle faults to the east which carry mylonitic gneiss and metasedimentary rocks in their hanging walls.

The quartzite consists of a reddish brown- to orange-weathering, massive, medium- to fine-grained, blocky quartzite which is milky-white to grey on a fresh surface. The rock is almost exclusively quartz with <1% fine-grained white mica and opaque oxides. While the quartzite has been extensively recrystallized, relict, individual, rounded grains and faint, continuous, planar laminations indicate this unit is of sedimentary origin, and not a metaigneous rock.

Stratigraphic Correlation

Stratigraphic correlation of this collection of metasedimentary units with known stratigraphy from surrounding regions in southeastern California and western Arizona remains unclear. Carbonate rocks of this type are unknown within the Proterozoic basement of this region, which consists predominantly of high-grade gneisses and intrusive rocks similar to the Mesquite Gneiss (e.g. Thomas et al., 1988; Orell, 1988; Podruski, 1979). Correlation, based on lithologic similarity, with units of the Paleozoic cratonal section (Grand Canyon affinity) seems a likely possibility; however, unit by unit correlation cannot be made with certainty based on present data. Intact Paleozoic cratonal stratigraphy is present in surrounding ranges to the southeast (Southern Plomosa

Mountains: Miller, 1970; Miller and McKee, 1971), south (Northern Dome Rock Mountains: Yeats, 1985) southwest (Big Maria Mountains: Hamilton, 1982) and west (Riverside Mountains: Carr and Dickey, 1980). While known occurrences of lower Mesozoic rocks in western Arizona (Reynolds, et al., 1987) would preclude such a predominance of carbonate rock within the section, the lithologies exposed at Mesquite Mountain bear a resemblance to a newly-described, lower Mesozoic section in the Moon Mountains directly to the south of Mesquite Mountain (Knapp, in prep.). Given the considerable disruption of the section, both Paleozoic and Mesozoic lithologies may be represented.

Stratigraphic correlation of the cherty calcite marble with units from surrounding areas in western Arizona and southeastern California is made difficult by the extent of metamorphism (diopside grade) and intense deformation recorded in the rock, and the lack of a demonstrably intact stratigraphic sequence. Based on compositional features alone, a tentative correlation is made with the Permian Kaibab Limestone, however the unit could correspond to a more cherty interval within Mississippian carbonate rocks of the Paleozoic platformal sequence (P. Stone, pers. comm.), or to part of an as yet poorly understood lower Mesozoic sequence of clastic and carbonate rocks exposed in surrounding areas (Reynolds et al., 1987; Knapp, in prep.).

The pure quartzite unit is most likely correlative with one of three identified quartzite units within the Phanerozoic section of western Arizona: the Cambrian Tapeats Sandstone, the Permian Coconino Sandstone, or the Jurassic Aztec Sandstone. Alternatively, this quartzite may be related to minor quartzite intervals which have been described within the lower Mesozoic section (Triassic Vampire Formation) from surrounding areas in Arizona (Reynolds et al., 1987; Marshak and Vander Meulen, in press; Knapp, in prep). Lack of stratigraphic association with other lithologies and lack of distinctive primary features make a more precise correlation of this quartzite unit impossible.

A similar sequence of mylonitic metasedimentary and metaigneous rocks is present in the Battleship Peak area of the southwestern-most Buckskin Mountains, about 40 km east of Mesquite Mountain. Marshak and Vander Meulen (in press) interpreted the protoliths of these rocks to be Mesozoic and Paleozoic in age. The deformed metasedimentary rocks consist of (1) white mylonitic quartzite, (2) micaceous and/or feldspathic mylonitic quartzite, (3) various marbles, (4) calc-silicate rock, and (5) quartz-epidote-feldspar schist. This sequence of lithologies outcrops over several square

kilometers, has a structural thickness of up to 800 m, and lies along a sheared contact with underlying mylonitic basement. Exposures of the Buckskin-Rawhide detachment fault structurally above this package of metasedimentary rocks indicates it is situated within the lower plate of the main detachment.

SEDIMENTARY ROCKS

Unmetamorphosed sedimentary rocks and sediments at Mesquite Mountain are restricted to deposits of (1) the upper Miocene to Pliocene Bouse Formation and (2) the Colorado River drainage system. These rocks and sediments were deposited subsequent to most deformation and record a period of tectonic quiescence in the region from Late Miocene time to Recent.

BOUSE FORMATION

Deposits of the upper Miocene to lower Pliocene Bouse Formation mantle bedrock exposures throughout the study area. The Bouse Formation was first described by Metzger (1968) on the basis of (1) a 767-foot type section from a well in Parker Valley, and (2) two reference sections, one of which is located along the western flank of Mesquite Mountain (SW1/4 sec. 26 and SE1/4 sec. 27, T. 8 N., R. 20 W., Gila and Salt River baseline and meridian). The Bouse Formation is named for Bouse Wash which trends roughly east-west along the northern edge of Mesquite Mountain

Metzger (1968) identified three units within the Bouse Formation: (1) a basal limestone, (2) interbedded clay, silt and sand (which comprises most of the formation), and (3) a distinctive tufa deposit that mantles topography and is thought to have formed at or near the water surface throughout Bouse Formation deposition. Recent work by Buising (1986, 1987) shows the Bouse Formation to be interfingered with conglomerate and sandstone of the underlying Osborne Wash association. The Bouse Formation is overlain by and interfingers with conglomerates interpreted as ancestral Colorado River gravels (Buising, 1987).

ALLUVIUM

Rocks mapped as alluvium consist predominantly of unconsolidated gravels and sand associated with the modern drainage system of the Colorado River and its tributaries, including Bouse Wash. These deposits include alluvium, colluvium, talus,

dune sand, and flood plain deposits of the Colorado River. No attempt has been made in the present study to distinguish these various Quaternary deposits on the geologic map.

IGNEOUS ROCKS

The volume of igneous rocks exposed at Mesquite Mountain (exclusive of granitic dikes and sills included with the Mesquite Gneiss) is relatively minor, and limited to intrusive rock types. These rocks range in composition from biotite granite to mafic intrusive dikes, and they are all of latest Cretaceous or Tertiary age. Three generations of intrusive activity are evident from the relation of these intrusive units to development of fabrics in the country rocks. Biotite granite bodies pre-date most or all of the mylonitic deformation, intermediate dikes appear to by syn-kinematic, and mafic to intermediate dikes are clearly post-tectonic.

BIOTITE GRANITE

Small, isolated bodies of biotite-bearing granite are distributed within the Mesquite Gneiss. These granites consist of coarse- to fine-grained, hypidiomorphic granular, tan to orange-weathering granite with the igneous assemblage quartz + potassium feldspar + plagioclase + biotite ± muscovite ± Fe-oxides. Accessory phases include zircon, sphene, and apatite, and alteration phases include chlorite and fine-grained white mica.

The largest of these granite bodies, at the south end of Mesquite Mountain, contains several large (10-15 m) blocks of the Mesquite Gneiss migmatite, indicating that intrusion of these granitic bodies post-dated development of the migmatite. Deformation within these granites varies from ultramylonitization to undeformed granite. The age of these granites is inferred to be latest Cretaceous to earliest Tertiary, based on the similarity to variably foliated, biotite granite sills in the Mesquite Gneiss which have been dated as Late Cretaceous.

GRANITIC PEGMATITE

Often present in association with metasedimentary rocks in the Mesquite Mountain fault zone are irregular pods of white- to light grey-weathering, very coarse-grained, granitic pegmatite. These rocks consist exclusively of large, angular potassium feldspar and quartz crystals in a matrix of finer-grained quartz and potassium feldspar. Based on their texture, these rocks are clearly of igneous origin, and were deformed along with the

metasedimentary rocks within the Mesquite Mountain fault zone. No direct connection of these rocks can be made with surrounding intrusive units, since they are found only within the Mesquite Mountain fault zone. The highly evolved composition suggests these pegmatites represent late-stage fluids from an intrusive body, and may be related to biotite granite which intrudes the Mesquite Gneiss. Age constraints can only be inferred from the fact that these pegmatites intrude the Mesozoic(?) metasediments of the MMFZ, and are deformed along with them in the fault zone. They may represent igneous activity which was associated with development of the Mesquite Mountain fault zone.

TONALITE DIKES

A series of porphyritic tonalite dikes (too small to be shown on the geologic map) are irregularly distributed within the Mesquite Mountain area. These dikes are typically 2 to 5 m in thickness, and are continuous over the scale of individual fault blocks. The primary mineralogy consists of plagioclase and quartz phenocrysts floating in a fine- to very fine-grained, equigranular groundmass of feldspar and quartz. Primary textures have been considerably obscured: phenocrysts are rounded and broken, and the groundmass shows clear evidence of thin shear bands of crushed, cryptocrystalline material. Dike margins do not typically show evidence of deformation, and dikes cross-cut both gneissic and mylonitic foliation in country rocks of the Mesquite Gneiss and biotite granite.

INTERMEDIATE DIKE ROCKS

Exposed only locally at the very southern end of Mesquite Mountain (too small to be shown on the geologic map) are several small intrusive dikes, two to three meters thick, which intrude the surrounding Mesquite Gneiss and granitic bodies. These dikes, which strike north to northeast and dip vertically, consist of brown-weathering, quartz- and feldspar-rich porphyry which contains abundant phenocrystic biotite. The rock is dark grey on a fresh surface with a mottled appearance that results from 3-5 mm, chalky-white feldspar phenocrysts.

Near contacts with the country rocks, these dikes have a primary(?) foliation parallel to the contact, but otherwise show little evidence of fabric development or deformation. These dikes clearly cut all other fabrics and contacts within the crystalline gneiss, but their age relation to dikes of basaltic(?) composition exposed along the southeast flank of Mesquite Mountain is unclear. Based on the phenocryst assemblage

plagioclase + quartz + biotite + hornblende(?) in a groundmass of fine- to very fine-grained quartz and feldspar, this rock is inferred to be of intermediate (andesitic to dacitic) composition.

DIABASE DIKES

Several northwest-trending, mafic dikes occur along the southeastern flank of Mesquite Mountain. These small dikes are 1 to 2 m thick, continuous for about half a kilometer, and are not found elsewhere at Mesquite Mountain The dikes have a seriate texture from large elongate (up to 2 mm) plagioclase grains to a variably sized groundmass of interlocking felty plagioclase. Large grains exhibit optical zoning. Pyroxene is also present as large, relict grains which have been highly altered to chlorite. Opaque oxides make up less than one percent of the rock.

These mafic dikes are significant in that they cut all fabrics and structures within the crystalline rocks. These rocks are probably related to mafic volcanic rocks of Miocene age known from the detachment terrain in the Whipple and Buckskin Mountains. Attempts to obtain a conventional K-Ar age for these rocks have failed due to the high calcium carbonate content of the rock as an alteration product.

DESCRIPTION OF STRUCTURES AND FABRICS

Structures and fabrics at Mesquite Mountain record a continuous progression from ductile, penetrative fabrics to more localized, brittle faulting. A total of eight deformational events are recognized, documenting the structural evolution of the crystalline basement at Mesquite Mountain since Late Cretaceous time. The relative timing of the development of these structural and fabric elements has been determined largely on the basis of cross-cutting relationships in the field. The sequence of structural events is described here in temporal order, beginning with the oldest recognizable fabric in the Mesquite Gneiss. Standard structural abbreviations (Turner and Weiss, 1963) are used to denote deformational phases (D), planar fabric elements (S), linear fabric elements (L), and fold phases (F). Where the relation of one fabric or structural element to another remains equivocal, a separate number has been assigned. Fabric elements are summarized on equal area stereonet plots (Figs. 1.5-1.9), and are statistically contoured

for 3% of the data per 1% area. Mean vectors are determined for the data sets and the 2σ cone of confidence is reported.

For the purpose of structural analysis, the Mesquite Mountain area can be divided into six structural domains as follows: (1) Mesquite Hill, (2) the south end, (3) the western flank, (4) the eastern flank, (5) the Mesquite Wash Hills, and (6) the north end. Boundaries of these structural domains are indicated in Figure 1.2. The south end (domain 2) is characterized by a series of klippen bounded by low-angle faults. The western flank comprises the extensive exposure of Mesquite Gneiss to the west of the northeast-southwest-trending ridgeline of the mountain (which includes Agency Peak), while the eastern flank is bounded by the ridge crest to the west and the Mesquite Wash Hills fault to the east. The Mesquite Wash Hills make up the low-lying exposures to the east of the Mesquite Wash Hills fault. The north end constitutes the northern two kilometers of Mesquite Mountain.

GNEISSIC LAYERING IN THE MESQUITE GNEISS (D1)

The earliest fabric element at Mesquite Mountain consists of compositional layering (S_1) within the Mesquite Gneiss. Evidence for relict, primary lithologic layering (S_0) within the migmatite is lacking, although the compositional layering now present may in part reflect original stratification within the sedimentary protolith of the gneiss. Gneissic layering is defined by alternating leucosomatic and mesosomatic bands which vary from several centimeters to one or two meters in thickness (Figs. 1.3 and 1.4). Layering is continuous for tens to hundreds of meters, but is typically contorted internally by folding. Development of this layering was associated with amphibolite facies metamorphism and extensive granitic injection. A stereonet plot of poles to gneissic foliation (n=77) in the Mesquite Gneiss (Fig. 1.5), reveals a predominant southwest to northwest dip, with a roughly bimodal distribution. Contouring of these data indicate a mean vector with a length of 0.641 oriented N84E 59, corresponding to an average attitude of gneissic foliation of N6W 41SW.

At least three styles of folds are developed within the migmatite, and are interpreted as F_1 structures. Intrafolial, isoclinal folds (F_{1a}) are ubiquitous within the gneiss, and are folded by later tight-to-open (50°-80°) (F_{1b}) and open (F_{1c}) folds. Many F_{1a} structures are preserved only as rootless isoclinal folds. Both F_{1b} and F_{1c} folds typically indicate a top-to-the-northeast asymmetry when viewed down plunge. Most of this folding appears to be synchronous with development of the migmatite. Figure 1.10

shows an example of this evidence, where a thin, granitic band defines part of the folded compositional layering, but truncates contiguous layering only 20 cm away. Despite the abundance of folding and transposition of layering within the gneiss complex, the compositional layering (S_1) exhibits a very consistent west to southwest dip of 20° to 65°.

DUCTILE FABRICS IN THE MESQUITE GNEISS (D2)

Mylonitic fabrics within the Mesquite Gneiss and associated granitic rocks are variably developed, and represent either temporally distinct deformational events or a single, progressive event. All mylonitic fabrics (S_2, S_3, and S_4) are characterized by a well-developed, mylonitic foliation (defined by oriented micas and flattened potassium feldspar and quartz grains), and stretched mineral lineation (defined by smeared quartz grains, aligned mica trains, and trails of crushed potassium feldspar). This fabric is most prominent near exposures of the Mesquite Mountain and Agency fault zones, but is also well developed within distributed zones of shear in the main body of Mesquite Gneiss. For the purpose of description, these fabrics are treated separately where they can be differentiated, but given the similarity of all mylonitic fabrics in the Mesquite Mountain area, it is difficult to distinguish separate generations in the absence of an associated structure. The stretched-mineral lineation is invariably present where the mylonitic fabric exists, and as such, attitudes which bear a lineation symbol on the geologic map (Plate 1-1) indicate a mylonitic fabric.

A locally intense, mylonitic foliation (S_2) and associated stretched mineral lineation (L_2) is developed heterogeneously within the Mesquite Gneiss. In general, discrete mylonitic shear zones are not recognized. Rather, the mylonitic fabric is gradational over distances of tens of meters from zones of intense shear to areas of unmylonitized gneiss. The orientation of the mylonitic fabric is very consistent, with a moderate southwestward dip. These mylonitic fabrics are always found to cross-cut and therefore post-date, the gneissic layering in the Mesquite Gneiss. In addition, biotite granites which intrude the Mesquite Gneiss bear this mylonitic fabric and are never seen to post-date mylonitization.

MESQUITE MOUNTAIN FAULT ZONE (D3)

The Mesquite Mountain fault zone (MMFZ) is exposed at low elevations along the western flank of Mesquite Mountain (domains 2, 3, and 6), and consists of an irregular, discontinuous band of highly deformed metasedimentary rocks which are enveloped

within the crystalline rocks of the Mesquite Gneiss (Plate 1-1; Figs. 1.2 and 1.11). Despite the discontinuous nature of the MMFZ, expressions of this structure are present along the entire length of the western flank of Mesquite Mountain. The fault zone is folded, but has a general eastward dip, and projects beneath Mesquite Mountain (Plate 1-2). Structural thickness of the MMFZ varies from < 1 to > 20 m, with abrupt variations in thickness along the trace of the fault zone. Numerous exposures of the MMFZ are marked only by the presence of thin tectonic slivers of metasedimentary rocks within mylonitic rocks of the Mesquite Gneiss. Where these distinctive metasedimentary rocks are absent, the MMFZ can be difficult to recognize.

Boundaries of the MMFZ are commonly characterized by a concordant, 20-50 cm-thick mylonite zone. An earlier mylonitic fabric (S_2) developed within the Mesquite Gneiss is clearly truncated in numerous places by the MMFZ and its associated mylonitic foliation (S_3) (Fig. 1.12). For this reason, the MMFZ is interpreted as a D_3 structure. Both upper and lower bounding surfaces of the MMFZ locally truncate gneissic (S_1) and mylonitic (S_2) foliation within the Mesquite Gneiss, however, at some localitites, the MMFZ and its associated mylonitic fabric parallel pre-existing fabrics in the Mesquite Gneiss. S_3 fabrics at the fault zone boundaries are typically ultramylonitic, with a pronounced south-southwest-plunging, stretched mineral lineation (L_3). Angular discordance of the S_3 fabric with the earlier S_2 mylonites is locally as much as 30-40° (Fig. 1.12).

Sedimentary rocks of Paleozoic and/or Mesozoic age have been ductilely deformed and metamorphosed at mid- to upper-greenschist facies conditions within the Mesquite Mountain Fault Zone. These rocks, consisting primarily of marble and calc-silicate rock, possess a transposition foliation (S_3) which is consistently concordant with the fault zone boundaries and associated mylonitic fabrics in the gneiss (Fig. 1.12). Within cherty portions of the marbles, rootless isoclines (F_3) defined by folded chert bands are common. Lenses of isoclinally folded, mylonitic gneiss and syn-tectonic granitic pegmatite occur within the metasedimentary band of the MMFZ. Along the western flank of peak 1625, mylonitic gneiss from the Mesquite Gneiss occupies the core of a large-amplitude (200 m), recumbent, isoclinal fold defined by metasedimentary rocks within the MMFZ. In other exposures, pods of mylonitic gneiss define rootless isoclinal folds within the metasedimentary rocks of the MMFZ (Fig. 1.13). These relationships suggest that lenses of the Mesquite Gneiss near the fault zone boundaries were entrained within the fault zone during ductile shearing.

Metamorphic assemblages associated with the S_3 fabric in the metasedimentary rocks of the MMFZ consist of quartz + calcite + biotite + chlorite ± epidote in calc-silicate rocks, and calcite + quartz + dolomite ± muscovite in calcite marbles. These assemblages are grown in the foliation, which is defined primarily by thin compositional banding and aligned minerals. In the cherty calcite marble, this metamorphic assemblage and fabric overprints a previous amphibolite facies (diopside-grade) metamorphism. This earlier metamorphic assemblage probably developed during thrust burial and amphibolite facies metamorphism of the sedimentary protolith of these rocks.

The magnitude of displacement on the Mesquite Mountain fault zone can only be treated in a speculative manner. No piercing points, stratigraphy, or lithologic variation within the Mesquite Gneiss can be correlated across the fault zone. The fabrics developed both within and near the fault zone are indicative of extremely high magnitudes of shear strain, but how this translates into net displacement across the zone is unclear. It is probably safe to infer that displacement is of the order of several hundreds of meters to tens of kilometers, in a zone of relatively localized shear. The sense of displacement on the MMFZ is indicated by shear sense in mylonitic rocks associated with the fault zone. Asymmetric porphyroclasts, S-C fabrics, and sygmoidal quartz bands define a predominant top-to-the-northeast shear sense for mylonites associated with the MMFZ.

AGENCY FAULT ZONE (D4)

The Agency fault zone outcrops as a relatively continuous structure along the lower, eastern flank of Mesquite Mountain (Plate 1-1; domains 4 and 6, Fig. 1.2), and consists of a gently- to moderately- west-dipping zone, 3-15 m thick, of highly sheared gneiss and lenses of deformed metasedimentary rock. The exposed extent of the fault zone consists of a three-kilometer segment, but the structure is inferred to continue along strike to both the north and south in the subsurface. A concordant mylonitic fabric is associated with the Agency fault zone, with a stretched mineral lineation oriented ~S30W, plunging 10-15°, similar to mylonitic foliation and lineation within other areas of the Mesquite Gneiss.

The geometry of the Agency fault zone, as determined by structural contouring, describes a domal surface consisting of three segments (Plate 1-1; Fig. 1.14). The middle segment, ~1.5 km long, strikes N10-35E, with westward dips from 30-45°. To the north, the fault zone dip shallows and wraps around to a more northeasterly strike, coincident with the disappearance of high-angle faults in its hanging wall (Plate 1-1).

Along the southern segment, exposed for about 0.5 km, the dip of the fault zone again shallows (15-20°) and curves around toward a strike which is due north. The Agency fault zone differs from the analogous Mesquite Mountain fault zone in four principal respects: (1) it is a relatively regular, continuous structure, (2) it does not exhibit the high degree of folding of the fault surface that the MMFZ does, (3) mylonitic fabrics developed along the fault zone are not as intense as those seen on the MMFZ, and (4) where exposed, the Agency fault zone dips antithetically (west) to the MMFZ. On this basis, the Agency fault zone is distinguished as a separate, younger structure from the Mesquite Mountain fault zone, despite the similarity in structural style and kinematic history. If the Agency fault zone is a younger structure, the projection of the fault zone to the west implies it truncates the MMFZ at depth beneath Mesquite Mountain (Plate 1-2).

Metasedimentary rocks incorporated within the Agency fault zone consist predominantly of orange, micaceous calcite marble; minor amounts of cherty, grey marble and quartzite are also present. The largest lenses of these metasedimentary rocks are indicated on the geologic map (Plate 1-1) and are exaggerated for clarity on the geologic cross sections (Plate 1-2). These metasedimentary rocks possess a well-developed foliation, but generally lack a discernible mineral lineation. Mylonitic gneiss within the Agency fault zone is typically altered to a bright red color which marks the trace of the fault zone along segments where metasedimentary rocks are absent. In places, these fault zone rocks exhibit cavernous weathering and brecciation, suggesting that movement on the Agency fault zone spanned a spectrum of rheological conditions.

Fabrics associated with the Agency fault zone (S_4) truncate both gneissic (S_1) and mylonitic (S_2) fabrics within the Mesquite Gneiss, similar to the Mesquite Mountain fault zone on the west flank of Mesquite Mountain. This relationship is seen both above and below the fault zone, and like the MMFZ, the Agency fault zone is in places concordant with pre-existing fabrics in the Mesquite Gneiss. Mesoscale folds in gneissic layering in the footwall of the Agency fault zone appear to have a top-to-the-southwest asymmetry when viewed down plunge. On the south wall of Pitchfork Canyon (domain 4), gneissic layering is folded in a large-amplitude (> 40 m), upright fold which plunges roughly S30W in the footwall of the Agency fault zone.

The sense of displacement on the Agency fault zone is inferred from kinematic indicators in mylonitic gneiss associated with the fault zone. A predominant top-to-the-northeast sense of displacement is indicated by all kinematic indicators. The magnitude of

displacement on this structure is not well constrained but is inferred to be of the order of hundreds of meters to kilometers.

The contorted and discontinuous geometry of the Mesquite Mountain fault zone has resulted, in part, from meso- to macroscale folding subsequent to movement within the fault zone. These folds are particularly evident in exposures of the MMFZ in the western flank (domain 3) of Mesquite Mountain. Fold axes plunge gently to moderately to the south-southwest, and fold the MMFZ along with the surrounding crystalline rocks. Both outcrop and map scale folds of the MMFZ are essentially parallel to mylonitic lineation. Since folding of the MMFZ must have post-dated movement on the fault zone, these folds are assigned to an F_4 phase of folding, and are interpreted as the result of deformation in the hanging wall of the Agency fault zone.

The orientation of all mylonitic fabrics is very consistent, with a moderate southwestward dip. Poles to mylonitic foliation (S_2, S_3, and S_4) within both the Mesquite Gneiss and mylonitic fault zones (Fig. 1.6; n=116) define a mean vector (length = 0.838) of N56E 50, with a 2σ confidence cone of five degrees. This mean pole orientation corresponds to an averaged strike and dip of N34W 40SW for mylonitic foliation at Mesquite Mountain. A stereonet plot of mylonitic stretching lineation (L_2, L_3, and L_4) associated with the mylonitic foliation (Fig. 1.7; n=116) shows a very tight clustering of the data about a south-southwest plunge. Data are distributed about a mean vector (length = 0.814) of S18W 42, with a 2σ confidence cone of six degrees. The angular distance between these mean vectors for mylonitic lineation and poles to mylonitic foliation is 82°, signifying that in a general sense, shear in the mylonites was dominated by dip slip.

A combined plot of gneissic (S_1) and mylonitic (S_2 through S_4) foliation (Fig. 1.8; n=193) emphasizes the general coincidence in orientation of the these two styles of fabrics: the angular separation of the mean vectors for these two data sets is only 18 degrees. This relationship suggests that (1) the direction of the maximum elongation (ε_3) was oriented essentially within the plane of the compositional layering of the basement complex during the development of ductile fabrics, and (2) either little appreciable rotation of the strain axes occurred during progressive mylonitization, or earlier phases of the mylonitic fabric were subsequently rotated into parallelism during continued shear.

The consistency in orientation of both mylonitic foliation and lineation (for all generations of these fabric elements), despite evidence for cross-cutting relations of

mylonitic fabrics is striking. Two possible interpretations can be offered for the correspondence in fabric orientations: (1) all pre-existing mylonitic fabrics were rotated into parallelism with the youngest and most intense fabric, or (2) all fabrics developed during the same progressive event associated with Tertiary extensional deformation. Since no clear evidence for a relict mylonitic fabric which pre-dates Tertiary mylonitization has been documented at Mesquite Mountain, the latter scenario is preferred.

DUCTILE HIGH-ANGLE FAULTS

A series of moderate- to steeply-dipping ductile faults occurs along the eastern flank of Mesquite Mountain within the crystalline rocks of the Mesquite Gneiss (Plate 1-1). At least five of these faults were recognized, all having a similar orientation (N50-65E, 40-60SE; Fig. 1.9), planar geometry, and spacing (20-30 m). These faults truncate both gneissic and mylonitic foliation within the Mesquite Gneiss, and are characterized by penetrative, mylonitic zones, 0.1-1 m thick, developed along the faults (Fig 1.15). Folds developed in both the hanging walls and footwalls of these faults exhibit a very ductile style, and indicate an apparent normal sense of displacement. Orientation of fold axes (S15-20W) for these folds are essentially parallel to mylonitic lineation (S10-15W) developed within the fault-related mylonites, implying an oblique-normal, northeast-southwest sense of displacement on this set of structures.

Although the intersection is not well exposed, the ductile high-angle faults appear to sole into the Agency fault zone low on the eastern flank of Mesquite Mountain. Given the similarity in ductile style of deformation and kinematic sense, this interpretation seems reasonable. Since no noticeable shallowing of the high-angle faults is seen down dip, they may actually be truncated by the Agency fault zone. An interpretation of synchronous movement is preferred, and these faults are designated part of the D_4 deformation.

The high-angle faults are most pronounced over the central, domal segment of the Agency fault zone, and are oriented roughly parallel to the transport direction (northeast) inferred from mylonitic lineation and fold axis orientations associated with the faults. As such, they do not conform to the expected geometry and orientation of faults associated with extension in an ENE-WSW direction. Walker et al. (1986) argue that orientation of normal faults need not be directly related to extension direction. One explanation for these ductile high-angle faults is that they represent accommodation structures within the

hanging wall of the Agency fault zone related to topography on the fault surface (Fig 1.14). They appear to have been active synchronously with the Agency fault zone, and are best developed over a domal high in the footwall of the fault zone.

LOW-ANGLE FAULTS (D5)

A series of klippen of intensely mylonitized gneiss, bounded by low angle faults, is exposed at the south end (domain 2) of Mesquite Mountain (Plates 1-1 and 1-2). These faults place variably sheared but typically mylonitic Mesquite Gneiss, and lesser amounts of deformed, metasedimentary and fine-grained, silicic intrusive rocks in the hanging wall against relatively unmylonitized Mesquite Gneiss in the footwall (Fig. 1.16). Small (2-4 m), isolated lenses of sheared metasedimentary rocks (usually micaceous calcite marble) occur along the contact. These low-angle faults strike generally north-northwest to northwest, with gentle southwesterly dips of 10-35°. Structural contouring of the fault surfaces suggests they deviate from smooth, curviplanar surfaces, particularly in the case of the large klippe which caps peak 1625'. Variations in dip on this fault surface range from 20-60° over short distances, and are perhaps due to folding which post-dated movement on the fault.

This system of faults displays a spectrum of fabrics, ranging from penetrative mylonitic foliation to extreme brecciation. Mylonitic fabrics are concordant with the fault contacts, and exhibit a well-developed stretched mineral lineation These faults and their associated fabrics clearly truncate both mylonitic foliation in the hanging wall and gneissic foliation in the footwall.

Sense of movement on these faults is indicated by shear-sense indicators within the mylonites (asymmetric porphyroclasts, mica fish, sygmoidal quartz ribbons) which demonstrate a consistent top-to-the-northeast sense of shear. The magnitude of displacement on these faults is unconstrained. Relatively high shear strains are indicated by the degree of mylonitization associated with the faults, but no reliable piercing points can be identified within the Mesquite Gneiss crystalline terrain. A minimum of 200-300 m of offset is suggested for the klippe on peak 1625', which truncates the folded Mesquite Mountain fault zone in the footwall, and the MMFZ does not appear in the hanging wall in the direction of transport.

Relative timing of movement on this set of faults is constrained by the fact that they cut the folded Mesquite Mountain fault zone (evident along the southwest flank of

peak 1625'), but are cut by northwest-striking, high-angle faults. While these klippen do not presently define a single, continuous surface, reconstruction of movement on the northwest-striking faults could reconstruct them as a single fault surface. The range of structural fabrics developed on these faults (mylonites to cataclasites) suggests they were active over a range of physical conditions within the crust. This observation is consistent with the relative timing of these structures between conditions of extreme mylonitization on the Mesquite Mountain fault zone and brittle faulting on high-angle faults. Absolute timing of movement on the set of low-angle faults is inferred to be mid-Tertiary (late Oligocene or early Miocene), and associated with the development of the Whipple-Buckskin-Rawhide detachment system.

HIGH-ANGLE BRITTLE FAULTS (D_6 & D_7)

Two families of steeply-dipping to vertical faults (D_6 and D_7) dissect the range and disrupt the continuity of all pre-existing structures. Recognition of these faults is based on (1) abrupt, linear breaks in topography, (2) discontinuities in the Mesquite Mountain and Agency fault zones and in gneissic banding within the Mesquite Gneiss, and (3) brecciation and disruption of the gneiss along the trace of these faults. Exposures of the actual fault surfaces are not common, but do exist.

One set of these faults is oriented N40-60W, with dips varying between ~70° northeast to ~70° southwest (Plates 1-1 and 1-2). Five faults are recognized within this group, and are identified as D_6 structures. The relative sense of displacement on these faults is unknown, because the original configuration of structural and lithologic features truncated by the faults is unconstrained. An apparent right-lateral sense of offset for these structures is suggested by the northwest extension of bedrock exposures along the southwest side of the large fault through the center of Mesquite Mountain. Given the relative consistency in attitude of the gneissic and mylonitic foliation in the Mesquite Gneiss, it would appear that no appreciable rotation has taken place between adjacent fault blocks. The general continuity of rock types and structures preserved from one fault block to another suggests that offsets on these faults are not great, and probably less than 2-3 km for any individual fault.

Given their brittle character, the timing of movement on these D_6 faults is constrained to post-date development of ductile fabrics and structures within the Mesquite Gneiss. Basal tufa deposits of the Bouse Formation overlap these fault surfaces, indicating that movement had ceased by the time of Bouse deposition in the late Miocene.

Miller and McKee (1971) described northwest-trending, right-slip faults in the southern Plomosa Mountains, to the southeast of Mesquite Mountain, with post mid-Miocene displacement of about 3-5 km. Middle to late Miocene right-slip faults of western Arizona, which show no evidence of activity since Pliocene time, may be part of an ancestral San Andreas fault system, implying westward migration of the locus of right-lateral slip along the North American plate margin in the late Tertiary.

A single, N50E-striking, vertical fault (D_7) occurs along the southeastern flank of Mesquite Mountain, and clearly truncates D_6 structures. This fault is similarly identified by a geomorphologic depression, and disruption of the bedrock along the trace of the fault. An apparent left-lateral sense of displacement is suggested by the *en echelon* pattern of two low, elongate, northeast-trending ridges of crystalline gneiss to the southeast of the fault. The relative timing of movement on this northeast-striking fault can be fairly well constrained: it truncates the family of northwest-striking high-angle faults, and is cut by a series of basaltic dikes along the southeast side of Mesquite Mountain (Plate 1-1). Both the movement on the fault and intrusion of the basaltic dikes across the fault are constrained to predate Bouse deposition in late Miocene time. Northeast-trending, high-angle faults of Tertiary age are uncommon in western Arizona.

MESQUITE WASH HILLS FAULT (D8)

The Mesquite Wash Hills fault (MWHF) is exposed for approximately 2 km of its length and forms the western boundary of the Mesquite Wash Hills (Plate 1-1). The fault is marked by both surface outcrop and geomorphologic expression within the stream drainages and gravel pediments of the low-lying area between the Mesquite Wash Hills and Mesquite Mountain proper. This structure is the youngest recognized at Mesquite Mountain, and is designated the D_8 deformation.

The MWHF is oriented N25-30E, dips 82-90° to the southeast, and juxtaposes highly brecciated mylonitic rocks of the Mesquite Gneiss in the hanging wall (to the southeast of the fault) against unconsolidated gravels which overlie the Bouse Formation (to the northwest of the fault) (Fig. 1.17). Brecciation of the gneisses within ~100 m of the main trace of the fault has produced angular gneissic clasts (up to small boulder size) in a matrix of angular pebble-sized clasts. This fault breccia exhibits cavernous weathering which marks much of the trace of the fault. Several other minor strands of the fault occur to the east within the bedrock gneisses, but disruption and brecciation decrease away from the main fault trace and generally die out laterally within 100 m of the fault.

The trace of the MWHF is evident on areal photographs as a lineament in alluvial gravels which continues along a more northerly strike (N10E) north of the Mesquite Wash Hills. Several minor gullies are abruptly truncated along this northern trace of the fault, which projects beyond the north end of Mesquite Mountain and into Bouse Wash. The change in strike in the MWHF is expressed in the topography by a discernible bend at the termination of exposures in the Mesquite Wash Hills to the east of the fault. Thus, the total length of the surface expression of the fault is approximately 4 km, along the eastern flank of Mesquite Mountain

A 5-20 cm-thick microbreccia is developed on the fault surface, and consists of small, angular to rounded grains of feldspar and lithic fragments in a well-indurated matrix of fine-grained rock powder (Fig. 1.17). No kinematic indicators are evident on the fault surface, and no convincing correlation of units can be made across the fault, but apparent offsets of minor stream drainages suggest primarily left-lateral displacement. The magnitude of displacement on the Mesquite Wash Hills fault is largely unconstrained, but probably on the order of hundreds of meters to several kilometers.

The age of movement on the MWHF is poorly defined. Brecciation of the mylonitic gneisses clearly post-dates all other fabrics recorded in these rocks. At its most southwesterly exposure, the MWHF apparently truncates the Agency fault zone (Plate 1-1), and given the contrast in deformational styles between these two structures, the MWHF is arguably younger. Thus, a lower age limit for movement on the MWHF system is inferred to be after mylonitic deformation of the crystalline gneiss, and movement on the Agency fault zone. Gravels in the footwall (or northeast side) of the MWHF overlie the Bouse Formation, and must be either correlative with or younger than Colorado River gravels of Pliocene age (Buising, 1987). Offset of minor stream drainages along the MWHF suggests that some displacement on the Mesquite Wash Hills fault is Quaternary, and provides evidence for some of the youngest faulting yet documented in the Colorado River Trough region. Activity on the Mesquite Wash Hills fault may thus be bracketed between cessation of movement on the Agency fault zone (mid-Miocene) and Recent, but may be characterized by several periods of movement. Other faults with post-Bouse Formation movement include the northwest-trending Havasu Springs fault, located along the southeastern end of Lake Havasu to the north (Davis et al., 1980).

DISCUSSION

The sequence, style, and timing of structural events documented at Mesquite Mountain shed new light on the development of the Whipple-Buckskin-Rawhide detachment system. Discussed below are factors relating to the timing and significance of the structural development at Mesquite Mountain.

AGE OF DEFORMATION

The relative timing of structures and fabrics at Mesquite Mountain requires a Tertiary (or possibly very latest Cretaceous) age for the development of these features. Based on U-Pb zircon dating of biotite granite from the Mesquite Gneiss, an age of 67.2 ± 1.4 Ma is implied for the development of this migmatite complex (Knapp and Walker, in prep.). The age of mylonitic fabrics within the lower Colorado River extensional corridor is controversial. Numerous workers have proposed either a Mesozoic or Tertiary age for formation of mylonites in this geologically complex terrain. Howard and John (1987) argue for a Late Cretaceous age for mylonites formed in Cretaceous plutons in both the Chemeheuvi and Iron Mountains of southeastern California. Mesozoic structures with associated ductile fabrics are now well-documented from the Maria fold and thrust belt (Reynolds et al., 1986, and Richard, 1988).

The age of mylonitic deformation at Mesquite Mountain is constrained to be younger than ~67 Ma based on U-Pb zircon dating of a biotite-granite sill from the Mesquite Gneiss (Knapp and Walker, in prep.). A number of observations corroborate a Tertiary age for mylonitic deformation at Mesquite Mountain, including (1) the style of the mylonitic fabrics, (2) the coincident orientation of mylonitic foliation and lineation from all mylonites, (3) evidence for a Mesozoic, amphibolite-grade metamorphism in the metasedimentary rocks which predates mylonitization in the Mesquite Mountain and Agency fault zones.

Reynolds et al. (1988) review the distinctions between Mesozoic to early Tertiary metamorphic fabrics and Tertiary mylonitic fabrics in western Arizona. Fabrics produced during Mesozoic and early Tertiary prograde metamorphism are generally schistose rather than mylonitic. Tertiary mylonitic fabrics, in contrast, are more strongly lineated, less schistose (except where ultramylonitic), and characterized by ubiquitous crystal-plastic deformation of quartz. As discussed earlier, all mylonitic fabrics at Mesquite Mountain exhibit a strong stretching lineation and textures indicative of crystal-plastic flow of quartz

and brittle behavior of potassium feldspar, rather than neomineralization. Thus, fabrics at Mesquite Mountain more closely resemble Tertiary mylonitic fabrics than metamorphic fabrics associated with Mesozoic deformation.

The relative age of this mylonitic fabric is constrained by two factors: first, it overprints all fabrics associated with development of the Mesquite Gneiss, and second, the conditions of temperature, pressure, and strain rate implied by the two styles of deformation (migmatiztion versus mylonitization) are considerably different. Mylonitization was characterized by crystal-plasticity, low- to mid-greenschist facies metamorphism, and accommodation of high strain, at relatively low temperatures judging from the purely brittle behavior of potassium feldspar. Migmatization and development of the Mesquite Gneiss, on the other hand, was associated with amphibolite facies metamorphism, *in situ* partial melting, and dynamic recrystallization. Given these factors, it seems unlikely that deformation associated with these different fabrics was closely spaced in time.

Conditions of mylonitization in the Mesquite Gneiss are reflected in microtextural features observed in thin section. Quartz consistently exhibits crystal-plastic behavior, and occurs as thin, elongate ribbons, or as domains of polygonally-recrystallized grains. Potassium feldspar typically occurs as angular to rounded porphyroclasts which show varying degrees of fracturing, but no obvious evidence of recrystallization or crystal-plastic behavior. Epidote appears to pre-date development of the mylonitic fabric, and forms trains of crushed grains along shear planes. Micas (mostly biotite) are sheared and bent, and often show extensive alteration. Secondary mineralization associated with mylonitization was limited primarily to fine-grained white mica and chlorite, indicating greenschist facies conditions.

Temperatures and pressures associated with mylonitic deformation are difficult to constrain. Rheological properties of the constituent minerals are dependent on both temperature and strain rate in the low temperature plasticity and power law creep regimes (e.g., Schmid, 1982). Conditions were apparently not suitable for dislocation creep to predominate in potassium feldspar. Independent evidence for temperatures of mylonitization in the Mesquite Mountain area comes from $^{40}Ar/^{39}Ar$ data (Knapp and Heizler, 1988b and in prep.). Hornblendes (T_c~500°C) from amphibolites in the Mesquite Gneiss yield Late Cretaceous ages, and show no evidence of Tertiary argon loss. Biotites (T_c~300°C) show closure to argon diffusion at around 30-33 Ma, and potassium feldspar (T_c~150-200°C) has a minimum apparent age of ~22 Ma.. These data

suggest that temperatures did not exceed ~300° C since mid-Oligocene time, and had cooled below 150° C by the early Miocene, for the structural levels exposed at Mesquite Mountain. A temperature range of 150-300° C seems probable for formation of these mylonites, and is consistent with the observed microtextures.

The general sequence of structural events at Mesquite Mountain is characterized by a progression from penetrative, ductile deformation to successively more brittle, localized deformation. The succession of mylonitic fabrics may be related to distinct episodes of deformation, or alternatively, may be expressions of a progressive, non-coaxial deformation. No distinction between these two models can be made on the basis of present data.

INCISEMENT OF DETACHMENT FOOTWALL

The significance of the Mesquite Mountain and Agency fault zones is best explained in terms of splays along lateral ramps within the footwall of the Whipple-Buckskin-Rawhide detachment system. Mesquite Mountain is situated directly on trend with the elongate "corrugations" in the detachment surface defined by the morphology of the Buckskin and Rawhide Mountains. In the case of the Agency fault zone, evidence for this ramp geometry is provided by the series of high-angle ductile faults which formed synchronously with the fault zone into which they sole. These faults are oriented essentially parallel to the extension direction for the detachment terrain, and kinematic indicators for these faults indicate they had a strongly oblique motion, in the direction of tectonic transport during extension. The present geometry of these faults, dipping ~60° to the southeast, suggests they are in the orientation in which they developed. Also implied by these relations is that the Agency fault zone is likely true to its original geometry and orientation, which forms a west-dipping, doubly-arched surface (Fig. 1.14).

The presence of Tertiary mylonitic fabrics throughout the hanging wall of both the Mesquite Mountain and Agency fault zones is indicative of incisement tectonics, as described by Davis and Lister (1988). Originally, the entire Mesquite Mountain block would have been situated in the lower plate of the detachment during the initial stages of mylonitization. During continued displacement on the detachment, pieces of the footwall were incorporated into the hanging wall. Exactly when this incisement occurred is uncertain, but mylonitic fabrics on the high-angle ductile faults in the hanging wall of the Agency fault zone suggest that incisement took place during the waning stages of ductile conditions. (i.e., the Mesquite Mountain block had reached a crustal level during its

ascent in the footwall where it was behaving with a rheology which was transitional from crystal-plastic to brittle.)

Within this scenario, the Mesquite Mountain and Agency fault zones are seen as similar structures, but are separated in time. Folding of the Mesquite Mountain fault zone took place after the structure became kinematically inactive and was being transported in the hanging wall of the Agency fault zone. Irregularities in the footwall to the Agency fault zone were responsible for inhomogeneous shear across this structure. These inferences have several implications: (1) that extensional strain in the detachment system was partitioned along numerous fault zones or strands of the major detachment fault, (2) that initiation of these strands took place under conditions where penetrative strain was becoming rheologically unfavorable, and (3) that large-scale irregularities in the fault zones (i.e., corrugations) were a primary feature, and not simply a function of post-detachment warping.

The style of deformation exhibited by isoclinal folding of the Mesquite Mountain fault zone in the hanging wall of the Agency fault zone may be analogous to microstructural features described by Lister and Snoke (1984), wherein C planes in S-C mylonites are folded during development of very high shear strains. With rotational simple shear, features originally oriented within the extensional field will pass into the shortening field. It is unclear whether such a deformation mechanism is plausible at the scale observed for the MMFZ, but high-strain and ductile folding of this structure subsequent to (or during the latter stages of) its formation clearly has occurred.

REGIONAL RELATIONS

Metamorphosed and deformed supracrustal rocks, of Paleozoic and Mesozoic age, in the footwall of the Whipple-Buckskin-Rawhide detachment system are known from several localities in west central Arizona. Marshak and Vander Meulen (in press) describe a sequence of metasedimentary and metaigneous rocks from the Battleship Peak area of the southern Buckskin Mountains. These metasedimentary rocks were deformed in a complex shear zone associated with Tertiary extension. Marshak and Vander Meulen (in press) documented several stages of deformation characterized by (1) development of mylonitic foliation and intrafolial isoclinal folds, (2) asymmetric, recumbent to inclined folds, and (3) development of ductile faults, kink folds, and brittle fractures and faults. Despite intense shearing and development of mylonitic fabrics along much of the exposure of the contact of these metasedimentary rocks, the deformed metasediments

locally discordantly truncate mylonitic fabrics within the underlying deformed basement, with no intervening extensive zone of shear. These workers interpreted the contact to be an unconformity at the base of the Paleozoic sequence. There is no evidence at Mesquite Mountain, however, that the original basement/cover contact is preserved. In addition, crystalline rocks bound the metasedimentary package from above at Mesquite Mountain, unlike the sequence in the Battleship Peak area of the Buckskin Mountains.

Rocks which are lithologically and structurally similar to the metasedimentary rocks of Mesquite Mountain are also known from the Rawhide Mountains (Shackleford, 1980) and the easternmost Buckskin Mountains (field trip with Bruce Bryant). In the Ives Wash area of the eastern Buckskin Mountains, mylonitic metasedimentary layers that consist of orange, calcite marble, quartzite, and calc-silicate rocks, are 4-5 m thick and laterally continuous for distances greater than 1 km. Tertiary mylonitic fabrics are very strongly developed here, and lenses of mylonitic gneiss are isoclinally folded within the metasedimentary rocks, in a fashion similar to the Mesquite Mountain fault zone. These areas are greater than 60 km distant from exposures at Mesquite Mountain, in the direction of tectonic transport of the detachment system.

Exposures in the northern Plomosa Mountains reveal a highly deformed sequence of metamorphosed sedimentary rocks beneath the Plomosa detachment fault. Scarborough and Meader (1983) described these units as part of a discontinuous, 0-50 m-thick zone, directly beneath the Plomosa detachment, which consists of tectonically interleaved lenses of carbonate, quartzite, and gneissic basement. These workers interpreted the metasedimentary rocks to be of Paleozoic protoliths, and inferred that normal movement on the Plomosa detachment fault was primarily a case of reactivation of an earlier thrust fault. The occurrence of the ductilely deformed metasedimentary rocks between the brittle detachment fault (above) and relatively unmylonitized gneissic basement (below) contrasts with exposures both at Mesquite Mountain and in the Buckskin Mountains.

These examples serve to illustrate several important points about the significance of the Mesquite Mountain and Agency fault zones exposed at Mesquite Mountain. Rocks of similar lithology, degree and style of deformation, and grade of metamorphism are extensively distributed within the footwall gneisses of the detachment systems. An area spanning >3,000 km^2 is represented by the distribution of these rocks, comprising a significant portion of the exposed extent of the footwall to the Whipple-Buckskin-Rawhide detachment. These ductilely deformed metasedimentary rocks occur in a

number of different structural settings: (1) enveloped within mylonitic crystalline gneisses (Mesquite Mountain, eastern Buckskin Mountains), (2) situated above mylonitic gneisses but directly below a detachment fault (western Buckskin Mountains), and (3) present above unmylonitized Precambrian gneiss and below a detachment fault (northern Plomosa Mountains).

At Mesquite Mountain, the age of the Mesquite Mountain and Agency fault zones is constrained to be Tertiary, and demonstrates that envelopment of the metasedimentary rocks along these structures was related to extensional tectonism. Marshak and Vander Meulen (in press) make a similar argument for the rocks of the Battleship Peak area, and in the eastern Buckskin Mountains, all rocks, including metasedimentary slivers and gneissic basement, are strongly transposed in the Tertiary mylonitic fabric (B. Bryant, pers. comm.). These relations emphasize that (1) the present configuration of the metasedimentary rocks is primarily a Tertiary feature, (2) reactivation of thrust faults (or pre-existing crustal weaknesses) was not the primary means for accommodation of extensional strain, and (3) these rocks probably provided a competence contrast with the basement gneisses, such that high shear strain was localized in the carbonate and metasedimentary rocks once they were entrained along the Tertiary structures.

CONTINUOUS PROGRESSION OF DEFORMATIONAL STYLE

Spencer (1984, 1985) develops cogent arguments about the effect of isostatic response of the crust during development of the detachment system. The time scales (tens to hundreds of thousands of years) for local isostatic readjustment of the crust are relatively short in comparison with those which characterized the development of the detachment system (Davis et al., 1980). Several studies now attribute large wavelength (5-20 km) irregularities and doming of detachment faults to such isostatic effects (Davis and Lister, 1988; Spencer and Reynolds, 1988; Wernicke and Axen, 1988). The presence of isostatic modification of the original geometry of the structures in the Mesquite Mountain area cannot be excluded, however it appears that many of the structural features maintain their original relative geometric relations on the scale of exposures at Mesquite Mountain.

NON-COINCIDENCE OF TERTIARY AND MESOZOIC STRUCTURES

Numerous thrust structures of the Maria fold and thrust belt are known from the region of west-central Arizona (Reynolds et al., 1986). These Mesozoic structures

initially carried Paleozoic and Mesozoic supracrustal rocks to considerable depths beneath crystalline thrust sheets, at greenschist to amphibolite facies conditions of metamorphism. As a result of later Tertiary extension within the detachment terrain, these structures were significantly modified. An important point, however, is that extension was not a matter of reactivation of these pre-existing planes of weakness. Many thrust structures of the Maria fold and thrust belt, although folded and dissected, remain with intact Mesozoic fabrics and metamorphic assemblages. In addition, evidence from the Mesquite Mountains area indicates that large amounts of extension were accommodated on structures such as the Mesquite Mountain and Agency fault zones, which are clearly of Tertiary age. These structures entrained metasedimentary rocks, which had previously been buried, as they intersected the older thrust faults.

CONCLUSIONS

The rocks and structures of the Mesquite Mountain area in west-central Arizona record a complex history of deformation in the footwall of the regional Whipple-Buckskin-Rawhide detachment system. The continuous progression of deformational styles from penetrative, ductile deformation to more localized, brittle faulting reflects a successively more shallow crustal setting for deformation in the footwall of the detachment system, and provides a genetic link between ductile and brittle structures. These structures and mylonitic fabrics are demonstrably Tertiary in age, based on the Late Cretaceous age of migmatization of the Mesquite Gneiss, and show a consistent top-to-the-northeast sense of shear. The Mesquite Mountain and Agency fault zones, which envelop deformed metasedimentary rocks within the gneissic basement, are interpreted as structures associated with incisement of the footwall to the detachment during the evolution of this regional extensional system. This process appears to have operated on the scale of large crustal blocks, because the mylonitic rocks of Mesquite Mountain clearly originated in the footwall, but now the entire mountain is situated in the hanging wall of a detachment splay, based on recent seismic data (Hauser et al., 1987). Tertiary extension is clearly superimposed on Mesozoic structures of the Maria fold and thrust belt of west-central Arizona, but reactivation of these thrust structures was not the main mechanism for accommodation of extension in the detachment terrain. Instead, new structures developed in response to extensional stress, and high strain was localized within less competent lithologies as they were entrained within these new structures.

ACKNOWLEDGEMENTS

Grateful appreciation is extended to the Tribal Council of the Colorado River Indian Tribes for permission to conduct field studies and collect samples on the Colorado River Indian Reservation. Thanks are also expressed to Chuck Lamb, Weldon Johnson, Curtiss Martin, and the staff of the Tribal Museum for friendship and logistical support during field work. Maureen Noonan, Scott Ritterbush, and Tom Knapp served admirably as field assistants for field work conducted from Fall 1986 to Fall 1987. Larry Busby, Les Bovee, and the staff of Buckskin Mountain State Park on the Colorado River afforded kind hospitality and a welcome retreat from the dry, dusty rigor of the desert. Numerous discussions with Jon Spencer, Steve Reynolds, Clark Burchfiel, Kip Hodges, Steve Richard, Paul Stone, Greg Davis, and many others greatly contributed to my understanding of the geology at Mesquite Mountain and in the Mojave-Sonoran Desert area at large. Scott Ritterbush is acknowledged for his penetrating study of shear sense in mylonitic rocks from Mesquite Mountain as an undergraduate research project. Stereonet analysis of structural data was greatly facilitated by the Stereonet computer program developed by Richard Allmendinger for the Macintosh. This research was supported primarily through the generosity of B.C. Burchfiel and his endowed Schlumberger Chair of Geology at M.I.T.

REFERENCES

Buising, A.V., 1986, The Bouse Formation and bracketing units, SE California and W Arizona: Investigations into the depositional and tectonic evolution of the proto-Gulf of California [abs.]: Geol. Soc. Amer. Abs. Progs., v. 18, no. 2, p. 90.

Buising, A.V., 1987, Mio-Pliocene depositional and tectonic evolution of the lower Colorado River area [abs.]: Geol. Soc. Amer. Abs. Progs., v. 19, no. 7, p. 605.

Buising, A.V., 1988, Contrasting subsidence histories, northern and southern proto-Gulf of California: Implications for proto-Gulf tectonic models [abs.]: Geol. Soc. Amer. Abs. Progs., v. 20, no. 3, p. 146-147.

Carr, W.J., and Dickey, D.D., 1980, Geologic map of the Vidal, California, and Parker SW, California-Arizona, quadrangles: U.S. Geol. Survey Misc. Invest. Map, I-1125, 1:24,000.

Davis, G.A., Anderson, J.L., Frost, E.G., and Shackelford, T.J., 1980, Mylonitization and detachment faulting in the Whipple-Buckskin-Rawhide Mountains terrane, southeastern California and western Arizona, *in* Crittenden, M.D., Jr., Coney, P.J., and Davis, G.H., eds., Cordilleran Metamorphic Core Complexes: Geol. Soc. Am. Mem. 153, p. 79-129.

Davis, G.A., and Lister, G.S., 1988, Detachment faulting in continental extension; Perspectives from the Southwestern U.S. Cordillera : Geol. Soc. Am. Special Paper 218, p. 133-159.

Davis, G.H., 1980, Structural characteristics of metamorphic core complexes, southern Arizona, *in* Crittenden, M.D., Jr., Coney, P.J., and Davis, G.H., eds., Cordilleran Metamorphic Core Complexes: Geol. Soc. Am. Mem. 153, p. 35-77.

Davis, G.H., 1983, Shear-zone model for the origin of metamorphic core complexes: Geology, v. 11, p. 342-347.

DeWitt, E., Sutter, J.F., Davis, G.A., and Anderson, J.L., 1986, $^{40}Ar/^{39}Ar$ age-spectrum dating of Miocene mylonitic rocks, Whipple Mountains, southeastern California [abs.]: Geol. Soc. Amer. Abs. Progs., v. 18, no. 6, p. 584.

Hamilton, W., 1982, Structural evolution of the Big Maria Mountains, northeastern Riverside County, southeastern California , *in* Frost, E.G., and Martin, D.L., eds., Mesozoic-Cenozoic Tectonic Evolution of the Colorado River Region, California, Arizona, and Nevada: San Diego, California, Cordilleran Publishers, p. 1-27.

Hauser, E.C., Gephart, J., Latham, T., Oliver, J., Kaufman, S., Brown, L., and Lucchitta, I., 1987, COCORP Arizona transect: Strong crustal reflections and offset moho beneath the transition zone: Geology, v. 15, p. 1103-1106.

Howard, K.A., and John, B.E., 1987, Crustal extension along a rooted system of imbricate low-angle faults; Colorado River extensional corridor, California and

Arizona, *in* Coward, M.P., Dewey, J.F., and Hancock, P.L., eds., Continental Extensional Tectonics: Geological Society of London Special Publication 28, p. 299-311.

Knapp, J. H., 1988, Ductile to brittle structural evolution at Mesquite Mountain, west-central Arizona [abs.]: Geol. Soc. Amer. Abs. Progs., v. 20, no. 3, p. 173.

Knapp, J.H., and Heizler, M.T., 1988a, $^{40}Ar/^{39}Ar$ geochronology of crystalline thrust nappes of the Late Cretaceous Maria fold and thrust belt, west-central Arizona [abs.]: Geol. Soc. Amer. Abs. Progs., v. 20, no. 3, p. 173.

Knapp, J.H., and Heizler, M.T., 1988b, Tertiary thermal history of west-central Arizona: Implications for mechanisms of crustal extension [abs.]: Geol. Soc. Amer. Abs. Progs., v. 20, no. 7, p. A16-A17.

Knapp, J.H., and Heizler, M.T., in prep., Thermal history of crystalline thrust nappes of the Maria fold and thrust belt, west-central Arziona.

Knapp, J.H., in prep., Mesozoic thrusting and Tertiary detachment faulting, Moon Mountains, west-central Arizona.

Knapp, J.H., and Walker, J.D., in prep., U-Pb geochronology of Mesozoic to Tertiary magmatism in west-central Arizona: Implications for tectonic evolution of the Maria fols and thrust belt.

Lister, G.S., and Snoke, A.W., 1984, S-C mylonites: Jour. Struc. Geol., v. 6, p. 617-638.

Marshak, S., and Vander Meulen, M., in press, Geology of the Battleship Peak area, southern Buckskin Mountains, Arizona: Structural style below the Buckskin Detachment fault, *in* Spencer, J.E., and Reynolds, S.J., eds., Geology of the Buckskin Mountains: Arizona Bureau of Geology and Mineral Technology Bull. 198.

Metzger, D.G., 1968, The Bouse Formation (Pliocene) of the Parker-Blythe-Cibola area, Arizona and California: U.S. Geol. Survey Prof. Paper 600-D, p. D126-D136.

Metzger, D.G., Loeltz, O.J., and Burdge, I., 1973, Geohydrology of the Parker-Blythe-Cibola area, Arizona and California: U.S. Geol. Survey Prof. Paper 486-G, 130 p.

Miller, F.K., 1970, Geologic map of the Quartzsite quadrangle, Yuma County, Arizona: U.S. Geol. Surv. Geol. Quad. Map GQ-841.

Miller, F.K., and McKee, E.H., 1971, Thrust and strike-slip faulting in the Plomosa Mountains, southwestern Arizona: Geol. Soc. Amer. Bull., v. 82, p. 717-722.

Orell, S.E., and Anderson, J.L., 1987, Proterozoic metamorphism in the Whipple Mountains, southeastern California: Geol. Soc. Amer. Abstr. Progs., v. 19, no. 6, p. 438.

Orell, S.E., 1988, *title?* M.S. thesis, Univ. Southern Calif., Los Angeles,

Podruski, J.A., 1979, Petrology of the upper plate crystalline complex of the eastern Whipple Mountains, southeastern California: M.S. thesis, Univ. Southern Calif., Los Angeles, 193 p.

Rehrig, W.A., and Reynolds, S.J., 1980, Geologic and geochronologic reconnaissance of a northwest-trending zone of metamorphic core complexes in southern and western Arizona, *in* Crittenden, M.D., Jr., Coney, P.J., and Davis, G.H., eds., Cordilleran Metamorphic Core Complexes: Geol. Soc. Am. Mem. 153, p. 131-157.

Reynolds, S.J., and Rehrig, W.A., 1980, Mid-Tertiary plutonism and mylonitization, South Mountains, central Arizona, *in* Crittenden, M.D., Jr., Coney, P.J., and Davis, G.H., eds., Cordilleran Metamorphic Core Complexes: Geol. Soc. Am. Mem. 153, p. 159-175.

Reynolds, S.J., 1982, Multiple deformation in the Harcuvar and Harquahala Mountains, west-central Arizona, *in* Frost, E.G., and Martin, D.L., eds., Mesozoic-Cenozoic Tectonic Evolution of the Colorado River Region, California, Arizona, and Nevada: San Diego, California, Cordilleran Publishers, p. 137-142.

Reynolds, S.J., and Spencer, J.E., 1985, Evidence for large-scale transport on the Bullard detachment fault, west-central Arizona: Geology, v. 13, p. 353-356.

Reynolds, S.J., Florence, F.P., Welty, J.W., Roddy, M.S., Currier, D.A., Anderson, A.V., and Keith, S.B., 1986, Compilation of Radiometric Age Determinations in Arizona: Ariz. Bur. Geol. Min. Tech. Bull. 197, p. 258.

Reynolds, S.J., Spencer, J.E., Richard, S.M., and Laubach, S.E., 1986, Mesozoic structures in west-central Arizona, *in* Beatty, B., and Wilkinson, P.A.K., eds., Frontiers In Geology and Ore Deposits of Arizona and the Southwest: Arizona Geological Society Digest, v. 16, p. 35-51.

Reynolds, S.J., Spencer, J.E., and DeWitt, E., 1987, Stratigraphy and U-Th-Pb geochronology of Triassic and Jurassic rocks in west-central Arizona, *in* Dickinson, W.R., and Klute, M.A., eds., Mesozoic Rocks of Southern Arizona and Adjacent Areas: Arizona Geological Society Digest, v. 18, p. 65-80.

Reynolds, S.J., Richard, S.M., Haxel, G.B., Tosdal, R.M., and Laubach, S.E., 1988, Geologic setting of Mesozoic and Cenozoic metamorphism in Arizona, *in* Ernst, W.G., ed., Metamorphism and Crustal Evolution of the Western United States (Rubey Volume VII): Englewood Cliffs, New Jersey, Prentice-Hall, p. 466-501.

Richard, S.M., 1982, Preliminary report on the structure and stratigraphy of the southern Little Harquahala Mountains, Yuma County, Arizona, *in* Frost, E.G., and Martin, D.L., eds., Mesozoic-Cenozoic Tectonic Evolution of the Colorado River Region, California, Arizona, and Nevada: San Diego, California, Cordilleran Publishers, p. 235-242.

Richard, S.M., 1983, Structure and stratigraphy of the southern Little Harquahala Mountains, Yuma County, Arizona: M.S. thesis, Univ. of Arizona, Tucson, 154 p.

Richard, S.M., 1988, Bedrock geology of the Harquahala Mountains, west-central Arizona: Mesozoic shear zones, cooling, and Tertiary unroofing: Ph.D. dissertation, Univ. of California, Santa Barbara, 230 p.

Richard, S.M., Reynolds, S.J., and Spencer, J.E., 1987, Mesozoic stratigraphy of the Little Harquahala and Harquahala Mountains, west-central Arizona, *in* Dickinson, W.R., and Klute, M.A., eds., Mesozoic Rocks of Southern Arizona and Adjacent Areas: Arizona Geological Society Digest, v. 18, p. 101-119.

Ross, C.P., 1923, The lower Gila region, Arizona: U.S. Geol. Surv. Water Supply Paper 498, 237 p.

Scarborough, R., and Meader, N., 1983, Reconnaissance geology of the northern Plomosa Mountains: Arizona Bureau of Geology and Mineral Technology Open-File Report 83-24, 35 p.

Schmid, S.M., 1982, Microfabric studies as indicators of deformation mechanisms and flow laws operative in mountain building, *in* Hsü, K.J., ed., Mountain Building Processes: Academic Press, London, p. 95-110.

Shackelford, T.J., 1980, Tertiary tectonic denudation of a Mesozoic-early Tertiary (?) gneiss complex, Rawhide Mountains, western Arizona: Geology, v. 8, p. 190-194.

Spencer, J.E., 1982, Origin of folds of Tertiary low-angle fault surfaces, southeastern California and western Arizona, *in* Frost, E.G., and Martin, D.L., eds., Mesozoic-Cenozoic Tectonic Evolution of the Colorado River Region, California, Arizona, and Nevada: San Diego, California, Cordilleran Publishers, p. 123-134.

Spencer, J.E., 1984, Role of tectonic denudation in warping and uplift of low-angle normal faults: Geology, v. 12, p. 95-98.

Spencer, J.E., 1985, Miocene low-angle normal faulting and dike emplacement at Homer Mountain and surrounding areas, southeastern California and southernmost Nevada: Geol. Soc. Amer. Bull., v. 96, p. 1140-1155.

Spencer, J.E., and Reynolds, S.J., in press, Tertiary structure, stratigraphy, and tectonics of the Buckskin Mountains, *in* Spencer, J.E., and Reynolds, S.J., Geology of the Buckskin Mountains: Arizona Bureau of Geology and Mineral Technology Bull. 198.

Thomas, W.M., Clark, H.S., Young, E.D., Orell, S.E., and Anderson, J.L., 1988, Proterozoic high-grade metamorphism in the Colorado River region, Nevada, Arizona and California, *in* Ernst, W.G., ed., Metamorphism and Crustal Evolution of the Western United States (Rubey Volume VII): Englewood Cliffs, New Jersey, Prentice-Hall, p. 526-537.

Turner, F.J., and Weiss, L.E., 1963, Structural analysis of metamorphic tectonites: New York, McGraw-Hill, 545 p.

Walker, J.D., Hodges, K.V., and Wernicke, B.P., 1986, The relation of tilt geometry to extension direction: Geol. Soc. Amer. Abs. Progs., v. 18, no. 2, p. 194-195.

Wernicke, B.P., and Axen, G.J., 1988, On the role of isostasy in the evolution of normal fault systems: Geology, v. 16, p. 848-851.

Wilson, E.D., Moore, R.T., and Cooper, J.R., 1969, Geologic map of Arizona: Arizona Bureau of Mines and U.S. Geol. Survey, scale 1:500,000.

Wilson, E.D., 1960, Geologic map of Yuma County, Arizona: Arizona Bureau of Mines, scale 1:375,000.

Yeats, K.J., 1985, Geology and structure of the northern Dome Rock Mountains, La Paz County, Arizona: M.S. thesis, Univ. of Arizona, Tucson, 123 p.

FIGURE CAPTIONS

Plate 1-1: Geologic map of Mesquite Mountain, Colorado River Indian Reservation, original scale 1:24,000 (xerox reduced version).

Plate 1-2: Geologic cross sections of Mesquite Mountain, scale 1:24,000, no vertical exaggeration.

Figure 1.1: Location map of Mesquite Mountain in the Mojave-Sonoran Desert area of southeastern California and western Arizona. Other mountain ranges referred to in text are indicated on map. Area of Figure 1.2 indicated by box with heavy line.

Figure 1.2: Structural domains at Mesquite Mountain, and informal names of geographic features.

Figure 1.3: Migmatitic fabric of Mesquite Gneiss, showing no evidence for overprinting of mylonitic fabric. Located in Cat-claw Canyon, but representative of Mesquite Gneiss where unaffected by later deformation.

Figure 1.4: Nature of contorted compositional layering and complex, disharmonic fold patterns within Mesquite Gneiss. Range of scales at which felsic segregation has occurred is evident. Lens cap for scale.

Figure 1.5: Equal-area stereonet and contour plot of poles to gneissic foliation (S_1) in Mesquite Gneiss, n=77. Contour interval is 3%/1% area. Mean vector has a length of 0.641, with an orientation N84E 59. Mean length is too low to calculate concentration factor by the approximate method.

Figure 1.6: Summary equal-area stereonet and contour plot of poles to mylonitic foliation (S_2, S_3, and S_4) at Mesquite Mountain, n=116. Contour interval is 3%/1% area. Mean vector has a length of 0.838, with an orientation N56E 50. Concentration factor is 6.8, and 2σ confidence cone is 5 degrees.

Figure 1.7: Summary equal-area stereonet and contour plot of mylonitic lineation (L_2, L_3, and L_4) at Mesquite Mountain, n=116. Contour interval is 3%/1% area. Mean vector has a length of 0.814, with an orientation of S18W 42. Concentration factor is 5.4, and 2σ confidence cone is 6 degrees.

Figure 1.8: Summary equal-area stereonet plot of poles to gneissic (S_1) and mylonitic foliation (S_2, S_3, and S_4), showing the general coincidence on orientation of these two fabric types (n=193). Open boxes represent gneissic foliation (S_1) and solid circles represent mylonitic foliation (S_2, S_3, and S_4).

Figure 1.9: Stereonet plot of attitudes of ductile high-angle faults in hanging wall of Agency fault zone along eastern side of Mesquite Mountain. Faults strike N50-65E, and dip 40-60SE.

Figure 1.10: Evidence for syntectonic migmatization of Mesquite Gneiss. Thin granitic band across center of photo is folded with compositional layering at right of photo, but truncates similar, contiguous layering in center of photo.

Figure 1.11: Typical exposure of Mesquite Mountain fault zone, consisting of 3-7 m band of metasedimentary rock (undulatory, resistant ledge across center of photo) enveloped within crystalline rocks of Mesquite Gneiss. Fault zone is bounded both above and below by discontinuous envelope of concordant mylonitic gneiss. Note discordance of MMFZ with both locally-developed, earlier mylonitic fabric (left of center) and with compositional layering within the Mesquite Gneiss. Width of view is about 150 m. Area of Figure 1 is just to left of center.

Figure 1.12: Close-up view of Mesquite Mountain fault zone, showing truncation of earlier mylonitic fabric developed in Mesquite Gneiss (right), by 0.5-1 m thick mylonite (dark band) developed parallel to fault zone boundary. Transposed compositional layering in banded calc-silicate unit (upper left) within fault zone is also parallel to fault zone boundaries.

Figure 1.13: Mesquite Mountain fault zone (MMFZ) as exposed along central portion of western flank of Mesquite Mountain. MMFZ is about 15 m thick and cuts diagonally across photo from upper left to lower right. Hinge of mesoscale isoclinal fold (right of center) of mylonitic Mesquite Gneiss is floating in orange, micaceous marble within fault zone.

Figure 1.14: Idealized geometry of Agency fault zone, showing elongate, domal morphology of the fault surface below Agency Peak, east side of Mesquite Mountain.

Figure 1.15: Ductile high-angle faults and associated drag fold structures within Mesquite Gneiss, hanging wall to Agency fault zone, east flank of Mesquite Mountain. Sense of shear on folds in both hanging wall and footwall imply normal sense of displacement. Mylonitic lineation in the fault zone trends S10-15W 25, and fold axes are oriented S15-20W 10-25, implying an oblique-normal sense of displacement.

Figure 1.16: Klippe of intensely mylonitized gneiss (dark cap at top of hill), bounded by gently NW-dipping fault. Footwall to fault consists of relatively unmylonitized Mesquite Gneiss (upper right of center; note compositional layering) and biotite-bearing granite (base of hill). View is toward west-northwest across Migmatite Wash at southern end of Mesquite Mountain; relief exposed is ~100 m.

Figure 1.17: Close up of Mesquite Wash Hills fault, oriented N26E 82SE, showing brecciation and cavernous weathering of basement gneisses near fault. Note thin (10-15 cm) microbreccia veneer (just above center) developed on fault surface. Orientation of fault gives apparent reverse sense of offset. Bush at top of photo is ~1 m high.

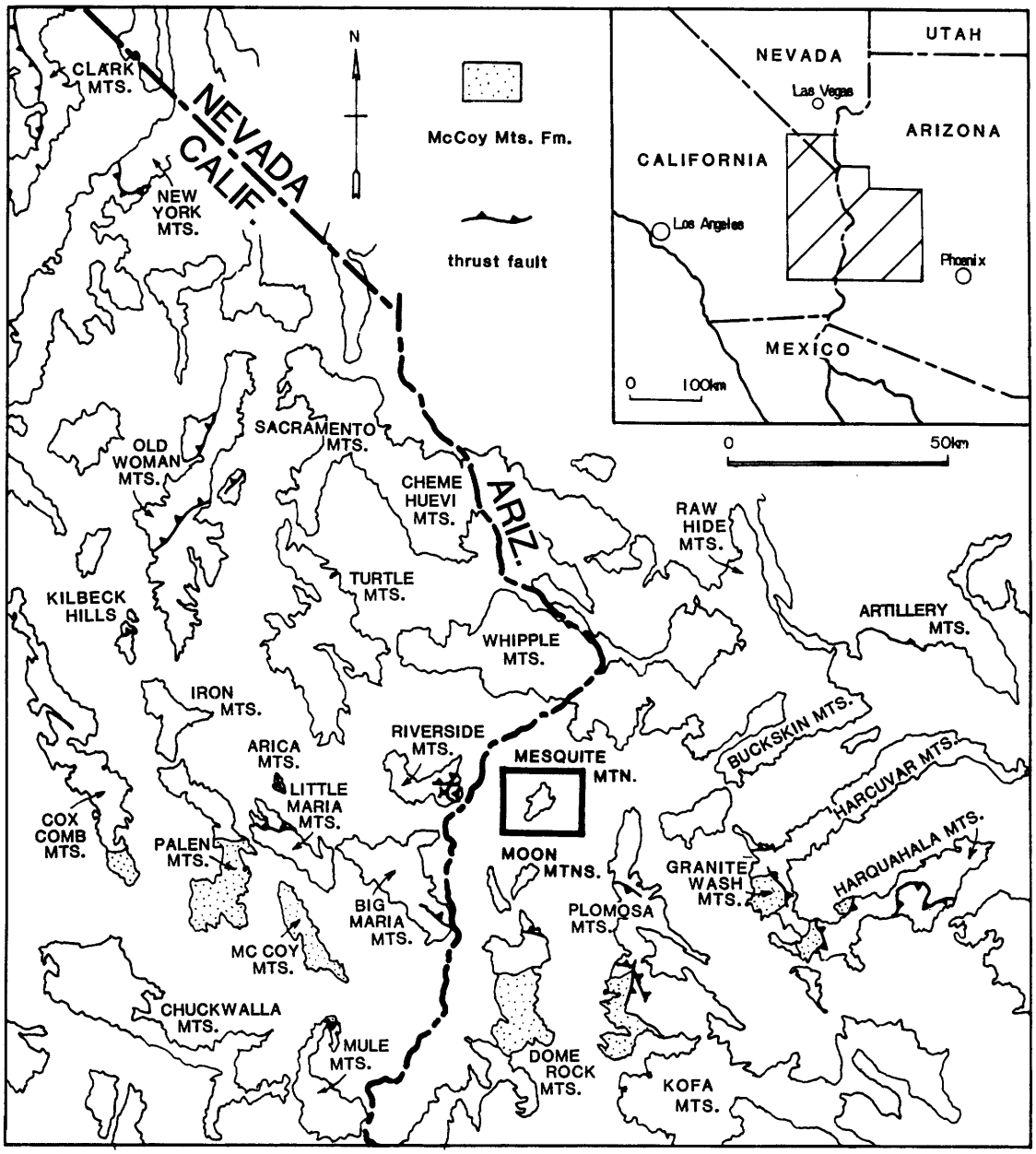
N
McCoy Mts. Fm.
thrust fault
NEVADA
CALIF.
ARIZ.
CLARK MTS.
NEW YORK MTS.
OLD WOMAN MTS.
SACRAMENTO MTS.
CHEME HUEVI MTS.
TURTLE MTS.
KILBECK HILLS
WHIPPLE MTS.
IRON MTS.
ARICA MTS.
LITTLE MARIA MTS.
RIVERSIDE MTS.
MESQUITE MTN.
COX COMB MTS.
PALEN MTS.
MOON MTNS.
BIG MARIA MTS.
MC COY MTS.
CHUCKWALLA MTS.
MULE MTS.
DOME ROCK MTS.
KOFA MTS.
PLOMOSA MTS.
GRANITE WASH MTS.
RAW HIDE MTS.
ARTILLERY MTS.
BUCKSKIN MTS.
HARCUVAR MTS.
HARQUAHALA MTS.
UTAH
NEVADA
Las Vegas
ARIZONA
CALIFORNIA
Los Angeles
Phoenix
MEXICO
0 100km
0 50km

Figure 1.1

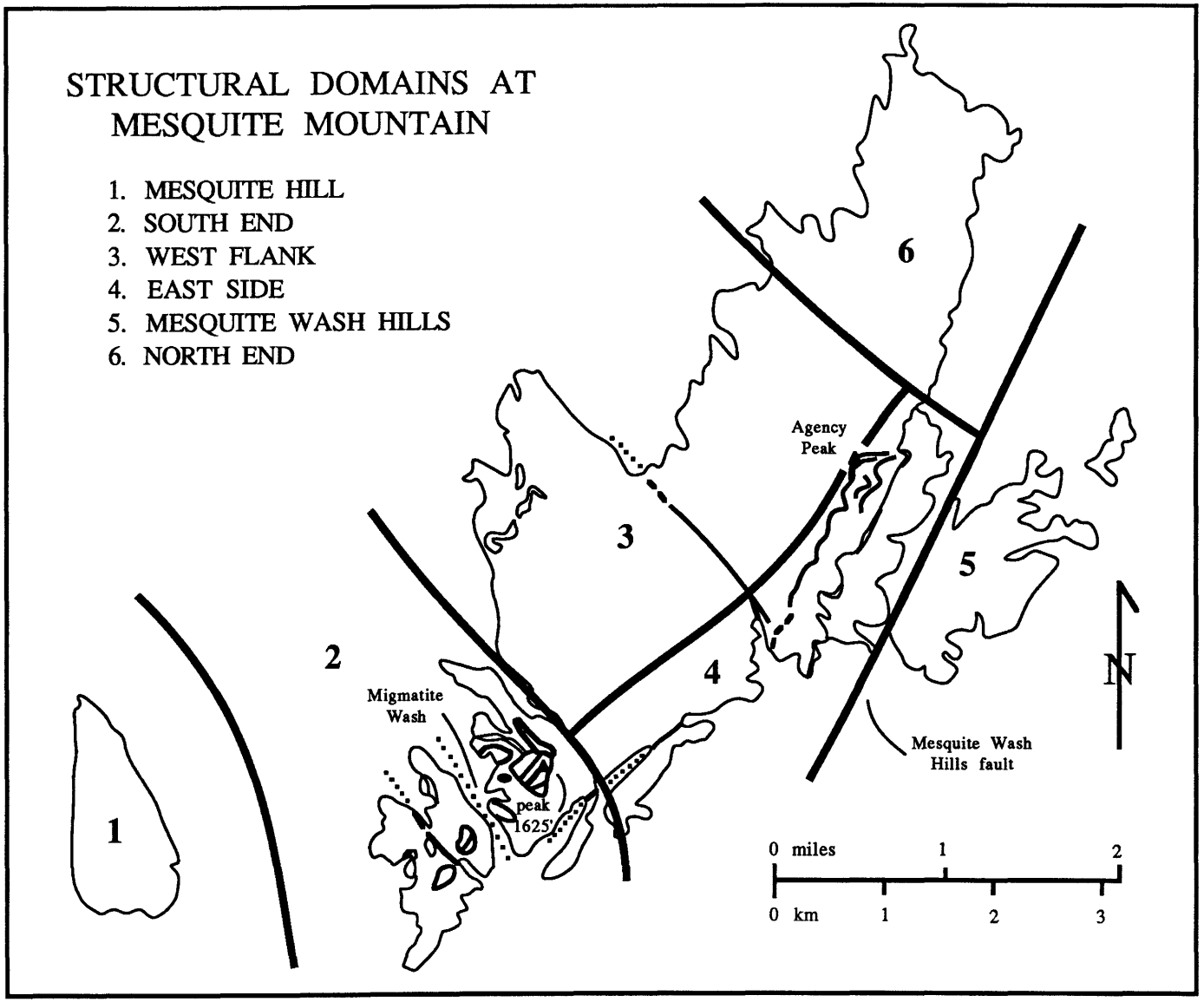
STRUCTURAL DOMAINS AT
MESQUITE MOUNTAIN
1. MESQUITE HILL
2. SOUTH END
3. WEST FLANK
4. EAST SIDE
5. MESQUITE WASH HILLS
6. NORTH END
1
2
3
4
5
6
Agency Peak
Migmatite Wash
peak 1625'
Mesquite Wash Hills fault
N
0 miles 1 2
0 km 1 2 3

Figure 1.2

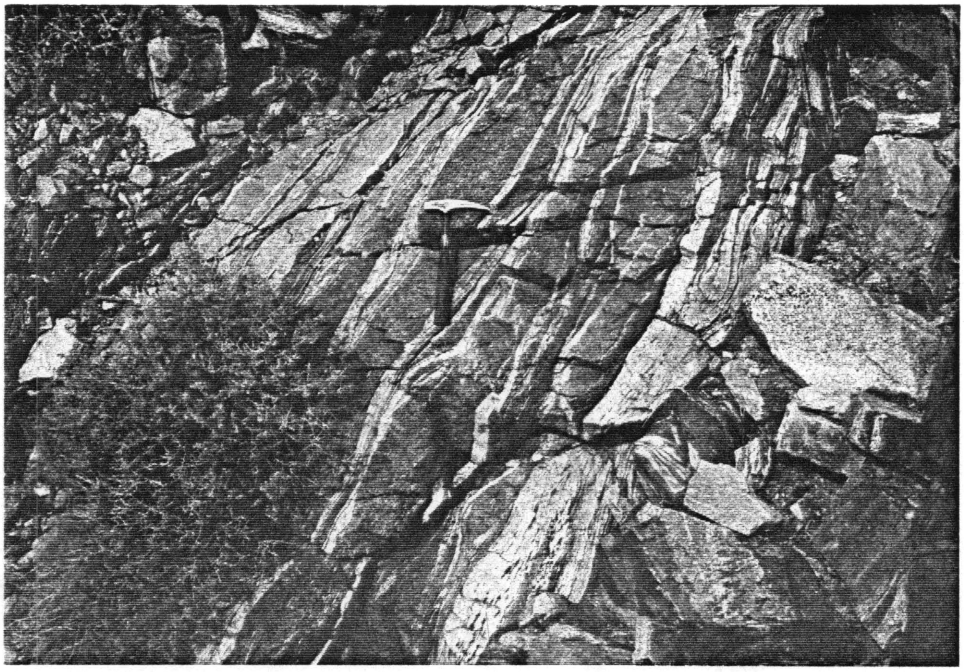

Figure 1.3

Figure 1.4

POLES TO GNEISSIC FOLIATION
IN MESQUITE GNEISS

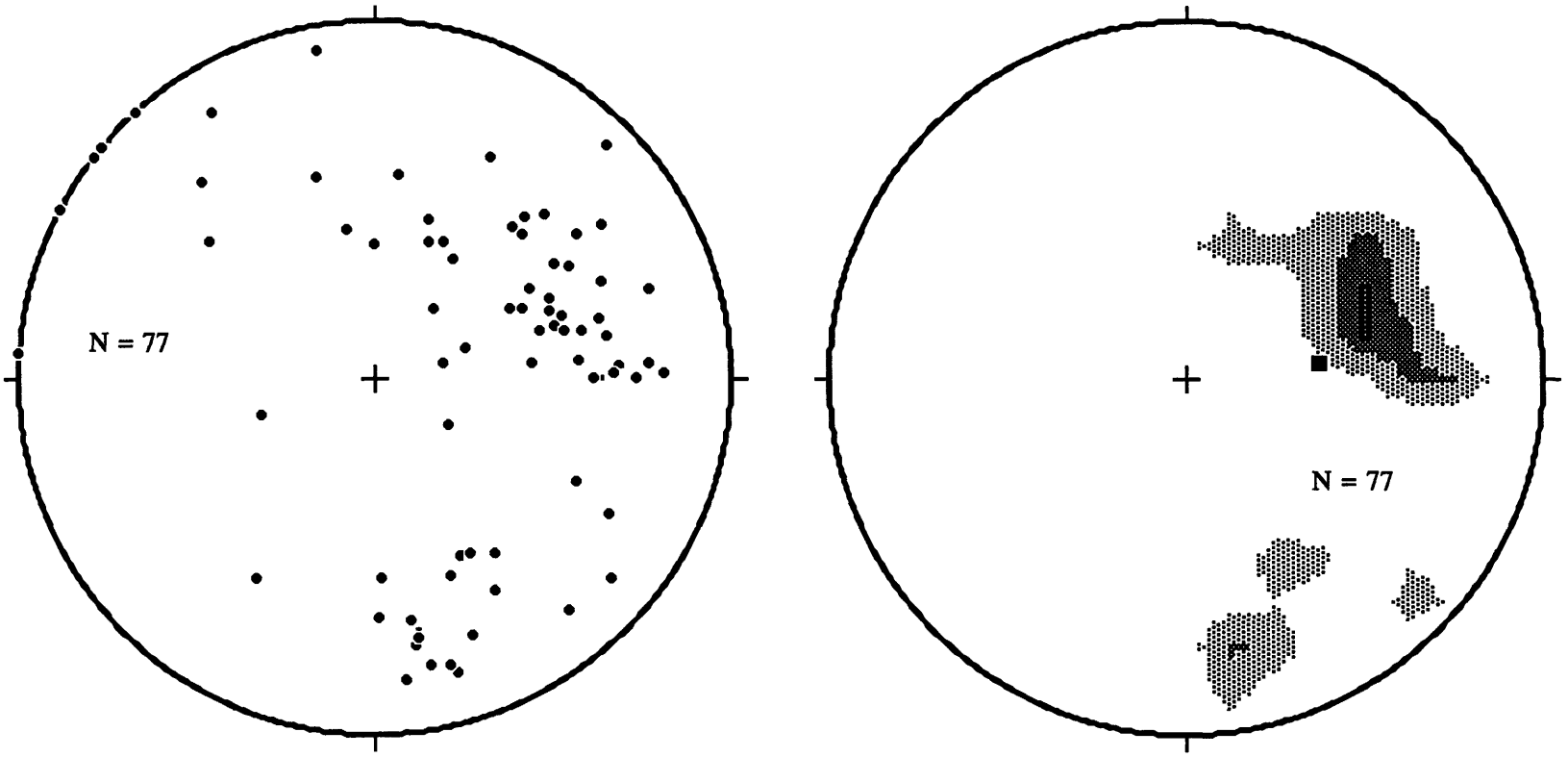

CONTOUR INTERVAL: 3% / 1% AREA

MEAN VECTOR: N84E 59 , 0.641

Figure 1.5

POLES TO MYLONITIC FOLIATION
IN MESQUITE GNEISS

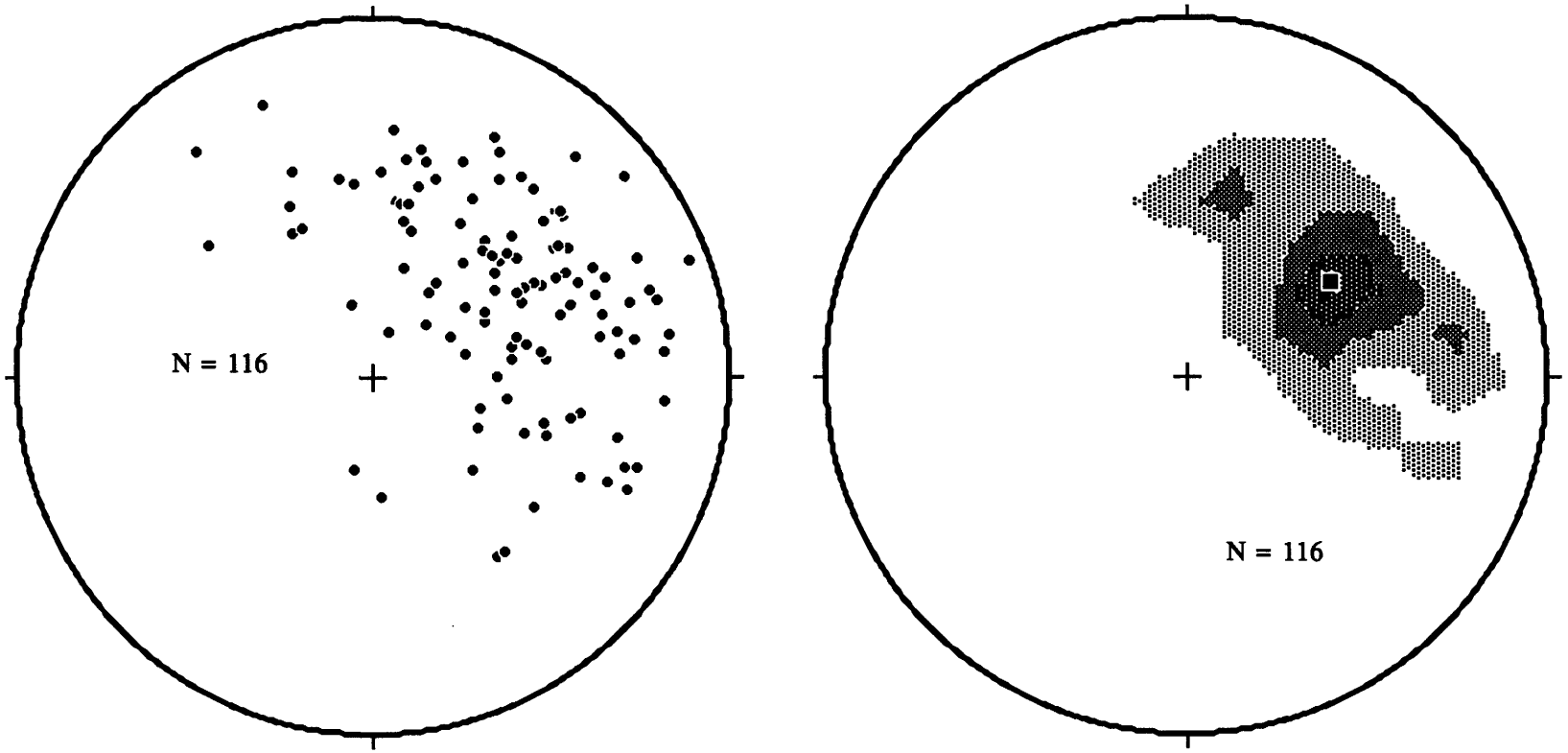

CONTOUR INTERVAL: 3% / 1% AREA

MEAN VECTOR: N56E 50, 0.838

Figure 1.6

MYLONITIC LINEATION IN
MESQUITE GNEISS

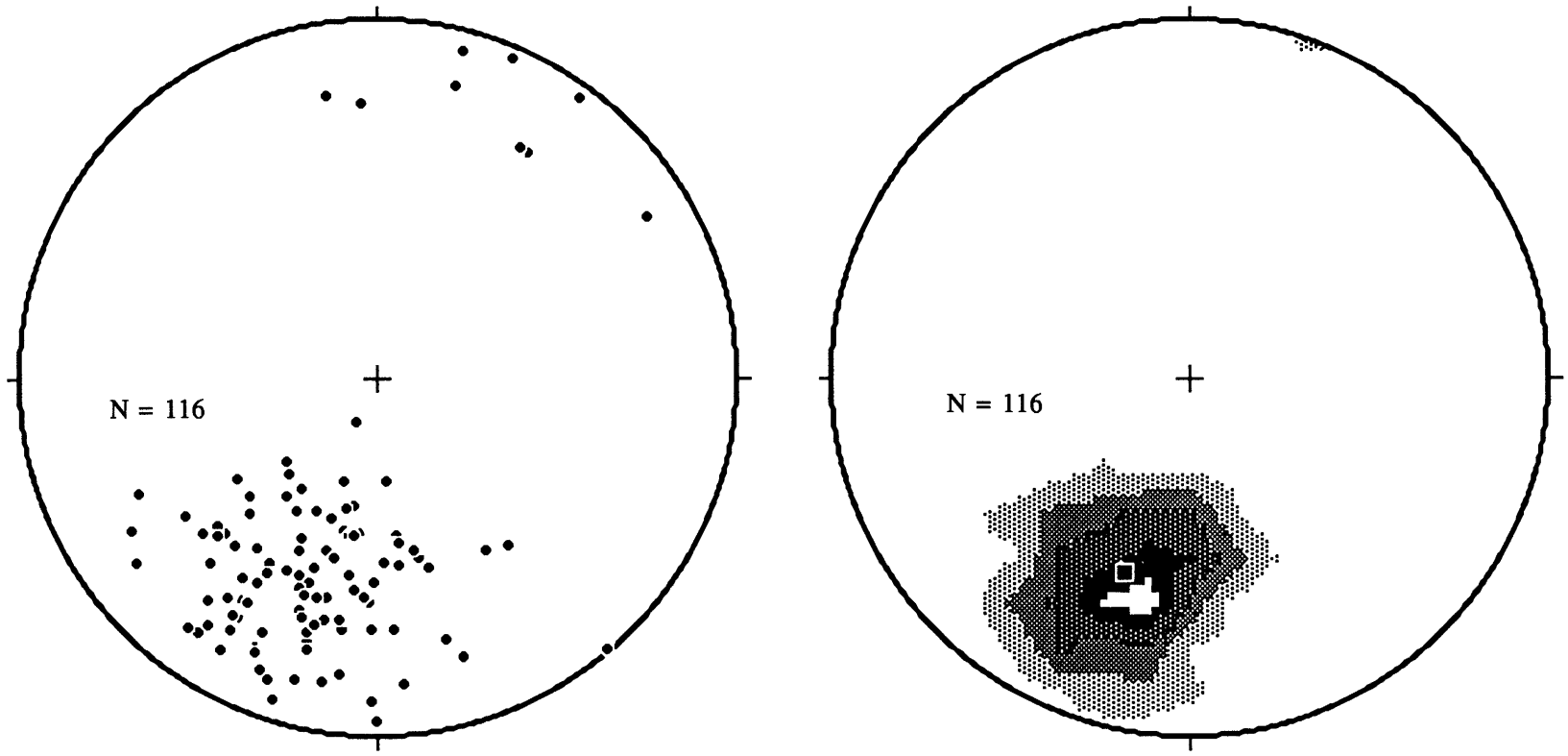

CONTOUR INTERVAL: 3% / 1% AREA

MEAN VECTOR: S18W 42, 0.814

Figure 1.7

SUMMARY OF POLES TO FOLIATION
IN MESQUITE GNEISS

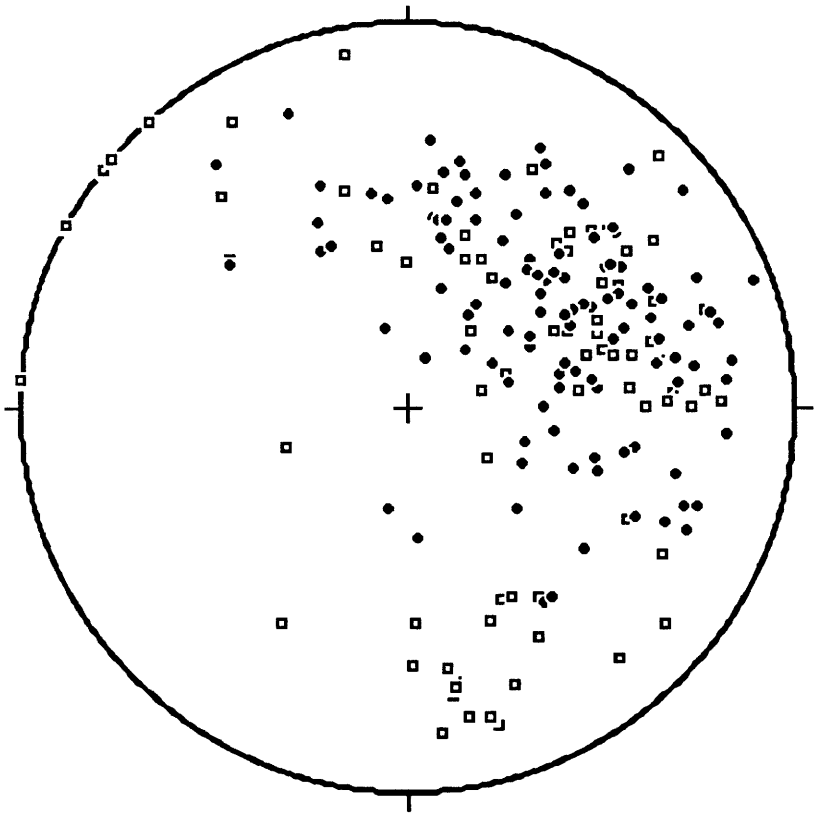

▫ GNEISSIC FOLIATION (n=77)

• MYLONITIC FOLIATION (n=116)

Figure 1.8

DUCTILE HIGH-ANGLE FAULTS,
EAST SIDE OF MESQUITE MTN.

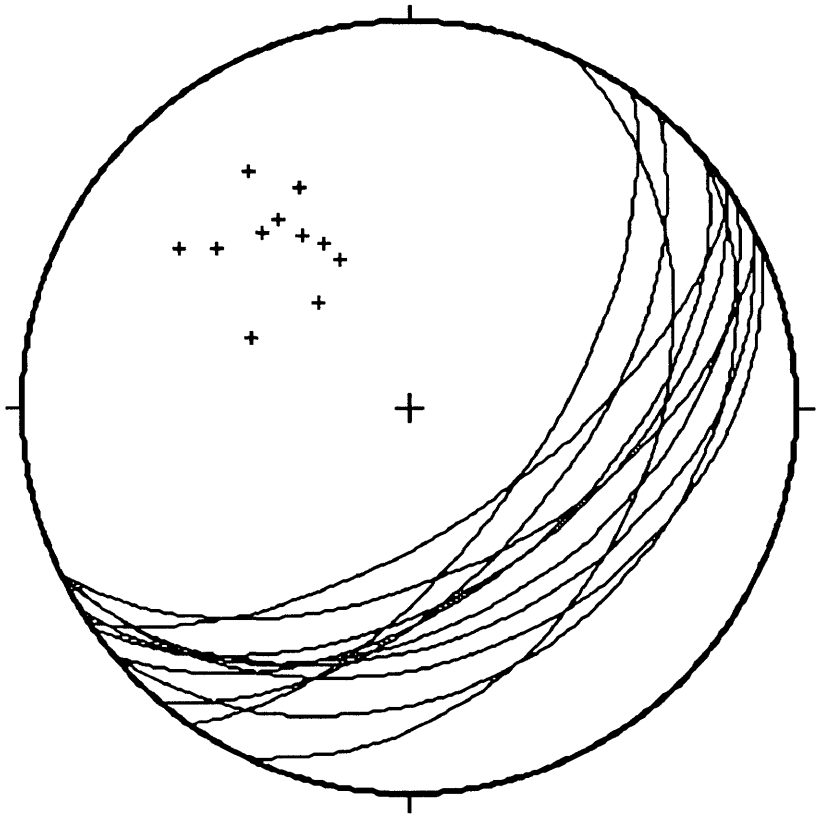

Figure 1.9

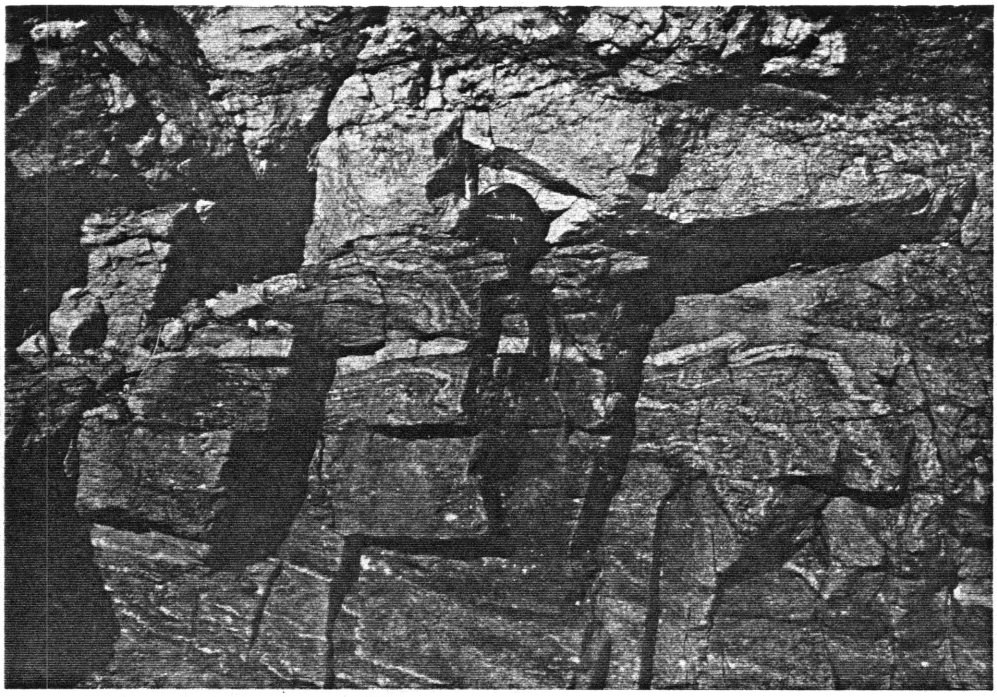

Figure 1.10

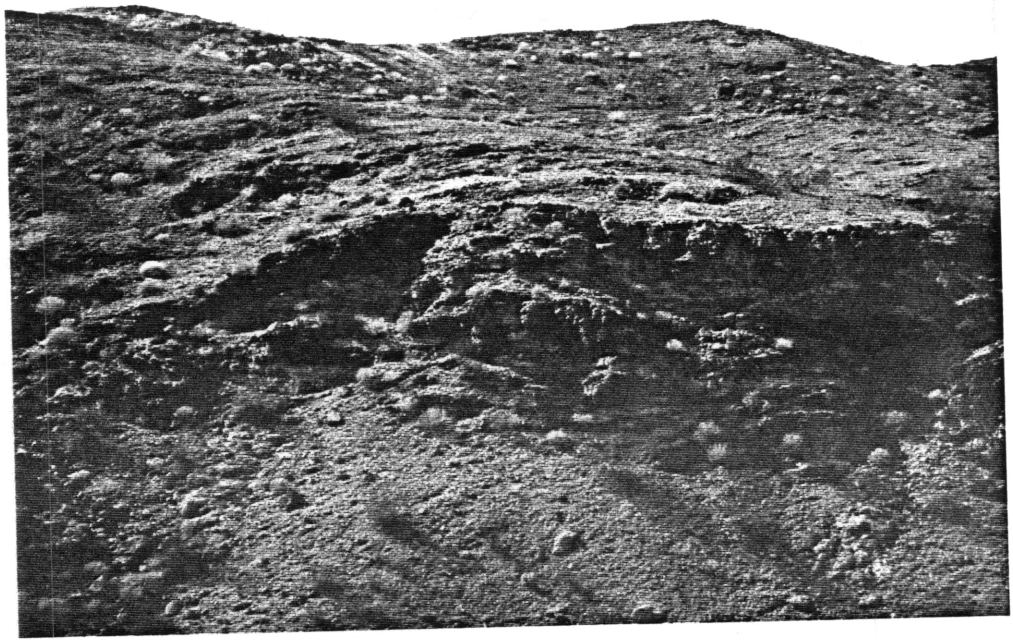

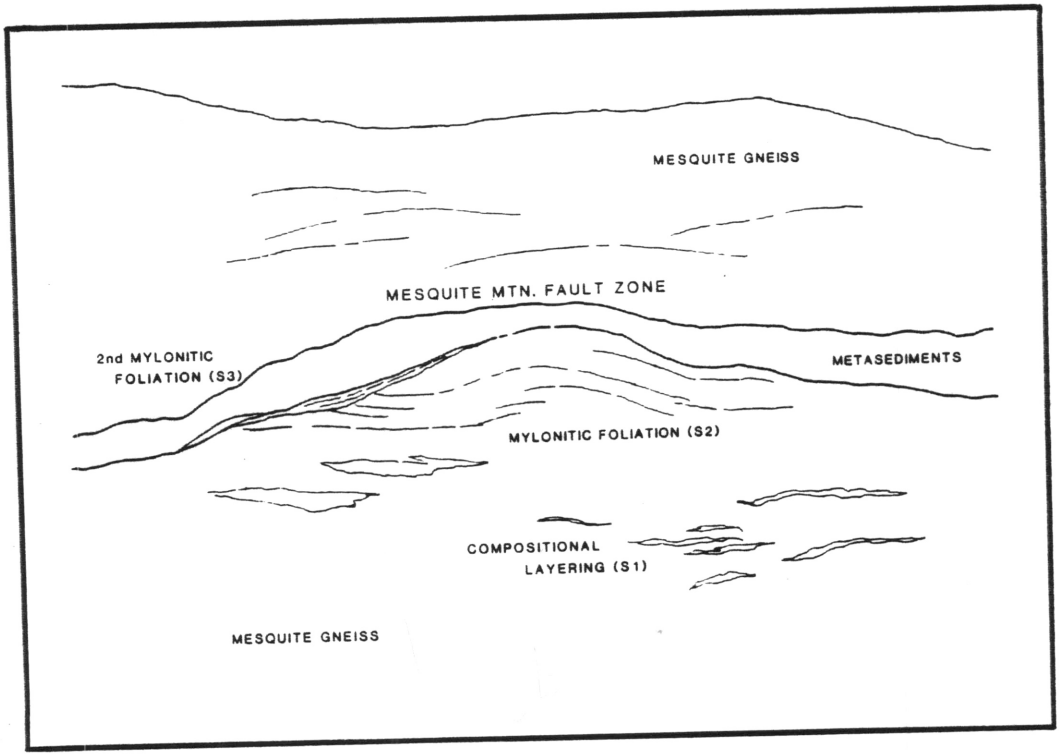
MESQUITE GNEISS
MESQUITE MTN. FAULT ZONE
2nd MYLONITIC FOLIATION (S3)
METASEDIMENTS
MYLONITIC FOLIATION (S2)
COMPOSITIONAL LAYERING (S1)
MESQUITE GNEISS

Figure 1.11

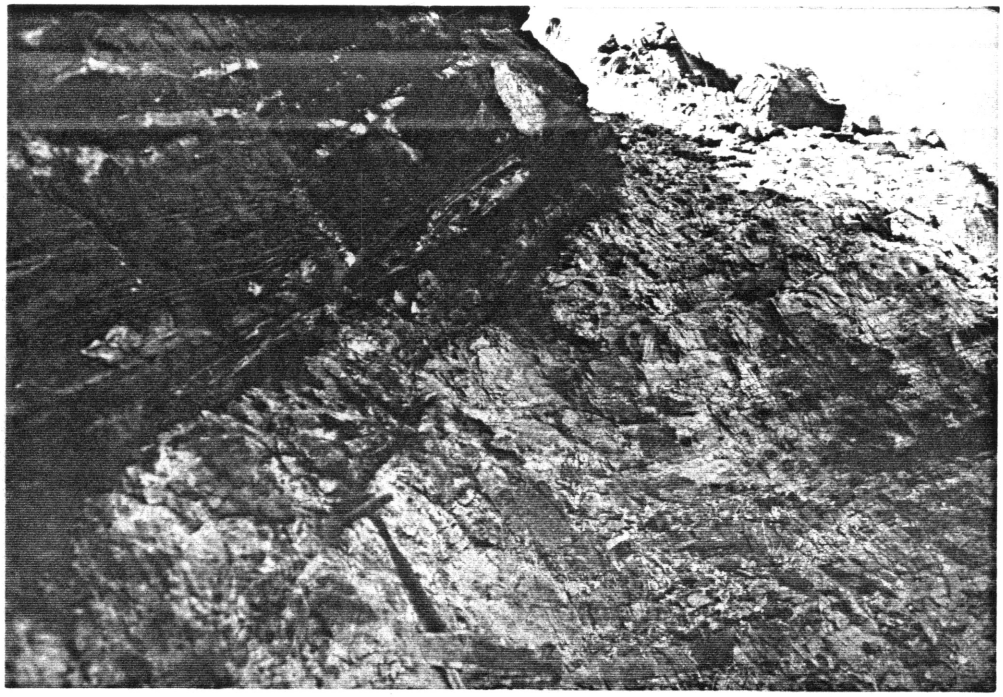

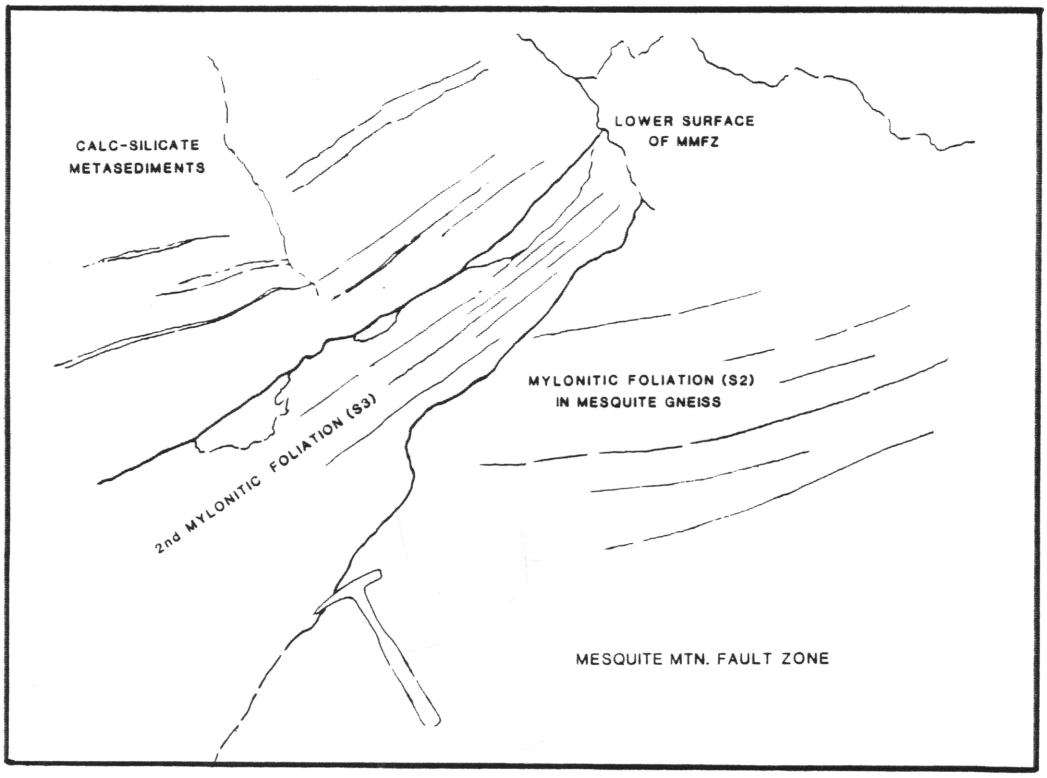
CALC-SILICATE
METASEDIMENTS
LOWER SURFACE
OF MMFZ
MYLONITIC FOLIATION (S2)
IN MESQUITE GNEISS
2nd MYLONITIC FOLIATION (S3)
MESQUITE MTN. FAULT ZONE

Figure 1.12

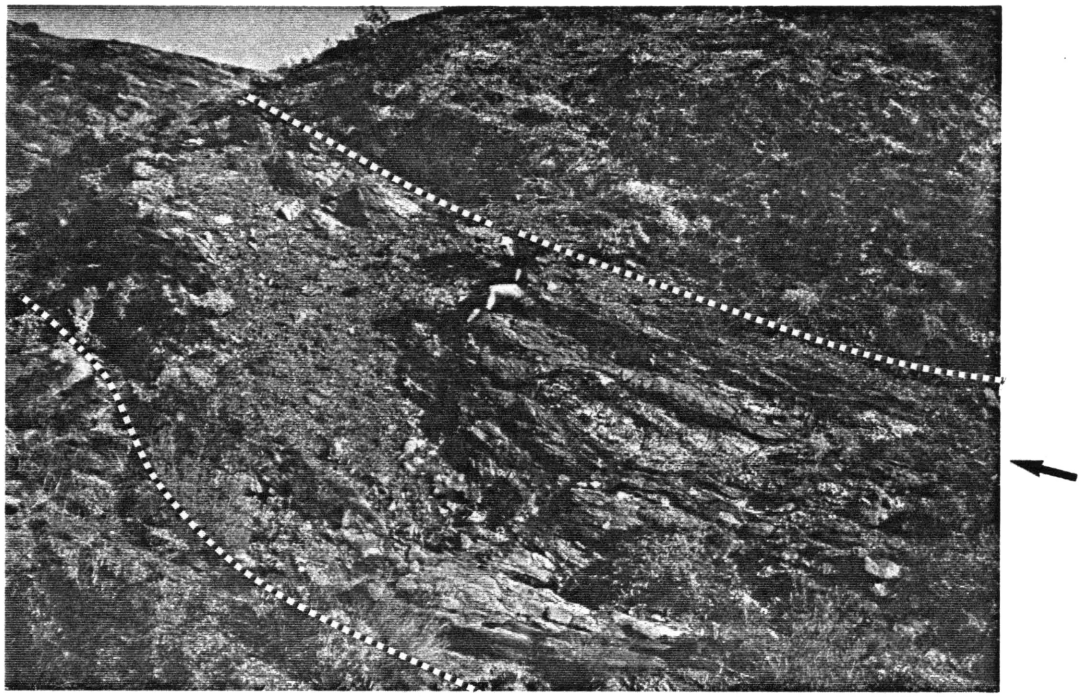

Figure 1.13

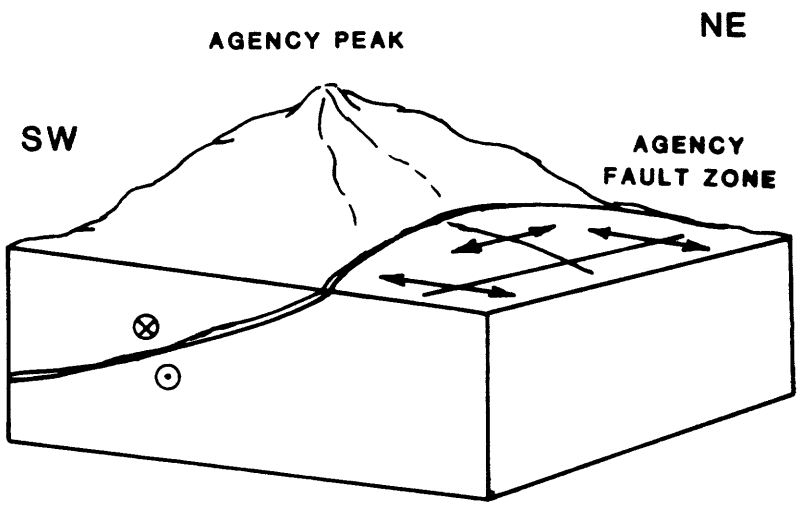

Figure 1.14

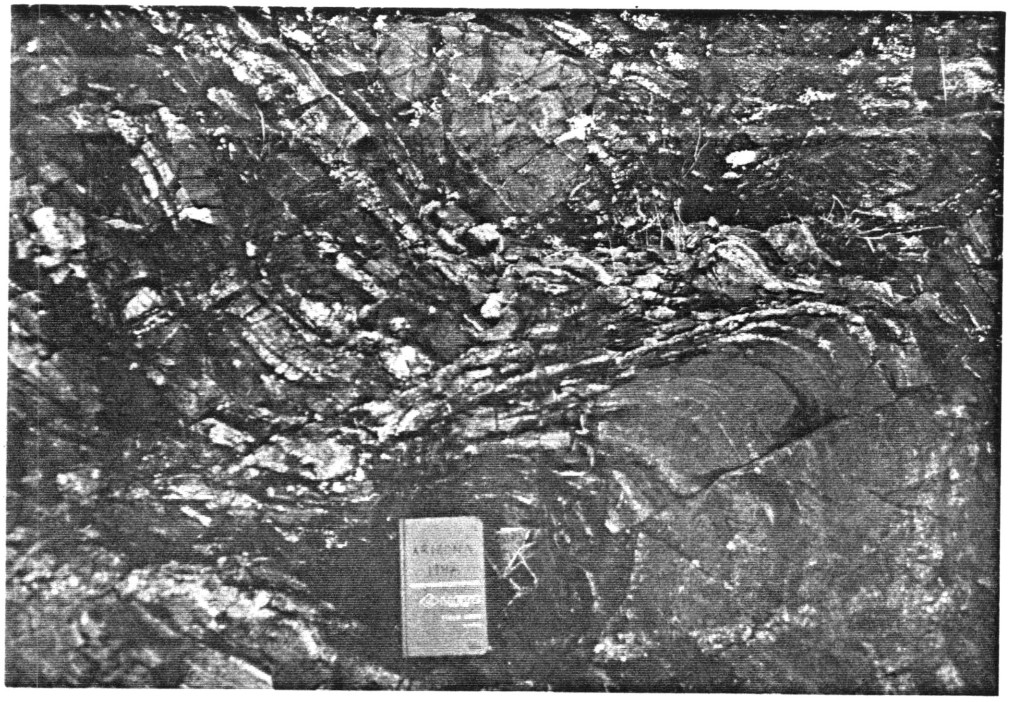

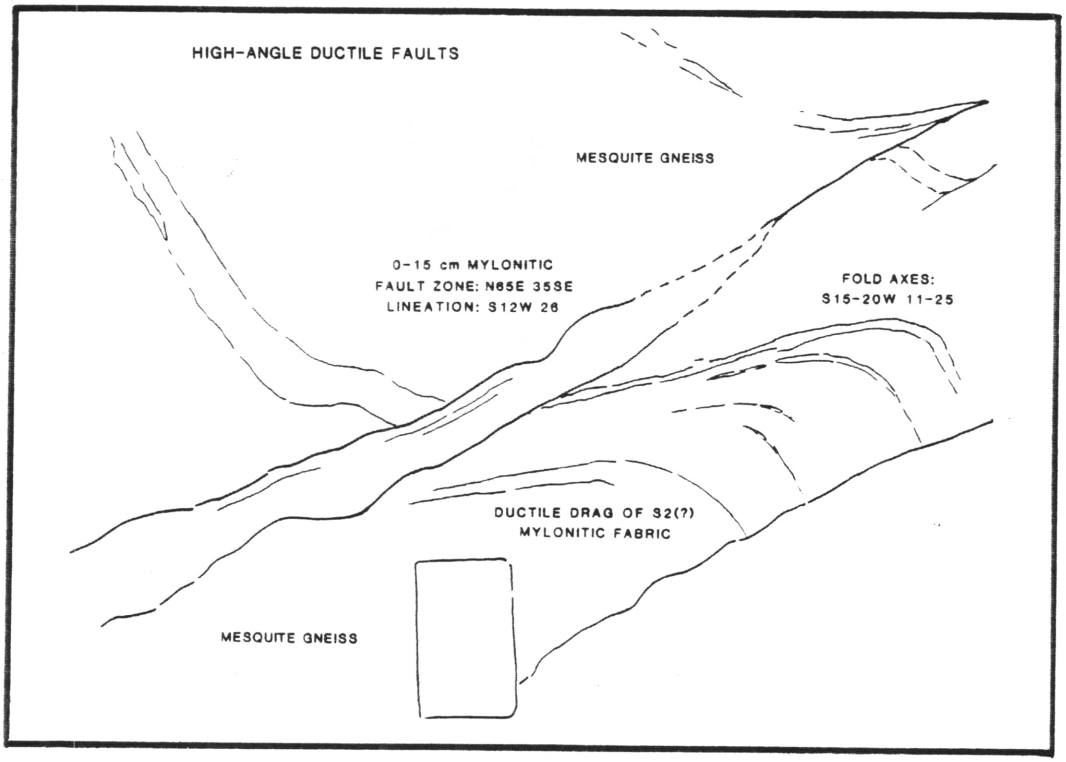
HIGH-ANGLE DUCTILE FAULTS
MESQUITE GNEISS
0-15 cm MYLONITIC
FAULT ZONE: N65E 35SE
LINEATION: S12W 26
FOLD AXES:
S15-20W 11-25
DUCTILE DRAG OF S2(?)
MYLONITIC FABRIC
MESQUITE GNEISS

Figure 1.15

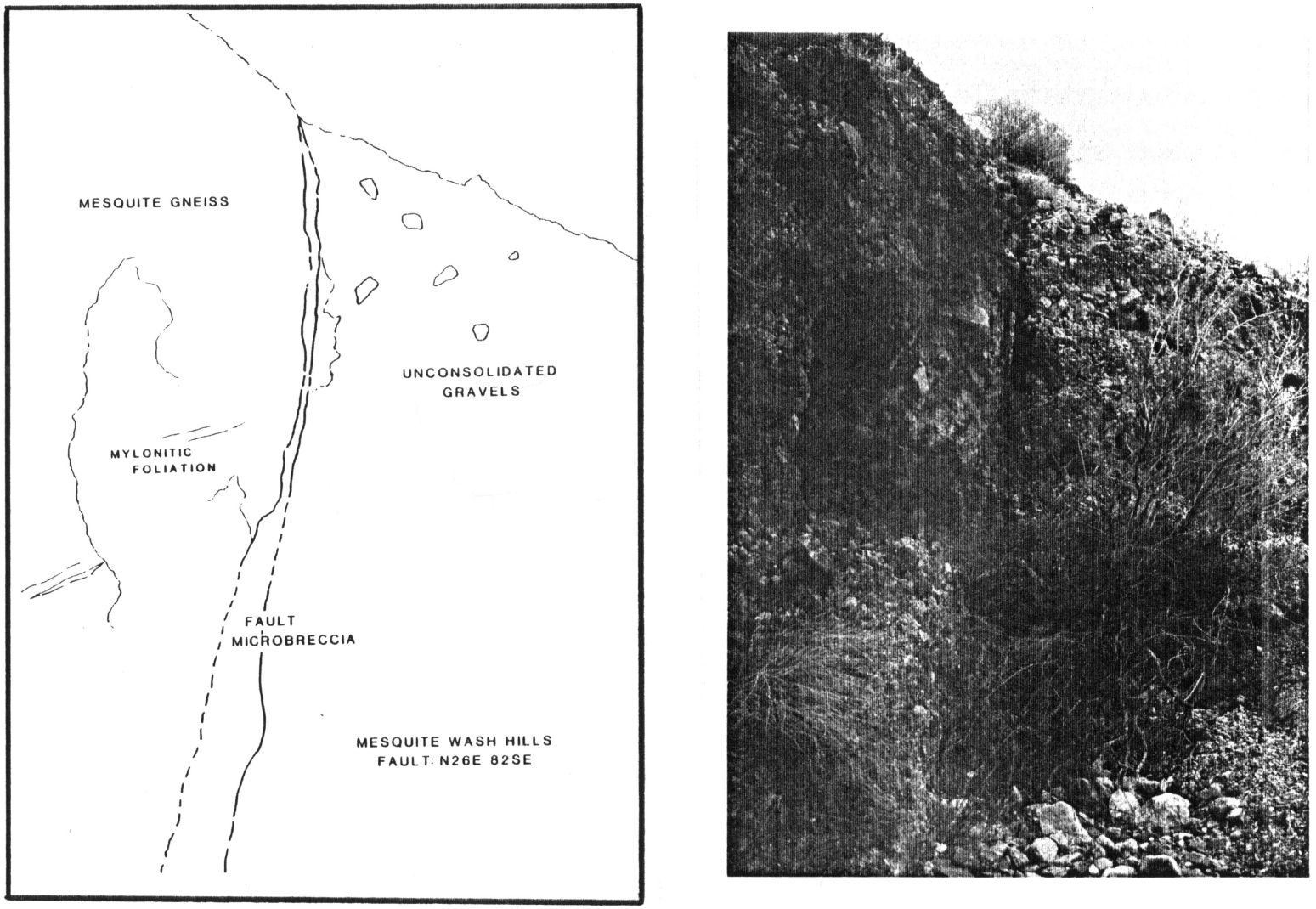
MESQUITE GNEISS
UNCONSOLIDATED
GRAVELS
MYLONITIC
FOLIATION
FAULT
MICROBRECCIA
MESQUITE WASH HILLS
FAULT: N26E 82SE

Figure 1.17

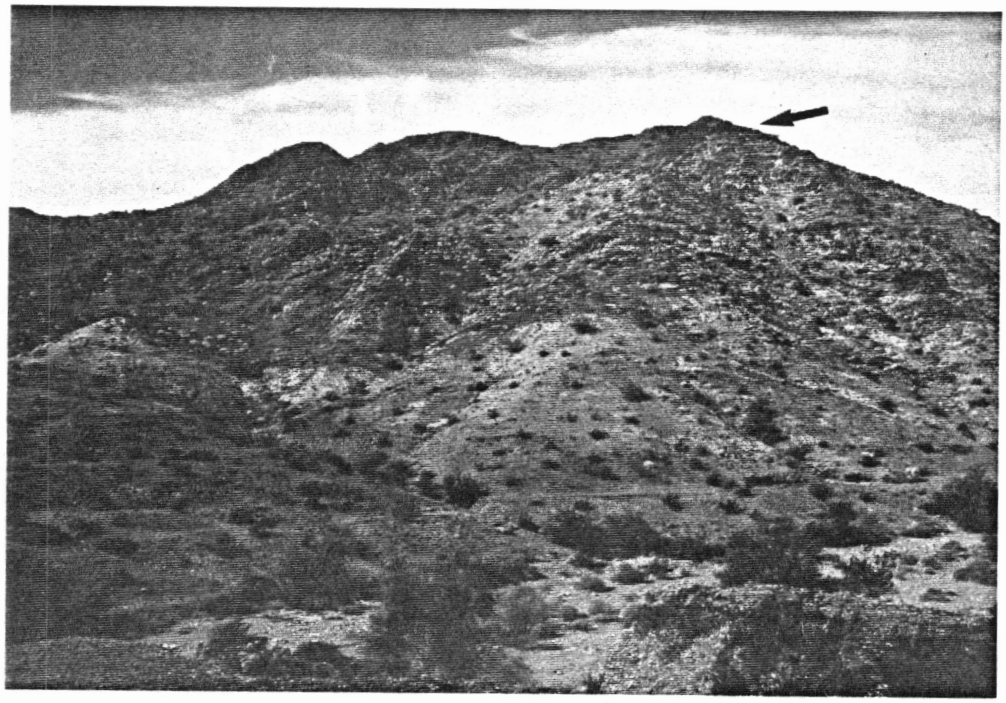

Figure 1.16

CHAPTER 2

MESOZOIC THRUSTING AND TERTIARY DETACHMENT FAULTING IN THE MOON MOUNTAINS, WEST-CENTRAL ARIZONA

James H. Knapp

ABSTRACT

The rocks and structures exposed in the Moon Mountains of the Colorado River Indian Reservation, west-central Arizona, record Mesozoic thrusting within the Maria fold and thrust belt, and superimposed Tertiary detachment faulting related to the regional Whipple-Buckskin-Rawhide detachment system. The major structures of the Moon Mountains are (1) the Valenzuela thrust fault, (2) the Moon Mountain detachment fault, and (3) the Copper Peak detachment fault. Lithologies consist primarily of Mesozoic and Tertiary intrusive rocks and crystalline gneisses of Precambrian age, with minor but important exposures of deformed and metamorphosed sedimentary and volcanic rocks. A newly-described section of metamorphosed, lower Mesozoic sedimentary rocks, the Valenzuela metasedimentary section, is assigned to the Buckskin Formation (Reynolds et al., 1987) of western Arizona.

The Valenzuela thrust fault, exposed in the southern Moon Mountains, carries an assemblage of megacrystic, Jurassic quartz syenite and Precambrian gneisses and schists over the deformed Valenzuela metasedimentary sequence. Footwall structure suggests initial tectonic transport of the hanging wall to the south, whereas later fabrics in both the hanging wall and footwall indicate northward transport, suggesting a multi-stage

kinematic history for this Mesozoic structure. Fabrics associated with the thrust fault indicate that amphibolite facies metamorphism accompanied deformation. The Valenzuela thrust system is correlated with the Tyson thrust system of the northern Dome Rock Mountains, implying a regional extent for this structure.

The Moon Mountain detachment fault, exposed along the eastern side of Moon Mountain, places a section of faulted and tilted Tertiary sedimentary rocks above gneisses, schists, and amphibolites of the Moon Mountains crystalline assemblage. At least two fabrics are present in the footwall gneisses. Gneissic compositional layering is concordant with the detachment fault, but primarily represents a Mesozoic feature. Ductile shear fabrics of Tertiary age are variably developed in gneisses and granites of the footwall, and indicate a consistent top-to-the-east shear sense associated with the detachment system. Strata in the hanging wall of the detachment show tilting which is strongly oblique to the inferred direction of movement for the detachment fault.

The Copper Peak detachment fault, exposed in the Copper Peak area of the northeastern Moon Mountains, carries sedimentary and volcanic rocks of Paleozoic(?), Mesozoic, and Tertiary age over a ductilely deformed footwall consisting primarily of granitic intrusive rocks. Ductile footwall fabrics exhibit a consistent top-to-the-northeast sense of shear. The development of these ductile fabrics is constrained to post-date intrusion of the Copper Peak granite (of probable mid-Tertiary age), and largely pre-date the intrusion of a late- to post-tectonic biotite granite (Tmbg) which yields an early Miocene (20.8 ± 3.2 Ma) U-Pb zircon age. The Copper Peak detachment is correlated with the Moon Mountain detachment fault, from which it is offset by an inferred, high-angle fault. The lack of penetrative ductile fabrics in Paleozoic/Mesozoic sedimentary rocks in the hanging wall of this fault is distinctive in the western Arizona region, and may constrain reconstruction of the detachment system.

Regional relations dictate that the Moon Mountain and correlative Copper Peak detachment faults are the western exposed limit of the Whipple-Buckskin-Rawhide detachment system at the latitude of the Moon Mountains. The presence of Tertiary ductile fabrics in the footwalls of these structures implies that the rocks originated at depths and temperatures sufficient to produce well-developed mylonitic fabrics, and that the actual breakaway (original surface break) for the detachment system is not preserved in this area. In addition, these east-dipping mylonitic fabrics dip antithetically to a much deeper-seated, west-dipping mylonitic zone that has been seismically imaged (Hauser et al., 1987) and correlated with mylonites of the Whipple and Buckskin Mountains. This

relation suggests that either (1) Tertiary mylonitization was characterized by anastamosing shear zones within a large section of the crust, or that (2) different phases of Tertiary mylonitization are represented in the lower plate of the Whipple-Buckskin-Rawhide detachment system.

The generation of large magnitudes of extension in mid-Tertiary time may have been related to inheritance of a thickened crust from Mesozoic shortening, but accommodation of extensional strain in the detachment system did not take place primarily along pre-existing thrust faults. Preservation of dissected but intact Mesozoic structures, such as the Valenzuela thrust fault, are well-documented in western Arizona, and indicate that the geometry of the detachment fault and related structures was not controlled by pre-existing zones of weakness. Localization of strain was probably more a function of both the local and regional stress regime and the evolving thermal structure of the crust.

INTRODUCTION

LOCATION AND GEOLOGIC SETTING

The Moon Mountains of the Colorado River Indian Reservation in west-central Arizona are located Mojave-Sonoran Desert region within the southern Basin and Range province of the western U.S. Cordillera (Fig. 2.1). Rocks exposed in this region record a complex history involving major compressional deformation, probably during a number of episodes in Mesozoic time, and large-magnitude extensional tectonism during Tertiary time. The Moon Mountains are centrally located within the Maria fold and thrust belt (Reynolds et al., 1986), which extends from the Coxcomb Mountains of southeastern California, to the Harquahala Mountains of central Arizona (Fig. 2.1). In addition, the Moon Mountains area is situated within the westernmost exposures of the regional Whipple-Buckskin-Rawhide detachment system of mid-Tertiary age, a system associated with profound crustal extension in the Colorado River extensional corridor (Howard and John, 1987)

Rocks exposed in the Moon Mountains consist primarily of crystalline gneisses and granitic intrusive rocks, with lesser amounts of sedimentary and volcanic supracrustal lithologies. These rocks range in age from Precambrian to Tertiary, and record a

complicated history of repeated deformation, metamorphism, and magmatism which characterizes much of the Mojave-Sonoran Desert area of the southwestern Cordillera. Detailed field mapping, structural analysis, and geochronology are presented in this study which document the presence of Mesozoic thrusting and associated fabrics, as well as Tertiary detachment faulting and associated structural elements in the Moon Mountains area.

Some confusion surrounds the geographic nomenclature of the Moon Mountains area. Moon Mountain is variably referred to solely as the peak which bears this name, or the entire area composed of the two elongate ridges which define the northernmost Dome Rock Mountains, north of Tyson Wash. For the purpose of this report, Moon Mountain will be used to refer to the peak which bears this name, and Moon Mountains will refer to the entire area made up of the two elongate ridges (Plate 2-1; Fig. 2.2). Several informal names have been used to designate certain geographic areas or elements, for the sake of ease of reference. These names are indicated on the sketch map in Figure 2.2, and include (1) Detachment Wash, (2) the Valenzuela area, (3) El Diablo Peak, (4) the Mojave Paint Basin, and (5) Copper Peak. The Valenzuela area refers to the region near and to the south of the Valenzuela Mine, in the southeastern part of the Moon Mountains. El Diablo Peak is the name given to peak 1337' in the Valenzuela area.

PREVIOUS WORK

Previous work within the Moon Mountains area has largely revolved around the mining resources and potential of the Colorado River region. The area was heavily mined in the late 1800's and early 1900's for base and precious metals, and is now the site of gold production from the Copperstone Mine, an open pit operation just to the north of the Copper Peak area in the northeastern Moon Mountains (see Spencer et al., 1988). Wilson et al. (1969) showed the generalized distribution of rock types for the Moon Mountains area on the Arizona state geologic map, identifying the presence of crystalline gneisses and metamorphosed Mesozoic rocks. James Baker, from San Diego State University, produced a brief, unpublished, senior honors thesis report on the general location of the Moon Mountain detachment fault, and a brief treatment of the rock types of the western half of the Moon Mountains. Buising (1988) included outcrops of the upper Miocene to lower Pliocene Bouse Formation at Moon Mountain in her study of the proto-Gulf of California in western Arizona and southeastern California. Metzger (1968, 1973) also makes mention of Bouse Formation deposits in the area of the Moon Mountains in

reports on the hydrogeology of the lower Colorado River trough. The present study constitutes the first thorough compilation and discussion of the rocks and structures of the Moon Mountains, including the geologic map compiled at a scale of 1:24,000 (Knapp, in press).

DESCRIPTION OF ROCK UNITS

Rocks exposed in the Moon Mountains consist predominantly of crystalline gneisses and granitic intrusive rocks, with lesser amounts of sedimentary and volcanic lithologies. These rocks range in age from Precambrian to Tertiary and record successive periods of sedimentation, magmatism, deformation, and metamorphism. Detailed descriptions of the rock units are presented below, and are categorized by metamorphic, sedimentary, and igneous rock types. Within each of these divisions, units are discussed in order of decreasing age, as deduced from field relationships and U-Pb zircon geochronology.

The general distribution of rock units in the Moon Mountains is primarily influenced by the major structures present in the area (Plate 2-1, Fig. 2.2). The footwalls of both the Moon Mountain and Copper Peak detachment faults are predominated by crystalline gneisses and granitic intrusive rocks; the hanging walls of these structures are devoid of these lithologies, and carry either Tertiary sedimentary rocks (Moon Mountain detachment) or sedimentary and volcanic rocks of Tertiary, Mesozoic, and Paleozoic(?) age (Copper Peak detachment). Supracrustal rocks of Mesozoic age are restricted primarily to two areas. A newly recognized sequence of metasedimentary rocks, herein referred to as the Valenzuela metasedimentary sequence, occurs beneath the Valenzuela thrust fault in the southeastern Moon Mountains. Metavolcanic rocks of inferred Mesozoic age are concentrated in the area of the Mojave Paint Basin, where they are surrounded by younger granitic intrusive rocks.

METAMORPHIC ROCKS

Metamorphic rocks of the Moon Mountains consist of gneisses, schists, and amphibolites of presumed Precambrian age, and a sequence of metamorphosed sedimentary rocks, herein named the Valenzuela metasedimentary section. These lithologies comprise roughly 35% of the bedrock exposure, and record multiple phases of deformation and metamorphism.

Rocks of inferred Precambrian age in the Moon Mountains have been divided into two lithotectonic units based on general lithologic characteristics and geographic distribution. The Moon Mountain crystalline assemblage is designated as the collection of gneisses and amphibolites which underlie Moon Mountain, in the footwall of the Moon Mountain detachment fault in the northwestern Moon Mountains (Plate 2-1; Fig. 2.2). The name Valen crystalline assemblage is used here for the sequence of gneisses and schists which outcrop along the eastern arm of the Moon Mountains, in the footwall of the Copper Peak detachment. These rock units are inferred to be primarily of Precambrian age based on lithologic similarity with Precambrian rocks from surrounding ranges (e.g. Whipple Mountains, Orell, 1988; Podruski, 1979), and constitute the oldest units exposed in the Moon Mountains area.

MOON MOUNTAIN CRYSTALLINE ASSEMBLAGE (mx, a)

The Moon Mountain crystalline assemblage, named for the crystalline rocks which compose Moon Mountain itself, is exposed over an area of roughly four to five square kilometers in the northwestern Moon Mountains (Plate 2-1). These rocks display fabrics associated with intense deformation and amphibolite facies metamorphism. Five main lithologies have been identified within the Moon Mountain crystalline assemblage, defining a crude tectonic stratigraphy. These five divisions, in structurally ascending order, are: (1) a lower injection complex, composed mostly of sheared augen gneiss which has been extensively intruded by dikes of the structurally lower Tyson Peak granite, (2) thinly-banded gneiss, (3) quartz-mica schist (4) hornblende-biotite schist, and (5) medium- to coarse-grained augen gneiss. These five units form a continuous, layered stratigraphy over several kilometers within the highly deformed rocks of the Moon Mountain crystalline assemblage. The maximum exposed structural thickness of this sequence is ~120 m, in the vicinity northwest of the Apache Mine. Due to the regional northeast dip of the section, lower structural levels are not exposed at the north end of Moon Mountain, and the top of the section has been truncated by a splay of the Moon Mountain detachment fault.

VALEN CRYSTALLINE ASSEMBLAGE (vx)

The Valen crystalline assemblage is named for exposures of gneisses, schists, and amphibolites which underlie Valen Peak and surrounding areas in the eastern arm of the Moon Mountains (Fig. 2.2). This heterogeneous assemblage of crystalline rocks outcrops over an area of about three square kilometers, and is characterized by a variety

of lithologies, including megacrystic augen gneiss, banded-gneiss, quartzofeldspathic schist, and amphibolite, in order of decreasing abundance. All lithologies possess a metamorphic fabric, which varies from a crude foliation defined by aligned porphyroclasts and matrix minerals in the coarse-grained augen gneisses (Fig. 2.3), to a well-developed foliation and metamorphic mineral lineation in the schists and amphibolites. Fabrics do not exhibit a consistent orientation in these rocks; foliation is typically moderate- to shallow-dipping, but is disrupted on a local scale by folding. Metamorphic lineation is similarly variable. Petrographic analysis of these rocks indicates these fabrics were developed at amphibolite or epidote amphibolite facies conditions of metamorphism.

The Valen crystalline assemblage is intruded by several younger granitic bodies. Along the northern boundary of this unit, biotite-bearing granites of lower Miocene age intrude the Valen crystalline assemblage. The southern boundary of the crystalline complex is marked by an intrusive contact with a large body of quartz syenite of Jurassic age. The southernmost exposures of the Valen assemblage are fault bounded, and are carried in the hanging wall of the Valenzuela Thrust, where they overlie rocks of the Valenzuela metasedimentary section.

VALENZUELA METASEDIMENTARY SEQUENCE

A section of deformed and metamorphosed sedimentary rocks, exposed in the Valenzuela area of the southeastern Moon Mountains, has been informally named the Valenzuela metasedimentary section. These rocks consist of schist, marble, quartzite, and calc-silicate rocks which have been metamorphosed at lower amphibolite facies, and are beneath the Valenzuela thrust fault. Due to the internal deformation within this section, the original stratigraphic order of this sequence cannot be reconstructed with certainty. The structural ordering consists of: (1) a basal section of calc-silicate rocks with abundant, isoclinally folded quartzite lenses, (thought to be quartzite pebbles and cobbles), (2) a thin interval (2-4 m) of thinly-bedded quartzite, (3) a section of interbedded schists and quartzites, (4) a thick interval of orange- to brown-colored micaceous marble, (5) a second, thin, discontinuous interval of schists, (6) a second interval of thinly bedded quartzite which typically marks the overlying thrust contact, and (7) a second interval of calc-silicate rocks (see Figs. 2.4a and b). This structural sequence appears to define a repetition of the lithologies in a large, overturned synform, opening toward the south. Attenuation in the upper limb has resulted in thinning and omission of units directly beneath the Valenzuela thrust. Since the original stratigraphic

order of the Valenzuela section is unknown, it is impossible to determine whether this fold constitutes a large syncline, overturned to the south as in the neighboring Big Maria Mountains, or a synformal anticline.

Calc-silicate Rocks (vc)

The base of the Valenzuela metasedimentary sequence consists of 10-12 m of greyish green-weathering calc-silicate rocks that contain numerous quartzite lenses (Fig. 2.5). Since the base of this unit is not exposed, the structural thickness represents a minimum. The contact with the overlying quartzite is sheared, but appears to be an original stratigraphic boundary. These rocks are typically medium- to fine-grained schists which contain the assemblage quartz + potassium feldspar + biotite + plagioclase + calcite + chlorite + epidote, with minor muscovite. Preserved as rootless isoclinal fold hinges are abundant lenses of pure vitreous quartz. In thin section, these quartz lenses are medium- to coarse-grained with interlocking grain boundaries, suggesting a hydrothermal origin; however, in outcrop, the lenses take on the appearance of deformed quartzite clasts.

Thinly-bedded Micaceous Quartzite (vq)

An interval of thin- to very thin-bedded, micaceous quartzite occurs both near the base and at the top of the structural section. This quartzite outcrops as a resistant ledge, typically 3 to 4 m thick. It marks the thrust contact with the overlying quartz syenite along much of the length of the Valenzuela thrust fault, is exposed above the basal unit of calc-silicate rocks, and is exposed in a klippe of the metasedimentary rocks that lie above the Valen crystalline assemblage to the west of the Graveside fault (Plate 2-3). Despite intense recrystallization and internal deformation, the unit appears to retain certain aspects of its sedimentary origin. The quartzite is a thin- to very thin-bedded, light to medium grey-weathering, laminated, medium- to fine-grained, micaceous quartzite with thin micaceous partings. The rock consists almost exclusively of quartz (90-95%) and muscovite (4-5%), with a minor amount of potassium feldspar.

The unit displays intense internal deformation, typified by isoclinal folding (Fig.2.6); contacts with adjacent units are sheared, but relatively intact. Beneath the Valenzuela thrust fault, the outcrop pattern of this quartzite unit defines a large recumbent fold, opening toward the south, and cored by rocks of the interbedded schist, quartzite, and micaceous marble.

Interbedded Schist and Quartzite (vs)

An interval of thin- to medium-interbedded schist and quartzite makes up a significant part of the section. This unit outcrops as a slope of silvery-grey to brown-weathering schists, with more resistant, quartz-rich layers forming small continuous ridges (Fig. 2.4a). The maximum structural thickness of this unit is about 40-45 m, but probably represents an overestimate due to the internal folding and thickening evident in the outcrop.

Schists from this unit are composed largely of quartz and muscovite. One sample was found to contain numerous kyanite porphyroclasts, with a matrix assemblage of quartz + muscovite + sillimanite(?) + epidote ± opaques oxides. This assemblage is indicative of amphibolite facies metamorphism, and sillimanite has grown within the fabric.

Micaceous Marble (vm)

A very distinctive lithology within the Valenzuela metasedimentary section consists of an orange-weathering, micaceous calcite marble. This unit forms a prominent, resistant ledge in the upper part of the section. Contacts with both the underlying interbedded schist and quartzite unit and the overlying part of the section are sheared, and the base of the marble changes from a concordant contact to one which cuts with marked discordance across the underlying part of the section (Figs. 2.4a and b).The marble outcrops as a "medium-bedded", coarse-grained, orange- to brown-weathering, micaceous marble. Structural thickness of the unit varies considerably along strike due thickening and attenuation of the unit, but ranges from ~2 to 10 m.

The marble contains the assemblage calcite + muscovite ± quartz. Some intervals are very micaceous, containing up to 10% muscovite. Due to the degree of recrystallization and internal deformation within this unit, essentially no primary features remain.

Stratigraphic Correlation

Stratigraphic correlation of the Valenzuela metasedimentary sequence with known stratigraphy from west-central Arizona and adjoining southeastern California suggests an early Mesozoic age for this section. A clear correlation can be made with the Tung Hill metasedimentary sequence (Yeats, 1985) of the northern Dome Rock Mountains, just to

the south of the exposures of the Valenzuela section. This correlation can be made on the basis of (1) the general succession of lithologies within the two sections, (2) similar structural position of these metasedimentary rocks beneath thrust faults which carry deformed augen gneiss in the hanging wall, and (3) the geographic proximity of the two sections, which are separated by no more than ~8 km.

Yeats inferred a lower Mesozoic age for the Tung Hill section based on the lack of resemblance with other known occurrences of Paleozoic and Mesozoic strata in the region, and Reynolds et al. (1987) correlated the Tung Hill section with the Buckskin Formation of the Buckskin Mountains, to the north. The type section for the Buckskin Formation is located in the Planet-Mineral Hill area of the Buckskin Mountains, and consists primarily of quartzose sandstone, siltstone, and conglomerate, with a variable calcareous component. While carbonate intervals are typically lacking in sections from western Arizona which have been correlated with the Buckskin Formation (Reynolds et al., 1987), more distal facies of the calcareous-rich siltstones could be marine carbonates (Spencer, pers. comm.). Evaporite intervals are characteristic within the lower Triassic section of the eastern Mojave Desert (Walker, 1985, 1988) and in the Buckskin Formation of western Arizona (Reynolds et al., 1987), but they have not been recognized in the Valenzuela section.

Reynolds et al. (1987) identify four divisions of Mesozoic supracrustal rocks in west-central Arizona. In ascending stratigraphic order, these are: (1) quartzose to slightly feldspathic sandstones, siltstones and conglomerates that depositionally overlie the Permian Kaibab Limestone, (2) quartzite and quartzofeldspathic sandstone with locally interbedded volcaniclastic rocks, (3) voluminous silicic volcanic, hypabyssal, and volcaniclastic rocks, and (4) a thick section of volcaniclastic rocks assigned to the McCoy Mountains Formation. In the eastern Mojave Desert of southeastern California, the lower Mesozoic Moenkopi Formation consists of marine and non-marine terrigenous, carbonate and evaporite rocks (Walker, 1985, 1988). Facies within the Moenkopi Formation vary from alluvial redbeds on the Colorado Plateau to mainly marine carbonate rocks in the central Mojave Desert.

SEDIMENTARY ROCKS

Sedimentary rocks and sediments of the Moon Mountains range in age from Paleozoic to Recent, and are represented by minor amounts of carbonate, quartzite, conglomerate, sandstone, siltstone, and unconsolidated gravels. These rocks are

restricted to the hanging walls of the Moon Mountain and Copper Peak detachment faults, where they are variably faulted, tilted, and brecciated. Several of these rock types occur only in the Copper Peak area as small outcrops in the hanging wall of the Copper Peak detachment.

COPPER PEAK AREA

Exposed in the vicinity of Copper Peak is a collection of units which occur only in the hanging wall of the Copper Peak detachment. These units include quartzite, cherty limestone, sandstone, and mafic volcanic rocks (Plate 2-1). While these lithologies comprise an insignificant percentage of the rocks exposed in the Moon Mountains, they occupy an important structural position, and bear on the geologic evolution of the Moon Mountains area.

Quartzite

The top of Copper Peak is composed of highly brecciated, vitreous white quartzite. This quartzite breccia consists of reddish-brown weathering, angular, small pebble- to large cobble-sized quartzite clasts in a matrix of sub-angular to sub-rounded, crushed, fine-grained quartz. Preserved in some of the larger quartzite clasts are relict primary sedimentary features, including thin silty laminations and medium- to fine-grained, well-rounded quartz sand grains in quartz cement. Despite the high degree of fracturing and brecciation of this quartzite, the rock does not appear to be significantly recrystallized or ductilely deformed, unlike other quartzites exposed in the Moon Mountains.

Stratigraphic correlation of this laminated, medium- to fine-grained quartz arenite cannot be made with certainty. Several correlations are possible: the Cambrian Bolsa Quartzite, the Permian Coconino Sandstone, the Jurassic Aztec Sandstone, or quartzites associated with lower Mesozoic rocks in west-central Arizona.

Cherty Carbonate Rocks

A small irregular mound of brecciated, cherty limestone occurs at the northern base of Copper Peak. This rock outcrops in irregular blocks of greyish brown-weathering, laminated, cherty limestone which has been highly brecciated internally. Laminations and dark brown, irregular nodules of chert and/or silty material weather more resistantly than the medium- to fine-grained calcite matrix, giving the rock a rough,

mottled surface. Despite the high degree of fracturing and internal brecciation within the unit, the laminations and silty partings appear to be a primary sedimentary feature of the rock. Orientation of bedding is inconsistent, varying from one block to the next due to the extreme disruption of the outcrop.

The protolith of this limestone breccia is inferred to be one of the carbonate units that characterize the cratonal Paleozoic section of western Arizona. Cherty carbonates are unknown from Precambrian, Mesozoic, or Cenozoic strata in this region. Since the unit outcrops in structural isolation in the hanging wall of the Copper Peak detachment, a stratigraphic succession cannot be inferred. The rock occurs in close proximity to highly brecciated, laminated quartz arenite which caps the top of Copper Peak and may correspond to either the Cambrian Bolsa Quartzite or the Permian Coconino Sandstone of the Paleozoic cratonal section. Of the limestone units of Paleozoic age, the Permian Kaibab Limestone is known to contain chert-rich intervals (Richard, 1982). Based on this fact and the proximity to quartz arenite of possible Permian age, a correlation with the Permian Kaibab Limestone is preferred.

Conglomerate

Several small, poorly-exposed outcrops of coarse, pebbly sandstone and fine-grained conglomerate are found just north of Copper Peak in the hanging wall of the Copper Peak detachment. Structural thickness of this clastic section is difficult to assess due to incomplete exposure. A minimum thickness of ~15 m can be estimated from the available exposure. Contacts with surrounding units are also cryptic; however, the sediments appear to be intercalated with mafic volcanic rocks. These sedimentary rocks are dark brown-weathering, massive to thick-bedded, with medium- to small-sized, sub-angular to sub-rounded pebbles floating in a medium- to coarse-grained, sandy matrix composed primarily of quartz, feldspar, and lithic fragments. Pebble lithologies include basalt, quartzite, and carbonate. Formational affinity of individual clasts is difficult to determine based on small grain size.

The rocks have been strongly tilted based on the orientation of faintly-developed, fining upward sequences which indicate a westward facing in these rocks. The bedding is oriented ~N10W, dipping 80° SW to vertical. Based on lithology and clast composition and comparison with sediments of known Tertiary age, these terrigenous rocks are inferred to be of Tertiary age, and were apparently associated with subaerial basin deposition during development of the regional detachment system of western

Arizona and southeastern California. Spencer et al. (1988) indicate the presence of monolithologic sedimentary breccias derived from the Jurassic quartz porphyry in association with these fine-grained, terrigenous sediments. Tilting of these sediments, to vertical attitudes, is probably associated with rotation in the hanging wall of the Copper Peak detachment, as is the case for extension-related sediments in many other parts of the detachment system (cf Davis et al., 1980, in the Whipple Mountains).

MOON MOUNTAIN AREA

A sequence of conglomerates and sandstones which has been faulted and tilted in the hanging wall of the Moon Mountain detachment fault is exposed over an area of about two square kilometers to the east of Detachment Wash.

Monolithologic Conglomerate (Tcs)

Monolithologic conglomerate occupies the lowest exposed levels of this section, and rests in fault contact against crystalline gneisses of the Moon Mountain crystalline assemblage on the Moon Mountain detachment fault. This unit consists exclusively of poorly-sorted (pebble- to boulder-size), angular to sub-angular, clasts of greenish grey-weathering, quartz porphyry in a clast-supported conglomerate.

BOUSE FORMATION (Tmb)

Deposits of the upper Miocene to lower Pliocene Bouse Formation mantle bedrock exposures throughout the study area. The Bouse Formation was first described by Metzger (1968) on the basis of a 767-foot type section from a well in Parker Valley, and two reference sections, one of which is located along the western flank of Mesquite Mountain (SW1/4 sec. 26 and SE 1/4 sec. 27, T.8 N., R.20W., Gila and Salt River baseline and meridian).

Metzger (1968) identified three units within the Bouse Formation: (1) a basal limestone, (2) interbedded clay, silt and sand (which comprises most of the formation), and (3) a distinctive tufa deposit that mantles topography and is thought to have formed at or near the water surface throughout Bouse Formation deposition. Recent work by Buising (1987; 1988) shows the Bouse Formation to be interfingered with conglomerate and sandstone of the underlying Osborne Wash association. The Bouse Formation is overlain by and interfingers with conglomerates interpreted as ancestral Colorado River gravels (Buising, 1987).

ALLUVIUM (Qal)

Rocks mapped as alluvium consist predominantly of unconsolidated gravels and sands associated with the modern drainage system of the Colorado River and its tributaries. These deposits include alluvium, colluvium, talus, dune sand, and flood plain deposits of the Colorado River. No attempt has been made in the present study to distinguish these various Quaternary deposits on the geologic map.

IGNEOUS ROCKS

MOJAVE PAINT BASIN METAVOLCANIC SEQUENCE (mv)

A series of deformed and metamorphosed volcanic rocks is exposed in the northern end of the eastern arm of the Moon Mountains, in what is informally referred to as the Mojave Paint Basin (Fig. 2.2). These rocks (indicated by "mv" on the geologic map) outcrop as recessive slopes of green to grey weathering, medium- to fine-grained rock in the area of low relief to the south of the Copper Peak area. Contacts with surrounding units are generally not well exposed, and are either intrusive or fault-bounded where the contact relations can be observed. Due to the extreme internal deformation within this unit and the lack of stratigraphic contacts with other units, the stratigraphic order is unknown.

QUARTZ PORPHYRY (Jqp)

Limited outcrops of silicic volcanic or sub-volcanic quartz porphyry are restricted to the area around the Mojave Paint Basin, the area near Copper Peak, and the hanging wall of the Copper Peak detachment, all in the northeastern Moon Mountains. This lithology forms resistant, rounded hills of massive, blocky-weathering, quartz porphyry which appears orange to dark brown on a weathered surface and greyish green on a fresh surface. Near the Copper Peak detachment fault, extensive secondary alteration has produced red- and yellow- weathering of the unit. The rock consists of medium- to coarse-grained phenocrysts of quartz, plagioclase, lithic fragments, potassium feldspar, and relict hornblende and biotite, floating in a very fine-grained groundmass of quartz and feldspar. The presence of embayed quartz grains, lithic fragments, many angular or broken phenocrysts, and the microcrystalline groundmass, suggest a volcanic origin for this rock. Other primary features are lacking, as the quartz porphyry typically forms a structureless mass.

Exposures of the quartz porphyry are typically fault-bounded, such that stratigraphic relations with surrounding units are unclear. Below Copper Peak, the quartz porphyry rocks are intruded by the Copper Peak granite, which produces a baked and altered zone near the contact. South of the Copper Peak granite, the quartz porphyry appears to be in stratigraphic contact with deformed metavolcanic rocks of the Mojave Paint Basin sequence, but the contact is not well-exposed. The stratigraphic ordering of these two units is not discernible within the map area, but based on regional relations, the quartz porphyry is inferred to overlie the metavolcanic sequence.

The age of the quartz porphyry is inferred strictly from regional relations. Similar silicic volcanic rocks are known from a wide area in the Mojave-Sonora desert region (Pelka, 1973a; Hamilton, 1982; Reynolds et al., 1987; Tosdal et al., 1988). These rocks consistently occupy a stratigraphic position above lower Mesozoic sedimentary rocks correlative with the Triassic Moenkopi Formation. Reynolds et al. (1987) reported slightly discordant U-Pb zircon data for quartz porphyry rocks form the Buckskin Mountains and Black Rock Hills which they interpreted to signify an emplacement age of 162 to 160 Ma. Granitic plutons of known Late Jurassic age intrude these quartz porphyry rocks in several ranges (Tosdal et al., 1988). Based on these relations, a Middle Jurassic age is inferred for the quartz porphyry rocks exposed in the Moon Mountains.

MAFIC VOLCANIC ROCKS (Tb)

Very minor, low-lying exposures of dark brown- to black-weathering, mafic volcanic rocks occur in association with coarse-grained sandstones north of Copper Peak, in the northernmost part of the map area. Contacts of these volcanic rocks with the surrounding bedrock are very poorly exposed, but the Copper Peak detachment fault is inferred to project beneath the outcrops of basalt. Flow features were not observed in these rocks, but igneous textures suggest they were rapidly quenched. Contacts with associated sedimentary rocks are not well exposed in the area near Copper Peak, so the possibility that these are hypabyssal dike rocks cannot be ruled out. Further to the north, outside the map area, Spencer et al. (1988) shows more exposures of these mafic volcanic rocks in the continuation of the hanging wall of the Copper Peak detachment fault. The age of these mafic volcanic rocks is inferred to be Tertiary. Judging from timing constraints for Tertiary volcanism in western Arizona, these volcanic rocks are probably of late Oligocene to mid Miocene age.

INTRUSIVE ROCKS

Granitic intrusive rocks, ranging in composition from quartz syenite to garnet two-mica granite, comprise the majority of rocks exposed in the Moon Mountains area. Large volumes of megacrystic, porphyritic quartz syenite (Jqs) occur in the southern Moon Mountains, and are known from a number of surrounding ranges in the Mojave-Sonora region (Hamilton, 1982; Yeats, 1985; Tosdal, 1988). Five separate bodies of biotite-bearing granite are identified: 1) the Tyson Peak granite (tpg), 2) the Copper Peak granite (cpg), (3) a biotite-bearing leucogranite (lg), (4) a small stock of biotite granite (Tmbg), and (5) a small hornblende-biotite granite stock (Thbg). The Tyson Peak granite is exposed along most of the length of the western arm of the Moon Mountains, and is named for Tyson Peak. The Copper Peak granite outcrops in the northeastern part of the Moon Mountains, and is named for Copper Peak. The biotite granites are all similar in composition and may be genetically related, but can be differentiated on the basis of texture, mineralogy, color index, and/or contact relations. Together these granitic rocks constitute ~45-50% of the exposed bedrock in the Moon Mountains.

Megacrystic Quartz Syenite (Jqs)

A large body of megacrystic quartz syenite is exposed at the southern end of the Moon Mountains, over an area of several square kilometers. The rock outcrops as rounded, resistant, dark hills. The quartz syenite is characterized by variable amounts (3-50%) of small (<1 cm) to very large (>15 cm), grey to purple, potassium feldspar megacrysts in a medium- to fine-grained groundmass of quartz + potassium feldspar + biotite + plagioclase, with epidote, chlorite, and minor white mica as secondary alteration products (Fig. 2.7). Accessory phases typically include sphene, zircon, apatite, and opaque oxides.

In the Valenzuela area, the quartz syenite intrudes the Valen crystalline assemblage, and is carried in the hanging wall of the Valenzuela thrust fault above the Valenzuela metasedimentary section. Intruding the quartz syenite are two groups of granitic dikes: one is a biotite-bearing leucogranite (lg) and the other is a set of garnet+biotite-bearing pegmatites and aplites. In the southwestern part of the Moon Mountains, the quartz syenite is intruded by the Tyson Peak granite.

Uranium-lead zircon dating of the megacrystic quartz syenite yields a late Middle Jurassic to early Late Jurassic age (160 ± 15; Knapp and Walker, in prep.). These rocks bear a strong resemblance to porphyritic Precambrian granites known from the Mojave-

Sonora region (Anderson, 1983), and can be difficult to distinguish in the field. All of the megacrystic quartz syenite rocks which form a relatively homogeneous, continuous body at the southern end of the Moon Mountains are correlated with the unit which was dated from the hanging wall of the Valenzuela thrust fault in the Valenzuela area. Other bodies of similar, phenocryst-rich, megacrystic granite occur within both the Moon Mountain crystalline assemblage and Valen crystalline assemblage, and may be either Precambrian or Jurassic in age.

Leucogranite (lg)

Irregular pods and bands of deformed, gneissic leucogranite are present within rocks of the Valenzuela area in the southeastern Moon Mountains. These rocks weather a medium grey to brown, and occur in bodies up to tens of meters across, but more often are found as thin (<1 m), sheared dikes which are clearly intrusive into the surrounding units. The rock consists of medium- to fine-grained, biotite-bearing leucogranite, which contains primarily quartz, potassium feldspar, plagioclase, and biotite. The rock possesses a well-developed fabric with a strongly-developed foliation parallel to the fabric in the surrounding rocks. It is restricted solely to exposures in the Valenzuela area and in the southernmost Moon Mountains. In the Valenzuela area, this leucogranite intrudes the Jurassic quartz syenite, the Valenzuela metasedimentary section, and the Valen crystalline assemblage south of the Trail Pass fault.

Similar rocks are known from areas to the south of the Moon Mountains. Yeats (1985) mapped a bodies of gneissic leucogranite in the northern Dome Rock Mountains that are intrusive into both megacrystic granites and lower Mesozoic metasedimentary rocks. Tosdal (1988) has dated rocks thought to be of this same suite from the Dome Rock Mountains and areas further south in Arizona, and cites an early Late Jurassic (158 Ma) age of intrusion.

Garnet-bearing Pegmatites

A swarm of garnet-bearing pegmatite and aplite dikes is present in the Valenzuela area in the southeastern portion of the Moon Mountains. The dikes vary in width from 0.5-2 m and are continuous over 10's to 100's of meters. The highest concentration of these dikes occurs in the area of El Diablo peak, where they make up as much as 20-25% of the outcrop (Fig. 2.4b). The dikes are most prevalent within the quartz syenite, but occur also within the Valen crystalline assemblage (south of the Valenzuela cutoff), and

several garnet-bearing dikes are present in the base of the Valenzuela metasedimentary section. The dikes are not recognized elsewhere in the Moon Mountain area, and no granitic body is exposed structurally below the dikes as an obvious source for them.

The dikes consist compositionally of quartz (55-60%), potassium feldspar (15-20%), plagioclase (12-15), garnet (<1%), and muscovite (<1%), with minor amounts of biotite and Fe-Ti oxides. Zircon and apatite are present in trace amounts. The rock has a hypidiomorphic granular texture, and varies from fine- to coarse-grained between aplitic and pegmatitic varieties. Muscovite appears to be a primary phase, as it occurs as well-formed, cleanly terminated grains, and exists as inclusions in some feldspar grains. Garnet occurs as medium- to fine-grained, subhedral to euhedral grains, typically concentrated toward the centers of dikes.

These dikes clearly intrude a metamorphic foliation developed within the quartz syenite and Valen crystalline assemblage, however the dikes themselves are deformed. Due perhaps to the composition of these dikes, they do not have a well-developed fabric themselves, but are folded in complex patterns, and are cut by gently north-dipping shear planes (Fig. 2.8).

U-Pb zircon analysis of these dikes (Knapp and Walker, in prep) indicates they are Late Cretaceous in age, based on a lower intercept age of 71.1 ± 6.7 Ma (4 fractions). Hamilton (1982, 1984) described a similar swarm of muscovite-bearing pegmatites in the north-central and northwestern Big Maria Mountains to the west, which he inferred to be Late Cretaceous in age based on cross-cutting relations with Jurassic intrusive rocks and a K-Ar age of ~62 Ma (Martin et al., 1982).

Tyson Peak Granite (tpg)

The Tyson Peak granite (informal name) consists of a large, relatively homogeneous granitic body exposed over an area of several square kilometers in the southwestern part of the Moon Mountains (Plate 2-1, Fig. 2.2). This granite body intrudes gneisses of both the Moon Mountain crystalline assemblage (to the north) and the quartz syenite (to the south). Exposures of the Tyson Peak granite extend over eight kilometers from north to south, and a thickness of 150 m is represented. This must be taken as a minimum thickness as the base is nowhere exposed. Several satellite bodies of the granite occur within the quartz syenite. The granite is named for Tyson Peak, near the section corner for sections 1, 2, 11, and 12.

The unit consists of a medium- to coarse-grained porphyritic biotite granite, weathering to light greyish brown. Porphyritic potassium-feldspar crystals are 1-3 cm (with foliation bent around them), make up 20-25% of the rock, and sit in an equigranular, medium- to coarse-grained matrix of quartz (35%), feldspar (30%), and biotite (8-12%). Minor epidote is present as a secondary(?) phase. A moderate to well-developed foliation, defined by aligned biotite, elongate feldspar grains, and stretched quartz is present over much of the exposed extent of the granite. Abundant secondary white mica has grown within the plane of foliation where the rock is strongly foliated.

The contact of the porphyritic biotite granite with the surrounding crystalline country rock is highly sheared in places, but is clearly intrusive. Numerous aplitic dikes emanate from the granite body at the northern contact with gneisses of the Moon Mountain crystalline assemblage, and the abundance of these dikes decreases dramatically within ~100 m from the contact. In contrast, dikes are rare and a quartz-rich border phase is typically present along the southern contact of the granite, and blocks of the quartz syenite, up to 200-300 m across, occur within the granite near its margins. The granite contact is irregular on an outcrop scale, and clearly truncates an earlier foliation within the gneissic country rock (Fig. 2.9). Foliation is poorly developed within the margins of the granite, where the rock tends to be equigranular and crumbly with no preferred mineral orientation, and the mica has been extensively sericitized.

The age of the Tyson Peak granite is uncertain, but constrained to be post-Jurassic based on intrusive relations with the quartz syenite, and pre-Bouse Formation. The Tyson Peak granite bears a strong resemblance to foliated granite in the northern Dome Rock Mountains (just to the southeast, across Tyson Wash) named the Tyson Wash granite (Yeats, 1985). In that area, the Tyson Wash granite truncates the Tyson Wash thrust, here correlated with the Valenzuela thrust. These correlations would restrict the age of the Tyson Peak/Tyson Wash granite to be younger than ~71 Ma (post-Late Cretaceous). Outcrop examination of s-c fabrics within the Tyson Peak granite exhibit a top-to-the-northeast shear sense, consistent with kinematic indicators for the Moon Mountain detachment fault, and implying that the Tyson Peak granite pre-dates significant deformation in the footwall of the detachment.

Copper Peak Granite(cpg)

The Copper Peak granite is exposed over an area of ~2 km^2 surrounding and to the south of Copper Peak, in the northeastern part of the Moon Mountains. The unit

outcrops as low ridges and irregular hills of orangish brown-weathering granite. Numerous dikes of intermediate to mafic composition intrude the granite, and form more resistant, west-northwest trending ridges. Contacts of the Copper Peak granite with surrounding units are either (1) fault-bounded, or (2) not well exposed. Along the northern margin of the Copper Peak granite, the unit is truncated by the Copper Peak detachment fault. The southern boundary of the Copper Peak granite consists of an intermediate- to high-angle fault, which juxtaposes the granite against metamorphosed Jurassic and lower Mesozoic(?) volcanic and volcaniclastic rocks of the Mojave Paint Basin. Below the Copper Peak detachment, the Copper Peak granite is in direct contact with metamorphosed volcanic rocks of the Jurassic quartz porphyry (Jqp). The contact is not well exposed, but is inferred to be intrusive based on the baked, discolored nature of the quartz porphyry near the contact. Several blocks (5-10 m in diameter) of sheared, megacrystic quartz syenite occur as inclusions within the Copper Peak granite, indicating that significant deformation had affected the country rocks prior to intrusion of the Copper Peak granite.

The unit consists of a biotite-bearing, hypidiomorphic granite with the primary assemblage quartz + potassium feldspar + plagioclase + biotite. Secondary mineralization has resulted in chloritization of biotite and sericitization of feldspar. A weakly- to strongly-developed tectonic fabric is present over much of the exposed extent of the granite, and is characterized by flattened and stretched quartz grains and crushed potassium feldspar crystals. A consistent top-to-the-northeast shear sense is indicated by S-C fabrics (including bent micas and sygmoidal quartz ribbons) and asymmetric feldspar porphyroclasts beneath the Copper Peak detachment.

The age of the Copper Peak granite is constrained to be younger than Jurassic, based on intrusive relations with the Jurassic quartz porphyry, and is inferred to be Tertiary, based on compositional and textural similarity to other biotite-bearing granites in the Moon Mountains area. It may be roughly coeval with Tmbg, a biotite granite dated by U-Pb zircon to be 20.8 ± 3.2 (Knapp and Walker, in prep.).

Biotite Granite (Tmbg)

Outcrops of a small, unnamed stock of porphyritic biotite granite flank both the northern and southern margins of the Mojave Paint Basin area in the northeastern Moon Mountains. This granite forms steep, crumbly ridges and weathers to an orange-brown in knobby, rounded outcrops. The rock is typically a medium-grained biotite porphyry

with phenocrysts of feldspar (40%), quartz (30%), and biotite (~5%) set in a fine-grained groundmass of quartz and feldspar. Some portions are not nearly so porphyritic, and form a medium-grained, hypidiomorphic granular texture.

Contacts with surrounding units are intrusive. In northern exposures, this biotite granite intrudes the Copper Peak granite, and can be differentiated from the Copper Peak granite by a higher biotite content and consequent darker color. This biotite granite is clearly intrusive into rock of the Mojave Paint Basin metavolcanic sequence, which have been strongly mylonitized. The granite truncates mylonitic fabrics in these country rocks that indicate a predominant top-to-the-northeast asymmetry. The granite does possess a locally developed foliation consisting of flattened quartz grains and aligned micas, but the rock is generally not foliated, and is interpreted to be late- to post-tectonic with respect to development of mylonites in the footwall of the Copper Peak detachment. Along the southern margin of this granitic body lies another biotite granite (Thbg). Intrusive relations between these two granites are equivocal. The contact is marked by a distinct mineralogical and color change to the darker, hornblende-bearing granite to the south (Fig. 2.10), but (1) no baked contact is evident, (2) no dikes emanate from one body into the other, and (3) no textural evidence for quenching of one body against the other was observed. Several small outliers of the hornblende-bearing granite (Thbg) occur within the biotite granite (Tmbg), but their contacts are not well exposed, and they may either by included blocks in or intrusive outliers to the main body of hornblende-bearing granite.

U-Pb zircon dating of the Tmbg unit indicates it is early Miocene in age, based on a lower intercept of 20.8 ± 3.2 (Knapp and Walker, in prep.). The spatial association and similarity in composition of other biotite granites in the Moon Mountains area suggests that they may also be of early Miocene age. These granites usually possess only one foliation, where they are deformed, and the fabric is characteristically the Tertiary mylonitic fabric.

Hornblende-biotite Granite (Thbg)

A small stock of mesocratic, hornblende-bearing, biotite granite is exposed over about a square kilometer in the eastern Moon Mountains. The rock outcrops as resistant ridges of medium grey granite which weathers to a brownish dark grey with desert varnish, and is easily distinguishable from the neighboring biotite granite and rocks of the Valen crystalline assemblage. Most of the unit consists of a medium- to coarse-grained, hypidiomorphic granular, unfoliated granite, with potassium feldspar (40-50%), quartz

(25-30%), plagioclase (10-15%), biotite (8-10%), and hornblende (4-5%). Some portions are porphyritic, with potassium feldspar phenocrysts up to 1 cm making up 25% of the rock. Foliation, where present, is only moderately developed, but appears to be tectonic based on stretched and flattened quartz grains. The margins of the granite body are distinctly unfoliated, and discordantly truncate all fabrics in the Valen crystalline assemblage. This unit appears to intrude the Tmbg granite, and is therefore inferred to be early to mid-Miocene in age.

Basic to Intermediate Dike Rocks (Td)

Basic to intermediate dike rocks are irregularly distributed within the Moon Mountains, but are most prominent in the Copper Peak area, in the Moon Mountain crystalline assemblage in the vicinity of Moon Mountain, and in the Miocene granites to the south of the Mojave Paint Basin. These dikes are typically northwest to west-northwest trending and steeply dipping to vertical. Compositions range from diabase to biotite-porphyry dacite, but no regular variation in composition with location was observed. All dikes post-date development of ductile fabrics in the country rocks, however some faulting clearly post-dates dike emplacement.

In the Copper Peak area, a series of west-northwest-trending dikes intrudes the Copper Peak granite in the footwall of the Copper Peak detachment fault. These dikes are in turn cut by a high-angle fault which offsets the detachment, and may therefore place an upper age limit on movement of the Copper Peak/Moon Mountain detachment system. Along the western side of Moon Mountain, a large dike of intermediate composition intrudes across a series of north-northeast trending faults which cut a splay of the Moon Mountain detachment, placing an upper age limit on movement on this structure. These dikes are inferred to be mid- to late Miocene in age, based on the presence of widespread volcanism of this age known in the region.

DESCRIPTION OF STRUCTURES

The structural geology of the Moon Mountains records elements of both Mesozoic thrust faulting and Tertiary detachment faulting. These deformational episodes have been identified regionally in surrounding ranges, within the Late Cretaceous Maria fold and thrust belt (Reynolds, et al., 1986) and the mid-Tertiary Whipple-Buckskin-Rawhide-Bullard detachment terrain (Davis, et al., 1980; Reynolds and Spencer, 1985; numerous

other references.). In the Moon Mountains, three major structures are identified: (1) the Valenzuela thrust system, (2) the Moon Mountain detachment fault, and (3) the Copper Peak detachment fault.

VALENZUELA THRUST FAULT

The Valenzuela thrust fault is exposed in the Valenzuela area of the southeastern Moon Mountains, where it places crystalline rocks of the Valen assemblage and sheared, Jurassic quartz syenite above the deformed and metamorphosed Valenzuela section (Plate 2-3, Fig. 2.2). The thrust system is complicated by later folding and faulting, such that the present expression of the Valenzuela thrust consists of irregular, discontinuous segments.

Three major factors complicate understanding of the Valenzuela thrust system. First, the uncertainty of stratigraphic ordering and correlation of the Valenzuela metasedimentary sequence obscures a clear picture of structural juxtaposition, particularly in the northernmost exposure of the Valenzuela thrust. As a result, the thrust contact has been mapped at the sheared contact between rocks identified as part of the Valenzuela metasedimentary sequence, and lithologies which are clearly part of the Valen crystalline assemblage or the quartz syenite. Secondly, the Valenzuela thrust appears to be characterized by a multi-stage kinematic history, with evidence for both south- and north-directed phases of movement. Finally, the dismembered nature of the thrust system due to later folding and faulting considerably complicates the present geometry of the thrust system.

The nature of the Valenzuela thrust fault differs across the northeast-striking, high-angle Graveside fault. On the southern side, the Valenzuela thrust carries sheared gneisses of the Valen crystalline assemblage and quartz syenite above the deformed and metamorphosed Valenzuela section. The thrust contact is marked by a thin (5-10 cm) zone of mylonitic gneiss, which typically is in contact with either the thinly-bedded quartzite or micaceous carbonate of the Valenzuela section. The contorted nature of the Valenzuela thrust is due in part to folding of the fault surface subsequent to movement. Broad folding about northeast-southwest trending fold axes is suggested by the outcrop pattern of the thrust surface.

The southernmost exposures of the Valenzuela thrust fault dip moderately to gently to the southeast, and juxtapose gneissic quartz syenite above calc-silicate and

quartzite units of the Valenzuela section. The southeastward dip of the thrust beneath the hills of quartz syenite at the south end of the east arm of the Moon Mountains suggests that the Valenzuela thrust continues in the subsurface to the south. Exposures in the northern Dome Rock Mountains (Yeats, 1985) reveal the exact same structural juxtaposition across the Tyson thrust zone. Here, along the northeastern edge of the Dome Rock Mountains, the Tyson thrust places sheared megacrystic gneiss of the Tyson augen gneiss above a deformed and metamorphosed sedimentary section which Yeats (1985) referred to as the Tung Hill section. Where exposed, the Tyson thrust is a gently north-dipping feature, with abundant evidence for north-directed shear (Yeats, 1985).

MOON MOUNTAIN DETACHMENT FAULT

The Moon Mountain detachment fault is exposed for about 1.5 km of its length, along the eastern flank of the western arm of the Moon Mountains, in the vicinity of Moon Mountain (Plate 2-1, Fig. 2.2). The fault is marked by a very distinctive lithologic break, and alteration and discoloration of the gneissic basement rocks exposed in the footwall just below the fault. The detachment strikes generally north-northwest to south-southeast, with variable intermediate to shallow dips ranging from 20-40° to the east. Excellent exposures of the Moon Mountain detachment are present at the head of Detachment Wash (informal name), where the fault places a sequence of block-faulted and tilted Tertiary conglomerates and sandstones above mylonitized and subsequently brecciated gneisses of the Moon Mountain crystalline assemblage (Fig. 2.11). To the north of Detachment Wash, the detachment is covered by deposits of the late Miocene Bouse Formation, but a lower splay of the fault continues into the crystalline rocks, and cuts below the top of Moon Mountain. High angle faults with apparent normal displacement cut the crystalline rocks in the hanging wall of the splay, and appear to either merge with or be truncated by the splay of the Moon Mountain detachment.

Several notable structural relations are preserved in the footwall of the Moon Mountain detachment. The lower splay of the detachment which carries crystalline rocks of the Moon Mountain crystalline assemblage is cut by a large (3 m-wide) dike, which also appears to cross-cut high-angle faults in the hanging wall of the detachment splay. This intermediate dike, as well as the detachment splay, is in turn cut by a series of north-northeast-trending high-angle faults with an apparent normal sense of displacement, judging from offsets of the crude lithologic layering in the Moon Mountain crystalline assemblage rocks. Radiometric dating of these dikes could place important timing

constraints on the age of movement on this splay of the detachment, as well as movement on the main strand of the detachment.

The southeastward continuation of the Moon Mountain detachment is buried beneath Bouse Formation deposits, but is inferred to be present from ductile, northeast-directed fabrics in the Tyson Peak granite and the Jurassic quartz syenite in the southern Moon Mountains (Fig. 2.12). The trace of the detachment in the subsurface projects directly through the alluvial wash which separates the two arms of the Moon Mountains and into Tyson Wash. As discussed previously, rock types appear to be continuous across this separation in the southern Moon Mountains. In addition, rock types and structures (in particular the Valenzuela thrust system) appear to be continuous from the southern Moon Mountains into the northern Dome Rock Mountains. These relations suggest two possible alternatives for the continuation of the Moon Mountain detachment: (1) the detachment rapidly loses displacement toward the southeast, and essentially dies out in the southern Moon Mountains, or (2) the Moon Mountain detachment is truncated against a high-angle, subsurface fault, and is offset to the northeastern Moon Mountains, where it appears again as the Copper Peak detachment.

The magnitude of displacement on the Moon Mountain detachment system is difficult to estimate. No correlation of rock types can be made from the hanging wall to the footwall of the detachment. Ductile fabrics in the footwall gneisses are concordant with the detachment and are indicative of high shear strain. The juxtaposition of mylonitic gneisses and supracrustal sedimentary rocks across the detachment is suggestive of a large net throw on the fault in order to bring rocks from depths suitable for mylonitic deformation to near-surface conditions.

COPPER PEAK DETACHMENT

The Copper Peak detachment fault, exposed in the Copper Peak area at the northeastern edge of the Moon Mountains, carries an assemblage of sedimentary and volcanic rocks over a ductilely deformed footwall of granitic and Mesozoic volcanic rocks. The fault surface dips generally northeastward, and is marked by a 2-3 m zone of chloritized mylonitic gneiss. Ductile fabrics in the footwall are characterized by S-C mylonites within the granitic rocks, and decrease in intensity away from the fault.

Units preserved in the hanging wall of the Copper Peak detachment occur as fault-bounded slivers, and include Jurassic quartz porphyry, Tertiary sedimentary and mafic

volcanic rocks, and quartzite and carbonate of inferred Paleozoic age. Pre-Tertiary units are highly brecciated, and Tertiary strata exhibit steep westward dips.

The geometry of the Copper Peak detachment fault has been significantly modified by later faulting and folding. High-angle faults offset the detachment on either side of Copper Peak, and the exposure of the detachment below Copper Peak defines a long, narrow reentrant, probably as a result of folding of the the surface subsequent to displacement.

The Copper Peak detachment continues down dip in the subsurface northeast of the Moon Mountains. Spencer et al. (1988) describe the geology of the Copperstone Gold Mine to the northeast of Copper Peak, and attribute the gold mineralization in brecciated Jurassic quartz porphyry to fluid circulation along the developing detachment system and associated hanging wall structures.

The age of movement on the Copper Peak detachment is only roughly constrained by the presence of Tertiary-age sediments and mafic volcanic rocks which are tilted in the hanging wall, and the unconformable overlap of the Bouse Formation across the fault. Volcanic rocks from tilt blocks within other regions of the detachment terrain of western Arizona and southeastern California yield Miocene ages (Davis, 1980; Frost, ?), and likely represent the age of volcanic rocks in the Copper Peak detachment system. Spencer and Reynolds (1988) cite an age of about 20 Ma for similar sedimentary rocks which are tilted in the hanging wall of the Buckskin detachment.

The trace of the Copper Peak detachment is buried both to the northwest and southeast by deposits of the Bouse Formation. Geophysical data (proprietary gravity data from Cyprus Minerals Co.; J. Spencer, pers. comm.) suggest the Copper Peak detachment fault is truncated by a northeast-trending, high-angle fault along the western side of the eastern arm of the Moon Mountains (Plate 2-1, Fig. 2.2). No expression of this structure can be seen in the Bouse sediments or overlying alluvial cover, but the presence of such a fault is consistent with termination of the Moon Mountain detachment in the southern Moon Mountains, where lithologic units and structures appear to be continuous across the projection of the Moon Mountain detachment through Tyson Wash.

Correlation of the Copper Peak detachment with the Moon Mountain detachment is made on the basis of (1) similarity of geometry and style of the two detachments, (2) rough timing constraints indicating these are both mid-Tertiary features, and (3)

resolution of the continuation of the Moon Mountain detachment fault towards the southeast.

DISCUSSION

The geologic evolution of the Moon Mountains involved multiple phases of deformation and metamorphism. Structures associated with both the Maria fold and thrust belt and the Whipple-Buckskin-Rawhide detachment terrain are exposed here. The present study provides important new information about (1) the continuation of the Maria fold and thrust belt from exposures known to the west (Big Maria and Riverside Mountains) to exposed thrusts to the east (Plomosa, Granite Wash, Harquahala Mountains), (2) the conditions of metamorphism associated with thrusting, based on assemblages and fabrics developed in lower Mesozoic rocks, and (3) the timing of thrusting, and (4) another occurrence of lower Mesozoic sedimentary rocks in west-central Arizona. With regard to Tertiary extension, data from the Moon Mountains indicate that accomodation of extension did not primarily take place along pre-existing thrust faults, and that rocks directly in the footwall of the western-most exposures of the detachment system originated at relatively deep crustal levels, implying that the actual surface break of the detachment is not preserved at this latitude.

GEOMETRY OF THRUSTING

The geometry of Mesozoic thrust faulting in the Moon Mountains, as exhibited by the Valenzuela thrust fault, is complicated by a multi-stage history of movement on the thrust fault in addition to post-thrusting modification of the thrust. Footwall structure is defined by an apparent repetition of the section in the Valenzuela metasedimentary sequence in a large, recumbent, south-opening fold which is cored by the micaceous marble unit. Shearing of contacts within the section has disrupted a continuous stratigraphy, such that units have been omitted in the upper limb of the fold. Since the exact original stratigraphy of the Valenzuela section is unclear, it cannot be determined with certainty whether the fold represents a large, south-vergent syncline, or an overturned, synformal anticline with northward vergence. Two factors favor the former interpretation: (1) descriptions of the lower Mesozoic section from surrounding areas in Arizona and southeastern California indicate that the base of the section is characterized by calcareous sandstones, siltstones, and gypsum deposits (similar to the present exposed

base of the Valenzuela section), and (2) a large, south-facing, thrust-related syncline is preserved in Paleozoic rocks in the Boyer's Gap area just to the south of the Moon Mountains.

Reactivation of the Valenzuela thrust is demonstrated by fabric relations in both the hanging wall and footwall of the thrust. S-C relations within both the hanging wall gneisses and footwall sediments of the Valenzuela thrust exhibit a consistent top-to-the-northeast shear sense. The micaceous marble unit has been dismembered along the thrust contact, and boundaries of this unit truncate foliaiton in lower units of the Valenzuela sequence (Fig. 2.4a). In addition, folitaion in hanging wall gneisses is strongly discordant with the thrust contact, implying that slip has taked place subsequent to the fabric formation.

CORRELATION WITH TYSON THRUST

Similarities between the Valenzuela thrust system of the Moon Mountains and the Tyson thrust system (Yeats, 1985) from the northern Dome Rock Mountains allow a reliable correlation of these structures, and imply that they are of regional significance. The Tyson thrust zone of the northern Dome Rock Mountains is a northeast-dipping shear zone which places megacrystic augen gneiss (Tyson augen gneiss) above a deformed and metamorphosed sequence of metasedimentary rocks (Tung Hill section). Both the lithologic description and structural relation of these units correspond to the Valenzuela metasedimentary section and Valenzuela thrust fault exposed in the southern Moon Mountains (Fig. 2.14).

CONDITIONS OF METAMORPHISM

Basement-involved thrusting on the Valenzuela thrust fault was associated with lower amphibolite facies metamorphism. Evidence for this grade of metamorphism comes both from amphibolites of the Valen crystalline assemblage and schists of the Valenzuela metasedimentary section. Amphibolites of the Valen crystalline assemblage in the vicinity of the Valenzuela thrust exhibit an aligned mineral foliation and lineation, defined by elongate hornblende and epidote grains, which generally parallels the thrust contact. Aluminous schists from the interbedded schist and quartzite unit of Valenzuela section contain the assemblage quartz + muscovite+ sillimanite after kyanite. The presence of this assemblage in rocks of lower Mesozoic age clearly requires a period of amphibolite facies metamorphism subsequent to the age of deposition (Triassic?). Of

significance is the association of this assemblage with the Valenzuela thrust fault, demonstrating that this high-grade metamorphic event was associated with the emplacement of crystalline rocks of the upper plate.

TIMING OF THRUSTING

The age of thrusting on the Valenzuela thrust fault is relatively well constrained on the basis of U-Pb zircon geochronology. Jurassic quartz syenite, which is carried in the hanging wall of the thrust, is dated at 160 ± 15 Ma, and provides a lower limit on the age of thrusting. Garnet-bearing granitic pegmatite and aplite dikes, which were intruded during the latest, north-directed phase of movement on the Valenzuela thrust, yield a lower intercept age of 71.1 ± 6.7 Ma. The entire history of movement is therefore bracketed between late Middle Jurassic and Late Cretaceous, and the latest phase of movement was clearly Late Cretaceous in association with the Maria fold and thrust belt.

TERTIARY DETACHMENT FAULTING

The Moon Mountain and correlative Copper Peak detachment faults of the Moon Mountains are part of the regional mid-Tertiary detachment system of western Arizona and southeastern California. This major extensional terrain is evidenced along a 300 km tract within the lower Colorado River region (Howard and John, 1987). The Moon Mountains area has been proposed as part of the breakaway zone for this regional extensional system based on: (1) the northeast-dipping geometry and top-to-the-northeast kinematic history of the detachment system, (2) the absence of detachment fault exposures for some 150 km further to the southwest, along the direction of tectonic transport, and (3) evidence from seismic data which show a shallow-dipping reflector within the subsurface connecting the Buckskin detachment fault with the Moon Mountain detachment fault (Hauser, et al., 1987).

GEOMETRY OF DETACHMENT SYSTEM

Reconstruction of the Whipple-Buckskin-Rawhide detachment system has typically been hindered by the lack of continuous stratigraphy and/or distinctive piercing points across the detachment fault. Severe disruption of Paleozoic and Mesozoic stratigraphy and facies trends during Mesozoic thrusting precludes restoration of these units, and the geometry of structures associated with the Maria fold and thrust belt is not sufficiently clear to allow a confident reconstruction of these structures. The situation is

complicated by the fact that a significant portion of the thrust belt was erosionally denuded during the early Tertiary.

Rocks in the hanging wall of the Copper Peak detachment fault may place important constraints on reconstruction of the detachment system. Significantly, brecciated limestone and quartzite, correlated with units of the Paleozoic cratonal section, appear to have escaped the ductile deformation and high-grade metamorphism which most Paleozoic rocks of west-central Arizona display. These units could not have been buried and metamorphosed to any significant degree during any of several phases of Mesozoic folding and thrusting, implying they were originally outside the main locus of deformation during development of the Maria fold and thrust belt. Similar strata of demonstrable Paleozoic age were reported by Scarborough and Meader (1983) from the hanging wall of the Plomosa detachment fault in the northern Plomosa Mountains. Unmetamorphosed and undeformed Paleozoic strata in the footwall of the detachment system are known from the southern Plomosa Mountains (Miller and McKee, 1971) The correspondence of these unmetamorphosed carbonates and quartzites in the segmented detachment system may help in restoration of the pre-Tertiary configuration of the Maria fold and thrust belt.

Constraints on the timing of deformation in the footwall of the Copper Peak detachment system suggest a Late Oligocene to Early Miocene age for development of mylonitic fabrics. The Copper Peak granite of the northeastern Moon Mountains exhibits ductile, top-to-the-northeast directed fabrics below the Copper Peak detachment. This granite is intruded by a similar biotite granite (Tmbg) which is late- to post-tectonic based on (1) intrusion of this granite into mylonites of inferred Tertiary age, and (2) only local development of a weak mylonitic fabric within the granite. The Tmbg biotite granite yields a U-Pb lower intercept age of 20.8 ± 3.2, reflecting the age at which the rocks in the lower plate of the Copper Peak detachment were no longer at appropriate conditions for mylonitization.

CONCLUSIONS

The rocks and structures exposed in the Moon Mountains of the Colorado River Indian Reservation, west-central Arizona, record Mesozoic thrusting within the Maria fold and thrust belt, and superimposed Tertiary detachment faulting related to the regional Whipple-Buckskin-Rawhide detachment system. The major structures of the Moon

Mountains consist of the Valenzuela thrust fault, the Moon Mountain detachment fault, and the Copper Peak detachment fault. Thrusting in the Moon Mountains resulted in the emplacement of crystalline basement rocks over supracrustal sedimentary rocks at amphibolite facies conditions of metamorphism. Movement on the thrust was characterized by a multi-stage history, with apparent evidence for an earlier phase of south-directed movement, and a final phase of north-directed shear. Dating of this later phase of thrusting at ~71 Ma is the first direct documentation of the age of thrusting in the Maria fold and thrust belt. The Valenzuela thrust system is correlated with the Tyson thrust system of the northern Dome Rock Mountains, implying a regional extent for this structure.

The Moon Mountain detachment fault in the northern Moon Mountains places a section of faulted and tilted Tertiary sedimentary rocks above gneisses, schists rocks of the Moon Mountains crystalline assemblage. At least two fabrics are present in the footwall gneisses. Gneissic compositional layering is parallel with the detachment fault, but primarily represents a Mesozoic feature. Ductile shear fabrics are variably developed in gneisses and granites of the footwall, and indicate a consistent top-to-the-east shear sense associated with the detachment systems. Strata in the hanging wall of the detachment show tilting which is strongly oblique to the inferred direction of movement for the detachment fault. Regional relations dictate that the Moon Mountain detachment fault is the exposed western limit at this latitude for the regionally extensive Whipple-Buckskin-Rawhide detachment system of southeastern California and western Arizona.

The Copper Peak detachment fault, exposed in the Copper Peak area of the northeastern Moon Mountains, carries sedimentary and volcanic rocks of Paleozoic(?), Mesozoic, and Tertiary age above a ductilely deformed footwall consisting primarily of granitic intrusive rocks. Ductile footwall fabrics exhibit a consistent top-to-the-northeast sense of shear. The Copper Peak detachment is correlated with the Moon Mountain detachment fault, from which it is offset by an inferred, high-angle fault. The lack of penetrative ductile fabrics in Paleozoic/Mesozoic sedimentary rocks in the hanging wall of this fault is distinctive in the western Arizona region, and may constrain reconstruction of the detachment system.

The timing of development of ductile fabrics in the footwall of the Copper Peak detachment is constrained by the ductilely deformed Copper Peak granite (of probable Tertiary age), and a late to post-tectonic biotite granite (Tmbg) which yields an early Miocene (20.8 ± 3.2) U-Pb zircon age. Despite pre-existing zones of weakness

introduced by basement-involved thrust faults of the Maria fold and thrust belt, accommodation of extensional strain in the Tertiary detachment system was largely accomplished by the initiation of new structures.

The Moon Mountain and Copper Peak detachment faults are the western exposed limit of the Whipple-Buckskin-Rawhide detachment system at the latitude of the Moon Mountains. The presence of Tertiary ductile fabrics in the footwalls of these structures implies that the rocks originated at depths and temperatures sufficient to produce well-developed mylonitic fabrics, and that the actual breakaway (original surface break) for the detachment system is not preserved in this area. In addition, these east-dipping mylonitic fabrics dip antithetically to and not much higher in the crust than the seismically imaged mylonitic zone associated with the Whipple-Buckskin-Rawhide detachment system, suggesting that either (1) Tertiary mylonitization was characterized by anastamosing zones within the crust or that (2) different phases of Tertiary mylonitization are represented in the lower plate of the Whipple-Buckskin-Rawhide detachment system.

ACKNOWLEDGEMENTS

Gratitude is expressed to the Tribal Council of the Colorado River Indian Tribes for permission to conduct this research on the Colorado River Indian Reservation, and to Chuck Lamb, Weldon Johnson, Curtiss Martin, and the staff at the Tribal Museum for friendship and logistical support during this study. Grateful appreciation is offered to Maureen Noonan, Scott Ritterbush and Tom Knapp for their patience and perseverance as field assistants. Thanks is also extended to the Rangers and staff of Buckskin Mountain State Park for their kind hospitality during my field studies. Helpful discussions, both in the field and elsewhere, with Steve Reynolds, Jon Spencer, Clark Burchfiel, Kip Hodges, Bruce Bryant, Paul Stone, and Bryan Kriens greatly aided my understanding of the geology of the Moon Mountains area. This research was supported primarily through the generosity of Professor B.C. Burchfiel and the resources of his Schlumberger Chair at M.I.T.

REFERENCES

Buising, A.V., 1987, Mio-Pliocene depositional and tectonic evolution of the lower Colorado River area [abs.]: Geol. Soc. Amer. Abs. Progs., v. 19, no. 7, p. 605.

Buising, A.V., 1988, Contrasting subsidence histories, northern and southern proto-Gulf of California: Implications for proto-Gulf tectonic models [abs.]: Geol. Soc. Amer. Abs. Progs., v. 20, no. 3, p. 146-147.

Davis, G.A., 1980, Problems of intraplate extensional tectonics, western United States *in* Continental Tectonics: National Research Council, National Academy of Sciences, p. 45-89.

Davis, G.A., Anderson, J.L., Frost, E.G., and Shackelford, T.J., 1980, Mylonitization and detachment faulting in the Whipple-Buckskin-Rawhide Mountains terrane, southeastern California and western Arizona, *in* Crittenden, M.D., Jr., Coney, P.J., and Davis, G.H., eds., Cordilleran Metamorphic Core Complexes: Geol. Soc. Am. Mem. 153, p. 79-129.

Davis, G.H., 1980, Structural characteristics of metamorphic core complexes, southern Arizona, *in* Crittenden, M.D., Jr., Coney, P.J., and Davis, G.H., eds., Cordilleran Metamorphic Core Complexes: Boulder, Colorado, Geol. Soc. Amer., Inc., Geol. Soc. Am. Mem. 153, p. 35-77.

Frost, E.G., and Martin, D.L., 1982, *in* Frost, E.G., and Martin, D.L., eds., Mesozoic-Cenozoic Tectonic Evolution of the Colorado River Region, California, Arizona, and Nevada: San Diego, California, Cordilleran Publishers, 608 p.

Frost, E.G., and Okaya, D.A., in prep, Structural and tectonic elements of extensional crust in CALCRUST seismic profiles, Mojave-Sonoran Desert: Tectonics.

Frost, E.G., and Okaya, D.A., 1985, Geometry of detachment faulting in the Old Woman-Turtle-Sacramento-Chemehuevi Moutains Region of SE California: EOS, Trans. Am. Geophys. Un., v. 66, p. 46, 978.

Frost, E.G., Okaya, D.A., McEvilly, T.V., Hauser, E.C., Galvan, G.S., McCarthy, J., Fuis, G.S., Conway, C.M., Blom, R.G., and Heidrick, T.L., 1987, Crustal transect: Colorado Plateau-detachment terrane-Salton Trough, *in* Davis, G.H., and VandenDolder, E.M., eds., Geologic Diversity of Arizona and Its Margins: Excursions to Choice Areas: Tucson, Arizona, Ariz. Bur. Geol. Min. Tech., Field Trip Guidebook, 100th Ann. Mtg. , p. 398-422.

Hamilton, W., 1982, Structural evolution of the Big Maria Mountains, northeastern Riverside County, southeastern California, *in* Frost, E.G., and Martin, D.L., eds., Mesozoic-Cenozoic Tectonic Evolution of the Colorado River Region, California, Arizona, and Nevada: San Diego, California, Cordilleran Publishers, p. 1-27.

Hauser, E.C., Gephart, J., Latham, T., Oliver, J., Kaufman, S., Brown, L., and Lucchitta, I., 1987, COCORP Arizona transect: Strong crustal reflections and offset moho beneath the transition zone: Geology, v. 15, p. 1103-1106.

Howard, K.A., and John, B.E., 1987, Crustal extension along a rooted system of imbricate low-angle faults; Colorado River extensional corridor, California and Arizona, *in* Coward, M.P., Dewey, J.F., and Hancock, P.L., eds., Continental Extensional Tectonics: Geological Society of London Special Publication 28, p. 299-311.

Knapp, J.H., and Heizler, M.T., 1988a, $^{40}Ar/^{39}Ar$ geochronology of crystalline thrust nappes of the Late Cretaceous Maria fold and thrust belt, west-central Arizona [abs.]: Geol. Soc. Amer. Abs. Progs., v. 20, no. 3, p. 173.

Knapp, J.H., and Heizler, M.T., 1988b, Tertiary thermal history of west-central Arizona: Implications for mechanisms of crustal extension [abs.]: Geol. Soc. Amer. Abs. Progs., v. 20, no. 7, p. A16-A17.

Martin, D.L., Krummenacher, D., and Frost, E.G., 1982, K-Ar geochronologic record of Mesozoic and Tertiary tectonics of the Big Maria-Little Maria-Riverside Mountains terrane, *in* Frost, E.G., and Martin, D.L., eds., Mesozoic-Cenozoic Tectonic Evolution of the Colorado River Region, California, Arizona, and Nevada: San Diego, California, Cordilleran Publishers, p. 518-549.

Metzger, D.G., 1968, The Bouse Formation (Pliocene) of the Parker-Blythe-Cibola area, Arizona and California: U.S. Geol. Survey Prof. Paper 600-D, p. D126-D136.

Reynolds, S.J., 1982, Multiple deformation in the Harcuvar and Harquahala Mountains, west-central Arizona, *in* Frost, E.G., and Martin, D.L., eds., Mesozoic-Cenozoic Tectonic Evolution of the Colorado River Region, California, Arizona, and Nevada: San Diego, California, Cordilleran Publishers, p. 137-142.

Reynolds, S.J., and Rehrig, W.A., 1980, Mid-Tertiary plutonism and mylonitization, South Mountains, central Arizona, *in* Crittenden, M.D., Jr., Coney, P.J., and Davis, G.H., eds., Cordilleran Metamorphic Core Complexes: Boulder, Colorado, Geol. Soc. Amer., Inc., Geol. Soc. Am. Mem. 153, p. 159-175.

Reynolds, S.J., Florence, F.P., Welty, J.W., Roddy, M.S., Currier, D.A., Anderson, A.V., and Keith, S.B., 1986, Compilation of Radiometric Age Determinations in Arizona: Ariz. Bur. Geol. Min. Tech. Bull. 197, p. 258.

Reynolds, S.J., Richard, S.M., Haxel, G.B., Tosdal, R.M., and Laubach, S.E., 1988, Geologic setting of Mesozoic and Cenozoic metamorphism in Arizona, *in* Ernst, W.G., ed., Metamorphism and Crustal Evolution of the Western United States (Rubey Volume VII): Englewood Cliffs, New Jersey, Prentice-Hall, p. 466-501.

Reynolds, S.J., Spencer, J.E., and DeWitt, E., 1987, Stratigraphy and U-Th-Pb geochronology of Triassic and Jurassic rocks in west-central Arizona, *in* Dickinson, W.R., and Klute, M.A., eds., Mesozoic Rocks of Southern Arizona and Adjacent Areas: Arizona Geological Society Digest 18, p. 65-80.

Reynolds, S.J., Spencer, J.E., Richard, S.M., and Laubach, S.E., 1986, Mesozoic structures in west-central Arizona, *in* Beatty, B., and Wilkinson, P.A.K., eds., Frontiers In Geology and Ore Deposits of Arizona and the Southwest: Arizona Geological Society Digest 16, p. 35-51.

Spencer, J.E., Reynolds, S.J., Anderson, J.L., Davis, G.A., Laubach, S.E., Richard, S.M., and Marshak, S., 1987, Field-trip guide to parts of the Harquahala, Granite Wash, Whipple, and Buckskin Mountains, west-central Arizona and southeastern California, *in* Davis, G.H., and VandenDolder, E.M., eds., Geologic Diversity of Arizona and Its Margins: Excursions to Choice Areas: Tucson, Arizona, Ariz. Bur. Geol. Min. Tech., Field Trip Guidebook, 100th Ann. Mtg. , p. 351-364.

Spencer, J.E., and Reynolds, S.J., in press, Middle Tertiary tectonics of Arizona and adjacent areas, *in* Jenny, J.P., and Reynolds, S.J., eds., Geologic evolution of Arizona: Arizona Geological Society Digest 17.

Tosdal, R.M., Haxel, G.B., and Wright, J.E., in press, Jurassic geology of the Sonoran Desert region, southern Arizona, southeastern California, and northernmost Sonora: Construction of a continental-margin magmatic arc, *in* Jenny, J.P., and Reynolds, S.J., eds., Geologic evolution of Arizona: Arizona Geological Society Digest 17.

Walker, J.D., 1985, Permo-Triassic paleogeography and tectonics of the southwestern United States: Ph.D. dissertation, Cambridge, M.I.T., 224 p.

Walker, J.D., 1988, Permian and Triassic rocks of the Mojave Desert and their tectonic implications for timing and mechanisms of continental truncation: Tectonics, v. 7, p. 685-709.

Wilson, E.D., Moore, R.T., and Cooper, J.R., 1969, Geologic map of Arizona: Arizona Bureau of Mines and U.S. Geol. Survey, scale 1:500,000.

Yeats, K.J., 1985, Geology and structure of the northern Dome Rock Mountains, La Paz County, Arizona: M.S. thesis, Tucson, Univ. of Arizona, 123 p.

FIGURE CAPTIONS

Plate 2-1: Geologic map of the Moon Mountains, Colorado River Indian Reservation, scale 1:24,000 (xerox reduced version).

Plate 2-2: Geologic cross sections of the Moon Mountains, scale 1:24,000, no vertical exaggeration.

Plate 2-3: Detailed geologic map of the Valenzuela area, southeastern Moon Mountains, scale ~1:12,000.

Figure 2.1: Location map of the Moon Mountains in the Mojave-Sonoran Desert area.

Figure 2.2: Geologic sketch map of the Moon Mountains, showing major structures, distribution of rock units, and geographic names used in text.

Figure 2.3: Augen gneisses typical of Valenzuela crystalline assemblage, showing well-developed fabric defined by flattened and aligned K-feldspar porphyroclasts. Predominant shear sense is not evident in rocks of this lithology. Lens cap for scale.

Figures 2.4a and b: Panoramic view of the Valenzuela area, southern Moon Mountains, showing (1) Valenzuela metasedimentary section (right side 4a), (2) Valenzuela Thrust fault (center), and (3) El Diablo peak (left side 4b). Thrust fault is marked by contact of dark resistant cap of Jqs with more recessive units of metasedimentary section, just above distinctive ledge of light-colored marble. Southeast-dipping Graveside fault trends up major drainage (center of 4b), and separates exposures of the Valenzuela thrust from El Diablo peak, which is extensively intruded by garnet-bearing pegmatites. Note (1) discordance of marble unit with underlying units of Valenzuela metasedimentary section (right of 4a), (2) discordance of west-dipping foliation in gneisses of hanging wall with trace of thrust, and (3) relative absence of pegmatite dikes to east (right) of Graveside fault as compared to El Diablo peak on the west. View spans NE to E. Northern Plomosa Mountains.visible in distance. Exposed relief is approximately 150 m.

Figure 2.5: Basal calc-silicate unit of Valenzuela metasedimentary sequence, with lenses of pure, vitreous quartzite floating in a fine-grained matrix of quartz + potassium feldspar + biotite + epidote ± muscovite. Hinges of rootless isoclinal folds are preserved in the quartz bands, which are interpreted as deformed quartzite pebbles and cobbles. Lens cap for scale.

Figure 2.6: Fold hinges of rootless isoclines developed in thinly-bedded quartzite of Valenzuela metasedimentary section, below Valenzuela thrust fault, southern Moon Mountains. View is toward the ESE; hammer for scale.

Figure 2.7: Well-developed S-C fabric in Jurassic quartz syenite of hanging wall of Valenzuela thrust, indicating top-to-the-north (right) shear sense. S surfaces are sub-horizontal, sygmoidal in cross–section, and cut by c planes which dip gently to the right. Hammer for scale.

Figure 2.8: View of garnet-bearing, granitic pegmatite dikelets which intrude discordantly across metamorphic foliation in amphibolite schists of Valenzuela crystalline assemblage, but are cut by N-dipping shear planes which appear synchronous with the foliation development. Dikes are interpreted to be syn- to late-kinematic with development of this fabric, which indicates a top-to-the-N (left) sense of shear. Footwall of Valenzuela Thrust fault. Lens cap for scale.

Figure 2.9: Detail of intrusive contact of porphyritic biotite granite with foliated gneisses formed from megacrystic quartz syenite. Undulatory contact is discordant to foliation in gneisses of country rock, and granite has only poorly developed fabric here. Southern margin of main body of porphyritic granite, southern Moon Mountains. Lens cap for scale.

Figure 2.10: Contact of hornblende-biotite granite (upper left) and biotite granite (lower right) in central Moon Mountains, marked by line of dark to light color contrast running from left center to upper right. Relief is about 180 m.

Figure 2.11: Moon Mountain detachment as exposed in Detachment Wash, just south of Moon Mountain Rocks in hanging wall are massively bedded, unsorted, angular, monolithic conglomerates derived from quartz porphyry. Footwall gneisses are highly sheared and retrograded rocks of the Moon Mountain crystalline assemblage. Detachment dips ~40° NE. Daypack (just below center) for scale.

Figure 2.12: Intense ductile deformation developed within Jurassic quartz syenite (Jqs), southern Moon Mountains. White streaks of feldspar were originally potassium feldspar megacrysts. Lens cap for scale.

Figure 2.13: Deformed sygmoidal lens of granite within footwall gneisses of Moon Mountain detachment, clearly indicating a top-to-the-northeast (left) asymmetry of shear. Granitic dikes are related to intrusion of porphyritic biotite granite, which outcrops just to west at mouth of Detachment Wash. Hammer for scale.

Figure 2.14: Geologic sketch map of the southern Moon Mountains and the northern end of the Dome Rock Mountains. Mapping from this report and Yeats (1985). Units shown include (1) porphyritic biotite granite (Tyson Peak granite and Tyson Wash granite), (2) megacrystic Jurassic quartz syenite, (3) lower Mesozoic sedimentary rocks (Valenzuela metasedimentary section, Tung Hill metasedimentary section), (4) gneissic leucogranite, (5) Precambrian crystalline rocks, and (6) cratonal Paleozoic section.

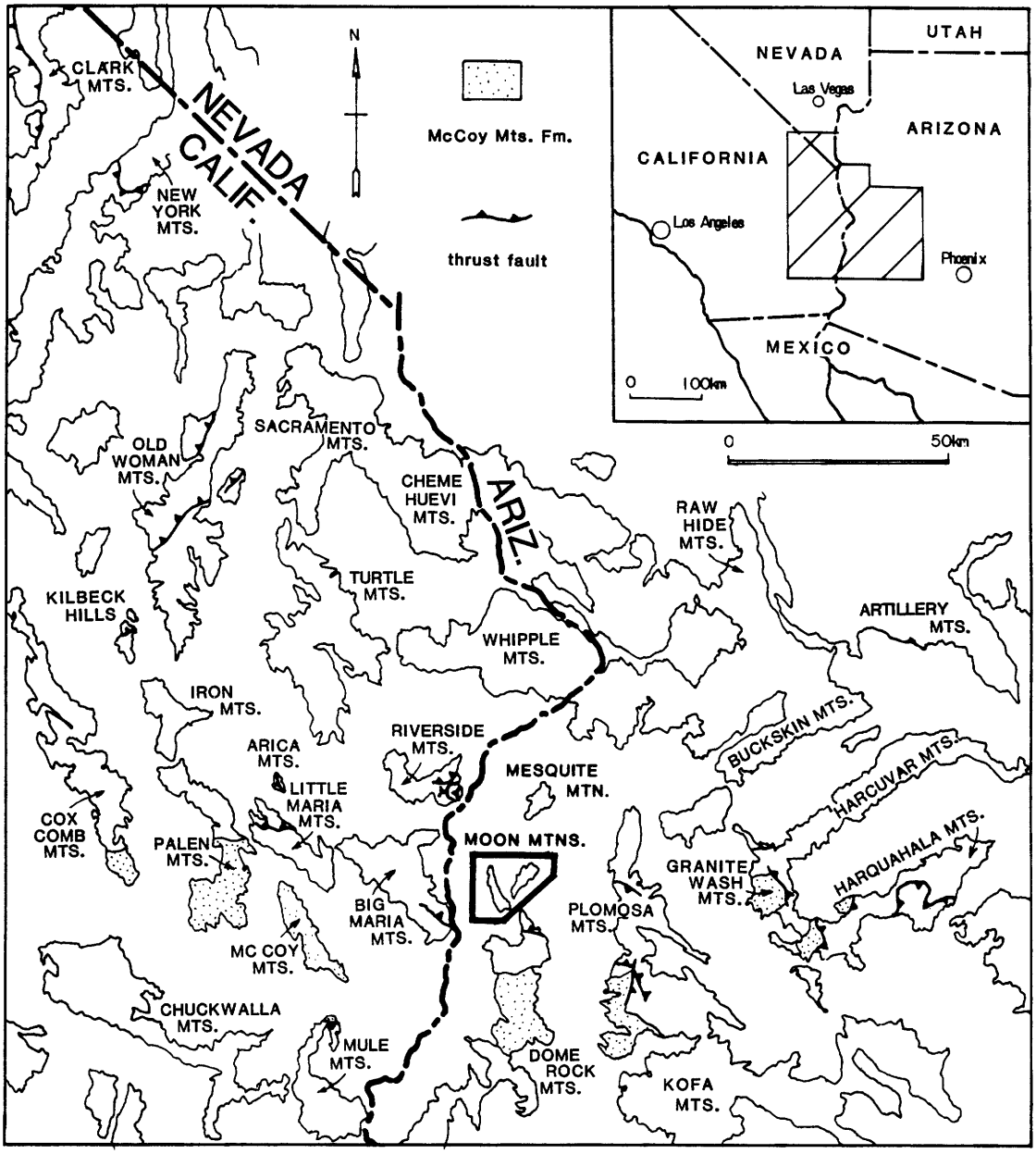
N
McCoy Mts. Fm.
thrust fault
NEVADA
CALIF.
ARIZ.
CLARK MTS.
NEW YORK MTS.
OLD WOMAN MTS.
SACRAMENTO MTS.
CHEME HUEVI MTS.
TURTLE MTS.
KILBECK HILLS
IRON MTS.
ARICA MTS.
LITTLE MARIA MTS.
COX COMB MTS.
PALEN MTS.
RIVERSIDE MTS.
MESQUITE MTN.
MOON MTNS.
BIG MARIA MTS.
MC COY MTS.
CHUCKWALLA MTS.
MULE MTS.
DOME ROCK MTS.
KOFA MTS.
PLOMOSA MTS.
GRANITE WASH MTS.
RAW HIDE MTS.
WHIPPLE MTS.
ARTILLERY MTS.
BUCKSKIN MTS.
HARCUVAR MTS.
HARQUAHALA MTS.
UTAH
NEVADA
Las Vegas
ARIZONA
CALIFORNIA
Los Angeles
Phoenix
MEXICO
0 100km
0 50km

Figure 2.1

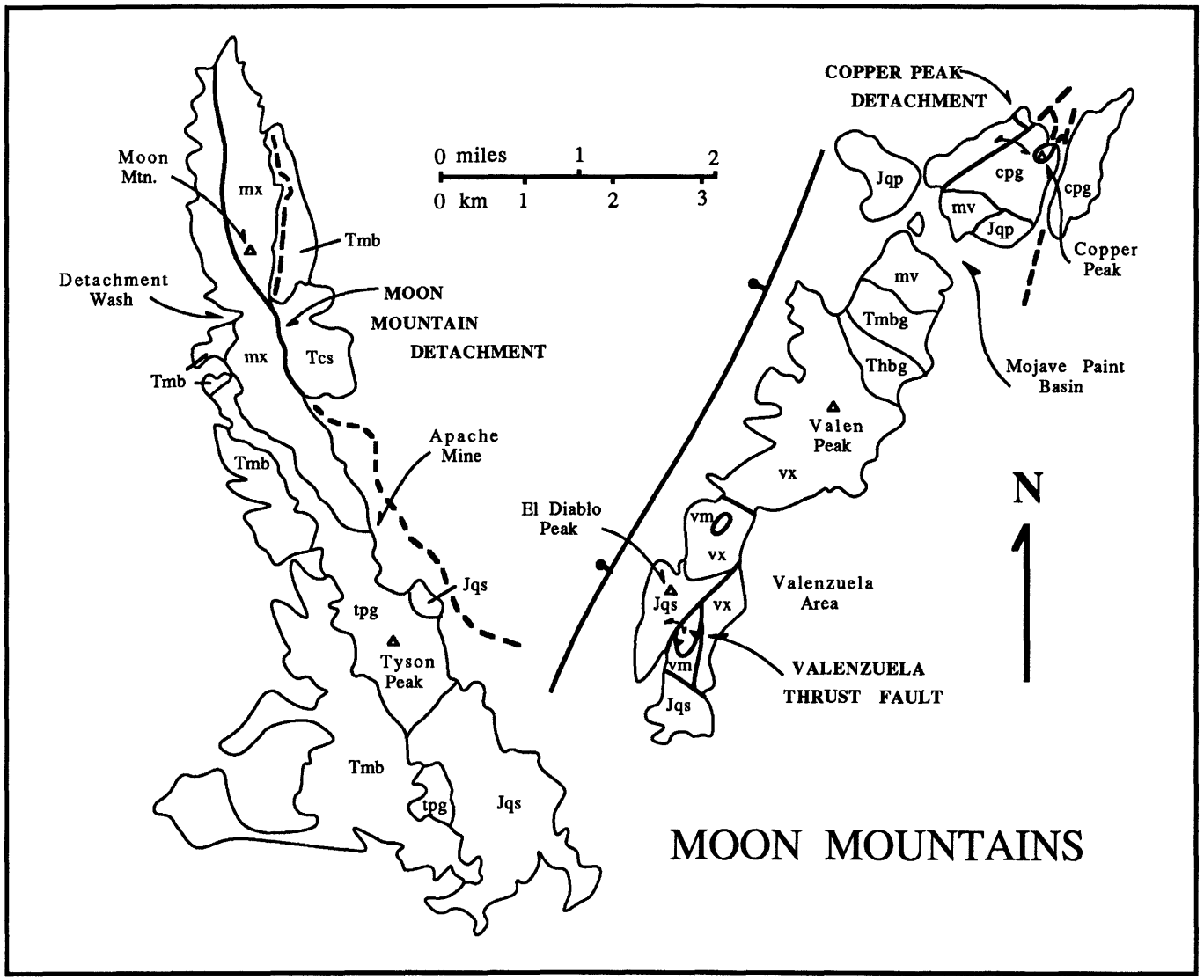
COPPER PEAK
DETACHMENT
Moon
Mtn.
mx
0 miles 1 2
0 km 1 2 3
Tmb
Detachment
Wash
MOON
MOUNTAIN
DETACHMENT
mx
Tcs
Tmb
Tmb
Apache
Mine
Jqs
tpg
Tyson
Peak
Tmb
tpg
Jqs
Jqp
cpg
cpg
mv
Jqp
Copper
Peak
mv
Tmbg
Thbg
Mojave Paint
Basin
Valen
Peak
vx
N
El Diablo
Peak
vm
vx
Valenzuela
Area
Jqs
vx
vm
VALENZUELA
THRUST FAULT
Jqs
MOON MOUNTAINS

Figure 2.2

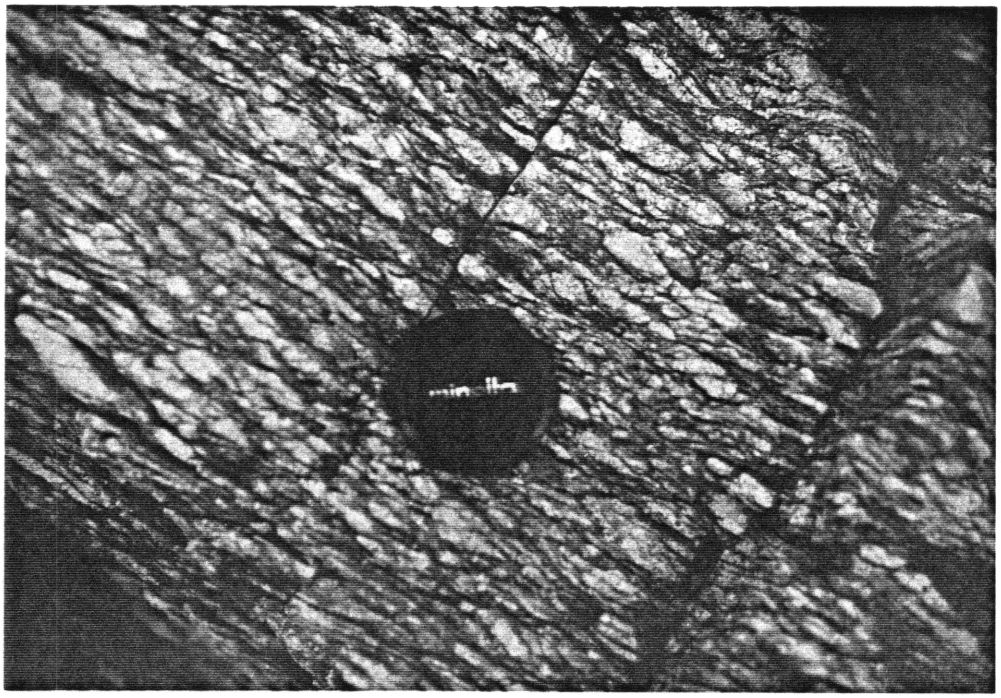

Figure 2.3

Figure 2.4a

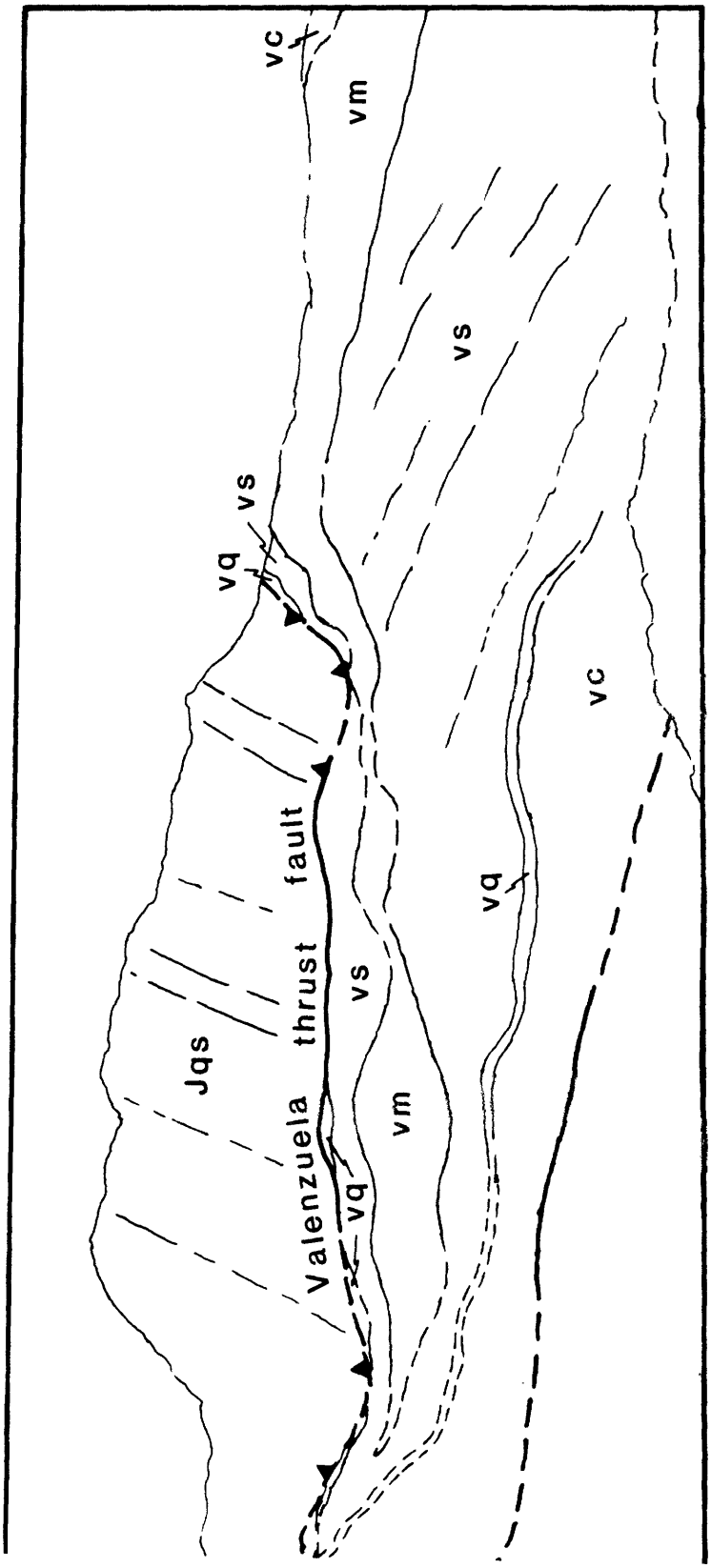

Figure 2.4a

Figure 2.4b

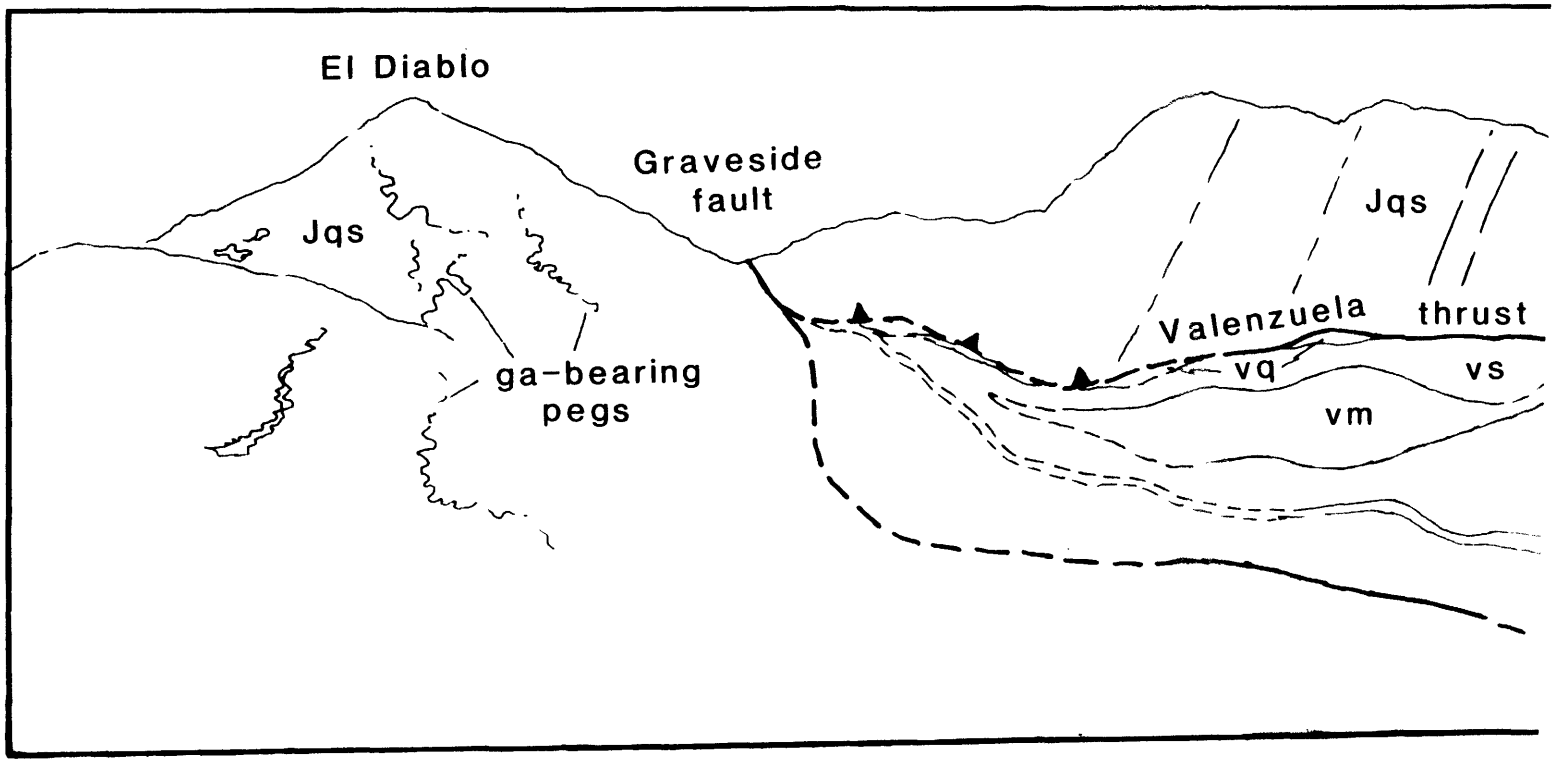
El Diablo
Graveside
fault
Jqs
Jqs
Valenzuela
thrust
vq
vs
vm
ga-bearing
pegs

Figure 2.4b

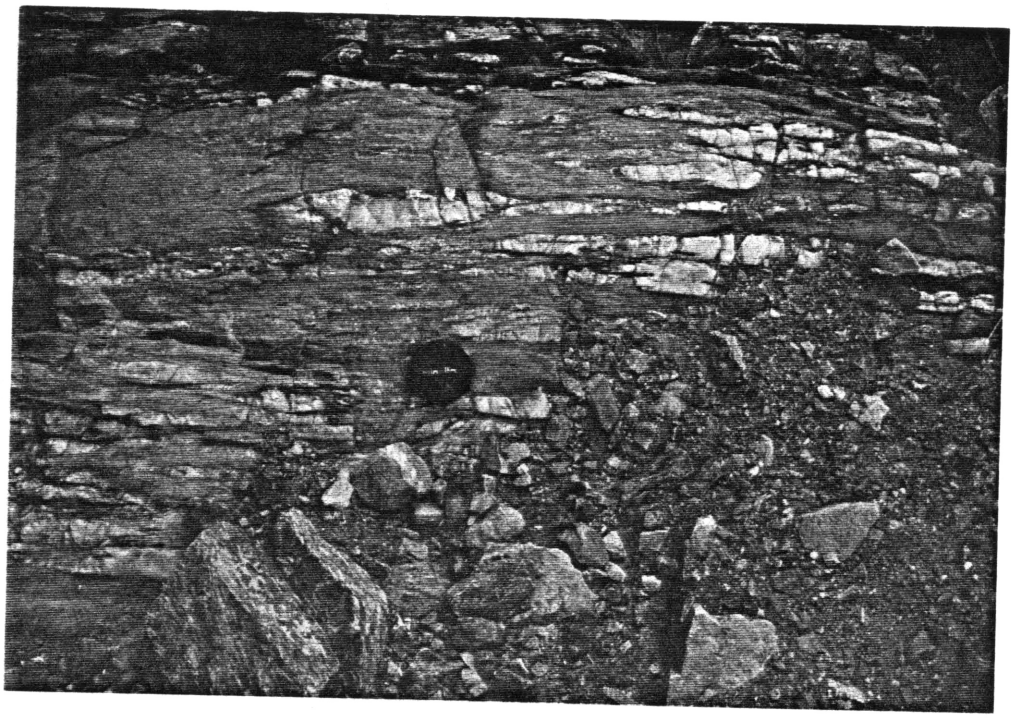

Figure 2.5

Figure 2.6

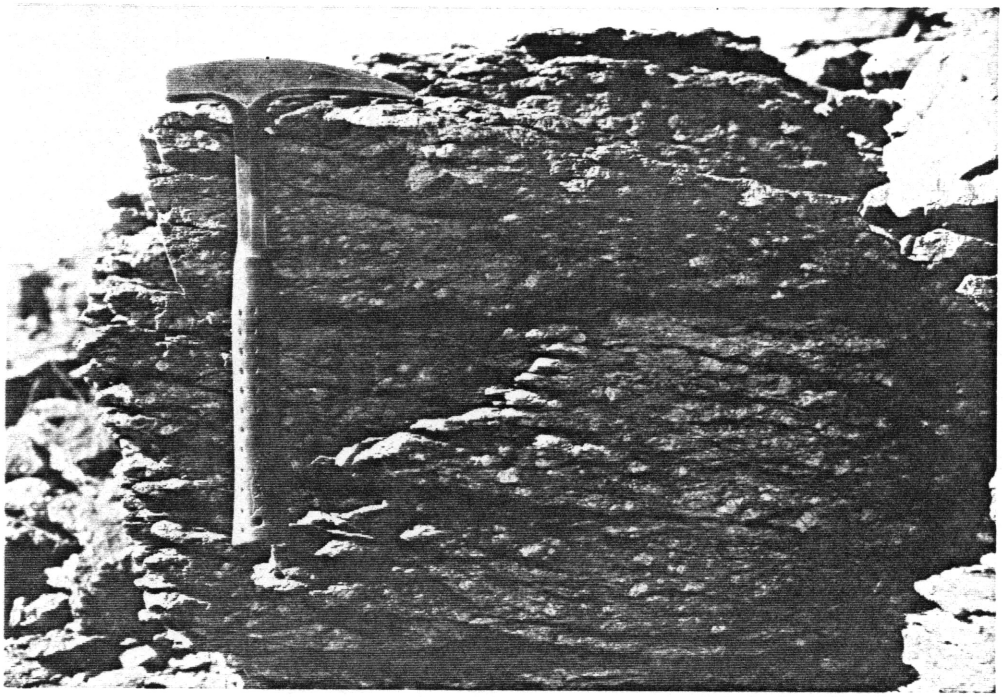

Figure 2.7

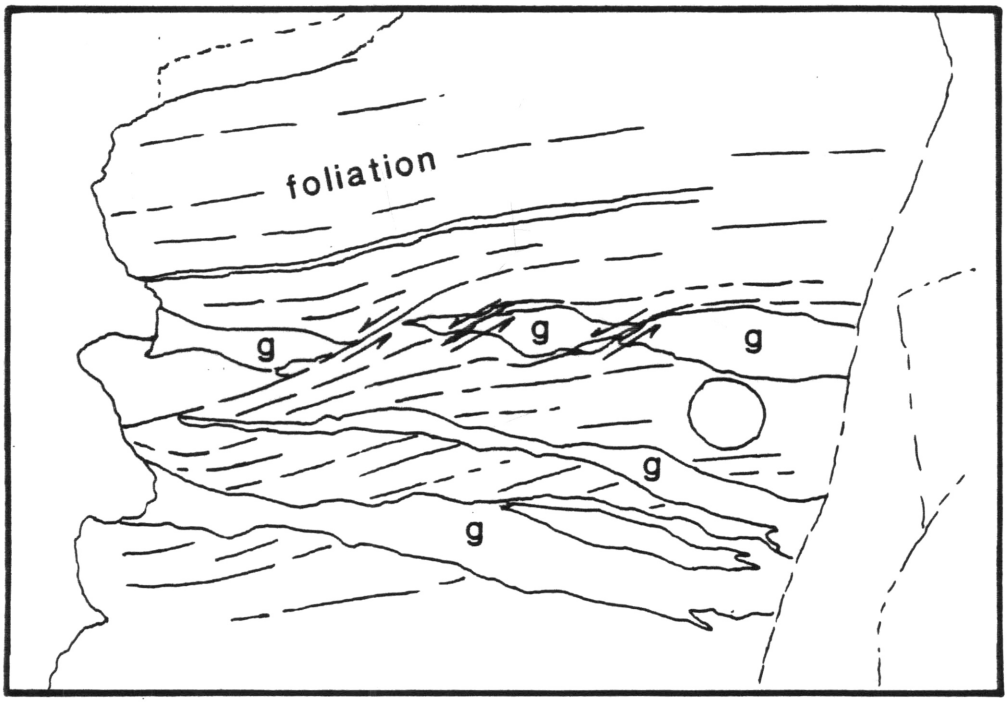

Figure 2.8

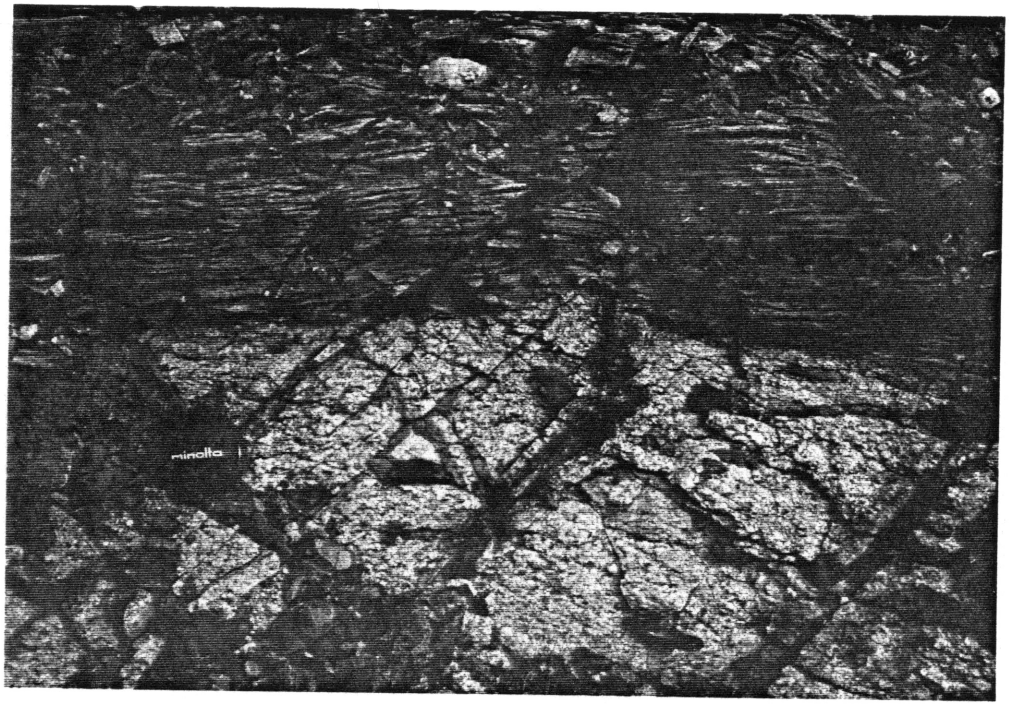

Figure 2.9

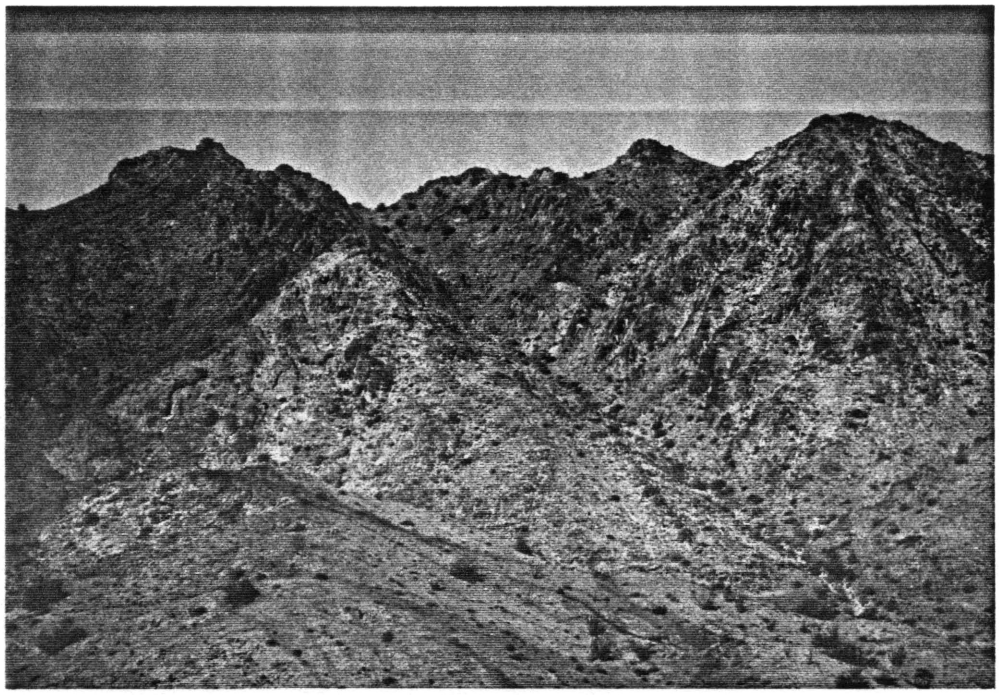

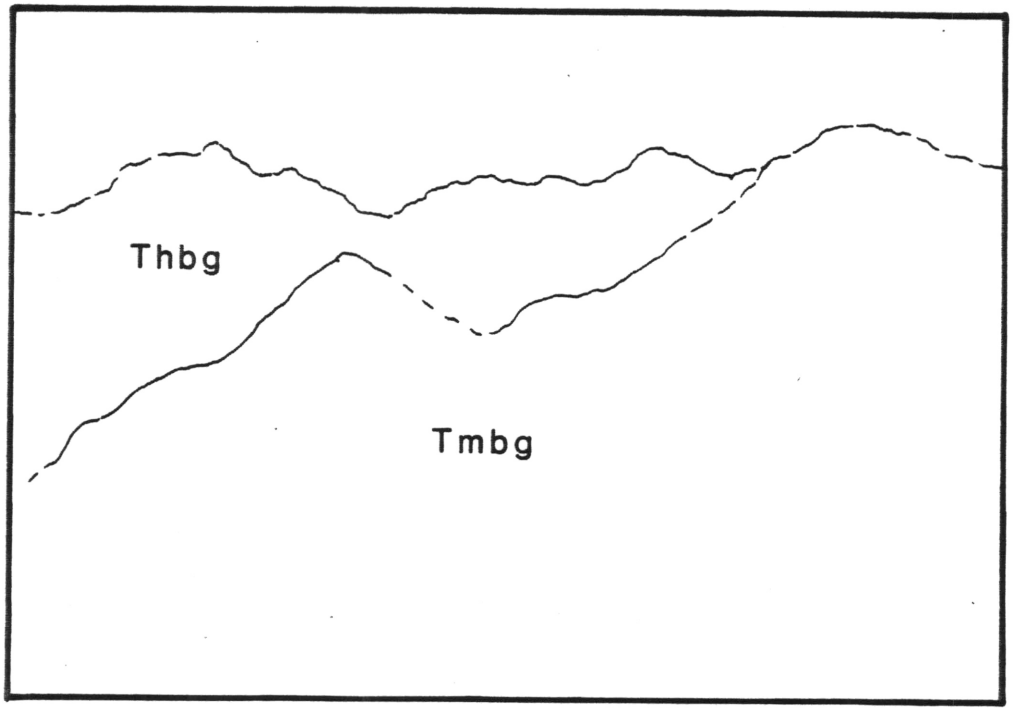

Figure 2.10

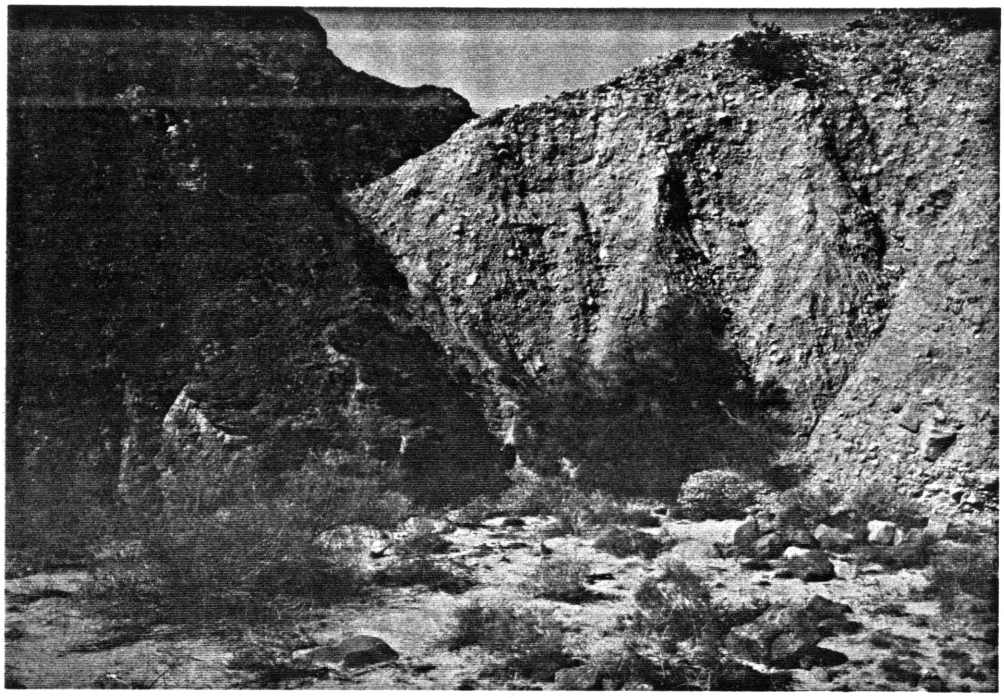

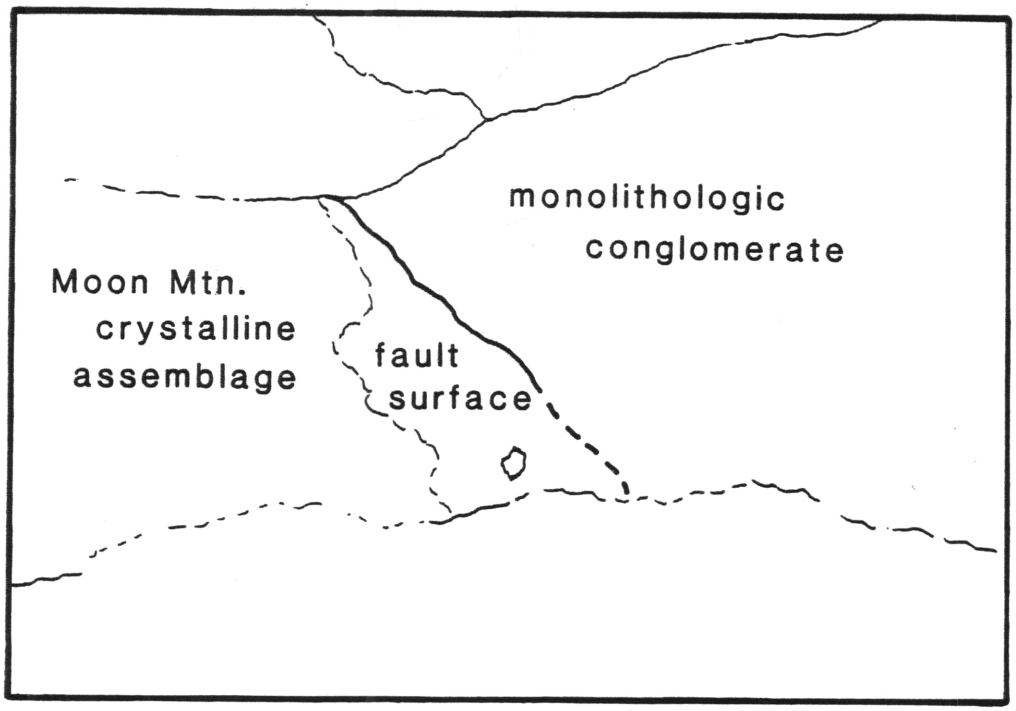
monolithologic
conglomerate
Moon Mtn.
crystalline
assemblage
fault
surface

Figure 2.11

Figure 2.12

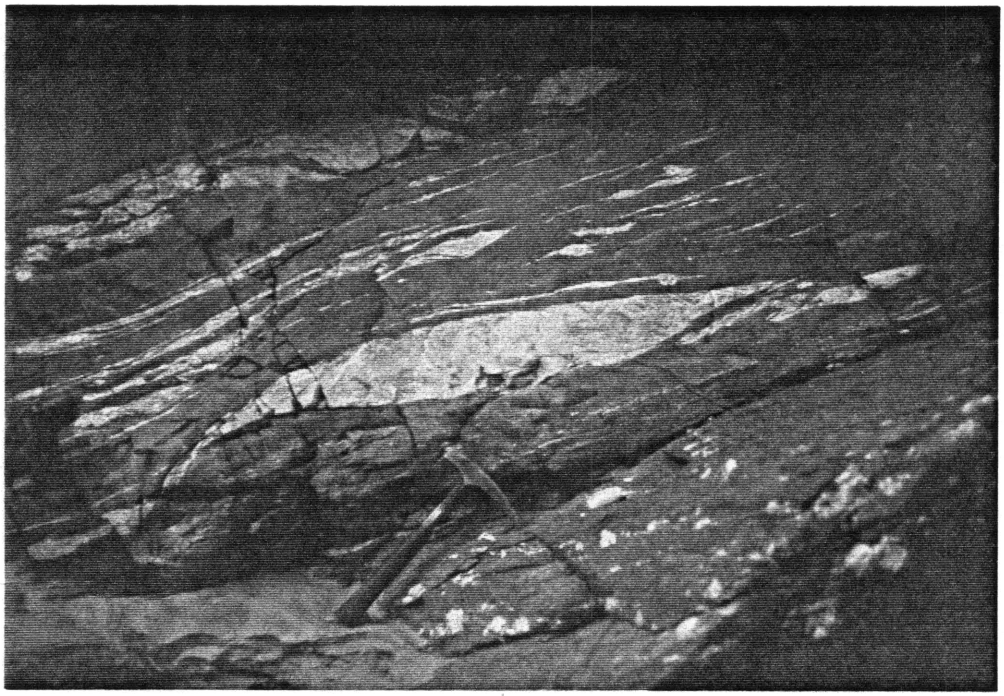

Figure 2.13

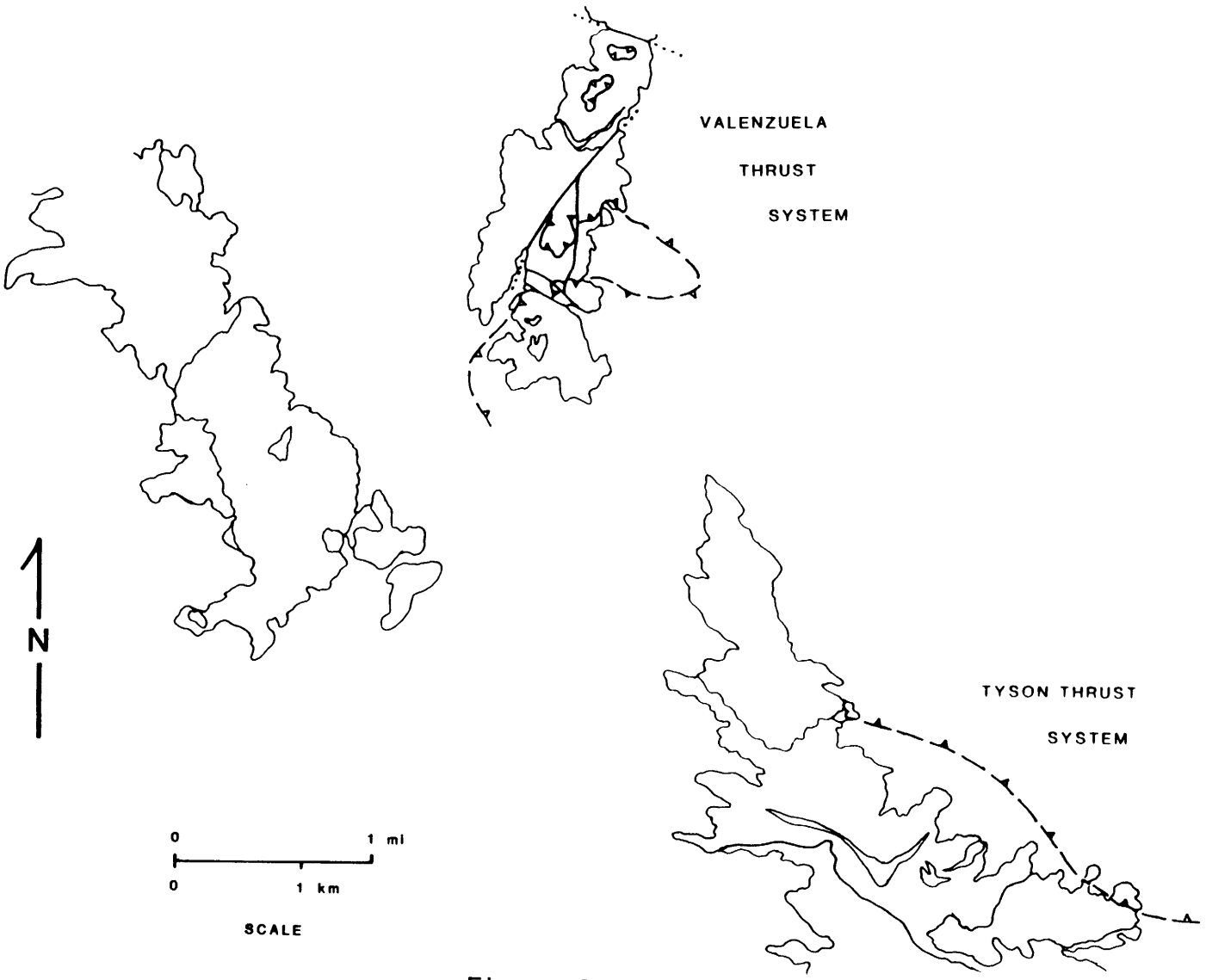
VALENZUELA
THRUST
SYSTEM
TYSON THRUST
SYSTEM
N
0
1 mi
0
1 km
SCALE

Figure 2.14

CHAPTER 3

THERMAL HISTORY OF CRYSTALLINE THRUST NAPPES OF THE MARIA FOLD AND THRUST BELT, WEST-CENTRAL ARIZONA

James H. Knapp and Matthew T. Heizler

ABSTRACT

The thermal history of crystalline rocks of west-central Arizona is characterized by three distinct phases since Late Cretaceous time. Results from $^{40}Ar/^{39}Ar$ step-heating analyses of mineral suites from crystalline thrust nappes of the Maria fold and thrust belt document regional heating of the crust during basement-involved thrusting and crustal thickening in the early Late Cretaceous (~80-90 Ma), followed by uplift and slow cooling (5-10°C/m.y.) throughout the latest Cretaceous and early Tertiary. Tectonic denudation associated with crustal extension in the late Oligocene-early Miocene resulted in rapid uplift and cooling of mid-crustal rocks in the footwall of the Whipple-Buckskin-Rawhide-Harcuvar detachment system. Potassium feldspars (Tc ~150-250°C) yield saddle-shaped release spectra with very consistent minimum apparent ages ranging from 28-22 Ma. These data are consistent with either of two models: (1) rapid exhumation of mid- to upper-crustal levels in the detachment terrain coincident with the time that the regional geothermal gradient cooled through closure of potassium feldspar to argon diffusion, or (2) a renewed thermal pulse, reaching > 150-200°C at the crustal levels presently exposed, associated with the early stages of extension and presumably related to the cause for crustal weakening.

Hornblende spectra indicate significant thermal heterogeneity within the region during Late Cretaceous time, which we interpret to reflect differing structural levels within the thrust belt. Data from the northern Plomosa Mountains suggest this area attained maximum temperatures of ~300°C during Cretaceous time, whereas surrounding areas record temperatures of ~450°C (northern Granite Wash Mountains) to >500°C (Mesquite Mountain) at this time. Both biotite and potassium feldspar release spectra imply that the northern Plomosa area could not have remained above closure temperatures for argon diffusion in these phases throughout the early Tertiary, yet these potassium feldspars exhibit pronounced argon loss at ~26 Ma. Steep gradients on several potassium feldspar spectra may be related to excess argon in highly retentive crystallographic sites, but one well-behaved potassium feldspar strongly suggests that these gradients are attributable to episodic argon loss rather than protracted cooling. Evidence of a consistent Tertiary thermal signature throughout the region, including areas which do not possess Tertiary fabrics or igneous rocks, suggests the crustal geotherm was elevated regionally during the onset of extension.

INTRODUCTION

The thermal structure and evolution of the continental lithosphere has become an important area of research. In particular, the thermal response of the crust to thrusting and thickening during orogenesis has been the focus of a number of studies in collisional belts (for example, England and Thompson, 1984; Selverstone et al., 1984; Hodges and Royden, 1984). While such studies have demonstrated that basement-involved thrusts have a dominant effect in the thermal evolution of collisional terrains, Andean-type orogens have largely been overlooked in this respect.

The Maria fold and thrust belt of the Mojave-Sonoran Desert area is a region of basement-involved deformation within the Cordilleran thrust belt of western North America. The presence of a number of crystalline thrust nappes here provides a unique opportunity to address the role of basement-involvement in the thermal evolution of an Andean-type orogen. In addition, the Mojave-Sonoran Desert region has been the locus of profound continental extension, which has directly overprinted structures and fabrics associated with several different, as yet unresolved, compressional episodes. Use of $^{40}Ar/^{39}Ar$ analysis affords the opportunity to assess the thermal consequences of these various deformational and metamorphic episodes in an area where more conventional

means of analysis have been hindered by lack of sufficient structural, petrologic, and geochronologic data.

LOCATION AND GEOLOGIC BACKGROUND

The Maria fold and thrust belt (as first defined by Reynolds et al., 1986) is an east-west trending segment of deformation within the Mesozoic Cordilleran thrust belt of western North America (Fig. 3.1), which extends some 250 km along strike from the Coxcomb Mountains in southeastern California to the Harquahala Mountains of west-central Arizona (Fig. 3.2). Included within this deformational belt are all or parts of the Palen, Mc Coy, Big Maria, Little Maria, Riverside, Mesquite, Moon, Dome Rock, Buckskin, Plomosa, Granite Wash, Harcuvar, Little Harquahala, and Harquahala Mountains (Fig. 3.2).

Within this belt of Mesozoic deformation, a number of major thrust faults place Proterozoic and Mesozoic crystalline rocks above Mesozoic and Paleozoic strata, with evidence for multiple episodes of deformation. Reynolds et al. (1986) describe a set of large, southeast- to south-vergent folds and locally associated thrusts which are discordantly cut by thrusts that verge southwest, south, north, and northeast, and interleave Paleozoic and Mesozoic sedimentary rocks with crystalline rocks. The sense of vergence of these structures not only varies considerably within the Maria fold and thrust belt, but deviates significantly from the consistent eastward vergence which characterizes the Cordilleran thrust belt throughout much of its length (Fig. 3.1).

The predominantly east-west strike of the Maria fold and thrust belt is perpendicular to the northerly trend of the Mesozoic thrust belt extending south from Canada. In the region of extensive Laramide deformation to the east in Colorado and New Mexico, structural trends strike generally north-south. Here, at the same latitude as the Maria fold and thrust belt, eastward vergence of large basement uplifts is inferred to have resulted from east-west convergence of the North American and Farallon plates in Late Cretaceous through early Tertiary time (Tweto, 1975).

Similarly, the Maria fold and thrust belt lies at an oblique orientation to the zone of Sevier-age and earlier deformation projecting southward from Utah and southern Nevada. The Sevier thrust belt, characterized by imbricate east-vergent thrust sheets within Paleozoic and Mesozoic strata, displays the thin-skinned, décollement style of deformation typical of the thrust belt further along strike to the north in the U.S. and

Canada, and to the south in Mexico. Work in recent years has extended the Sevier thrust belt from southern Nevada into the ranges of southeastern California in the Mojave region (Burchfiel and Davis, 1971, 1977; Miller et al., 1982). The southernmost known extent of this zone consists of a northeast-striking, southeast-vergent, basement-cored thrust nappe in the Old Woman Mountains of the central Mojave Desert (Miller et al., 1982; Fig. 3.2). Hoisch et al. (1988) argue for a Late Cretaceous age of deformation and associated metamorphism.

A number of factors have been cited as the cause for the distinctive region of basement-involved thrusting in the Mojave-Sonora area of the southwestern Cordillera. Burchfiel and Davis (1975, 1981) argued that the southwestern edge of the North American plate was truncated by several events in late Paleozoic and Mesozoic time, thus exposing the edge of the craton before the initiation of subduction-dominated tectonics during Mesozoic time (see also Walker, 1985, 1987). Facies of Paleozoic platform carbonates are transitional from a thick miogeoclinal sequence to a relatively thin cratonal (Grand Canyon) section within the Mojave-Sonora area. Basement-involved deformation is thought to have resulted from the lack of a thick Paleozoic miogeoclinal wedge with associated anisotropies (Burchfiel and Davis, 1975). These same authors propose a model for Mesozoic deformation in the western Cordillera whereby intracratonal westward underthrusting along the western edge of North America resulted in large part from heating and softening of the crust through extensive arc magmatism. Consequently, deformation was localized at the ductility transition from the relatively hot arc terrain in the west to the comparatively cool cratonal crust in the east.

Other workers (Miller et al., 1982; Hoisch et al., 1988) have argued that deformation and accompanying metamorphism largely preceded magmatic activity at mid- to upper-crustal levels. Hoisch (1985) concludes that in the Big Maria Mountains of southwestern California, synkinematic metamorphism resulted from circulation of large volumes of hot fluids rather than conductive cooling from plutonism. Similarly, in the Old Woman Mountains, post-kinematic granitic plutons derived from crustal anatexis were emplaced after the thermal peak of metamorphism (Miller et al., 1982). Recent studies in western Arizona (e.g. Reynolds et al., 1986) suggest that deformation and metamorphism in the basement-involved terrain typically pre-dated intrusion of large volumes of granitic magma.

Most work within the Maria fold and thrust belt has been concentrated within the past two decades. Hamilton (1964) was one of the earliest workers in this area to

recognize basement-involved Mesozoic deformation, and Reynolds et al. (1980) first described overthrusts of crystalline nappes in the eastern end of the Maria fold and thrust belt. Pelka (1973), Harding (1982), and Harding and Coney (1985), conducted detailed studies on the Mesozoic McCoy Mountains Formation. Mapping efforts within the Maria fold and thrust belt have included: LeVeque (1982) in the Palen Mountains; Emerson (1982) in the Little Maria Mountains; Ellis (1982), and Hamilton (1984) in the Big Maria Mountains; Carr and Dickey (1980), and Lyle (1982) in the Riverside Mountains; Miller (1970), Scarborough and Meader (1983), Stoneman (1985), and Davis (1985) in the Plomosa Mountains; Yeats (1985) in the Dome Rock Mountains; Richard (1983), and Spencer et al. (1985) in the Little Harquahala Mountains; Laubach (1986) in the Granite Wash Mountains; and Cunningham (1986) in the northern Granite Wash Mountains. Reynolds et al. (1986) provide a useful summary of the Arizona portion of the Maria fold and thrust belt.

The age of deformational events in the Maria fold and thrust belt is not well-constrained. Most of the deformation is known to involve the Mesozoic McCoy Mountains Formation and its equivalents. This thick section of volcaniclastic and sedimentary rocks parallels the strike of the Maria fold and thrust belt in a west-northwest - east-southeast linear trough (Fig. 3.2). However, the age of these sedimentary rocks and the tectonic setting of the depositional basin remains controversial. Based on inferred interbedding of the basal McCoy Mountains Formation with underlying Jurassic volcanic rocks, and paleomagnetic data from the lower McCoy Mountains Formation, Harding et al. (1983), and Harding and Coney (1985) argued that the McCoy Mountains Formation was deposited and deformed in rapid succession prior to late Middle to early Late Jurassic time. Other workers have proposed a post-mid-Cretaceous age for the McCoy Mountains Formation based on the presence of fossilized angiosperm wood in the upper part of the section (Pelka, 1973; Hamilton, 1982). Stone et al. (1987) argue convincingly for an early Late-Cretaceous age for at least the upper, fossil-bearing part of the McCoy Mountains Formation. An upper bound is placed on the deformation in the Granite Wash and Little Harquahala Mountains by Late Cretaceous plutons which are undeformed (Reynolds et al., 1986).

Crystalline rocks of the Maria fold and thrust belt are ideally suited for $^{40}Ar/^{39}Ar$ thermochronology analysis. These lithologies possess a variety of potassium-bearing minerals, including hornblende, biotite, muscovite, and potassium feldspar. In many cases, coexisting phases can be recovered from the same sample, insuring consistency in

the deformational and thermal history the minerals experienced. Closure temperatures for the argon isotopic system have been determined both empirically and experimentally. For the present study, the following approximate closure temperatures are assumed: hornblende, 500°C (Harrison, 1981); muscovite, 350°C (Harrison and McDougall, 1981); biotite, 300°C (Harrison et al., 1985); and potassium feldspar, 150-200°C (Harrison and McDougall, 1982; Harrison and Bé, 1983). These values are derived with geologically reasonable cooling rates in a slowly-cooled, regional metamorphic terrain (5-10°C/Ma). This suite of minerals provides a temperature range from ~500°C to ~150°C in tracking the cooling history of the crust following heating associated with thrusting and crustal thickening.

Previous studies addressing the thermal history of the Mojave-Sonora region of southeastern California and western Arizona are few in number, and most have been presented within the last two years. Hoisch et al. (1988) presented evidence for Late Cretaceous metamorphism in the Big Maria, Old Woman, and Piute Mountains of southeastern California. Several $^{40}Ar/^{39}Ar$ analyses indicate resetting of hornblende between 70 to 80 Ma and subsequent rapid cooling based on only slightly discordant ages for muscovite and biotite. Thermobarometric studies by these workers produced temperatures estimates ranging from ~450 to 600°C and pressure determinations corresponding to depths ranging from 9 to greater than 12 km (see Hoisch et al., 1988) during Late Cretaceous syntectonic metamorphism in southeastern California. Richard and Fryxell (in prep.) discuss results of $^{40}Ar/^{39}Ar$ analysis from the Buckskin, Rawhide, Harcuvar, and Harquahala Mountains to the east of the study area described here. Foster (in prep.) presents $^{40}Ar/^{39}Ar$ data from the eastern Mojave region, including the Old Woman, Piute, Turtle, Chemehuevi, Sacramento, Marble, and Ship Mountains (see Fig. 3.2).

Samples for this study were collected from areas within five different mountains or ranges in west-central Arizona in an attempt to develop a regional understanding of the thermal history of the Maria fold and thrust belt (Fig. 3.3). The study area covers more than 2,000 km^2 within the central portion of the Maria fold and thrust belt, where numerous basement-involved structures of Mesozoic age have been identified (see Reynolds et al., 1986 for a review). A brief discussion of the geologic setting for each of the five areas is presented below, working from west to east across the study area.

MESQUITE MOUNTAIN

Mesquite Mountain is located on the Colorado River Indian Reservation (Figs. 3.3 and 3.4), where bedrock exposures consist primarily of deformed, migmatitic gneiss (the Mesquite Gneiss) and lesser amounts of intrusive and metasedimentary rocks (Knapp, in prep.). Rocks of this area record a polydeformational history characterized by a continuous progression from penetrative, mylonitic deformation to successively more localized, brittle faulting in the footwall of the Whipple-Buckskin-Rawhide detachment system (Knapp, 1988). Granitic material, both developed *in situ* and derived and injected from lower crustal levels, makes up to 30-40 volume % of the gneiss. U-Pb zircon analysis from concordant granitic sills in the Mesquite Gneiss indicate a latest Cretaceous age (67.2 ± 1.4 Ma) of injection and migmatization (Knapp and Walker, in prep). Deformation, partial melting, and injection in the Mesquite Gneiss are interpreted to be the result of Late Cretaceous, basement-involved thrusting and crustal thickening in the Maria fold and thrust belt. Structures and fabrics which post-date development of the migmatite are exclusively mid-Tertiary in age, and related to crustal extension in the Whipple-Buckskin-Rawhide detachment system of the lower Colorado River trough (Knapp, in prep.).

MOON MOUNTAINS

The Moon Mountains are located at the western end of the study area, within the Colorado River Indian Reservation (Fig. 3.3). The rocks and structures here record both Mesozoic thrust faulting, associated with the Maria fold and thrust belt, and Tertiary detachment faulting, related to the Whipple-Buckskin-Rawhide detachment system (Knapp, in prep.). Rock types consist primarily of Mesozoic and Tertiary intrusive rocks and crystalline gneisses of Precambrian age, with minor but important exposures of deformed and metamorphosed sedimentary and volcanic rocks. The major structural elements of the range are the Valenzuela thrust fault, in the southern Moon Mountains, and the Moon Mountain detachment system, which dominates the northern Moon Mountains (Fig. 3.5).

The Valenzuela thrust fault carries sheared gneissic and granitic rocks in the hanging wall above a deformed and metamorphosed section of lower Mesozoic sedimentary rocks (Valenzuela metasedimentary section) in the footwall (Knapp, in prep.). Thrusting was associated with amphibolite facies metamorphism, based on the presence of kyanite and sillimanite in schists of the Valenzuela sequence. A multi-stage

history of movement on the Valenzuela thrust system is implied by both south- and north-directed kinematic indicators. The timing of deformation is constrained by U-Pb zircon data from quartz syenites carried in the hanging wall, which indicate a late Middle Jurassic (160 Ma) age for these rocks, while a Late Cretaceous (71 Ma) age for the most recent movement on the thrust is constrained by syn- to late-kinematic, garnet-bearing pegmatites in the footwall (Knapp and Walker, in prep.). The Valenzuela thrust system is correlated with the Tyson thrust system (Yeats, 1985) of the northern Dome Rock Mountains based on (1) their similarity in structural style, (2) the juxtaposition of similar rock types across the faults, (3) evidence for both south- and north-directed movement on the structures, and (4) their spatial proximity (exposures are separated by ~5 km).

The Moon Mountain detachment fault is exposed in the northwestern Moon Mountains (Fig. 3.5), and carries a section of highly faulted and tilted Tertiary sediments in the hanging wall above mylonitic crystalline rocks in the footwall. Ductile fabrics below the detachment are characterized by dynamic recrystallization of both potassium feldspar and biotite in Proterozoic gneisses, and are typically concordant with the east- to northeast-dipping detachment surface. A later mylonitic fabric is locally developed in these gneisses and the Mesozoic granitic rocks which intrude them. These mylonites, as well as lineations on the detachment fault, indicate a consistent top-to-the-east shear sense on the detachment system. The Moon Mountain detachment fault constitutes the westernmost exposure of the Whipple-Buckskin-Rawhide detachment system at this latitude.

NORTHERN DOME ROCK MOUNTAINS

The northern Dome Rock Mountains area (Figs. 3.2 and 3.3) lies at the southern edge of the Maria fold and thrust belt, and in the context of the present study, is situated furthest to the southwest in the footwall from the exposed extent of the Whipple-Buckskin-Rawhide detachment system. Precambrian and Mesozoic crystalline rocks and Paleozoic and Mesozoic supracrustal rocks here are involved in a series of north-dipping shear zones and large-scale folds (Fig. 3.6). Yeats (1985) mapped the area at a scale of 1:12,000, and identified the major rock units and structures present. Three major structures are identified within the northern Dome Rock Mountains. From north to south, these are the 1) Tyson thrust, 2) Tung Hill shear zone, and 3) Boyer's Gap shear zone (Fig. 3.6).

The Tyson thrust system, as mapped by Yeats (1985), is a gently northeast-dipping shear zone which places crystalline rocks of the Tyson augen gneiss over a deformed, metasedimentary sequence named the Tung Hill section. Both upper and lower plate rocks possess a well-developed mylonitic foliation and lineation, both of which intensify near the thrust contact. Data collected by Yeats indicates that the shear sense on the Tyson thrust is ambiguous, and described evidence for both south- and northeast-directed shear on the fault. The Tyson thrust fault is correlated with the Valenzuela thrust fault of the neighboring Moon Mountains to the north. Based on this correlation, a late Jurassic (160 Ma) crystallization age is inferred for the protolith of the Tyson augen gneiss (in the hanging wall of the thrust), and a Late Cretaceous history of movement on the thrust is implied (Knapp, in prep.).

The Boyer's Gap shear zone (Fig. 3.6) separates two lithologically distinct terrains within the northern Dome Rock Mountains, placing Precambrian crystalline rocks and overlying Paleozoic strata above undated metamorphic and Jurassic intrusive rocks along a north-dipping, ductile shear zone (Reynolds et al., 1986). A large, south- to southwest-facing, overturned syncline is defined by the Paleozoic units and their underlying crystalline basement. Based on S-C fabric relations, Yeats (1985) inferred a two-stage kinematic history for the Boyer's Gap shear zone: (1) south-southeast to southwest directed thrusting, followed by (2) predominantly left-lateral shearing. The stratigraphic separation from Precambrian gneiss in the hanging wall to Mesozoic(?) supracrustal rocks in the footwall requires a minimum throw of several kilometers on the shear zone. The timing of movement on the Boyer's Gap shear zone is constrained to post-date deposition of Mesozoic (McCoy Mountains Formation?) rocks in the footwall. An upper age limit for displacement is not well constrained.

NORTHERN PLOMOSA MOUNTAINS

The northern Plomosa Mountains are centrally located within the study area, and contain extensive exposures of Precambrian crystalline rocks and Tertiary sedimentary and volcanic units, with minor amounts of Mesozoic intrusive and Paleozoic and Mesozoic metasedimentary rocks (Figs. 3.2 and 3.3). As in many of the ranges of west-central Arizona, these rocks record both Mesozoic thrusting and Tertiary detachment faulting. The Deadman thrust fault, first identified by Scarborough and Meader (1983), is a southwest-dipping thrust fault which carries Precambrian crystalline rocks above a deformed and metamorphosed sequence of Paleozoic and Mesozoic sedimentary rocks (Fig. 3.7). Stoneman (1985) provides a detailed treatment of the structural relations of

the Plomosa Pass area in the northern Plomosa Mountains, and describes greenschist facies conditions of metamorphism associated with the thrusting. Based on asymmetric shear fabrics and fold vergence, Stoneman inferred a northeast- to east- directed sense of displacement on the Deadman thrust fault. Ductile fabrics indicate thrusting occurred by plastic behavior of the rocks, and deformation is seen to diminish at structurally higher levels within the gneiss in the hanging wall.

Stoneman (1985) describes the crystalline basement exposed in the Northern Plomosa Mountains as a heterogeneous complex of migmatitic gneiss and megacrystic granite of probable Precambrian age. The layered gneiss consists of dark grey and white, thinly banded migmatite which is interleaved with thick lenses of coarse-grained, hornblende-biotite gneiss. This layered gneiss has been pervasively intruded by foliated, megacrystic granite, ranging from relatively fresh porphyritic granite to highly deformed and metamorphosed granitic augen gneiss.

NORTHERN GRANITE WASH MOUNTAINS

The Northern Granite Wash Mountains are situated in the eastern end of the Maria fold and thrust belt (Figs. 3.2 and 3.3), and contain a complex series of imbricate thrust faults which interleave crystalline gneiss and granite with deformed and metamorphosed Paleozoic and Mesozoic sedimentary rocks. Reynolds et al. (1986) first identified numerous thrust sheets which were emplaced during Mesozoic tectonism at greenschist facies conditions of metamorphism, and Cunningham (1986) produced a geologic map of the northern Granite Wash Mountains (~10 km^2) at a scale of 1:10,000. The area can be divided into two main structural domains: (1) a northeast-striking belt of northwest-dipping imbricate thrust sheets which place gneissic Precambrian basement over Paleozoic and Mesozoic(?) metasedimentary units (the Cobralla thrust system), and (2) a sequence of northwest-striking, stacked thrust sheets which dip toward the northeast and place crystalline basement rocks above metasedimentary rocks and orthogneisses (the Hercules thrust system) (Fig. 3.8). On the basis of structural geometry and cross-cutting cleavages, Reynolds et al. (1986) argued that southeast-directed thrusting in the Cobralla thrust system predated southwest-directed thrusting and imbrication on the Hercules thrust system. Involvement of Mesozoic sedimentary rocks in both phases of the deformation places an approximate lower age limit on the timing of thrusting.

A large (> 25 km^2) granitic body, named the Tank Pass granite, intrudes the sequence of thrusts and discordantly truncates all fabrics and structures within the

northern Granite Wash Mountains. The granite body here is undeformed except for a local, weakly-developed foliation that becomes progressively more developed toward the northeast. These relations imply that intrusion of the granite was late to post-tectonic, and provide an upper limit on the age of deformation. Rehrig and Reynolds (1980) reported early Tertiary K-Ar ages (44.1 to 55.1 Ma) on biotite from the Tank Pass Granite which they interpreted as cooling ages, and inferred a Late Cretaceous crystallization age for the pluton. Since (1) the metamorphic aureole around the granite appears to be small (> 100 m), (2) dikes emanating from the granite are rare, and (3) the contact with the surrounding country rock is sharp, it would appear that the Tank Pass Granite did not have a widespread or prolonged thermal effect on the area. Samples for the present study were all collected within ~2 km of the northern exposed margin of the Tank Pass Granite, within the Cobralla and Hercules thrust systems.

The northern Granite Wash Mountains form part of the footwall of the Bullard detachment fault, exposed at the northeastern end of the adjoining Harcuvar Mountains, yet they contain no evidence of Tertiary fabrics or structures related to the detachment system (Rehrig and Reynolds, 1980; Reynolds and Spencer, 1985). Tertiary mylonitic gneisses, with a southwest-plunging lineation, are exposed below the Harcuvar detachment, and less than 20 km to the north, in the southwestern Buckskin Mountains, gneisses in the footwall of the Buckskin detachment fault are extensively mylonitized (Marshak and Vander Meulen, 1988; Spencer and Reynolds, 1988). The rocks of the northern Granite Wash Mountains preserve intact Mesozoic structures and fabrics apparently because they were at higher crustal levels than rocks which experienced penetrative mylonitic deformation during Tertiary extension in the lower Colorado River area. In addition, only minor amounts of Tertiary intrusive rocks, consisting of felsic dikes, have been identified in the northern Granite Wash Mountains, whereas abundant Tertiary magmatism has been documented throughout much of the remainder of the detachment system (Moon Mountains: Knapp, in prep.; Buckskin Mountains:, Bryant and Wooden, in press; Whipple Mountains: Wright et al., 1986).

40Ar/39Ar ANALYSIS

METHODOLOGY / TECHNIQUES

Where thrust-related structures have been identified (northern Dome Rock Mountains, northern Plomosa Mountains, northern Granite Wash Mountains), samples were taken from crystalline rocks carried in the hanging wall of these structures. Care was taken to obtain fresh, unaltered samples, and no samples were collected near intrusive dikes to avoid the influence of local thermal anomalies.

High purity mineral separates were obtained through conventional heavy liquid and magnetic separation techniques. In general, samples were > 98% pure. Some hornblende and biotite separates contained minor impurities of chlorite intergrowths. Muscovite and potassium feldspar fractions contained few visible impurities, which were limited mainly to quartz and plagioclase. A summary of sample weights and calculated J values is given in Table 1. Samples were irradiated with fast neutrons at the University of Michigan reactor in three different packages. Samples were analyzed on a Nuclide mass spectrometer at the State University of New York at Albany. Analyses of interlaboratory standard biotite demonstrate analytical reproducibility of better than 1%. Age spectra generated from the step-heating analysis of the samples (Figs. 3.9 through 3.13) plot the apparent age (in millions of years) versus the cumulative ^{39}Ar released over the whole experiment. Total errors are shown as 1σ on the age spectra plots.

DATA REDUCTION

Data from the step-heating analyses for each sample are presented in Tables 2a through 2y. A summary of all age data (minimum apparent ages, plateau ages, and isochron ages) is provided in Table 3. The decay constant for natural production of $^{40}Ar^*$ from ^{40}K is taken from Steiger and Jäger (1977) to be $5.543(\pm0.010) \times 10^{-10}$ per annum, and accounts for the combined decay mechanisms of ^{40}K to $^{40}Ar^*$. The ^{40}Ar line blank on the Nuclide gas source mass spectrometer at SUNY Albany is calculated from frequent air argon analyses to be $2x10^{-14}$ moles. Isotopic ratios ($^{40}Ar/^{39}Ar$ and $^{36}Ar/^{39}Ar$) were corrected for line blank and $^{37}Ar/^{39}Ar$ ratios were corrected for ^{37}Ar decay. Correction factors for reactor-produced, Ca-derived Ar and ^{40}K-derived Ar for the three different irradiations are given in Table 1.

Uncertainties in apparent ages are quoted at the 1σ level in data tables (Table 2), but 2σ values are used in the determination of statistically significant age plateaux and 2σ errors are quoted in Table 3. The criteria set forth by Fleck et al. (1977) are followed in

the determination of age plateaux. Calculation of plateau ages involves weighting of the age of each fraction in the plateau based on the percentage of gas it constitutes in the plateau. Dalrymple et al. (1988) point out that the conventional Ar isochron plot and the so-called "inverse" isotope correlation plot yield the same information in the interpretation of $^{40}Ar/^{39}Ar$ incremental heating data, provided correlated errors are accounted for in the former. The choice of which correlation diagram to use then becomes one of convenience in visual interpretation. For this purpose, we have chosen the inverse correlation method to present our $^{40}Ar/^{39}Ar$ data. Values of $^{39}Ar/^{40}Ar$ and $^{36}Ar/^{40}Ar$ ratios are corrected for line blank, and uncertainties for these corrected ratios are quoted at 2σ.

Regression of isochron data follows the algorithms established by York (1966, 1969) for least-squares regression, and employs a computer program developed by L. McKenna (unpublished). Two regression methods are used: York 2 calculates a regression based on correlated errors; York 1 is a regression for data that scatter outside of analytical error. High values for the York 2 mean standard weighted deviation (MSWD) of isotope correlation trends are not unusual, since complete separation of thermally distinct reservoirs of argon is unlikely. For this study, a value of 2.5 for the MSWD on the York 2 regression was taken as an acceptable upper limit (following McDougall and Harrison, 1988, and references cited therein) for use of this regression technique. Where the York 2 regression has been used (MSWD < 2.5), the MSWD is cited in the text; otherwise, the results of the York 1 regression are quoted. Values of the MSWD for the York 2 regression on all isotope correlation plots are presented in Table 3. Isotope correlation plots with regression lines are shown in Figures 3.14 through 3.18.

Heizler and Harrison (1988) review the analysis and interpretation of inverse isotope correlation plots. Only consecutive steps in the heating schedule are considered for isochron analysis, since the isochron regression represents a mixing line between two end-member reservoirs. Age gradients, produced by diffusional loss during slow cooling or episodic argon loss, will result in a heterogeneous radiogenic component in the sample, and can produce an apparent isochron age. Isotope correlation plots which yield ages for steps which define an age gradient on the age spectrum have not been treated as reliable ages.

RESULTS

A total of 24 mineral separates from the five areas of the study area were analyzed. The group included four hornblendes, three muscovites, nine biotites, and

eight potassium feldspars, seven of which came from samples with coexisting biotites. A summary of the results is presented in Table 3, which catalogues the number of heating steps, minimum apparent age, and where appropriate, the plateau and isochron ages, for each of the samples. In all, 401 heating steps were made on the 24 samples. Seven of the biotites and potassium feldspars are co-existing pairs. Presented below is a discussion of the samples analyzed for each of the areas, moving from north to south and east to west through the study area. Detailed descriptions of the individual rock samples and mineral separates can be found in the appendix.

MESQUITE MOUNTAIN

Mineral samples from the Mesquite Mountain area include two hornblende, two biotite, and a potassium feldspar separate from the crystalline rocks of the Mesquite Gneiss, a migmatitic gneiss which predominates the outcrop at Mesquite Mountain Samples 87M4 and 87M13 come from amphibolite layers, while samples 87M2 and 87M18 were taken from biotite-feldspar rich, melanosomatic layers within the Mesquite Gneiss. Two fractions were analyzed from hornblende sample 87M4 (labelled separately as 1 and 2) to verify reproducibility of the results for this spectrum. Sample localities are indicated in Figure 3.4.

Three hornblende separates - two from sample 87M4 and a third from 87M13 - were analyzed from the Mesquite Mountain area, and results are shown in Tables 2a-f (raw data) and Figures 3.9a-f (age spectra). All three spectra show evidence of essentially complete degassing in the Late Cretaceous. Sample 87M4(1) yields a "plateau" over 43.2 % of the ^{39}Ar released (steps 7-12) corresponding to an age of 76.3 ± 0.67 Ma (Fig. 3.9a). An isochron age (MSWD = 0.87) for steps 3-12 is of the same age within error, yielding an age of 75.4 ± 0.6 Ma (Fig. 3.14a). For the second split of this sample (87M4(2)), steps 10-12, comprising 50.5 % of the total gas, define a plateau at 83.2 ± 0.87 Ma (Fig. 3.9b). While at first the results from these two splits of the same sample appear discordant, inspection of the age spectra reveal that they yield very similar spectra, with about half of the gas given off at around 76 Ma, and the other half released at around 83 Ma.

Hornblende from sample 87M13, located in the central part of Mesquite Mountain, yields a similar age spectrum, with a plateau age defined at 77.5 ± 0.78 Ma (Fig. 3.9c). Isotope correlation analysis of this sample (MSWD = 0.27) reveals an age of 68.5 $^{+1.2}_{-3.6}$ Ma, with an initial $^{40}Ar/^{36}Ar$ ratio of 254 ± 18 (Fig. 3.14c). The very low

MSWD of 0.27 in this case results from regression of only three points. All three hornblende spectra are indicative of minor excess argon evolved during the low temperature steps, but this excess component generally constitutes less than five percent of the total gas. For all three separates, greater than 90% of all argon records ages between 67.8 and 84.7 Ma. We interpret these spectra to reflect essentially complete outgassing of these hornblendes during Late Cretaceous time, which may also correspond to the crystallization age of these hornblendes, since the amphibolite facies metamorphic fabric is concordant with gneissic layering in the Mesquite Gneiss.

The two biotite fractions analyzed from the Mesquite Gneiss (87M2 and 87M18) lie at opposite ends of Mesquite Mountain and are separated geographically by about 6 km (Fig. 3.4). Given the southwest-dipping structural grain of the Mesquite Mountain area, the vertical structural separation of these samples is estimated to be ~3 km. These two biotites reveal very similar, relatively flat age spectra, but statistical plateaus are not defined due to the gently concave-downward shape of the spectra (Figs. 3.9d and 3.9e). Sample 87M2, from the southern end of Mesquite Mountain, released almost 80% of the total argon gas between the narrow age range of 30.2 and 32.4 Ma, correlating very well with an isochron age of ~30 Ma. The isochron analysis of this sample reveals two statistically distinct trapped components which yield identical ages (30.1 ± 1.7 and 30.3 ± 0.2 Ma) but different initial $^{40}Ar/^{36}Ar$ ratios of 284 and 346, respectively, for steps 1-3 (York 1) and steps 4-8 (MSWD = 2.03) (Fig. 3.14d).

Sample 87M18, from the northern end of Mesquite Mountain, evolved > 95% of the argon gas between the apparent ages of 30.6 and 35.8 Ma (Fig. 3.9e), and yielded an isochron (MSWD = 1.74) for steps 9-11 (~20% of the total gas) corresponding to an age of $33.3\ ^{+0.8}_{-0.9}$ Ma (Fig. 3.14e). Minimum apparent ages for these samples are 20.8 ± 2.2 Ma (87M2) and 19.9 ± 1.0 Ma (87M18), and along with sloped portions of the low-temperature steps of the spectra, may signify diffusive loss. In summary, these biotites give ages of about 30 to 33 Ma, and constitute the youngest mica ages documented in this study.

A single potassium feldspar was analyzed from the Mesquite Gneiss, and comes from sample 87M18 at the north end of Mesquite Mountain. This microcline separate exhibits a saddle-shaped spectrum (Fig. 3.9f), and based on a minimum apparent age of 21.9 ± 0.8 Ma, records closure to argon diffusion in early Miocene time. With the

exception of very minor (> 2%) excess argon generated during the lowest temperature steps, this sample contains no gas which shows an apparent age older than 56.0 Ma.

MOON MOUNTAINS

Six mineral separates were analyzed from the Moon Mountains, including two muscovites (86MM25, MM87-8), two biotites (86MM23, MM87-7), and two potassium feldspars (86MM23, MM87-7). These samples were collected from crystalline rocks in two structurally distinct settings: from within the Valenzuela thrust system in the southern Moon Mountains, and from the footwall of the Moon Mountain detachment fault, in the northwestern Moon Mountains (Fig. 3.5). Step heating data for these six samples are presented in Tables 2g through 2l, and age spectra are shown in Figures 3.10a-f.

The release spectrum for muscovite from sample 86MM25 defines a plateau over 55% of the gas released (steps 3-6), corresponding to an age of 49.9 ± 0.6 Ma (Fig. 3.10a). Steps 3-10 of this sample yield an isochron age (York 1) of $49.6^{+0.9}_{-1.2}$ Ma with an initial $^{40}Ar/^{36}Ar$ ratio of atmospheric composition (Fig. 3.15a). Similarly, muscovite from sample MM87-8 yields a plateau age of 50.1 ± 0.2 Ma over 55% (steps 5-9) of the gas released (Fig. 3.10b). More than 80% of the total gas was evolved over the age range of 49.3 to 52.6 Ma. Increments 5-9 of sample MM87-8 define an isochron age (MSWD = 2.04) of $48.9^{+1.2}_{-4.1}$ Ma with an initial $^{40}Ar/^{36}Ar$ ratio of 449 (Fig. 3.15b). Minimum apparent ages for both of these muscovite samples are between 29 and 32 Ma, and occur at the lowest temperature steps. The initial, concave-downward portion of both release spectra may reflect diffusional loss profiles in these micas.

A biotite and potassium feldspar pair were analyzed from each of samples MM87-7 and 86MM23. Biotites from both of these samples yield similar, flat spectra, but statistical plateaux are a deceptive means of treating the data. Only 46% of the gas lies within a statistical plateau (age = 51.7 ± 0.2 Ma) for biotite MM87-7, but greater than 90% of the gas is released between the ages of 51.3 and 53.7 Ma; 99.3% of the gas is between the ages 48.1 and 54.5 Ma (Fig. 3.10c). Isochron analysis (York 1) of steps 1-10 reveal an age of 52.6 ± 0.2 Ma and an initial $^{40}Ar/^{36}Ar$ ratio of 282 (Fig. 3.15c). In the case of biotite from sample 86MM23, ~93% of the total gas is released between the ages of 46.3 and 51.2 (Fig. 4d), yet no statistical plateau can be defined due to the high precision of measurement of argon ratios. An isochron age (York 1) of $48.0^{+0.2}_{-0.3}$ Ma and an initial $^{40}Ar/^{36}Ar$ value of 274 are indicated by steps 3-9 of this sample (Fig. 3.15d).

We interpret both sets of data to represent closure of these biotites to argon diffusion at around 50 Ma. These ages are concordant within uncertainty with corresponding muscovites from the same two areas.

Potassium feldspar analyses from the Moon Mountains area yield saddle-shaped release spectra (Figs. 3.10e and f), which are probably indicative of excess argon contamination. Minimum apparent ages for these spectra are 23.4 ± 0.4 Ma (MM87-7) and 22.4 ± 0.4 Ma (86MM23), reflecting the maximum age at which these samples could have last become closed to argon diffusion. While not a plateau, steps 10-14 of sample 86MM23 make up ~36% of the total gas in this spectrum, and are all of the same apparent age (22.5 Ma) within error. Other than very small (< 1%) volumes of gas generated at the lowest temperature steps, these samples contain no gas which corresponds to ages older than ~60 Ma (Tables 2i and l).

Two features are immediately apparent from the Moon Mountains $^{40}Ar/^{39}Ar$ data. First, these two suites of samples, from conspicuously different structural settings in the Moon Mountains, give remarkably similar results, suggesting that the two areas experienced similar temperature conditions during the Late Cretaceous thermal event and subsequent Tertiary cooling history. Secondly, muscovite (T_C ~350°C) and biotite (T_C ~300°C) ages from the Moon Mountains are concordant at ~50 Ma, yet potassium feldspars from this area yield minimum apparent ages which are significantly younger (22.5-23.5 Ma). These data would appear to require very rapid cooling (>30°C/m.y.) of this terrain through the 350-300°C temperature range during the Middle Eocene, followed by either (1) a dramatic deceleration in the cooling rate (to ~3°C/m.y.) through the middle Tertiary (i.e. Fig. 15b), or (2) a secondary thermal event in Oligocene time sufficient to substantially reset potassium feldspar (T_C ~150-200°C) but not significantly affect the micas.

NORTHERN DOME ROCK MOUNTAINS

Two samples were analyzed from the northern Dome Rock Mountains: one from gneisses in the hanging wall of the Tyson thrust (87D20) and a second from the crystalline gneisses which form the base of the large Paleozoic syncline in the hanging wall of the Boyer's Gap shear zone (87D9) (Fig. 3.6). Both a biotite and potassium feldspar separate were analyzed from each sample, and results are presented in Tables 2m through 2p and Figures 3.11a-d.

Biotites show comparatively flat age spectra, with most of the argon gas evolved over the apparent age span of 50-60 Ma for both samples. As with many of the mica samples, strict plateau ages are not defined. A total of ~90 % of the gas (steps 3-10) in biotite 87D9 is given off between the ages of 53.9 and 57.1 Ma (Fig. 3.11a) and, similarly for biotite 87D20, ~80 % of the total gas (steps 3-9) is evolved between the apparent ages of 51.0 and 55.2 Ma (Fig. 3.11b) Isochron ages of 55.7 ± 0.3 Ma (87D9, steps 3-8, York 1) and $47.9^{+1.1}_{-1.2}$ Ma (87D20, steps 2-7, MSWD = 2.06) fall within or near this same range (Table 3, Figs. 3.16a and 3.16b). The high 40/39 ratios for steps 1, 10, and 11 of sample 87D20 are probably best explained by minor chlorite contamination of the sample.

The two potassium feldspar separates show similar, saddle-shaped age spectra, with minimum apparent ages of 26.4 ± 2.6 Ma (87D20) and 28.8 ± 0.4 Ma (87D9) (Figs. 3.16c and d). These samples do not show well-behaved age plateaux, but steps 10-13 of 87D20 yield an isochron age (MSWD = 0.9) of $26.5^{+1.2}_{-1.5}$ Ma, concordant within uncertainty of the minimum apparent age (Fig. 3.16c). For both samples, the higher temperature portions of the spectra are indicative of gas which is held in more retentive sites than the gas which is generated from coexisting biotites, a feature which is apparent in many of the western Arizona samples. The explanation for this behavior is not entirely clear, but may be related to anion siting of argon within the crystal structure of these feldspars. Given the complex structural and thermal history which all of these samples have experienced, it may not be surprising to find a multiplicity of site retentivities in potassium feldspar, developed through a combination of recrystallization of the feldspar and successive redistribution of argon within the grains.

NORTHERN PLOMOSA MOUNTAINS

The northern Plomosa Mountains are centrally located within the study area and contain exposures of the Deadman thrust fault of the Maria fold and thrust belt (Fig. 3.3). Samples from the Plomosa Pass area of the northern Plomosa Mountains were collected from crystalline rocks of Precambrian age carried in the hanging wall of the Deadman thrust fault (Fig. 3.7). A total of four mineral separates from three samples were studied, including a hornblende (86NP1), a biotite (87P7) and two potassium feldspars (87P5 and 87P7). Results of the step-heating analyses are provided in Tables 2q through t and age-spectrum plots are shown in Figures 3.12a-d.

A single hornblende separate (86NP1) from the northern Plomosa Mountains yields a highly disturbed age spectrum, with increments ranging in apparent age from a minimum of 159.9 ± 6.4 Ma to a maximum of 466.4 ± 1.2 Ma (Fig. 3.12a). A plot of the K/Ca ratio shows an initially high value for amphibole, decreasing from 0.8 to 0.1 over the first 20% of the gas released, and corresponding to a very erratic portion of the age spectrum. This behavior is suggestive of biotite contamination, however, biotite was not noticeable as grains in the mineral separate or as intergrowths in hornblende. While this hornblende does not exhibit a statistical plateau, ~52% of the gas was released in three steps (12-14) at apparent ages between 364.0 ± 0.6 and 373.0 ± 1.4 Ma (Fig. 3.12a). An isotope correlation plot (York 1) of steps 8-13 indicates an age of $265.1^{+9.0}_{-10}$ Ma (Fig. 3.17a), but this age does not correspond to a time interval of known regional tectonic significance in the area, and may well be an artifact of the monotonically decreasing age of these steps.

The age spectrum for biotite from sample 87P7 is also highly irregular, with apparent ages ranging from ~28 to 119 Ma over the eleven steps of the heating schedule (Fig. 3.12b). No semblance of a plateau is apparent, and the data are not well-behaved on an isochron plot, perhaps indicating that the sample contains separate but thermally indistinct reservoirs of argon gas. The minimum apparent age of 28.1 ± 1.9 Ma suggests that the sample lost some argon gas during the middle Tertiary, but the presence of a significant portion of the gas (>80%) with an apparent age greater than 90 Ma argues that the sample was not held above the closure temperature for argon diffusion in biotite (~300°C) either during or since Late Cretaceous time. This Proterozoic biotite has clearly experienced significant argon loss, but the timing of that loss can at best be attributed to some post-Proterozoic event based solely on the $^{40}Ar/^{39}Ar$ data.

Potassium feldspar samples from the Plomosa Pass area (87P5 and 87P7) exhibit release spectra which are markedly distinct from other feldspars in the study area (Figs. 3.12c and d). While these samples show the type of saddle-shaped spectra and minimum apparent ages which characterize all the potassium feldspars, both 87P5 and 87P7 reveal a significant portion (45-50%) of the total gas which was evolved at the highest temperature of the heating experiments, and yields apparent ages greater than 120 Ma. No age plateaux are defined by the data, but steps 22-24 (32% of the gas) of sample 87P5 all have ages of ~125.5 Ma. Steps 5-13 of sample 87P7 yield an age of $22.2^{+1.2}_{-1.5}$ Ma (MSWD = 2.29) on an isotope correlation plot (Fig. 3.17b). Minimum apparent ages for 87P5 and 87P7 are 27.2 ± 0.2 Ma and 25.8 ± 1.2 Ma, respectively. Argon which is

released at the highest temperature steps in these potassium feldspars might be located in relatively retentive, anionic sites, since apparent ages for these steps are older than those observed for biotite in 87P7. Alternatively, the steep ^{40}Ar gradients revealed in these samples may be the result of episodic argon loss in the middle Tertiary. At present, these two possibilities are difficult to distinguish. Regardless of the interpretation, it seems unlikely that the potassium feldspars from the northern Plomosa Mountains could have been held above or even near the closure temperature for argon diffusion in microcline (~150-200°C) throughout the Late Cretaceous and early Tertiary (80-100 Ma), and still retain such a significant portion of gas.

Data from the northern Plomosa Mountains are generally characterized by irregular spectra which do not show simple behavior of argon systematics. The age spectrum for hornblende is clearly disturbed, which we interpret to reflect partial outgassing of this Proterozoic hornblende, probably during Mesozoic tectonism. Partial resetting of this hornblende may have taken place during Jurassic or older deformation known from the Mojave-Sonora area, and may have had no relation to the late Cretaceous thermal disturbance. Significantly, this sample does not reflect the degree of resetting indicated by the other hornblendes from western Arizona. Both biotite and potassium feldspar contain abundant amounts of argon gas which yield apparent ages much older than the late Cretaceous thermal event recorded in surrounding areas of the Maria fold and thrust belt, yet feldspars show most recent closure to argon diffusion in the late Oligocene. Collectively, these data imply that (1) the northern Plomosa Mountains area did not attain temperatures in excess of ~250-300°C during basement involved thrusting, (2) that these modest temperatures could not have been maintained throughout the early Tertiary, and consequently, (3) a second thermal event was responsible for episodic loss of argon in potassium feldspar, but did not significantly affect either hornblende or biotite.

NORTHERN GRANITE WASH MOUNTAINS

Samples from the northern Granite Wash Mountains include a hornblende, a muscovite, two biotites, and a potassium feldspar, covering the temperature range of ~500-150°C for this area. Three of the samples (87G30, 87G16, and 87G29) come from the Cobralla thrust system in the eastern part of the area, and sample 87G36 (biotite and potassium feldspar) was collected from the Hercules thrust system in the western part of the area (Fig. 3.8). These localities were chosen in order to constrain the temperature-

time history of crystalline rocks which are carried within these two thrust systems, and to potentially differentiate the timing of deformation between the two systems.

Hornblende from sample 87G30 exhibits a disturbed spectrum for which no plateau age can be defined (Fig. 3.13a). Comparison with the K/Ca profile suggests that the low temperature part of the spectrum reflects minor biotite contamination of the sample. The significance of the variation in the K/Ca ratio at the highest temperature steps is not clear, but these steps (10-18) produce a well-defined (MSWD = 1.68) isochron age of 129.0 $^{+4.3}_{-6.4}$ Ma and a trapped initial $^{40}Ar/^{36}Ar$ ratio of 380 ± 62 (Fig. 3.18a). Several of the intermediate temperature steps yield apparent ages of ~80 Ma. A minimum apparent age for this sample of 55.5 ± 8.6 Ma may reflect minor disturbance of this phase subsequent to late Cretaceous time. We interpret this sample to record partial resetting in association with late Cretaceous heating. The significance of the age of the higher temperature steps may be a relict of a Jurassic thermal event, but this interpretation cannot be argued with much certainty.

In the argon release spectrum for muscovite from sample 87G16 (Fig. 3.13b), a plateau age of 53.7 ± 0.6 Ma over 50% of the gas is defined by steps 5-8. However, essentially all the argon gas is released over the range of apparent ages from 48.3 to 55.2 Ma, signifying closure to argon diffusion in early Tertiary time. An isochron plot (MSWD = 2.30) of steps 2-10 yields an age of 55.1 $^{+0.2}_{-0.3}$ Ma and an initial $^{40}Ar/^{36}Ar$ ratio of 256 (Fig. 3.18b).

The $^{40}Ar/^{39}Ar$ age spectrum for biotite sample 87G29 is clearly disturbed, and reveals a generally concave-downward profile with the apparent age increasing from 19.8 ± 0.6 to 49.8 ± 0.4 Ma over the first 45% of the gas released (Fig. 3.13c). While no statistical plateau is generated by these data, the final ~50% of the remaining gas yields apparent ages in the range 46.6 ± 0.2 to 52.9 ± 0.2 Ma. Inverse isotope correlation analysis of steps 4-8 yields an age (York 1) of 45.2 $^{+4.4}_{-9.1}$ Ma and a trapped component with isotopic composition of $^{40}Ar/^{36}Ar$ = 334, accounting for ~55% of the total argon gas released (Fig. 3.18c).

Biotite from sample 87G36 yields a relatively flat release spectrum; however, based on the critical value test, no plateau is evident (Fig. 3.13d). More than 85% of the total gas is evolved between the ages of 38.9 and 42.6 Ma. Analysis of the step-heating data on an inverse isotope correlation diagram reveals trapped components of two distinct

isotopic compositions, corresponding to $^{40}Ar/^{36}Ar$ ratios of 253 (steps 1-7) and 542 (steps 8-10). Both components reflect an identical age, within error, of 40.5 ± 0.6 Ma (Fig. 3.18d). Several cases have been reported (e.g. Heizler and Harrison, 1988) of isotopic heterogeneity in biotites, but in other cases (Roddick et al., 1980), biotites are known to produce flat release spectra even in the presence of excess argon. Sample 87G36 is another convincing example that distinct isotopic reservoirs can survive laboratory step-heating of biotites.

A potassium feldspar separate from sample 87G36 exhibits the type of saddle-shaped spectra which characterizes all the potassium feldspar analyzed in this study (Fig. 3.13e). A minimum apparent age of 20.2 ± 1.2 Ma is the same age, within uncertainty, of 21.4 ± 0.2 Ma indicated by inverse isotope correlation (MSWD = 2.39) of steps 5-16 (Fig. 3.18e). Other than minor excess argon given off during the very lowest and highest temperature steps, this sample contains no gas which corresponds to ages older than 41.0 Ma.

The data for the northern Granite Wash Mountains are summarized in Figure 8e, and define a regular progression in time for closure of the phases to argon diffusion. Of particular note are the fact that hornblende is disturbed and shows only partial resetting, apparently in response to the Late Cretaceous thermal event in the Maria fold and thrust belt. Mica ages are consistent with slow cooling from this thermal perturbation through the early Tertiary. Potassium feldspar yields the lowest minimum apparent age of all feldspars analyzed in this study, and reflects unroofing of the northern Granite Wash Mountains in the footwall of the Whipple-Buckskin-Rawhide detachment system. As discussed previously, no Tertiary fabrics or structures are known from the northern Granite Wash Mountains, which presumably were situated at higher crustal levels than those which experienced extensive mylonitization during the mid Tertiary. Significantly, however, the area was still above closure to argon diffusion in potassium feldspar during this time.

INTERPRETATION AND DISCUSSION

Thermochronology of crystalline rocks from western Arizona based on $^{40}Ar/^{39}Ar$ step-heating analysis provides a foundation for understanding the thermal evolution and tectonic history of basement thrust nappes in the Maria fold and thrust belt. This region is exceedingly complex geologically due to the number of deformational and metamorphic

events which have been superimposed here. Thermochronology affords a means of assessing the age, duration, and extent of these various events where stratigraphic and geochronologic control is largely lacking.

Results from each of the five study areas are discussed below and implications of the thermal history for tectonic interpretations are considered. Temperature-time plots, which show time, in millions of years, versus temperature, in degrees Centigrade, are presented in Figures 3.19-3.23. The inferred cooling paths represent interpolation between the data points. It should be emphasized that these paths are not considered to be the most realistic cooling paths, but rather the simplest interpretation based on the resolution of the present data. The actual cooling histories are probably more realistically characterized by faster cooling (i.e. steeper paths) during the early stages and progressively slower cooling with time, assuming that elevation of heat flow was an episodic event in the Late Cretaceous rather than a protracted phenomenon. Nominal uncertainties in closure temperature for the various minerals are assumed to be ±25°C. The actual closure temperatures will be a function of cooling rate, diffusion geometry, and effective diffusion radius, and may exceed this assumed range, especially in the case of potassium feldspar. Also depicted on the temperature-time plots is the general time span over which detachment faulting in the Whipple-Buckskin-Rawhide system was occurring. These constraints come primarily from the Whipple Mountains (Davis et al, 1980, and many other references; Spencer and Reynolds, 1988), and are bracketed between ~21 to 18 Ma for much of the displacement on the detachment system.

MESQUITE MOUNTAIN

Resetting of argon systematics in metamorphic hornblende at Mesquite Mountain occurred in Late Cretaceous time, between the ages of ~76-83 Ma. Since these ages represent closure of these phases to argon diffusion during cooling of the terrain, they represent minimum estimates on the degree and timing of the thermal perturbation. Independent evidence from U-Pb zircon data indicate a latest Cretaceous (67.2 ± 1.4 Ma) age for the timing of migmatization of the Mesquite Gneiss (Knapp and Walker, in prep.). Together the $^{40}Ar/^{39}Ar$ and U-Pb zircon data imply that (1) temperatures in the Mesquite Mountain area were in excess of 450-500°C, and probably at least 650° based on the evidence for *in situ* partial melting, (2) development of the Mesquite Gneiss migmatite was a protracted event, based on the ~10 m.y. spread between the older $^{40}Ar/^{39}Ar$ hornblende ages and the younger U-Pb zircon age for a concordant granitic sill

in the migmatite, and (3) that the later stages of migmatization were cooler and characterized by injection, which did not result in the resetting of argon systematics in hornblende. The timing of this migmatization is closely coincident with known age ranges of thrusting in the Maria fold and thrust belt (e.g.. Reynolds et al., 1986). While no thrust faults are exposed in the immediate area of Mesquite Mountain, we interpret migmatization of the Mesquite Gneiss as a deep-seated response to basement-involved thrusting and crustal thickening in Late Cretaceous time.

Biotite and potassium feldspar data show closure to argon diffusion at ~30-33 Ma and ~22 Ma, respectively. Shown in Figure 3.19 is the inferred temperature-time history for this area, based on these data. Hornblende and biotite analyses define a cooling rate of ~5°C/m.y. for Late Cretaceous and early Tertiary time, while apparent acceleration of the cooling rate, to ~20°C/m.y., occurred in Late Oligocene to Early Miocene time in response to exhumation of these rocks in the footwall of the Whipple-Buckskin-Rawhide detachment terrain. These data are consistent with relatively slow cooling over the temperature range 500-300°C until the onset of extension.

MOON MOUNTAINS

A schematic temperature-time history for the Moon Mountains is presented in Figure 3.20, and emphasizes the very rapid cooling rate (~30°C/m.y.) over the temperature interval of 350-300°C indicated by concordant ages for muscovite and biotite from this area. The steepness of this cooling path is suggestive of tectonic unroofing of these rocks in Middle Eocene time, however no known geologic data from western Arizona have documented extension of this age. Potassium feldspar minimum apparent ages, in contrast, require a substantial deceleration of the cooling rate to an average ~3°C/m.y. through mid-Tertiary time. The intriguing possibility is raised by these data that extension in west-central Arizona may have been initiated at a much earlier time than has previously been thought, and that geologic evidence for this early stage of tectonism has largely been obscured by later phases of extension. Foster et al. (1988) reported $^{40}Ar/^{39}Ar$ data from the Old Woman-Piute Mountains area to the northwest which record very rapid cooling of this nature at an even earlier age, in Late Cretaceous time, following a regional, amphibolite facies metamorphic event. The observed spread in mica and potassium feldspar minimum apparent ages might be attributed to reheating of these rocks, to temperatures sufficient to partially reset argon systematics in potassium feldspar but not affect micas, in association with the early stages of Miocene extension.

NORTHERN DOME ROCK MOUNTAINS

Analyses from the northern Dome Rock Mountains indicate that the area experienced significant heating and resetting of argon systematics in Late Cretaceous time. Significantly, biotites and potassium feldspars from rocks either known or inferred to be of Jurassic and Precambrian age exhibit essentially identical systematics. These data clearly demonstrate the fact that resetting of argon systematics in Late Cretaceous time was very efficient; little evidence remains of Proterozoic-age gas in the considerably older gneiss (87D9). The temperature-time history represented by these data (Fig. 3.21) covers only the temperature range from 300° to 150°C, and is most easily interpreted as a slow-cooling path at a rate of ~5°C/m.y. throughout middle Tertiary time. The potassium feldspars from this area yield some of the oldest minimum apparent ages found in this study, consistent with the distal position of the northern Dome Rock Mountains with respect to the exposed detachment terrain. These rocks would have been some of the earliest to be exhumed in the lower plate of the detachment. The minimum apparent ages indicate these rocks were at high enough crustal levels by late Oligocene time to have cooled through the closure temperature for microcline.

NORTHERN PLOMOSA MOUNTAINS

The northern Plomosa Mountains constitute an anomalous area within the thermal regime of the Late Cretaceous Maria fold and thrust belt. Spectra from all phases analyzed from the northern Plomosa Mountains are generally disturbed, and show much older ages than all surrounding areas. We interpret the older ages in the northern Plomosa Mountains area as indicative of significantly cooler temperatures here during Late Cretaceous time, and correspondingly higher levels within the Maria fold and thrust belt.

Shown in Figure 3.22 is the temperature-time history which can be deduced from these data for the northern Plomosa Mountains. Based on the nature of both hornblende and biotite spectra from crystalline rocks in the hanging wall of the Deadman thrust fault, it would appear unlikely that the Plomosa Pass region attained temperatures any higher than ~300°C for a sufficient time to significantly reset these minerals. Potassium feldspars from this area show closure to argon diffusion in late Oligocene time, at around 27 to 28 Ma. These data define an average cooling rate for the northern Plomosa Mountains of ~2°C/Ma, in contrast to the average 4°C/Ma cooling histories for the other study areas.

Also of major importance is the similarity of the lower temperature portions of the potassium feldspar spectra from the northern Plomosa Mountains to potassium feldspars from the other four areas. All potassium feldspars show minimum apparent ages between 20.2 ± 1.2 and 28.8 ± 0.4 Ma, yet the Late Cretaceous history of the northern Plomosa area is clearly different. This area could not have remained at elevated temperatures (i.e. above closure for argon diffusion in potassium feldspar) throughout early Tertiary time if it was at a much lower temperature to begin with than surrounding areas and cooled at a similar rate. We interpret these relations to be indicative of a renewed thermal pulse associated with mid-Tertiary extension. Moreover, the magnitude of this Tertiary thermal event can be fairly well estimated. Potassium feldspars, with closure temperatures in the range of 150°-200°C, were all significantly affected by the event, whereas biotites and muscovites show a variable, but always less pronounced response to the renewed heating.

NORTHERN GRANITE WASH MOUNTAINS

Spectra for samples from the northern Granite Wash Mountains are summarized in Figure 3.23, and indicate a history of thermal perturbation in Late Cretaceous time followed by slow cooling through early Tertiary time until rapid exhumation during late Oligocene to early Miocene extension. Metamorphic hornblende from amphibolite carried in the hanging wall of the Cobralla thrust system reflects partial resetting during this thermal event, but the hornblende contains an abundance of significantly older gas, indicating that outgassing was by no means complete. Assuming a closure temperature of ~450-500° C for metamorphic hornblende, we estimate that the northern Granite Wash Mountains area probably attained temperatures on the order of 400° to 500° C, the actual temperature being inversely proportional to the length of time which these elevated temperatures were maintained.

Muscovite and biotite from the northern Granite Wash Mountains reveal age spectra consistent with a period of slow cooling subsequent to the Late Cretaceous event. Biotites yield rather erratic spectra, and may reflect loss associated with renewed heating during the Tertiary extensional event. Significantly, rocks of the northern Granite Wash Mountains show no evidence of Tertiary fabrics or structures. Tertiary igneous rocks have been identified in this area, and may be related to reheating of the crust in association with extension.

YOUNGING OF AGES FROM SW TO NE

A correlation of ages - whether plateau ages, isochron ages, or minimum apparent ages - with structural position is evident within the study area. For both biotite and potassium feldspar samples, ages are successively younger from south to north, and generally from west to east. The oldest ages recorded for both biotite and potassium feldspar (with the exception of the northern Plomosa Mountains) are found in the northern Dome Rock Mountains area. The youngest ages observed come from the Mesquite Mountain area, inferred on these and other grounds to be the lowest structural levels exposed in the study area.

RELATION TO THRUST BELT GEOMETRY

Structures of the Maria fold and thrust belt are predominantly east-west trending, with vergence to the south. This geometry would dictate deeper structural levels to the north, where the basement-involved structures appear to have rooted. This geometry is cryptically reflected in the $^{40}Ar/^{39}Ar$ data from west-central Arizona, where hornblende shows progressively more thorough re-setting from south (northern Plomosa Mountains) to north (Mesquite Mountain) over a distance of ~25 km, across the strike of the Maria fold and thrust belt. It should be noted that this correlation can be made in only a qualitative sense, because an accurate reconstruction of Mesozoic structures in the Maria fold and thrust belt cannot be made on the basis of existing constraints.

RELATION TO DETACHMENT GEOMETRY

Our present understanding of the Whipple-Buckskin-Rawhide detachment system implies that rocks from the five study areas are situated in the footwall of this regionally extensive fault system. All five areas are located to the south and west of exposures of the detachment in the Whipple, Buckskin, and Harcuvar Mountains, however several detachment faults are exposed within the study area (notably the Moon Mountain and Plomosa detachments). Seismic data from western Arizona (Hauser et al., 1987, McCarthy and Thompson, 1988) image a reflector in the shallow crust which connects the Moon Mountain and Plomosa detachments as splays with the main detachment surface to the northeast. Such a relationship would require that the study area consists of three structural domains with respect to the detachment system, in large crustal horses separated by the detachment splays. The $^{40}Ar/^{39}Ar$ data indicate that all domains in the study area were subject to partial resetting of potassium feldspar during the time from late Oligocene to early Miocene. An accurate reconstruction of the detachment system cannot

presently be made, such that the relative depths of the five areas cannot by accurately assessed.

THICK-SKINNED INVOLVEMENT OF BASEMENT

Several inferences concerning the nature of basement-involved thrusting in the Maria fold and thrust belt can be made from the argon data. A summary of hornblende spectra from western Arizona is shown in Figure 20a, and emphasizes the variation in the degree of resetting during the Late Cretaceous thermal event. Based on this variation of temperatures indicated by hornblende samples from Mesquite Mountain (87M4(1); complete resetting), the northern Granite Wash Mountains (87G30; partial resetting), and the northern Plomosa Mountains (86NP1; disturbed), we conclude that different structural levels of the thrust belt are represented. These data are in agreement with other geochronologic and petrologic data for these areas. Based on U-Pb zircon dating of a granitic sill associated with migmatization in the Mesquite Gneiss, it is apparent that the rocks at Mesquite Mountain were partially melted in response to crustal thickening. In contrast, Cunningham (1986) documents primarily upper greenschist facies conditions of metamorphism associated with Late Cretaceous deformation in the northern Granite Wash Mountains. According to Stoneman (1985), the northern Plomosa Mountains area only exhibits mid- to upper greenschist facies metamorphism associated with thrusting.

In addition, it would appear that basement-involved deformation in the Maria fold and thrust belt was considerably thick-skinned. While it is impossible to directly estimate depths simply on the basis of temperature data, it seems reasonable to speculate that the high temperatures implied by the $^{40}Ar/^{39}Ar$ data, and the metamorphic conditions recorded in many of the rocks are indicative of depths in excess of 8-10 km. This thickness of thrust nappes is certainly on the same order of those involving décollement-style thrusting within the Cordilleran thrust belt further to the north. Present exposures of basement thrust sheets in the Maria fold and thrust belt typically preserve no more than one to three kilometers structural thickness, implying that a minimum of five to nine kilometers of overburden has been removed from these thrust nappes between a combination of erosion during early Tertiary time and tectonic denudation in the mid- to late Tertiary.

Attempts to accurately constrain the unroofing history for rocks of west-central Arizona are hindered by the lack of reliable depth versus time or depth versus temperature relations. Crustal geotherms were undoubtedly transient through time, and the relative

effects of static conductive relaxation versus cooling due to tectonic denudation cannot be discerned. In the case of very accelerated cooling rates in the Miocene, independent geologic data indicate that tectonic denudation and consequent rapid cooling were the primary influences on the thermal structure, despite continued input of magma and heat into the middle and upper crust.

CONCLUSIONS

The thermal history of crystalline rocks in the Maria fold and thrust belt of west-central Arizona is characterized by three distinct phases:

(1) regional heating associated with basement-involved thrusting and crustal thickening in Late Cretaceous time,

(2) uplift and slow cooling, at an average rate of 5-10°C/m.y. throughout early Tertiary time, and

(3) rapid cooling associated with tectonic denudation in late Oligocene to early Miocene time.

The thermal event associated with basement-involved thrusting dates the time of deformation in the Maria fold and thrust belt as Late Cretaceous, and based on resetting of hornblende, with a closure temperature for argon diffusion of ~500°C, we infer that basement involvement was relatively thick-skinned.

Hornblende spectra from Mesquite Mountain, the northern Granite Wash Mountains, and the northern Plomosa Mountains document significant heterogeneity during the Late Cretaceous thermal event, ranging from complete resetting to only minor disturbance of argon systematics. We interpret these variations to reflect different structural levels within the Maria fold and thrust belt.

Based on muscovite and biotite ages from west-central Arizona, the early Tertiary was characterized by a period of slow cooling, at rates between 5-10°C / m.y., assuming an average, linear cooling rate. More realistically, cooling histories are probably characterized by faster cooling rates initially, and slower cooling during the later part of the cooling path. Extremely rapid cooling resulted from tectonic denudation of mid-crustal levels in west-central Arizona in late Oligocene to early Miocene time.

Data from both the northern Plomosa Mountains and the Moon Mountains suggest the period of Tertiary extension and core complex development was characterized by a renewed heating event, reaching temperatures high enough at the crustal levels presently exposed to partially reset potassium feldspar, and associated with the early stages of extension.

ACKNOWLEDGEMENTS

This research was made possible through the generosity of Dr. Mark Harrison at SUNY Albany , who provided both technical and material support in abundance. JHK expresses gratitude to the Tribal Council of the Colorado River Indian Tribes for permission to collect samples from the Moon Mountains and Mesquite Mountain on the Colorado River Indian Reservation. Maureen Noonan provided able field assistance during collection of the samples. Appreciation is extended to Brian Wernicke for use of rock crushing and mineral separation facilities at Harvard University. Thanks to Larry McKenna for assistance with critical comments on statistical regression of the argon data. This work has benefitted greatly from discussions with Jon Spencer, Steve Reynolds, Kip Hodges, Dave Foster, Joan Fryxell, Laurence Page, Liz Schermer, and Steve Richard.

APPENDIX 1

SAMPLE DESCRIPTIONS

MESQUITE MOUNTAIN

Sample 87M4 is an amphibolite layer (~1 m thick) from within the Mesquite Gneiss at the southern end of Mesquite Mountain (Fig. 3.4).

Sample 87M13 comes from an amphibolite lens in the Mesquite Gneiss in the central part of Mesquite Mountain (Fig. 3.4).

Sample 87M2 was collected from a mesosomatic layer of the Mesquite Gneiss at the southern end of Mesquite Mountain (Fig. 3.4).

Sample 87M18 was collected at the northern end of Mesquite Mountain from a biotite-rich, mesosomatic layer within the Mesquite Gneiss (Fig. 3.4).

MOON MOUNTAINS

Sample 86MM25, collected from the Valenzuela metasedimentary section in the footwall of the Valenzuela thrust (Fig. 3.5), is a quartz + muscovite + sillimanite ± kyanite schist. Muscovite from this sample, making up ~15-20% of the rock, is medium- to fine-grained and grown in the well-developed foliation. Grains are typically intergrown with quartz and aluminosilicate phases and have ragged terminations, but are unaltered. Amphibolite facies metamorphism and development of the fabric in this rock was associated with emplacement of the Valenzuela thrust nappe in the Late Cretaceous (Knapp, in prep.).

Sample MM87-8 is a muscovite-rich, quartzofeldspathic schist, collected from the gneisses in the footwall of the Moon Mountain detachment fault (Fig. 3.5). Medium- to coarse-grained muscovite forms up to 40% of the rock, and occurs as cleanly terminated grains which show no sign of alteration. Shearing of muscovite, and surrounding quartz and potassium feldspar grains suggests the rock was deformed subsequent to crystallization of the present metamorphic assemblage. Type II mica "fish" (Lister and Snoke, 1984) are ubiquitous, forming a fabric inclined to the compositional layering in the rock. The metamorphic fabric in this rock is interpreted to be a Mesozoic feature, and subsequent shearing is attributed to deformation in the footwall of the detachment fault (Knapp, in prep.). The sample was taken from ~50 m structurally below the Moon Mountain detachment, within ~10 m of sample MM87-7.

Sample MM87-7 is a strongly sheared, banded orthogneiss from the footwall gneisses of the Moon Mountain detachment fault (Fig. 3.5). The rock consists of abundant, lens-shaped potassium feldspar porphyroclasts, surrounded by finer-grained quartz, potassium feldspar, plagioclase, biotite, and minor muscovite and hornblende. Biotite from this sample is medium- to fine-grained and grown parallel to compositional layering in the rock. Grains are cleanly terminated and show no signs of alteration or retrogradation. Potassium feldspar occurs in domains of polygonally recrystallized, medium to fine grains with polygonal or serrate boundaries. Based on metamorphic textures, recrystallization of the potassium feldspar megacrysts occurred during growth of the biotite. Potassium feldspars are very fresh, and show abundant tartan twinning typical of microcline. The age of these banded gneisses is inferred to be Precambrian, based on similarity to crystalline rocks of known Precambrian age from the region (see Knapp, in prep.) This sample was collected ~50 m below the Moon Mountain detachment fault, within ~10 m of sample MM87-8.

Sample 86MM23 is a sheared, megacrystic quartz syenite collected from the hanging wall of the Valenzuela thrust fault in the southern Moon Mountains (Fig. 3.5). This unit is correlated with the Tyson augen gneiss (Yeats, 1985) of the northern Dome Rock Mountains (87D20). U-Pb zircon geochronology indicates a late Middle Jurassic (160 ± 15 Ma) crystallization age for this rock (in Knapp and Walker, in prep.). The potassium feldspar separate was sized to an 80-100 mesh fraction, and contained <2% contamination of quartz and plagioclase. Some grains (<10%) showed orangish-brown iron staining due to minor inclusions of opaque oxides and biotite.

NORTHERN DOME ROCK MOUNTAINS

Sample 87D9 comes from a variably sheared, megacrystic syenogranite which sits in sharp, non-conformable contact with the basal Cambrian strata of the Paleozoic cratonal section (Fig. 3.6). The rock is characterized by abundant (30-40%), large (1-5 cm), rectangular potassium feldspar (microcline) megacrysts set in a matrix of finer-grained quartz (25-30%), potassium feldspar (15-20%), plagioclase (5-15%), and biotite (5-10%), with secondary muscovite, chlorite, and minor epidote. The rock is variably deformed, ranging from intact, potassium feldspar megacrysts floating in a crudely foliated groundmass, to mylonitic rocks in which potassium feldspar porphyroclasts are crushed and the matrix is highly sheared. Potassium feldspar is variably sericitized and biotite shows evidence of chloritic alteration along grain boundaries. Although this unit has not been dated radiometrically, Yeats (1985) argues for a Precambrian age based on (1) stratigraphic relations with the overlying Paleozoic section and (2) lithologic similarity to megacrystic granites from the Big Maria Mountains dated at about 1.4 b.y. (U-Pb zircon by L.T. Silver, cited in Hamilton, 1982). The sample sits at the base of the lower limb of the north-dipping syncline of Paleozoic rocks in Boyer's Gap, and is structurally about 100 m above the underlying Boyer's Gap shear zone.

Sample 87D20 was collected from the Tyson augen gneiss, which is carried in the hanging wall of the Tyson thrust (Fig. 3.6). Yeats (1985) describes the Tyson augen gneiss as a medium-grained, biotite-rich gneiss with up to 30% rectangular potassium feldspar (microcline) porphyroclasts. The sample consists of a highly sheared gneiss with porphyroclasts of both potassium feldspar and quartz floating in a sheared matrix of fine-grained biotite, quartz, and feldspar. Potassium feldspars are broken and crushed, but some large (2-3 cm) porphyroclasts remain. Biotite constitutes ~20% of the rock, and shows some chloritic alteration, while potassium feldspars show evidence of sericitization. Based on structural position and lithologic similarity, the Tyson augen gneiss is correlated with the megacrystic quartz syenite gneiss of Jurassic age carried in the Valenzuela thrust plate (see Moon Mountains section and Knapp, in prep.). Sample 87D20 is taken from near the Tyson thrust, about 30 m above the contact with the underlying metasedimentary rocks.

NORTHERN PLOMOSA MOUNTAINS

Sample 86NP1 comes from an amphibolite lens within the migmatitic layered gneiss sequence in the hanging wall of the Deadman thrust fault, about 30 m above the thrust contact (Fig. 3.7). The rock is medium- to coarse-grained, and consists predominantly of hornblende and plagioclase, with minor biotite, chlorite, opaque oxides, and epidote. Hornblende comprises 45-50% of the rock, and many grains are altered along fractures and cleavage planes to fine-grained mica and quartz(?). Biotite occurs in small, monominerallic domains rather than as an alteration around hornblende grains. The rock does not possess a tectonic fabric, as both hornblende and plagioclase occur as equant grains in a granoblastic texture. Stoneman (1985) inferred a Precambrian age for these gneisses based on similarity with known Precambrian gneisses from other areas in Arizona.

Sample 87P5 is a quartzofeldspathic orthogneiss from crystalline rocks in the hanging wall of the Deadman thrust fault in the Plomosa Pass area (Fig. 3.7). The rock consists of quartz (25-30%), plagioclase (50-55%), potassium feldspar (15-20%), and very minor biotite and chlorite. The rock shows evidence of deformation under conditions of cataclastic flow. Feldspar grains are typically rounded, and abundant, small fragments of feldspar and quartz make up the matrix for larger (medium to coarse) porphyroclast grains. Quartz has been strained and exhibits undulatory extinction, but in numerous cases has behaved by brittle fracturing. Biotite occurs as aggregates of very small, ragged grains and has been mostly altered to chlorite. Potassium feldspar exhibits tartan twinning (microcline), and generally appears unaltered. The age of these gneisses is inferred to be Precambrian (Stoneman, 1985). The sample was collected from ~200 m structurally above the southwest-dipping Deadman thrust fault.

Sample 87P7 is a thinly-banded, biotite-rich, quartzofeldspathic gneiss from the Precambrian crystalline rocks in the hanging wall of the Deadman thrust fault (Fig. 3.7). The rock contains the assemblage quartz (20-25%), plagioclase (35-40%), potassium feldspar (15-20%), and biotite (8-10%), with minor chlorite, epidote, and opaque oxides. Biotite is medium- to fine-grained, in ragged grains which occur as aggregates and irregular bands. Many biotite grains exhibit chloritic alteration between lamellae. Potassium feldspar is medium- to coarse-grained, usually in inclusion-free, irregular grains which exhibit well-developed tartan twinning (microcline). Although the rock shows evidence of shearing (polygonal recrystallization of quartz), potassium feldspars show only a slight cloudy alteration. Epidote occurs primarily as a vein-filling,

secondary mineralization. Potassium feldspar was sized to a 80-100 mesh fraction. The biotite separate contained ~5% chloritic intergrowths, and minor (< 1%) epidote contamination.

NORTHERN GRANITE WASH MOUNTAINS

Sample 87G16 is a metamorphosed quartzite from the crystalline rocks in the hanging wall of the Cobralla thrust system (Fig. 3.8), which consists almost exclusively of quartz and ~5% muscovite. Muscovite grains are medium to fine, cleanly terminated unaltered grains, and are aligned parallel to surrounding elongate quartz grains.

Sample 87G29 is taken from a medium-grained, quartz-biotite schist (unit XMZg6 or XMZg4) which sits within a sequence of crystalline gneisses and schists carried in the upper plate of a complex sequence of thrusts in the Cobralla area (Cunningham, 1986). This sample sits about 200 m above the highest thrust in the sequence (Fig. 3.8) within a unit Cunningham (1986) describes as "foliated granodiorite" [XMZg3: medium-grained metagranodiorite with quartz + plagioclase + alkali feldspar + biotite ± muscovite ± chlorite]. Biotite from this sample looks very fresh in thin section, with many clearly truncated grains. Both biotite and epidote (which comprises up to several percent of the modal abundance of the rock) are grown within the plane of the foliation, which is defined by mm-scale compositional segregations and the orientation of the biotites themselves.

Sample 87G30 is a medium- to fine-grained amphibolite collected from crystalline rocks carried in the hanging wall of the Cobralla thrust system of the northern Granite Wash Mountains (Fig. 3.8). Hornblende, which makes up ~40% of the rock, occurs typically as composites of small (> 0.5 mm) hornblende grains with quartz, epidote, and chlorite. Some hornblendes appear helicitic, whereas others appear to have reacted to form the composite grains. The rock does not possess a well-developed fabric, and based on the degree of retrogression (apparent also in reaction of plagioclase to epidote) and shearing of grains, appears to have experienced deformation and retrogression (greenschist to epidote-amphibolite facies) subsequent to amphibolite facies metamorphism. (These features might be interpreted in terms of an amphibolite facies metamorphism in pre-Cretaceous time (Jurassic or Proterozoic?) and greenschist to epidote-amphibolite facies metamorphism associated with emplacement of crystalline thrust nappes in the Late Cretaceous.)

Sample 87G36 is taken from a strongly foliated, coarse-grained augen gneiss which is carried as a fault-bounded structural package [Cunningham's structural unit #5] within the Hercules Thrust system of the northern Granite Wash Mountains. The rock consists of medium- to coarse-grained potassium feldspar augen in a matrix of finer-grained quartz, potassium feldspar, and biotite. The rock shows a well-developed tectonic fabric with sheared and aligned feldspar augen and matrix micas forming a planar fabric.

REFERENCES

Baldwin, S.L, and Harrison, T.M., 1988, Diffusion of ^{40}Ar in metamorphic hornblende [abs.]: EOS, v. 69, no. 16, p. 522.

Burchfiel, B.C., and Davis, G.A., 1971, Clark Mountain thrust complex in the cordillera of southeastern California: Geologic summary and field trip guide: Riverside, University of California, Campus Museum Contribution 1, p. 1-28.

Burchfiel, B.C., and Davis, G.A., 1972, Structural framework and evolution of the southern part of the Cordilleran orogen, western United States: Am. Jour. Sci., v. 272, p. 97-188.

Burchfiel, B.C., and Davis, G.A., 1975, Nature and controls of Cordilleran orogenesis, western United States: Extensions of an earlier synthesis: Am. Jour. Sci., v. 275-A, p. 363-396.

Burchfiel, B.C., and Davis, G.A., 1977, Geology of the Sagamore Canyon-Slaughterhouse Spring area, New York Mountains, California: Geological Society of America Bulletin, v. 88, p. 1623-1640.

Burchfiel, B.C., and Davis, G.A., 1981, Mojave Desert and environs, *in* Ernst, W.G., ed., The Geotectonic Development of California, (Rubey Volume I): Englewood Cliffs, New Jersey, Prentice-Hall, p. 217-252.

Carr, W.J., and Dickey, D.D., 1980, Geologic map of the Vidal, California, and Parker SW, California-Arizona, quadrangles: U.S. Geol. Survey Misc. Invest. Map, I-1125, 1:24,000.

Cunningham, W.D., 1986, Superposed thrusting in the northern Granite Wash Mountains, La Paz County, Arizona: M.S. thesis, Tucson, Univ. of Arizona, 112 p.

Dalrymple, G.B., Lanphere, M.A., and Pringle, M.S., 1988, Correlation diagrams in $^{40}Ar/^{39}Ar$ dating: Is there a correct choice?: Geophys. Res. Letters, v. 15, p. 589-591.

Davis, G.A., Anderson, J.L., Frost, E.G., and Shackelford, T.J., 1980, Mylonitization and detachment faulting in the Whipple-Buckskin-Rawhide Mountains terrane, southeastern California and western Arizona, *in* Crittenden, M.D., Jr., Coney, P.J., and Davis, G.H., eds., Cordilleran Metamorphic Core Complexes: Geol. Soc. Am. Mem. 153, p. 79-129.

Davis, G.M., 1985, Geology of the southern Plomosa Mountains: M.S. thesis, Tempe, Arizona State Univ., 158 p.

Dodson, M.H., 1973, Closure temperature in cooling geochronological and petrological systems: Contrib. Mineral. Petrol., v. 40, p. 259-274.

Ellis, M.J., 1982, Structural analysis of the Big Maria Mountains, Riverside County, California, *in* Frost, E.G., and Martin, D.L., eds. , Mesozoic-Cenozoic Tectonic Evolution of the Colorado River Region, California, Arizona, and Nevada: San Diego, California, Cordilleran Publishers, p. 223-233.

Emerson, W.S., 1982, Geologic development and late Mesozoic deformation of the Little Maria Mountains, Riverside County, California, *in* Frost, E.G., and Martin, D.L., eds., Mesozoic-Cenozoic Tectonic Evolution of the Colorado River Region, California, Arizona, and Nevada: San Diego, California, Cordilleran Publishers, p. 245-254.

England, P.C., and Thompson, A.B., 1984, Pressure-temperature-time paths of regional metamorphism I: Heat transfer during the evolution of regions of thickened continental crust: Jour. Petrol., v. 25, p. 894-928.

Fleck, R.J., Sutter, J.F., and Elliot, D.H., 1977, Interpretation of discordant $^{40}Ar/^{39}Ar$ age-spectra of Mesozoic tholeiites from Antarctica: Geochim. Cosmochim. Acta, v. 41, p. 15-32.

Foster, D.A., Harrison, T.M., Menard, T., and Spear, F.S., 1988, Mesozic thermal history of the Old Woman-Piute Mountains [OWP] from $^{40}Ar/^{39}Ar$ geothermometry [abs.]: Geol. Soc. Amer. Abstr. Progs., v. 20, no. 3, p. 161.

Foster, D.A., Harrison, T.M., Miller, C.F., Howard, K.A., and John, B.E., 1988, Mesozoic and Cenozoic thermal history of the eastern Mojave Desert, California: Insights from $^{40}Ar/^{39}Ar$ geochronology [abs.]: Geol. Soc. Amer. Abs. Progs., v. 20, no. 7, p. A17.

Foster, D.A., and Harrison, T.M., 1989, this volume?

Hamilton, W., 1964, Geologic map of the Big Maria Mountains NE quadrangle, Riverside County, California, and Yuma County, Arizona: U.S. Geol. Survey Geol. Quad. Map, GQ-350.

Hamilton, W., 1982, Structural evolution of the Big Maria Mountains, northeastern Riverside County, southeastern California , *in* Frost, E.G., and Martin, D.L., eds., Mesozoic-Cenozoic Tectonic Evolution of the Colorado River Region, California, Arizona, and Nevada: San Diego, California, Cordilleran Publishers, p. 1-27.

Hamilton, W., 1984, Generalized geologic map of the Big Maria Mtns. region, northeastern Riverside County, southeastern California: U.S. Geol. Survey Open-File Report 84-407, 1:48,000 with 7 p.

Hamilton, W., 1987, Mesozoic geology and tectonics of the Big Maria Mountains region, southeastern California, *in* Dickinson, W.R., and Klute, M.A., eds., Mesozoic rocks of southern Arizona and adjacent areas: Ariz. Geol. Soc. Digest, v. 18, p. 33-47.

Harding, L.E., 1982, Tectonic significance of the McCoy Mountains Formation, southeastern California and southwestern Arizona: Ph.D. dissertation, Tucson, Univ. of Arizona, 197 p.

Harding, L.E., 1982, A progress report on the tectonic significance of the McCoy Mountains Formation, southeastern California and southwestern Arizona, *in* Frost, E.G., and Martin, D.L., eds., Mesozoic-Cenozoic Tectonic Evolution of the Colorado River Region, California, Arizona, and Nevada: San Diego, California, Cordilleran Publishers, p. 135.

Harding, L.E., Butler, R.F., and Coney, P.J., 1983, Paleomagnetic evidence for Jurassic deformation of the McCoy Mountains Formation, southeastern California and southwestern Arizona: Earth Planet. Sci. Letters, v.62, p. 104-114.

Harding, L.E. and Coney, P.J., 1985, The geology of the McCoy Mountains Formation, southeastern California and southwestern Arizona: Geol. Soc. Amer. Bull., v. 96, p. 755-769.

Harrison, T.M., 1981, Diffusion of ^{40}Ar in hornblende: Contrib. Mineral. Petrol., v. 78, p. 324-331.

Harrison, T.M., 1983, Some observations on the interpretation of $^{40}Ar/^{39}Ar$ age spectra: Isotope Geoscience, v. 1, p. 319-338.

Harrison, T.M., and Be', K., 1983, $^{40}Ar/^{39}Ar$ age spectrum analysis of detrital microclines from the southern San Joaquin Basin, California: An approach to determining the thermal evolution of sedimentary basins: Earth Planet. Sci. Letters, v. 64, p. 244-256.

Harrison, T.M., and McDougall, I., 1980a, Investigations of an intrusive contact, northwest Nelson, New Zealand - I. Thermal, chronological and isotopic constraints: Geochim. Cosmochim. Acta, v. 44, p. 1985-2003.

Harrison, T.M., and McDougall, I., 1980b, Investigations of an intrusive contact, northwest Nelson, New Zealand - II. Diffusion of radiogenic and excess ^{40}Ar in hornblende revealed by $^{40}Ar/^{39}Ar$ age spectrum analysis: Geochim. Cosmochim. Acta, v. 44, p. 2005-2020.

Harrison, T.M., and McDougall, I., 1981, Excess ^{40}Ar in metamorphic rocks from Broken Hill, New South Wales: Implications for $^{40}Ar/^{39}Ar$ age spectra and the thermal history of the region: Earth Planet. Sci. Letters, v. 55, p. 123-149.

Harrison, T.M., and McDougall, I., 1982, The thermal significance of potassium feldspar K-Ar ages inferred from $^{40}Ar/^{39}Ar$ age spectrum results: Geochim. Cosmochim. Acta, v. 46, p. 1811-1820.

Harrison, T.M., Duncan, I., and McDougall, I., 1985, Diffusion of ^{40}Ar in biotite: Temperature, pressure and compositional effects: Geochim. Cosmochim. Acta, v. 49, p. 2461-2468.

Harrison, T.M., and FitzGerald, J.D., 1986, Exsolution in hornblende and its consequences for $^{40}Ar/^{39}Ar$ age spectra and closure temperature: Geochim. Cosmochim. Acta, v. 50, p. 247-253.

Hauser, E.C., Gephart, J., Latham, T., Oliver, J., Kaufman, S., Brown, L., and Lucchitta, I., 1987, COCORP Arizona transect: Strong crustal reflections and offset moho beneath the transition zone: Geology, v. 15, p. 1103-1106.

Heizler, M.T., and Harrison, T.M., 1988, Multiple trapped argon isotope components revealed by $^{40}Ar/^{39}Ar$ isochron analysis: Geochim. Cosmochim. Acta, v. 52, p.1295-1303.

Hodges, K.V., and Royden, L., 1984, Geologic thermobarometry of retrograded metamorphic rocks: An indication of the uplift trajectory of a portion of the northern Scandinavian Caledonides: Journal of Geophysical Research, v. 89, p. 7077-7090.

Hoisch, T.D., 1985, Metamorphism in the Big Maria Mountains, southeastern California: Unpublished Ph. D. dissertation, Univ. of Southern California, Los Angeles, 264 p.

Hoisch, T.D., Heizler, M.T., Harrison, T.M., Miller, C.F., and Stoddard, E.F., 1988, Late Cretaceous regional metamorphism in southeastern California, *in* Ernst, W.G., ed., Metamorphic and Crustal Evolution of the Western United States (Rubey Volume VII): Englewood Cliffs, New Jersey, Prentice-Hall, p. 538-571.

Knapp, J. H., 1988, Ductile to brittle structural evolution at Mesquite Mountain, west-central Arizona [abs.]: Geol. Soc. Amer. Abs. Progs., v. 20, no. 3, p. 173.

Knapp, J.H., and Heizler, M.T., 1988a, $^{40}Ar/^{39}Ar$ geochronology of crystalline thrust nappes of the Late Cretaceous Maria fold and thrust belt, west-central Arizona [abs.]: Geol. Soc. Amer. Abs. Progs., v. 20, no. 3, p. 173.

Knapp, J.H., and Heizler, M.T., 1988b, Tertiary thermal history of west-central Arizona: Implications for mechanisms of crustal extension [abs.]: Geol. Soc. Amer. Abs. Progs., v. 20, no. 7, p. A16-A17.

Knapp, J.H., in prep., Mid-Tertiary detachment tectonics at Mesquite Mountain, west-central Arizona.

Knapp, J.H., in prep., Mesozoic thrusting and Tertiary detachment faulting, Moon Mountains, west-central Arizona.

Knapp, J.H., and Walker, J.D., in prep., U-Pb geochronology of Mesozoic to Tertiary magmatism in west-central Arizona: Implications for tectonic evolution of the Mojave-Sonora region.

Laubach, S.E., 1986, Polyphase deformation, thrust-induced strain and metamorphism, and Mesozoic stratigraphy of the Granite Wash Mountains, west-central Arizona: Ph.D. dissertation, Urbana-Champaign, Univ. of Illinois, 180 p.

Laubach, S.E., Reynolds, S.J., Spencer, J.E., and Marshak, S., 1984, Polyphase deformation history of Mesozoic metasedimentary rocks in western Arizona [abs.]: Geol. Soc. Amer. Abs. Progs., v. 16, p. 570.

LeVeque, R.A., 1982, Stratigraphy and structure of the Palen Formation, Palen Mountains, southeastern California, *in* Frost, E.G., and Martin, D.L., eds., Mesozoic-Cenozoic Tectonic Evolution of the Colorado River Region, California, Arizona, and Nevada: San Diego, California, Cordilleran Publishers, p. 267-273.

Lister, G.S., and Snoke, A.W., 1984, S-C mylonites: Jour. Struc. Geol., v. 6, p. 617-638.

Lyle, J.H., 1982, Interrelationship of late Mesozoic thrust faulting and mid-Tertiary detachment faulting in the Riverside Mountains, southeastern California, *in* Frost, E.G., and Martin, D.L., eds., Mesozoic-Cenozoic Tectonic Evolution of the Colorado River Region, California, Arizona, and Nevada: San Diego, California, Cordilleran Publishers, p. 470-491.

Marshak, S., and Vander Meulen, M., in press, Geology of the Battleship Peak area, southern Buckskin Mountains, Arizona: Structural style below the Buckskin Detachment fault, *in* Spencer, J.E., and Reynolds, S.J., eds., Geology of the Buckskin Mountains: Arizona Bureau of Geology and Mineral Technology Bull. 198.

Maruyama, S., Liou, J.G., and Susuki, K., 1982, The peristerite gap in low-grade metamorphic rocks: Contrib. Mineral. Petrol., v. 81, p. 268-276.

McCarthy, J., and Thompson, G.A., 1988, Seismic imaging of extended crust with emphasis on the western United States: Geol. Soc. Am. Bull., v. 100, p. 1361-1374.

McDougall, I., and Harrison, T.M., 1988, Geochronology and thermochronology by the $^{40}Ar/^{39}Ar$ method: New York, Oxford University Press, 212 p.

Miller, F.K., 1970, Geologic map of the Quartzsite quadrangle, Yuma County, Arizona: U.S. Geol. Survey Geol. Quad. Map GQ-841.

Miller, F.K., and McKee, 1971, Thrust and strike-slip faulting in the Plomosa Mountains, southwestern Arizona: Geol. Soc. Amer. Bull., v. 82, p. 717-722.

Miller, C.F., Howard, K.A., and Hoisch, T.D., 1982, Mesozoic thrusting, metamorphism, and plutonism, Old Woman-Piute Range, southeastern California, *in* Frost, E.G., and Martin, D.L., eds., Mesozoic-Cenozoic Tectonic Evolution of the Colorado River Region, California, Arizona, and Nevada: San Diego, California, Cordilleran Publishers, p. 561-581.

Pelka, G.J., 1973, Geology of the McCoy and Palen Mountains, southeastern California: Ph.D. dissertation, Santa Barbara, Univ. of California, 162 p.

Powell, R., and Evans, J., 1983, A new geobarometer for the assemblage biotite-muscovite-chlorite-quartz: Jour. Metam. Geol., v. 1, p. 331-336.

Rehrig, W.A., and Reynolds, S.J., 1980, Geologic and geochronologic reconnaissance of a northwest-trending zone of metamorphic core complexes in southern and western Arizona, *in* Crittenden, M.D., Jr., Coney, P.J., and Davis, G.H., eds., Cordilleran Metamorphic Core Complexes: Geol. Soc. Am. Mem. 153, p. 131-157.

Reynolds, S.J., Keith, S.B., and Coney, P.J., 1980, Stacked overthrusts of Precambrian crystalline basement and inverted Paleozoic sections emplaced over Mesozoic strata, west-central Arizona, *in* Jenny, J.P., and Stone, C., eds., Studies in Western Arizona: Ariz. Geol. Soc. Digest, v. 12, p. 45-52.

Reynolds, S.J., 1982, Multiple deformation in the Harcuvar and Harquahala Mountains, west-central Arizona, *in* Frost, E.G., and Martin, D.L., eds., Mesozoic-Cenozoic Tectonic Evolution of the Colorado River Region, California, Arizona, and Nevada: San Diego, California, Cordilleran Publishers, p. 137-142.

Reynolds, S.J., Florence, F.P., Welty, J.W., Roddy, M.S., Currier, D.A., Anderson, A.V., and Keith, S.B., 1986, Compilation of Radiometric Age Determinations in Arizona: Ariz. Bur. Geol. Min. Tech. Bull. 197, 258 p.

Reynolds, S.J., and Spencer, J.E., 1985, Evidence for large-scale transport on the Bullard detachment fault, west-central Arizona: Geology, v. 13, p. 353-356.

Reynolds, S.J., Spencer, J.E., Richard, S.M., and Laubach, S.E., 1986, Mesozoic structures in west-central Arizona, *in* Beatty, B., and Wilkinson, P.A.K., eds., Frontiers In Geology and Ore Deposits of Arizona and the Southwest: Arizona Geological Society Digest , v. 16, p. 35-51.

Rice, J.M., 1977, Progressive metamorphism of impure dolomitic limestone in the Marysville aureole, Montana: Amer. Jour. Sci., v. 277, p. 1-24.

Richard, S.M., 1983, Structure and stratigraphy of the southern Little Harquahala Mountains, Yuma County, Arizona: M.S. thesis, Tucson, Univ. of Arizona, 154 p.

Richard, S.M., and Fryxell, J., this volume?

Roddick, J.C., Cliff, R.A., and Rex, D.C., 1980, The evolution of excess argon in alpine biotites--A $^{40}Ar/^{39}Ar$ analysis: Earth Planet. Sci. Lett., v. 48, p 185-208.

Scarborough, R., and Meader, N., 1983, Reconnaissance geology of the northern Plomosa Mountains, La Paz County, Arizona: Ariz. Bur. Geol. Min. Tech. Open-File Report 83-24, 35 p.

Selverstone, J., Spear, F.S., Franz, G., and Morteani, G., 1984, High-pressure metamorphism in the southwest Tauern Window, Austria: P-T paths from hornblende-kyanite-staurolite garbenschists: Jour. Petrol., v. 25, p. 501-531.

Spear, F.S., Selverstone, J., Hickmott, D., Crowley, P., and Hodges, K.V., 1984, P-T paths from garnet zoning: A new technique for deciphering tectonic processes in crystalline terranes: Geology, v. 12, p. 87-90.

Spencer, J.E., and Reynolds, S.J., in press, Tertiary structure, stratigraphy, and tectonics of the Buckskin Mountains, *in* Spencer, J.E., and Reynolds, S.J., Geology of the Buckskin Mountains: Arizona Bureau of Geology and Mineral Technology Bull. 198.

Spencer, J.E., Richard, S.M., and Reynolds, S.J., 1985, Geologic map of the Little Harquahala Mountains, west-central Arizona: Ariz. Bur. Geol. Min. Tech. Open-File Report 85-9, p. 18, 3 sheets.

Steiger, R.H., and Jäger, E., 1977, Subsommission on geochronology: Convention on the use of decay constants in geo- and cosmochronology: Earth Plan. Sci. Letters, v. 1, p. 369-371.

Stone, P., Page, V.M., Hamilton, W., and Howard, K.A., 1987, Cretaceous age of the upper part of the McCoy Mountains Formation, southeastern California and southwestern Arizona, and its tectonic significance: Reconciliation of paleobotanical and paleomagnetic evidence: Geology, v. 15, p. 561-564.

Stoneman, D.A., 1985, Structural geology of the Plomosa Pass area, northern Plomosa Mountains, La Paz County, Arizona : M.S. thesis, Tucson, Univ. of Arizona, 99 p.

Tweto, O., 1975, Laramide (Late Cretaceous-Early Tertiary) orogeny in the southern Rocky Mountains, *in* Curtis, B.F., ed., Cenozoic History of the Southern Rocky Mountains: Geol. Soc. Amer. Mem. 144, p. 1-44.

Walker, J.D., 1985, Permo-Triassic paleogeography and tectonics of the southwestern United States: Ph.D. dissertation, Cambridge, M.I.T., 224 p.

Walker, J.D., 1987, Permian to Middle Triassic rocks of the Mojave Desert, *in* Dickinson, W.R., and Klute, M.A., eds., Mesozoic rocks of southern Arizona and adjacent areas: Ariz. Geol. Soc. Digest, v. 18, p. 1-14.

Whitney, J.A., and Stormer, J.R., 1977, The distribution of $NaAlSi_3O_8$ between coexisting microcline and plagioclase and its effect on geothermometric calculations: Amer. Min., v. 62, p. 687-691.

Wright, J.E., Anderson, J.L., and Davis, G.A., 1986, Timing of plutonism, mylonitization, and decompression in a metamorphic core complex, Whipple Mountains, California [abs.]: Geol. Soc. Am. Abstr. Prog., v. 18, p. 201.

Yeats, K.J., 1985, Geology and structure of the northern Dome Rock Mountains, La Paz County, Arizona: M.S. thesis, Tucson, Univ. of Arizona, 123 p.

York, D., 1969, Least-squares fitting of a straight line with correlated errors: Earth Plan. Sci. Letters, v. 5, p. 320-324.

FIGURE CAPTIONS

Table 1: Summary of sample weights and calculated J values for samples from this study. Samples are grouped by mineral type, and correction factors for the three irradiation packages are given.

Table 2: Data tables of results of step-heating analyses for all samples in this study, grouped by area:

Tables 2a-f: Mesquite Mountain

Tables 2g-l: Moon Mountains

Tables 2m-p: northern Dome Rock Mountains

Tables 2q-t: northern Plomosa Mountains

Tables 2u-y: northern Granite Wash Mountains

Table 3: Summary of age data for all samples of this study. Included are total number of heating steps, minimum apparent age, and where appropriate, plateau age with 2σ uncertainty, steps in plateau, amount of gas in plateau, isochron age with 2σ uncertainty, steps in isochron, initial $^{40}Ar/^{36}Ar$ ratio, York regression used, and MSWD for York 2 regression.

Figure 3.1: Sketch map of the Cordillera of the western United States, showing the position of the Maria fold and thrust belt (MFTB) of the Mojave-Sonoran Desert area with respect to the east-vergent Sevier thrust belt of Late Cretaceous age.

Figure 3.2: Location map of the study area in the central portion of the Maria fold and thrust belt, Mojave-Sonoran Desert area, southeastern California and west-central Arizona. Other mountain ranges mentioned in text are also indicated. Area of figure 3.3 shown in heavy box.

Figure 3.3: Geologic sketch map of the study area in west-central Arizona, showing the location of the five areas from which samples were collected. Areas covered by Figures 3.4 through 3.8 are indicated by the boxes.

Figure 3.4: Sketch map of Mesquite Mountain, on the Colorado River Indian Reservation, showing sample localities for this study. Most bedrock exposures here consist of the Mesquite Gneiss injection migmatite complex.

Figure 3.5: Geologic sketch map and sample location map for the Moon Mountains area on the Colorado River Indian Reservation. Major structures are labeled, including the Valenzuela thrust fault (southeastern Moon Mountains) and the Moon Mountain detachment fault (northern Moon Mountains). Legend: vx=Valen crystalline assemblage, mx=Moon Mountain crystalline assemblage, vm=Valenzuela metasedimentary rocks, Jqs=Jurassic quartz syenite, mv=metavolcanic rocks, Jqp=Jurassic quartz porphyry, tpg=Tyson Peak granite, cpg=Copper Peak granite, Tmbg=Miocene biotite granite, Thbg=Miocene hornblende-biotite granite, Tcs=Tertiary conglomerate and sandstone, and Tmb=Miocene Bouse Fm.

Figure 3.6: Geologic sketch map and sample locality map for the northern Dome Rock Mountains. Sample 87D9 sits in the hanging wall of the Boyer's Gap shear zone, and 87D20 sits in the hanging wall of the Tyson thrust fault. Mapping from Yeats (1985).

Figure 3.7: Geologic sketch map and sample location map for the Plomosa Pass area of the northern Plomosa Mountains. Sample locations are indicated in the crystalline rocks in the hanging wall of the Deadman thrust fault. Mapping from Stoneman (1985).

Figure 3.8: Geologic sketch map and sample location map for the northern Granite Wash Mountains. Cobralla and Hercules thrust systems are indicated. Legend: JXg=Precambrian and/or Jurassic crystalline rocks, MzPz=Paleozoic and Mesozoic metasedimentary rocks, Kt=Cretaceous Tank Pass Granite. Mapping from Reynolds et al.(1986) and Cunningham (1986).

Figure 3.9: $^{40}Ar/^{39}Ar$ age spectra for Mesquite Mountain samples.

a: 87M4(1) hornblende
b: 87M4(2) hornblende
c: 87M13 hornblende
d: 87M2 biotite
e: 87M18 biotite
f: 87M18 potassium feldspar

Figure 3.10: $^{40}Ar/^{39}Ar$ age spectra for Moon Mountains samples.

a: 86MM25 muscovite
b: MM87-8 muscovite
c: MM87-7 biotite

d: 86MM23 biotite
e: MM87-7 potassium feldspar
f: 86MM23 potassium feldspar

Figure 3.11: $^{40}Ar/^{39}Ar$ age spectra for samples from the northern Dome Rock Mountains.

a: 87D9 biotite
b: 87D20 biotite
c: 87D9 potassium feldspar
d: 87D20 potassium feldspar

Figure 3.12: $^{40}Ar/^{39}Ar$ age spectra for samples from the northern Plomosa Mountains.

a: 86NP1 hornblende
b: 87P7 biotite
c: 87P5 potassium feldspar
d: 87P7 potassium feldspar

Figure 3.13: $^{40}Ar/^{39}Ar$ age spectra for samples from the northern Granite Wash Mountains.

a: 87G30 hornblende
b: 87G16 muscovite
c: 87G29 biotite
d: 87G36 biotite
e: 87G36 potassium feldspar

Figure 3.14: Isotope correlation plots for Mesquite Mountain samples.

a: 87M4(1) hornblende
b: 87M4(2) hornblende
c: 87M13 hornblende
d: 87M2 biotite
e: 87M18 biotite

Figure 3.15: Isotope correlation plots for Moon Mountains samples.

a: 86MM25 muscovite
b: MM87-7 biotite
c: 86MM23 biotite

Figure 3.16: Isotope correlation plots for samples from the northern Dome Rock Mountains.

a: 87D9 biotite
b: 87D20 biotite
c: 87D20 potassium feldspar

Figure 3.17: Isotope correlation plots for samples from the northern Plomosa Mountains.

a: 86NP1 hornblende
b: 87P7 potassium feldspar

Figure 3.18: Isotope correlation plots for samples from the northern Granite Wash Mountains.

a: 87G30 hornblende
b: 87G16 muscovite
c: 87G29 biotite
d: 87G36 biotite
e: 87G36 potassium feldspar

Figure 3.19: Temperature-time history for the Mesquite Mountain area, reflecting ~5°C/m.y. cooling rate for the latest Cretaceous and early Tertiary, with acceleration of the cooling rate to ~20°C/m.y. associated with tectonic denudation.

Figure 3.20: Temperature-time history for the Moon Mountains, reflecting very rapid cooling (~30°C/m.y.) during the early Tertiary, followed by slow cooling through the middle Tertiary.

Figure 3.21: Temperature-time history for the northern Dome Rock Mountains area. Only the temperature interval from ~300-150°C is covered, and reflects s cooling rate of ~5°C/m.y. for this area.

Figure 3.22: Temperature-time history for the northern Plomosa Mountains area. Shown in the heavy line is the cooling path (~2°C/m.y.) predicted by simple interpolation between data points. Lighter curve reflects cooling from >300°C in Late Cretaceous time, and re-heating during early stages of extension, as suggested by biotite and potassium feldspar spectra for this area.

Figure 3.23: Temperature-time history for the northern Granite Wash Mountains area, consistent with slow-cooling throughout the Tertiary at 5-10°C/m.y.

Table 1
$^{40}Ar/^{39}Ar$ sample weights and J values

sample #	phase	weight (mg)	J value (E-3)
87M4(1)	hornblende	314.13	6.433
87M4(2)	hornblende	299.31	4.790
87M13	hornblende	298.85	4.898
86NP1	hornblende	338.32	6.366
87G30	hornblende	297.36	5.593
86MM25	muscovite	88.24	4.861
MM87-8	muscovite	89.68	4.837
87G16	muscovite	76.06	6.466
87M2	biotite	86.82	6.333
87M18	biotite	78.63	6.403
86MM23	biotite	92.97	6.469
MM87-7	biotite	101.04	4.886
87D9	biotite	99.58	6.352
87D20	biotite	99.07	6.370
87P7	biotite	80.82	6.467
87G29	biotite	83.05	6.386
87G36	biotite	84.46	6.468
87M18	K-feldspar	100.79	6.363
86MM23	K-feldspar	106.65	6.354
MM87-7	K-feldspar	111.64	4.889
87D9	K-feldspar	103.32	6.392
87D20	K-feldspar	101.77	6.382
87P5	K-feldspar	145.22	6.294
87P7	K-feldspar	113.20	6.418
87G36	K-feldspar	104.17	6.410

correction factors:

	40/39 K	36/37 Ca	39/37 Ca
group 1	0.033	0.00222	0.000825
group 2	0.1333	0.000195	0.000751
group 3	0.0279	0.000204	0.000742

Table 2

$^{40}Ar/^{39}Ar$ data tables

a - y

87M4(1) HORNBLENDE

STEP #	TEMP (°C)	40Ar/39Ar	37Ar/39Ar	36Ar/39Ar	39Ar (E-13 mol)	total %39Ar	40Ar* %	40Ar*/39Ar(K)	K-Ar age (Ma)	error in age
1	750	232.9	2.636	6.568E-01	0.384	1.05	16.6	39.04	404.2	27.3
2	820	73.13	2.198	2.085E-01	0.104	1.34	14.9	11.65	130.4	20.5
3	920	37.58	4.889	1.054E-01	0.263	2.06	17.0	6.749	76.7	9.1
4	980	39.58	7.880	1.098E-01	0.518	3.48	18.8	7.668	86.9	4.6
5	1020	23.64	8.282	5.825E-02	0.712	5.43	28.5	6.985	79.3	2.9
6	1040	13.90	7.026	2.525E-02	1.14	8.55	47.9	6.907	78.4	2.3
7	1060	9.601	6.773	1.145E-02	2.63	15.8	67.7	6.666	75.8	1.0
8	1080	8.825	6.735	8.718E-03	4.03	26.8	74.4	6.695	76.1	0.4
9	1100	8.920	6.756	8.839E-03	2.90	34.7	73.9	6.756	76.8	0.8
10	1120	8.941	6.794	8.725E-03	2.88	42.6	74.3	6.814	77.4	0.9
11	1140	9.100	6.882	9.585E-03	1.98	48.1	71.5	6.724	76.4	0.7
12	1160	11.13	6.907	1.685E-02	1.36	51.8	57.2	6.609	75.1	1.5
13	1200	8.745	6.565	6.506E-03	1.40	55.6	79.3	7.259	82.3	1.5
14	1450	8.107	6.672	4.215E-03	16.2	100.0	89.3	7.306	82.9	0.1

87M4(2) HORNBLENDE

STEP #	TEMP (°C)	40Ar/39Ar	37Ar/39Ar	36Ar/39Ar	39Ar (E-13 mol)	total %39Ar	40Ar* %	40Ar*/39Ar(K)	K-Ar age (Ma)	error in age
1	750	201.9	2.715	4.987E-01	0.284	2.17	27.0	54.78	420.4	16.7
2	820	25.78	3.270	2.578E-02	0.078	2.77	67.8	18.38	152.2	21.1
3	920	11.72	6.528	1.841E-02	0.129	3.75	53.2	6.678	56.8	4.4
4	980	10.97	9.235	3.005E-03	0.764	9.59	95.6	10.68	90.0	1.7
5	1020	9.509	6.731	4.964E-03	0.902	16.5	87.5	8.462	71.7	1.0
6	1040	9.920	6.756	3.867E-03	2.12	32.7	91.9	9.203	77.8	1.0
7	1060	9.388	6.893	3.855E-03	1.23	42.1	91.2	8.681	73.5	1.8
8	1080	9.165	7.163	2.097E-03	0.723	47.6	96.2	8.997	76.1	1.0
9	1100	9.881	7.332	5.142E-03	0.249	49.5	85.4	8.824	74.7	5.3
10	1120	10.19	7.049	2.933E-03	0.693	54.8	94.1	9.771	82.5	2.2
11	1140	10.49	6.836	3.001E-03	1.65	67.4	94.7	10.04	84.7	0.7
12	1270	10.18	6.710	2.754E-03	4.26	100.0	95.5	9.792	82.7	0.5

87M13 HORNBLENDE

STEP #	TEMP (°C)	40Ar/39Ar	37Ar/39Ar	36Ar/39Ar	39Ar (E-13 mol)	total %39Ar	40Ar* %	40Ar*/39Ar(K)	K-Ar age (Ma)	error in age
1	700	524.7	2.181	1.291E+00	0.195	0.527	27.3	143.5	960.6	23.7
2	800	31.97	1.859	4.865E-02	0.164	0.970	54.3	17.70	150.0	37.9
3	850	14.04	3.813	6.265E-03	0.121	1.30	83.4	12.43	106.6	9.0
4	920	13.20	5.930	1.502E-02	0.265	2.01	67.0	9.131	78.9	7.9
5	960	11.50	8.035	1.069E-02	0.204	2.56	73.4	8.850	76.6	5.4
6	990	9.337	5.276	3.577E-03	0.351	3.51	89.1	8.604	74.5	3.0
7	1000	9.352	4.661	2.853E-03	1.09	6.46	92.8	8.792	76.1	2.1
8	1010	9.507	4.544	3.283E-03	1.84	11.4	91.9	8.813	76.2	0.8
9	1020	9.699	4.513	2.974E-03	2.43	18.0	93.1	9.095	78.6	0.5
10	1030	9.772	4.473	3.309E-03	1.98	23.3	92.0	9.066	78.4	1.3
11	1040	9.480	4.505	2.569E-03	3.47	32.7	94.3	8.995	77.8	0.4
12	1060	8.797	4.493	2.422E-03	4.98	46.2	94.4	8.352	72.3	0.5
13	1075	8.306	4.458	2.503E-03	4.46	58.2	93.7	7.833	67.9	0.5
14	1090	8.252	4.465	2.233E-03	3.91	68.8	94.6	7.859	68.1	0.6
15	1105	8.553	4.503	3.409E-03	1.43	72.7	90.3	7.815	67.8	0.9
16	1130	9.021	4.561	3.213E-03	1.04	75.5	91.2	8.347	72.3	1.0
17	1160	9.542	4.577	3.518E-03	2.75	82.9	91.4	8.780	76.0	1.2
18	1200	9.284	4.459	3.014E-03	5.61	98.1	92.8	8.663	75.0	0.2
19	1450	10.20	4.472	7.927E-03	0.715	100.0	78.3	8.126	70.4	2.1

87M2 BIOTITE

STEP #	TEMP (°C)	40Ar/39Ar	37Ar/39Ar	36Ar/39Ar	39Ar (E-13 mol)	total %39Ar	40Ar* %	40Ar*/39Ar(K)	K-Ar age (Ma)	error in age
1	600	23.99	0.1697	7.490E-02	1.56	1.29	7.6	1.835	20.8	1.1
2	670	4.612	0.1815	7.518E-03	4.93	5.36	50.9	2.370	26.9	0.5
3	750	3.519	0.0260	2.784E-03	14.5	17.3	75.4	2.665	30.2	0.2
4	800	3.765	0.0137	3.043E-03	12.4	27.6	74.9	2.834	32.1	0.2
5	850	3.815	0.0172	3.158E-03	8.60	34.6	74.3	2.850	32.3	0.3
6	950	3.935	0.0463	3.525E-03	10.4	43.2	72.4	2.864	32.4	0.1
7	1050	3.452	0.0898	2.301E-03	19.2	59.1	79.3	2.745	**31.1**	**0.1**
8	1150	3.021	0.0371	8.952E-04	32.1	85.6	90.0	2.726	**30.9**	**0.1**
9	1350	3.702	0.0904	1.953E-03	17.5	100.0	83.4	3.098	35.1	0.1

87M18 BIOTITE

STEP #	TEMP (°C)	40Ar/39Ar	37Ar/39Ar	36Ar/39Ar	39Ar (E-13 mol)	total %39Ar	40Ar* %	40Ar*/39Ar(K)	K-Ar age (Ma)	error in age
1	600	10.35	0.0631	2.908E-02	3.58	3.26	16.6	1.728	19.9	0.5
2	700	3.852	0.0583	3.882E-03	14.1	16.1	69.2	2.676	30.6	0.1
3	760	3.795	0.0125	2.771E-03	16.3	30.9	77.3	2.944	33.7	0.1
4	820	3.919	0.0102	2.551E-03	16.4	45.8	79.7	3.133	**35.8**	**0.2**
5	900	3.910	0.0257	2.562E-03	9.31	54.3	79.4	3.122	**35.7**	**0.2**
6	980	3.854	0.0977	3.088E-03	9.60	63.0	75.2	2.915	33.4	0.2
7	1050	3.574	0.1192	2.572E-03	10.9	72.9	77.6	2.789	31.9	0.2
8	1100	3.531	0.0731	2.203E-03	9.74	81.8	80.3	2.852	32.6	0.2
9	1150	3.506	0.0976	1.664E-03	10.0	90.9	84.7	2.988	34.2	0.2
10	1220	3.850	0.1515	2.488E-03	8.80	98.9	79.8	3.092	35.4	0.3
11	1350	7.558	0.5536	1.358E-02	1.24	100.0	46.0	3.550	40.5	2.1

87M18 K-FELDSPAR

STEP #	TEMP (°C)	40Ar/39Ar	37Ar/39Ar	36Ar/39Ar	39Ar (E-13 mol)	total %39Ar	40Ar* %	40Ar*/39Ar(K)	K-Ar age (Ma)	error in age
1	450	495.5	0.1446	1.538E+00	0.110	0.121	8.19	41.00	418.2	57.3
2	500	147.2	0.2345	4.027E-01	0.055	0.181	18.1	28.19	297.6	63.0
3	550	81.48	0.1822	2.028E-01	0.094	0.284	24.8	21.53	231.7	20.8
4	580	25.38	0.1807	5.373E-02	0.118	0.414	32.0	9.483	105.7	9.2
5	610	18.87	0.1653	4.239E-02	0.194	0.626	29.5	6.322	71.2	8.9
6	640	28.43	0.2877	7.416E-02	0.133	0.772	20.2	6.503	73.1	9.0
7	670	9.953	0.1636	2.381E-02	0.387	1.20	25.7	2.895	32.9	9.1
8	700	7.604	0.1617	1.509E-02	0.556	1.81	36.7	3.123	35.5	3.4
9	750	5.668	0.1380	1.024E-02	1.53	3.48	43.7	2.618	29.8	1.3
10	820	3.982	0.1178	5.095E-03	3.05	6.83	59.1	2.451	27.9	0.3
11	900	3.036	0.1146	2.172E-03	8.87	16.6	76.6	2.369	27.0	0.2
12	970	2.409	0.1381	1.154E-03	4.37	21.4	81.0	2.044	23.3	0.3
13	1020	2.192	0.1207	7.748E-04	4.92	26.7	84.5	1.938	22.1	0.2
14	1100	2.341	0.0776	1.336E-03	8.40	36.0	79.9	1.918	21.9	0.4
15	1160	2.839	0.0643	2.505E-03	7.59	44.3	71.3	2.070	23.6	0.1
16	1200	3.677	0.0970	4.452E-03	4.27	49.0	61.5	2.335	26.6	0.3
17	1240	5.095	0.1685	7.726E-03	4.69	54.1	53.6	2.790	31.8	0.4
18	1280	5.958	0.2013	8.592E-03	5.82	60.5	56.2	3.400	38.6	0.2
19	1320	5.638	0.1421	5.781E-03	10.1	71.6	68.7	3.906	44.3	0.1
20	1360	5.514	0.1151	4.418E-03	14.0	86.9	75.4	4.183	47.4	0.2
21	1400	5.540	0.1150	4.137E-03	7.67	95.3	76.6	4.292	48.6	0.2
22	1550	6.295	0.1717	4.460E-03	4.24	100	77.3	4.956	56.0	0.3

86MM25 MUSCOVITE

STEP #	TEMP (°C)	40Ar/39Ar	37Ar/39Ar	36Ar/39Ar	39Ar (E-13 mol)	total %39Ar	40Ar*%	40Ar*/39Ar(K)	K-Ar age (Ma)	error in age
1	600	26.56	0.4053	7.852E-02	2.17	6.93	12.6	3.355	29.2	1.3
2	670	7.465	0.2996	1.233E-02	2.46	14.8	50.8	3.812	33.1	0.6
3	740	9.385	0.0563	1.245E-02	2.83	23.8	60.3	5.682	**49.2**	**0.8**
4	800	6.905	0.0309	3.563E-03	5.15	40.3	84.1	5.826	**50.4**	**0.7**
5	840	6.323	0.0164	1.596E-03	5.76	58.6	91.9	5.825	**50.4**	**0.3**
6	870	6.108	0.0326	1.484E-03	3.62	70.2	92.0	5.644	**48.8**	**0.4**
7	900	6.486	0.0545	3.784E-03	4.01	83.0	82.1	5.343	46.3	0.7
8	950	6.071	0.1931	2.450E-03	1.01	86.2	86.4	5.332	46.2	2.5
9	1000	6.555	0.0905	3.075E-03	2.64	94.7	85.3	5.624	48.7	0.8
10	1100	6.755	0.1197	3.540E-03	1.03	97.9	83.0	5.689	49.2	1.3
11	1350	8.094	0.8169	3.388E-03	0.643	100	86.2	7.119	61.4	1.5

MM87-8 MUSCOVITE

STEP #	TEMP (°C)	40Ar/39Ar	37Ar/39Ar	36Ar/39Ar	39Ar (E-13 mol)	total %39Ar	40Ar*%	40Ar*/39Ar(K)	K-Ar age (Ma)	error in age
1	600	12.22	0.1020	2.868E-02	1.73	1.52	30.3	3.724	32.2	0.8
2	670	6.102	0.0215	4.803E-03	3.51	4.59	76.0	4.656	40.2	0.8
3	740	5.660	0.0136	2.328E-03	4.15	8.23	87.0	4.945	42.6	0.4
4	800	6.045	0.0064	2.060E-03	8.95	16.1	89.3	5.409	46.6	0.2
5	840	6.221	0.0025	1.247E-03	13.3	27.7	93.5	5.825	**50.1**	**0.2**
6	870	6.143	0.0024	8.221E-04	13.5	39.6	95.5	5.872	**50.5**	**0.2**
7	900	6.051	0.0032	9.891E-04	9.30	47.7	94.5	5.731	**49.3**	**0.2**
8	930	6.037	0.0010	6.537E-04	9.36	55.9	96.2	5.816	**50.1**	**0.2**
9	1000	6.117	0.0019	9.141E-04	17.0	70.8	95.0	5.819	**50.1**	**0.1**
10	1050	6.247	0.0020	5.850E-04	13.4	82.6	96.7	6.046	52.0	0.2
11	1150	6.240	0.0019	3.140E-04	18.3	98.6	98.0	6.119	52.6	0.1
12	1350	5.970	0.0955	1.441E-03	1.57	100	91.5	5.522	47.6	2.1

MM87-7 K-FELDSPAR

STEP #	TEMP (°C)	40Ar/39Ar	37Ar/39Ar	36Ar/39Ar	39Ar (E-13 mol)	total %39Ar	40Ar*%	40Ar*/39Ar(K)	K-Ar age (Ma)	error in age
1	450	188.8	0.1248	1.920E-01	0.058	0.063	69.3	132.1	898.6	80.7
2	500	116.1	0.0557	6.016E-02	0.165	0.241	84.2	98.30	708.0	13.6
3	550	44.78	0.0023	1.644E-02	0.468	0.746	88.7	39.89	321.5	3.8
4	580	11.80	0.0158	6.202E-03	0.865	1.68	83.4	9.940	85.6	2.6
5	610	7.917	0.0042	4.504E-03	1.24	3.02	82.0	6.558	56.9	1.3
6	640	6.734	0.0105	2.615E-03	1.99	5.16	87.5	5.934	51.6	1.2
7	670	4.670	0.0082	1.819E-03	3.55	8.99	87.4	4.105	35.8	0.8
8	700	3.678	0.0086	1.547E-03	4.53	13.9	86.3	3.194	27.9	0.4
9	750	3.351	0.0078	9.715E-04	9.43	24.1	90.3	3.037	26.6	0.2
10	800	2.974	0.0105	9.459E-04	6.39	31.0	89.2	2.667	23.4	0.4
11	870	3.216	0.0147	4.614E-04	7.79	39.4	94.5	3.053	26.7	0.3
12	900	2.791	0.0176	2.137E-04	5.10	44.9	96.1	2.701	23.7	0.7
13	960	3.067	0.0189	1.101E-03	4.79	50.0	87.9	2.715	23.8	0.4
14	1020	3.176	0.0120	6.630E-04	4.05	54.4	92.3	2.953	25.9	0.6
15	1080	3.501	0.0088	5.409E-04	5.86	60.7	94.2	3.314	29.0	0.4
16	1130	4.263	0.0100	8.557E-04	4.81	65.9	93.0	3.983	34.8	0.4
17	1180	5.953	0.0187	2.386E-03	5.42	71.8	87.4	5.221	45.5	0.4
18	1210	7.480	0.0183	2.340E-03	3.22	75.2	90.0	6.762	58.7	0.6
19	1240	7.351	0.0052	1.938E-03	13.0	89.3	91.7	6.751	58.6	0.1
20	1280	6.926	0.0036	1.860E-03	7.11	96.9	91.5	6.349	55.1	0.2
21	1330	7.201	0.0035	2.906E-03	2.29	99.4	87.2	6.315	54.9	1.0
22	1360	11.44	0.0704	1.404E-02	0.259	99.7	61.5	7.268	63.0	7.9
23	1430	14.41	0.1549	2.769E-02	0.177	99.9	41.5	6.210	54.0	16.6
24	1550	18.67	0.1321	3.247E-02	0.121	100	46.5	9.056	78.2	22.0

MM87-7 BIOTITE

STEP #	TEMP (°C)	40Ar/39Ar	37Ar/39Ar	36Ar/39Ar	39Ar (E-13 mol)	total %39Ar	40Ar*%	40Ar*/39Ar(K)	K-Ar age (Ma)	error in age
1	600	16.36	0.0403	3.656E-02	4.00	3.95	33.8	5.531	48.1	0.7
2	670	6.533	0.0049	2.018E-03	10.1	13.9	90.3	5.909	51.3	0.2
3	750	6.238	0.0036	9.076E-04	22.4	36.1	95.2	5.942	51.6	0.2
4	800	6.149	0.0046	3.989E-04	13.8	49.7	97.5	6.004	52.2	0.1
5	850	6.370	0.0235	5.596E-04	6.65	56.3	96.8	6.178	53.7	0.2
6	930	6.544	0.0185	1.912E-03	7.64	63.8	90.8	5.952	51.7	0.3
7	990	6.207	0.0041	5.185E-04	15.3	78.9	97.0	6.026	52.4	0.1
8	1030	6.300	0.0088	4.571E-04	9.51	88.3	97.3	6.138	53.3	0.2
9	1080	6.371	0.0223	8.478E-04	5.92	94.2	95.4	6.094	52.9	0.3
10	1150	6.459	0.1202	5.572E-04	5.23	99.3	96.8	6.274	54.5	0.5
11	1350	10.79	1.299	5.271E-03	0.690	100	84.9	9.292	80.1	2.5

86MM23 BIOTITE

STEP #	TEMP (°C)	40Ar/39Ar	37Ar/39Ar	36Ar/39Ar	39Ar (E-13 mol)	total %39Ar	40Ar*%	40Ar*/39Ar(K)	K-Ar age (Ma)	error in age
1	650	7.587	0.0850	1.599E-02	8.27	7.00	37.2	2.835	32.8	0.2
2	750	-	-	-	-	-	-	-	-	-
3	820	5.055	0.0092	2.652E-03	22.8	26.3	83.7	4.239	48.8	0.1
4	880	5.433	0.0174	4.213E-03	12.4	36.8	76.3	4.156	47.9	0.2
5	950	5.076	0.0529	3.470E-03	15.8	50.2	79.0	4.021	46.3	0.1
6	1050	4.733	0.0545	2.031E-03	24.6	71.0	86.6	4.104	47.3	0.1
7	1120	4.680	0.0243	1.319E-03	19.0	87.1	90.8	4.259	49.0	0.2
8	1180	4.822	0.0454	1.476E-03	12.0	97.2	90.0	4.356	50.1	0.2
9	1250	5.882	0.1122	4.769E-03	2.94	99.7	74.7	4.448	51.2	1.2
10	1350	15.04	0.2619	3.012E-02	0.347	100	39.2	6.125	70.1	5.1

86MM23 K-FELDSPAR

STEP #	TEMP (°C)	40Ar/39Ar	37Ar/39Ar	36Ar/39Ar	39Ar (E-13 mol)	total %39Ar	40Ar*%	40Ar*/39Ar(K)	K-Ar age (Ma)	error in age
1	450	193.8	0.0211	5.177E-01	0.179	0.115	20.7	40.79	415.8	155
2	500	42.60	0.0821	1.016E-01	0.160	0.218	27.5	12.55	138.4	9.5
3	550	17.05	0.0381	2.344E-02	0.415	0.484	55.3	10.09	112.1	3.3
4	580	5.537	0.0235	5.037E-03	0.587	0.861	62.9	4.017	45.5	1.9
5	610	4.158	0.0203	3.839E-03	0.929	1.46	63.7	2.992	34.0	1.1
6	640	3.483	0.0239	2.745E-03	1.35	2.32	68.5	2.640	30.0	0.8
7	670	2.931	0.0246	2.411E-03	2.04	3.63	68.9	2.187	24.9	0.5
8	700	2.647	0.0200	1.563E-03	3.30	5.75	77.0	2.153	24.5	0.7
9	750	2.521	0.0227	1.305E-03	4.11	8.39	79.6	2.104	24.0	0.3
10	800	2.183	0.0265	6.092E-04	8.95	14.1	88.1	1.972	22.5	0.2
11	870	2.092	0.0356	3.051E-04	15.9	24.3	92.8	1.971	22.5	0.1
12	950	2.106	0.0469	3.128E-04	19.2	36.7	93.0	1.984	22.6	0.1
13	990	2.143	0.0472	4.409E-04	7.13	41.2	89.6	1.983	22.6	0.1
14	1030	2.214	0.0446	7.478E-04	5.15	44.6	84.9	1.963	22.4	0.4
15	1100	2.392	0.0442	8.515E-04	7.30	49.2	85.8	2.110	24.0	0.2
16	1140	2.560	0.0349	9.991E-04	7.38	54.0	85.0	2.234	25.4	0.2
17	1180	2.912	0.0367	1.423E-03	8.55	59.5	82.8	2.461	28.0	0.1
18	1210	3.236	0.0398	2.009E-03	7.22	64.1	79.0	2.612	29.7	0.3
19	1260	3.536	0.0478	2.197E-03	11.3	71.4	79.8	2.857	32.5	0.2
20	1320	3.633	0.0255	1.825E-03	25.2	87.5	83.8	3.062	34.8	0.1
21	1360	3.322	0.0144	1.964E-03	15.4	97.4	80.8	2.710	30.8	0.1
22	1450	4.298	0.0223	1.964E-03	3.69	99.8	83.1	3.686	41.8	0.1
23	1550	12.45	0.2728	1.015E-02	0.327	100	67.5	9.438	105.1	4.3

87D9 BIOTITE

STEP #	TEMP (°C)	40Ar/39Ar	37Ar/39Ar	36Ar/39Ar	39Ar (E-13 mol)	total %39Ar	40Ar*%	40Ar*/39Ar(K)	K-Ar age (Ma)	error in age
1	600	18.19	0.0773	4.043E-02	2.30	1.52	34.0	6.215	69.9	0.9
2	670	6.352	0.0961	7.037E-03	5.67	5.28	66.5	4.246	48.0	0.4
3	750	5.525	0.0161	2.438E-03	16.6	16.3	86.2	4.773	53.9	0.2
4	800	5.396	0.0058	1.657E-03	19.0	28.9	90.1	4.874	55.0	0.1
5	850	5.359	0.0060	1.711E-03	16.0	39.5	89.7	4.821	54.4	0.2
6	900	5.699	0.0110	2.956E-03	9.82	46.0	83.8	4.793	54.1	0.2
7	950	5.883	0.0235	3.579E-03	6.90	50.5	81.1	4.794	54.1	0.2
8	1000	5.745	0.0223	3.221E-03	7.44	55.5	82.5	4.762	53.8	0.4
9	1100	5.286	0.0071	8.968E-04	28.7	74.5	94.2	4.988	56.3	0.1
10	1200	5.340	0.0156	8.362E-04	29.9	94.3	94.7	5.061	57.1	0.1
11	1350	7.322	0.0716	3.645E-03	8.64	100.0	84.6	6.217	69.9	0.2

87D20 BIOTITE

STEP #	TEMP (°C)	40Ar/39Ar	37Ar/39Ar	36Ar/39Ar	39Ar (E-13 mol)	total %39Ar	40Ar*%	40Ar*/39Ar(K)	K-Ar age (Ma)	error in age
1	600	18.32	0.1146	2.512E-02	3.79	4.15	59.2	10.87	120.8	0.3
2	670	6.764	0.0532	5.797E-03	6.18	10.9	73.9	5.022	56.8	0.4
3	750	5.257	0.0370	2.448E-03	11.7	23.7	85.4	4.503	51.0	0.3
4	800	5.391	0.0290	2.598E-03	9.82	34.5	84.9	4.592	52.0	0.2
5	850	5.720	0.0512	3.670E-03	7.09	42.2	80.1	4.606	52.2	0.3
6	880	5.948	0.1546	4.261E-03	4.66	47.3	77.9	4.667	52.8	0.3
7	950	5.695	0.4214	3.461E-03	7.82	55.9	81.6	4.669	52.9	0.2
8	1000	5.431	0.7457	2.150E-03	10.1	66.9	88.3	4.815	54.5	0.1
9	1100	5.226	0.3955	1.152E-03	20.2	89.0	93.2	4.880	55.2	0.1
10	1200	10.88	2.758	2.882E-03	8.86	98.7	93.3	10.20	113.6	0.4
11	1350	41.17	8.731	1.446E-02	1.15	100.0	90.6	37.71	388.4	1.9

87D9 K-FELDSPAR

STEP #	TEMP (°C)	40Ar/39Ar	37Ar/39Ar	36Ar/39Ar	39Ar (E-13 mol)	total %39Ar	40Ar*%	40Ar*/39Ar(K)	K-Ar age (Ma)	error in age
1	450	553.8	0.0959	1.141E+00	0.157	0.102	39.1	216.6	1568	57.9
2	500	135.4	0.0597	1.545E-01	0.181	0.220	66.0	89.72	817.8	43.2
3	550	52.68	0.0179	4.952E-02	0.524	0.562	71.9	38.02	392.4	3.9
4	580	14.87	0.0213	1.447E-02	0.907	1.15	70.5	10.56	117.9	2.9
5	610	11.69	0.0285	9.301E-03	1.14	1.90	75.7	8.911	99.9	1.9
6	640	9.053	0.0603	7.687E-03	1.97	3.18	74.2	6.753	76.2	1.1
7	670	6.283	0.0873	5.705E-03	2.12	4.56	72.2	4.570	51.9	1.2
8	700	4.682	0.0977	3.365E-03	2.90	6.45	77.6	3.661	41.7	0.6
9	750	4.633	0.0762	2.927E-03	4.66	9.49	80.4	3.740	42.6	0.3
10	800	3.195	0.0248	1.593E-03	6.25	13.6	83.9	2.693	30.8	0.5
11	870	2.965	0.0102	1.101E-03	12.5	21.7	87.7	2.607	29.8	0.2
12	950	2.827	0.0128	9.285E-04	8.28	27.1	88.8	2.520	28.8	0.2
13	1020	3.041	0.0121	1.241E-03	7.23	31.8	86.5	2.642	30.2	0.3
14	1100	3.546	0.0108	1.830E-03	8.70	37.5	83.6	2.973	34.0	0.2
15	1140	4.658	0.0103	3.062E-03	7.17	42.2	79.6	3.721	42.4	0.2
16	1180	5.648	0.0114	3.861E-03	7.56	47.1	79.0	4.475	50.9	0.3
17	1220	6.490	0.0119	3.989E-03	8.63	52.7	81.2	5.279	59.9	0.5
18	1260	7.167	0.0073	3.811E-03	14.7	62.3	83.8	6.008	68.0	0.2
19	1300	7.313	0.0031	3.335E-03	23.0	77.3	86.0	6.295	71.2	0.1
20	1350	7.105	0.0020	3.020E-03	28.8	96.1	86.9	6.180	69.9	0.1
21	1400	7.275	0.0063	2.841E-03	5.32	99.6	87.8	6.403	72.4	0.3
22	1550	11.12	0.0143	8.121E-03	0.661	100.0	77.1	8.688	97.5	5.8

87D20 K-FELDSPAR

STEP #	TEMP (°C)	40Ar/39Ar	37Ar/39Ar	36Ar/39Ar	39Ar (E-13 mol)	total %39Ar	40Ar* %	40Ar*/39Ar(K)	K-Ar age (Ma)	error in age
1	450	272.2	0.0477	5.198E-01	0.231	0.282	43.2	118.6	1017	18.7
2	500	116.0	0.0181	1.200E-01	0.279	0.623	68.3	80.51	748.0	6.0
3	550	52.60	0.0027	3.973E-02	0.654	1.42	76.5	40.83	417.7	2.8
4	580	16.39	0.0200	2.311E-02	0.783	2.38	56.0	9.529	106.5	3.1
5	610	11.65	0.0137	1.695E-02	0.890	3.47	54.1	6.609	74.5	3.0
6	640	9.998	0.0235	1.294E-02	1.14	4.86	58.8	6.143	69.4	1.3
7	670	7.803	0.0149	1.215E-02	2.44	7.84	52.2	4.181	47.5	0.7
8	700	4.701	0.0192	7.979E-03	1.23	9.34	45.3	2.312	26.4	1.3
9	750	11.94	0.0164	2.148E-02	0.763	10.3	44.1	5.561	62.9	2.2
10	800	3.700	0.0086	4.108E-03	5.03	16.4	64.6	2.454	28.0	0.2
11	870	8.235	0.0208	1.773E-02	0.715	17.3	34.9	2.964	33.8	3.2
12	950	4.318	0.0093	5.716E-03	1.85	19.6	56.6	2.597	29.7	1.1
13	1020	3.225	0.0127	2.572E-03	6.62	27.6	73.7	2.433	27.8	0.3
14	1100	4.416	0.0100	3.780E-03	10.5	40.5	73.2	3.267	37.2	0.3
15	1140	5.257	0.0087	4.806E-03	12.2	55.4	71.8	3.804	43.3	0.2
16	1180	5.598	0.0097	5.177E-03	8.93	66.3	71.4	4.036	45.9	0.3
17	1210	5.887	0.0069	4.718E-03	14.1	83.5	75.3	4.460	50.6	0.1
18	1250	7.618	0.0119	7.570E-03	2.66	86.8	68.5	5.349	60.6	1.2
19	1290	8.501	0.0084	6.730E-03	5.11	93.0	75.4	6.480	73.1	0.4
20	1350	9.394	0.0045	7.856E-03	4.11	98.0	74.0	7.040	79.3	0.3
21	1400	13.90	0.0278	2.120E-02	1.04	99.3	52.9	7.604	85.5	2.3
22	1550	21.71	0.0738	3.494E-02	0.577	100.0	50.3	11.36	126.2	2.6

86NP1 HORNBLENDE

STEP #	TEMP (°C)	40Ar/39Ar	37Ar/39Ar	36Ar/39Ar	39Ar (E-13 mol)	total %39Ar	40Ar* %	40Ar*/39Ar(K)	K-Ar age (Ma)	error in age
1	800	50.61	0.6006	3.535E-02	3.85	6.10	79.2	40.19	411.0	0.9
2	900	27.90	0.7757	2.206E-02	2.13	9.48	76.1	21.41	230.5	0.8
3	930	27.17	1.007	3.469E-02	0.653	10.5	60.7	16.97	185.0	4.2
4	970	25.40	1.527	3.699E-02	0.756	11.7	55.8	14.55	159.9	3.2
5	1020	25.89	3.307	1.721E-02	2.26	15.3	80.4	21.05	226.8	0.7
6	1040	42.72	4.288	2.395E-02	1.75	18.1	83.5	36.02	372.4	1.2
7	1060	48.56	4.791	1.405E-02	2.18	21.5	91.6	44.87	453.3	1.0
8	1080	48.50	5.036	8.971E-03	3.33	26.8	94.9	46.34	466.4	0.6
9	1100	46.20	5.105	7.349E-03	4.49	33.9	95.7	44.52	450.1	0.7
10	1120	43.94	5.163	7.428E-03	3.98	40.2	95.4	42.23	429.6	0.6
11	1140	40.97	5.163	5.487E-03	2.77	44.6	96.4	39.82	407.6	0.8
12	1160	37.05	5.085	4.534E-03	6.71	55.3	97.0	36.16	373.8	0.5
13	1180	36.07	5.058	4.735E-03	6.48	65.5	96.7	35.12	364.0	0.3
14	1220	36.60	5.023	3.290E-03	19.9	97.1	98.1	36.07	373.0	0.7
15	1450	32.73	4.506	1.007E-02	1.84	100	91.0	30.13	316.6	0.8

87P7 BIOTITE

STEP #	TEMP (°C)	40Ar/39Ar	37Ar/39Ar	36Ar/39Ar	39Ar (E-13 mol)	total %39Ar	40Ar* %	40Ar*/39Ar(K)	K-Ar age (Ma)	error in age
1	600	28.77	0.2607	8.909E-02	1.58	2.09	8.41	2.429	28.1	1.9
2	700	8.727	0.3740	8.162E-03	5.89	9.90	72.0	6.309	72.1	0.2
3	760	10.47	0.1167	5.266E-03	7.96	20.4	84.7	8.889	100.8	0.2
4	820	10.64	0.0282	2.767E-03	9.53	33.1	91.8	9.791	110.8	0.2
5	880	10.86	0.0376	4.216E-03	5.72	40.7	88.0	9.584	108.5	0.3
6	950	10.37	0.0870	4.950E-03	5.21	47.6	85.3	8.881	100.7	0.3
7	1020	10.89	0.1504	9.359E-03	5.42	54.7	74.1	8.102	92.1	0.7
8	1100	8.757	0.0750	1.440E-03	14.4	73.8	94.7	8.304	94.4	0.2
9	1150	9.741	0.0993	2.218E-03	8.29	84.8	92.8	9.060	102.7	0.3
10	1220	10.94	0.2645	1.849E-03	9.11	96.9	94.7	10.38	117.2	0.3
11	1350	12.78	0.7599	7.653E-03	2.35	100	81.9	10.54	119.0	0.9

87P5 K-FELDSPAR

STEP #	TEMP (°C)	40Ar/39Ar	37Ar/39Ar	36Ar/39Ar	39Ar (E-13 mol)	total %39Ar	40Ar* %	40Ar*/39Ar(K)	K-Ar age (Ma)	error in age
1	450	229.5	0.1300	5.967E-01	0.109	0.040	22.7	53.16	520.7	29.1
2	500	45.97	0.0867	8.273E-02	0.206	0.116	44.4	21.50	228.9	10.9
3	550	23.07	0.0283	2.143E-02	0.567	0.324	69.8	16.71	180.4	3.0
4	580	7.932	0.0168	7.245E-03	0.644	0.561	66.1	5.759	64.2	1.3
5	610	9.077	0.0402	8.741E-03	1.23	1.01	68.2	6.464	71.9	0.7
6	640	9.392	0.0570	7.856E-03	1.70	1.64	72.7	7.042	78.2	0.7
7	670	6.729	0.0707	4.913E-03	2.22	2.45	75.5	5.249	58.6	0.5
8	700	5.079	0.0756	4.306E-03	2.36	3.32	71.4	3.779	42.4	0.5
9	750	7.094	0.0768	5.893E-03	1.73	3.95	72.1	5.325	59.5	1.2
10	800	5.448	0.0610	4.284E-03	4.32	5.54	74.6	4.153	46.6	0.5
11	870	4.972	0.0489	3.547E-03	6.59	7.96	77.1	3.894	43.7	0.1
12	920	2.854	0.0261	1.374E-03	9.08	11.3	83.1	2.417	27.2	0.1
13	970	2.938	0.0234	1.255E-03	4.86	13.1	83.4	2.536	28.6	0.4
14	1020	3.412	0.0179	1.489E-03	8.73	16.3	84.8	2.940	33.1	0.2
15	1080	4.357	0.0181	1.916E-03	7.33	19.0	84.9	3.759	42.2	0.3
16	1130	5.215	0.0161	2.130E-03	11.5	23.2	86.6	4.554	51.0	0.1
17	1170	6.726	0.0195	2.712E-03	11.6	27.5	87.1	5.893	65.7	0.2
18	1210	8.686	0.0242	3.042E-03	16.4	33.5	89.0	7.756	86.0	0.1
19	1240	10.23	0.0248	3.145E-03	15.1	39.0	90.3	9.269	102.3	0.2
20	1260	11.15	0.0193	2.652E-03	13.9	44.1	92.4	10.33	113.7	0.1
21	1280	11.83	0.0153	2.378E-03	18.6	51.0	93.6	11.10	121.8	0.2
22	1300	12.10	0.0117	2.042E-03	26.8	60.8	94.6	11.46	**125.7**	**0.3**
23	1320	12.10	0.0083	2.039E-03	30.6	72.1	94.6	11.47	**125.7**	**0.2**
24	1340	12.08	0.0093	1.785E-03	30.5	83.3	95.2	11.52	**126.3**	**0.3**
25	1360	12.18	0.0085	1.864E-03	20.3	90.7	95.0	11.60	127.1	0.1
26	1390	12.27	0.0073	1.572E-03	18.0	97.3	95.7	11.77	129.0	0.2
27	1430	12.54	0.0080	1.794E-03	5.00	99.2	94.8	11.98	131.1	0.4
28	1460	14.89	0.0318	2.422E-03	0.080	99.2	91.2	14.14	153.8	2.1
29	1550	14.90	0.0409	2.051E-03	2.17	100	94.3	14.26	155.1	0.9

87P7 K-FELDSPAR

STEP #	TEMP (°C)	40Ar/39Ar	37Ar/39Ar	36Ar/39Ar	39Ar (E-13 mol)	total %39Ar	40Ar* %	40Ar*/39Ar(K)	K-Ar age (Ma)	error in age
1	450	108.3	0.0676	2.530E-01	0.506	0.408	30.7	33.51	351.5	3.9
2	500	88.50	0.1185	1.379E-01	0.139	0.521	51.8	47.73	482.1	20.2
3	550	46.13	0.0577	4.399E-02	0.289	0.754	69.2	33.10	347.6	5.6
4	580	15.88	0.0647	1.383E-02	0.410	1.08	68.8	11.77	131.3	2.3
5	610	10.64	0.1173	1.250E-02	0.562	1.54	60.0	6.922	78.4	3.0
6	640	9.727	0.1976	8.717E-03	0.901	2.27	69.4	7.132	80.7	1.6
7	670	6.878	0.2182	6.945E-03	1.22	3.25	66.0	4.808	54.8	1.4
8	700	4.970	0.1948	4.729E-03	1.44	4.41	66.8	3.553	40.7	1.0
9	750	3.782	0.1084	2.709E-03	5.09	8.52	76.2	2.956	33.9	0.4
10	800	3.201	0.0563	1.580E-03	2.37	10.4	79.3	2.705	31.1	0.4
11	870	3.640	0.0420	1.790E-03	5.49	14.9	82.6	3.081	35.3	0.4
12	920	2.555	0.0415	9.373E-04	5.97	19.7	85.2	2.248	25.8	0.3
13	970	2.771	0.0453	1.139E-03	5.15	23.8	83.8	2.404	27.6	0.3
14	1020	3.597	0.0424	1.171E-03	4.92	27.8	87.1	3.221	36.9	0.4
15	1080	5.245	0.0397	1.952E-03	6.00	32.7	87.0	4.638	52.9	0.2
16	1130	6.691	0.0406	2.186E-03	6.32	37.8	88.8	6.015	68.3	0.3
17	1170	8.389	0.0510	2.945E-03	6.90	43.3	88.5	7.489	84.7	0.5
18	1210	10.95	0.0630	3.736E-03	7.39	49.3	89.1	9.818	110.2	0.2
19	1240	12.74	0.0574	3.420E-03	8.46	56.1	91.4	11.70	130.6	0.2
20	1270	14.16	0.0354	2.457E-03	9.86	64.1	94.3	13.40	148.9	0.2
21	1300	14.68	0.0187	1.735E-03	14.2	75.5	96.1	14.14	156.7	0.2
22	1320	13.86	0.0108	1.380E-03	13.5	86.4	96.6	13.42	149.1	0.2
23	1350	13.54	0.0110	1.386E-03	10.7	95.1	96.4	13.10	145.6	0.2
24	1380	13.84	0.0162	1.834E-03	5.07	99.2	95.2	13.27	147.4	0.1
25	1420	18.76	0.0202	4.818E-03	0.666	99.7	88.7	17.30	190.0	3.6
26	1550	90.87	0.0761	1.380E-02	0.373	100	92.5	85.29	787.6	3.5

87G30 HORNBLENDE

STEP #	TEMP (°C)	40Ar/39Ar	37Ar/39Ar	36Ar/39Ar	39Ar (E-13 mol)	total %39Ar	40Ar*%	40Ar*/39Ar(K)	K-Ar age (Ma)	error in age
1	700	82.73	1.365	2.353E-01	0.631	2.22	15.9	13.16	128.1	4.1
2	800	31.85	3.081	8.906E-02	0.434	3.75	17.4	5.590	55.5	4.3
3	850	44.22	6.881	1.283E-01	0.354	5.00	14.7	6.605	65.4	8.1
4	920	20.16	17.85	3.763E-02	1.11	8.91	49.1	10.07	98.9	2.1
5	960	11.73	12.71	1.461E-02	1.48	14.1	67.9	8.089	79.8	1.9
6	990	9.759	6.747	5.651E-03	6.34	36.5	85.4	8.387	82.7	0.5
7	1000	11.55	6.123	8.816E-03	3.39	48.4	79.1	9.207	90.6	1.4
8	1010	11.45	5.818	4.651E-03	3.46	60.6	89.5	10.32	101.3	0.8
9	1020	14.33	5.513	9.635E-03	2.93	71.0	81.2	11.72	114.5	1.3
10	1035	15.13	6.183	6.869E-03	0.514	72.8	86.9	13.39	130.2	4.0
11	1050	15.87	7.951	6.885E-03	0.987	76.2	88.7	14.25	138.3	1.5
12	1070	15.87	9.308	8.969E-03	1.20	80.5	85.4	13.72	133.4	1.9
13	1080	15.68	8.455	8.137E-03	1.12	84.4	86.4	13.72	133.4	1.1
14	1090	15.91	9.263	1.096E-02	0.777	87.2	81.5	13.16	128.2	5.0
15	1100	15.90	11.36	1.096E-02	0.980	90.6	82.4	13.30	129.4	4.7
16	1125	16.48	15.02	1.242E-02	0.887	93.7	81.6	13.70	133.2	2.1
17	1140	18.56	9.671	1.599E-02	1.05	97.4	76.4	14.36	139.4	2.8
18	1160	22.23	8.521	2.229E-02	0.242	98.3	70.7	16.10	155.6	9.0
19	1180	35.23	8.755	8.005E-02	0.121	98.7	33.1	12.03	117.4	9.0
20	1500	110.0	10.30	3.759E-02	0.363	100	90.1	100.1	802.3	4.2

87G16 MUSCOVITE

STEP #	TEMP (°C)	40Ar/39Ar	37Ar/39Ar	36Ar/39Ar	39Ar (E-13 mol)	total %39Ar	40Ar*%	40Ar*/39Ar(K)	K-Ar age (Ma)	error in age
1	650	62.23	0.2728	1.977E-01	0.533	0.717	6.0	3.795	43.7	2.9
2	750	7.893	0.0863	1.243E-02	1.38	2.57	52.2	4.193	48.3	1.1
3	800	6.998	0.0119	8.181E-03	1.63	4.77	63.9	4.548	52.3	0.5
4	850	5.996	0.0054	4.970E-03	3.89	10.0	74.3	4.495	51.7	0.6
5	900	5.510	0.0024	2.688E-03	9.36	22.6	84.7	4.683	53.8	0.2
6	950	5.236	0.0028	1.849E-03	13.3	40.5	88.7	4.657	53.5	0.3
7	990	5.445	0.0047	2.636E-03	7.33	50.3	84.7	4.633	53.3	0.3
8	1030	5.456	0.0032	2.380E-03	6.81	59.5	86.0	4.720	54.2	0.2
9	1100	5.154	0.0030	1.245E-03	14.4	78.9	92.0	4.753	54.6	0.2
10	1350	5.193	0.0166	1.219E-03	15.7	100.0	92.2	4.801	55.2	0.2

87G29 BIOTITE

STEP #	TEMP (°C)	40Ar/39Ar	37Ar/39Ar	36Ar/39Ar	39Ar (E-13 mol)	total %39Ar	40Ar*%	40Ar*/39Ar(K)	K-Ar age (Ma)	error in age
1	600	6.689	0.0690	1.668E-02	6.15	5.43	25.7	1.732	19.8	0.3
2	670	4.867	0.0809	7.421E-03	11.5	15.6	54.2	2.647	30.2	0.2
3	750	5.241	0.0294	5.287E-03	18.3	31.7	69.5	3.648	41.5	0.2
4	820	5.545	0.0167	4.841E-03	13.0	43.2	73.4	4.083	46.4	0.1
5	900	6.473	0.0418	6.969E-03	8.24	50.5	67.5	4.384	49.8	0.2
6	960	6.088	0.0779	6.255E-03	7.51	57.1	68.9	4.212	47.9	0.5
7	1020	5.486	0.1100	4.604E-03	12.3	68.0	74.5	4.100	46.6	0.1
8	1100	5.236	0.0337	3.338E-03	19.9	85.5	80.4	4.219	48.0	0.1
9	1250	5.608	0.1221	3.120E-03	14.6	98.4	82.9	4.662	52.9	0.1
10	1350	11.89	0.2276	1.994E-02	1.47	99.7	49.7	5.981	67.6	1.0
11	1450	37.42	0.4087	1.033E-01	0.334	100	18.1	6.891	77.7	4.8

87G36 BIOTITE

STEP #	TEMP (°C)	40Ar/39Ar	37Ar/39Ar	36Ar/39Ar	39Ar (E-13 mol)	total %39Ar	40Ar*%	40Ar*/39Ar(K)	K-Ar age (Ma)	error in age
1	600	11.70	0.1305	3.251E-02	3.37	2.77	17.6	2.069	24.0	0.5
2	670	5.526	0.2841	8.219E-03	6.24	7.89	55.5	3.084	35.6	0.5
3	780	4.143	0.0418	2.521E-03	16.3	21.3	81.0	3.368	38.9	0.1
4	850	4.235	0.0143	2.360E-03	15.2	33.7	82.5	3.506	40.4	0.2
5	920	4.218	0.0329	2.545E-03	11.2	42.9	81.1	3.435	**39.6**	**0.2**
6	1020	3.806	0.0533	1.350E-03	26.3	64.5	88.6	3.378	**39.0**	**0.2**
7	1100	4.336	0.0228	2.743E-03	6.73	70.0	80.0	3.494	40.3	0.2
8	1150	3.956	0.0369	7.781E-04	28.4	93.3	93.2	3.696	42.6	0.1
9	1250	4.754	0.2820	2.218E-03	7.06	99.1	85.4	4.085	47.0	0.3
10	1400	11.18	0.3414	1.468E-02	1.07	100	60.1	6.833	78.0	2.4

87G36 K-FELDSPAR

STEP #	TEMP (°C)	40Ar/39Ar	37Ar/39Ar	36Ar/39Ar	39Ar (E-13 mol)	total %39Ar	40Ar*%	40Ar*/39Ar(K)	K-Ar age (Ma)	error in age
1	450	266.0	0.1455	6.857E-01	0.141	0.144	23.5	63.36	614.9	8.6
2	500	136.0	0.0739	3.194E-01	0.219	0.368	30.1	41.59	426.4	25.9
3	550	44.81	0.0582	1.014E-01	0.404	0.781	32.2	14.82	163.7	4.5
4	580	13.99	0.0620	3.144E-02	0.531	1.32	31.3	4.671	53.2	3.4
5	610	11.57	0.0996	2.731E-02	0.883	2.23	28.6	3.474	39.7	2.0
6	640	9.644	0.2106	2.281E-02	1.53	3.79	28.9	2.885	33.1	1.6
7	670	5.892	0.2360	1.014E-02	1.69	5.52	46.5	2.879	33.0	1.5
8	700	5.191	0.2065	8.851E-03	0.602	6.13	42.5	2.557	29.3	3.1
9	750	4.815	0.0947	8.106E-03	0.607	6.76	42.4	2.393	27.5	2.8
10	800	2.372	0.0336	1.466E-03	9.80	16.8	78.7	1.908	21.9	0.1
11	870	2.293	0.0280	1.223E-03	3.09	19.9	77.4	1.900	21.8	0.3
12	900	2.094	0.0340	3.341E-04	5.30	25.4	89.8	1.965	22.6	0.2
13	960	2.170	0.0319	1.082E-03	4.30	29.7	79.6	1.819	20.9	0.5
14	1020	2.589	0.0221	2.703E-03	3.76	33.6	64.6	1.759	20.2	0.6
15	1080	2.508	0.0137	1.812E-03	4.27	38.0	73.9	1.940	22.3	1.1
16	1130	2.590	0.0146	2.011E-03	5.26	43.3	73.1	1.964	22.6	0.4
17	1180	3.051	0.0221	2.773E-03	7.04	50.5	70.5	2.200	25.3	0.3
18	1210	3.600	0.0285	3.048E-03	3.96	54.6	71.6	2.668	30.6	0.2
19	1240	3.849	0.0291	3.557E-03	6.71	61.4	70.5	2.767	31.7	0.3
20	1280	3.965	0.0200	3.116E-03	7.46	69.1	74.7	3.013	34.5	0.4
21	1320	3.954	0.0051	2.418E-03	12.4	81.7	80.3	3.207	**36.7**	**0.1**
22	1360	3.929	0.0018	2.044E-03	13.2	95.2	83.0	3.292	**37.7**	**0.2**
23	1400	4.291	0.0027	3.506E-03	3.18	98.5	72.4	3.222	**36.9**	**1.1**
24	1450	5.475	0.0070	6.296E-03	1.17	99.7	60.7	3.582	41.0	1.1
25	1550	12.73	0.0093	1.266E-02	0.301	100.0	62.2	8.957	100.7	3.7

Table 3
$^{40}Ar/^{39}Ar$ age summary

sample	phase	total # steps	min. app. age (Ma)	plateau age (Ma)	2σ std. dev.	steps in plateau	gas in plateau	isochron age (Ma)	2σ std. dev.	steps in isochron	initial 40/36 ratio	York fit	York 2 MSWD
87M4(1)	hornblende	14	75.1 ± 3.0	76.3	±0.67	7-12	43.2	75.4	± 0.6	3-12	302 ±	2	0.87
87M4(2)	hornblende	12	56.8 ± 8.8	83.2	±0.87	10-12	50.5	76.3	+0.6 -2.3	5-9	172 ±	2	0.96
87M13	hornblende	19	67.8 ± 1.8	77.5	±0.78	5-11	30.7	68.5	+1.2 -3.6	13-15	254 ± 18	2	0.27
87M2	biotite	9	20.8 ± 2.2	31.0	±0.15	7-8	42.3	30.1, 30.3	±1.7, ±0.2	1-3, 4-8	284 ±, 346 ±	1, 2	5.55, 2.03
87M18	biotite	11	19.9 ± 1.0	35.8	±0.15	4-5	23.4	33.3	+0.8 -0.9	9-11	356 ±	2	1.74
87M18	K-feldspar	22	21.9 ± 0.8	-	-	-	-	-	-	-	-	-	-
86MM25	muscovite	11	29.2 ± 2.6	49.9	±0.55	3-6	55.4	49.6	+0.9 -1.2	3-10	293 ±	1	2.66
MM87-8	muscovite	12	32.2 ± 1.6	50.1	±0.16	5-9	54.8	48.9	+1.2 -4.1	5-9	449 ±	2	2.04
MM87-7	biotite	11	48.1 ± 1.4	51.7	±0.22	2-4	45.7	52.6	± 0.2	1-10	282 ±	1	4.53
MM87-7	K-feldspar	24	23.4 ± 0.8	-	-	-	-	-	-	-	-	-	-
86MM23	biotite	10	32.8 ± 0.4	-	-	-	-	48.0	+0.2 -0.3	3-9	274 ±	1	8.26
86MM23	K-feldspar	23	22.4 ± 0.8	22.5	±0.13	10-14	36.2	-	-	-	-	-	-
87D9	biotite	11	48.0 ± 0.8	54.2	±0.90	5-8	26.6	55.7	± 0.3	3-8	248 ±	1	2.74
87D9	K-feldspar	22	28.8 ± 0.4	-	-	-	-	-	-	-	-	-	-
87D20	biotite	11	51.0 ± 0.6	52.4	±0.24	4-7	32.2	47.9	+1.1 -1.2	2-7	420 ±	2	2.06
87D20	K-feldspar	22	26.4 ± 2.6	-	-	-	-	26.5	+1.2 -1.5	10-13	331 ±	2	0.9
86NP1	hornblende	15	159.9 ± 6.4	-	-	-	-	265.1	+9.0 -10.0	8-13?	?	?	4.09
87P7	biotite	11	28.1 ± 3.8	-	-	-	-	-	-	6-9?	-	-	-
87P7	K-feldspar	26	25.8 ± 0.6	-	-	-	-	22.2	+1.2 -1.5	5-13	735 ±	2	2.29
87P5	K-feldspar	29	27.2 ± 0.2	145.6	±0.36	22-24	32.3	-	-	-	-	-	-
87G30	hornblende	20	55.5 ± 8.6	-	-	-	-	129.0	+4.3 -6.4	10-18	380 ± 62	2	1.68
87G16	muscovite	10	43.7 ± 5.8	53.7	±0.61	5-8	49.5	55.1	+0.2 -0.3	2-10	256 ±	2	2.3
87G29	biotite	11	19.8 ± 0.6	-	-	-	-	45.2	+4.4 -9.1	4-8	334 ±	1	8.27
87G36	biotite	10	24.0 ± 1.0	39.2	±0.15	5-6	30.8	40.5	± 0.6	1-7, 8-10	253 ± ,542 ±	1, 2	6.62, 1.12
87G36	K-feldspar	25	20.2 ± 1.2	37.2	±0.32	21-23	29.4	21.4	± 0.2	5-16	349 ±	2	2.39

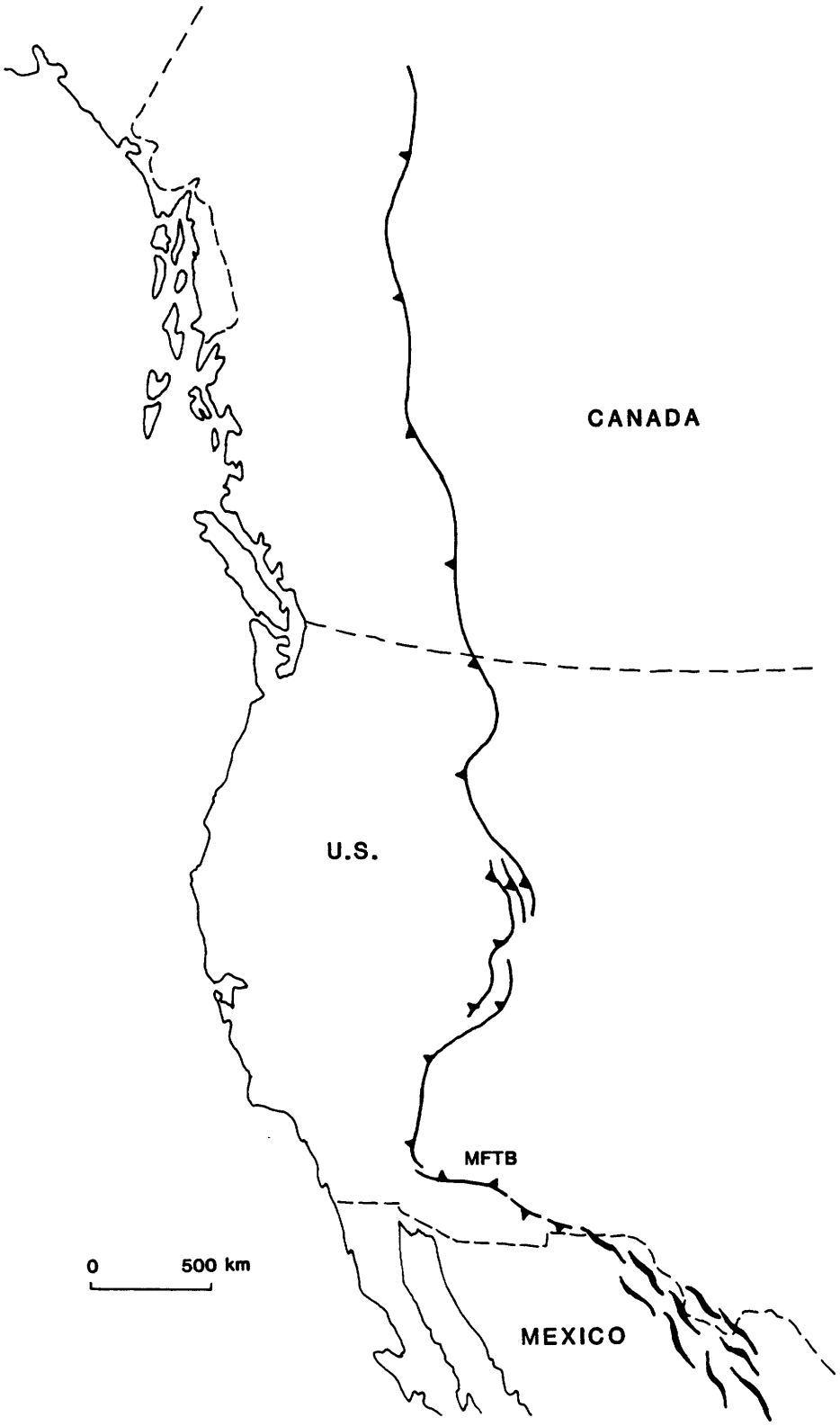

Figure 3.1

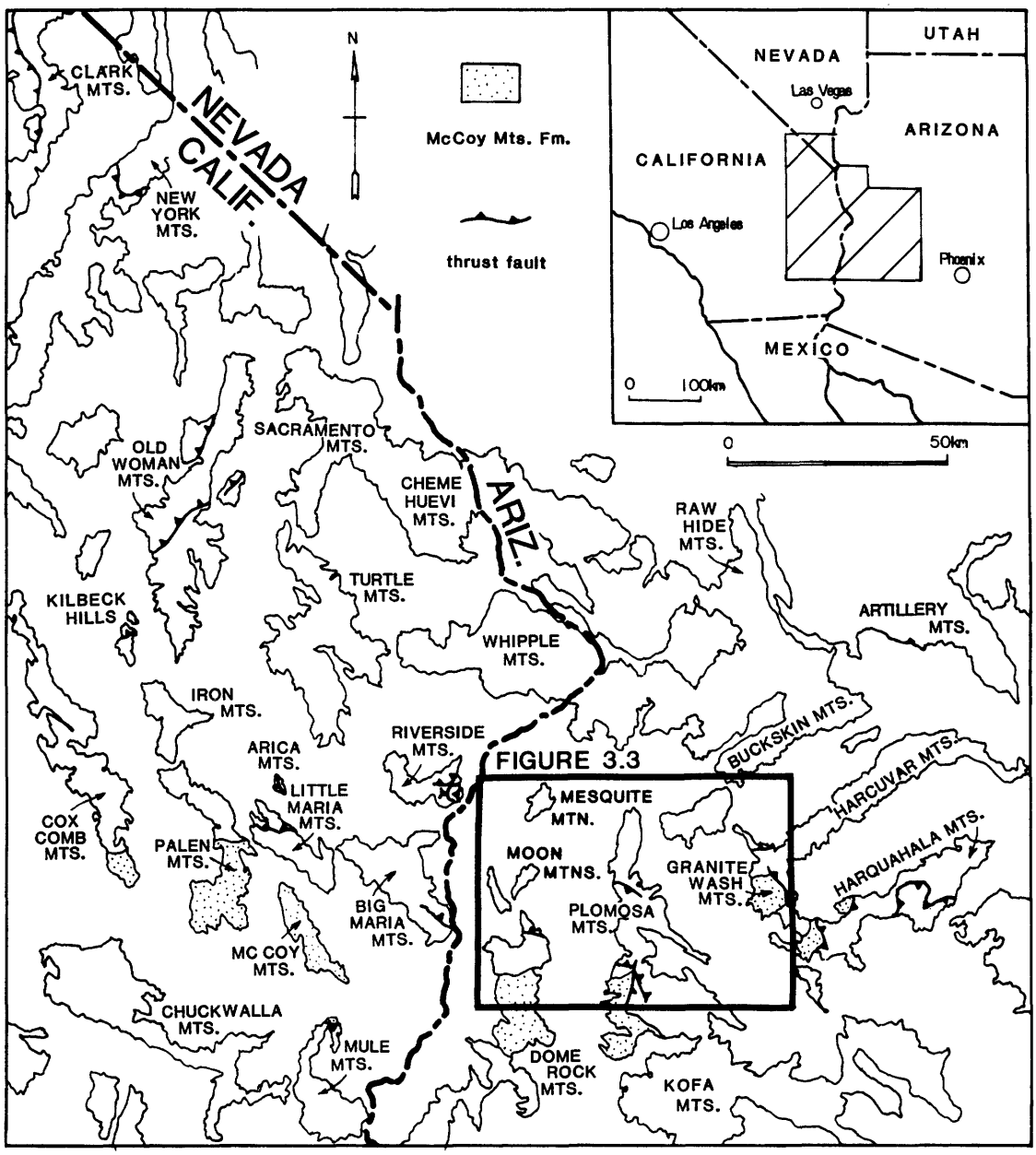
N
McCoy Mts. Fm.
thrust fault
NEVADA
CALIF.
ARIZ.
CLARK MTS.
NEW YORK MTS.
OLD WOMAN MTS.
SACRAMENTO MTS.
CHEME HUEVI MTS.
TURTLE MTS.
KILBECK HILLS
WHIPPLE MTS.
IRON MTS.
ARICA MTS.
LITTLE MARIA MTS.
RIVERSIDE MTS.
FIGURE 3.3
COX COMB MTS.
PALEN MTS.
BIG MARIA MTS.
MC COY MTS.
CHUCKWALLA MTS.
MULE MTS.
DOME ROCK MTS.
KOFA MTS.
MESQUITE MTN.
MOON MTNS.
PLOMOSA MTS.
GRANITE WASH MTS.
RAW HIDE MTS.
ARTILLERY MTS.
BUCKSKIN MTS.
HARCUVAR MTS.
HARQUAHALA MTS.
NEVADA
UTAH
ARIZONA
CALIFORNIA
Las Vegas
Los Angeles
Phoenix
MEXICO
0 100km
0 50km

Figure 3.2

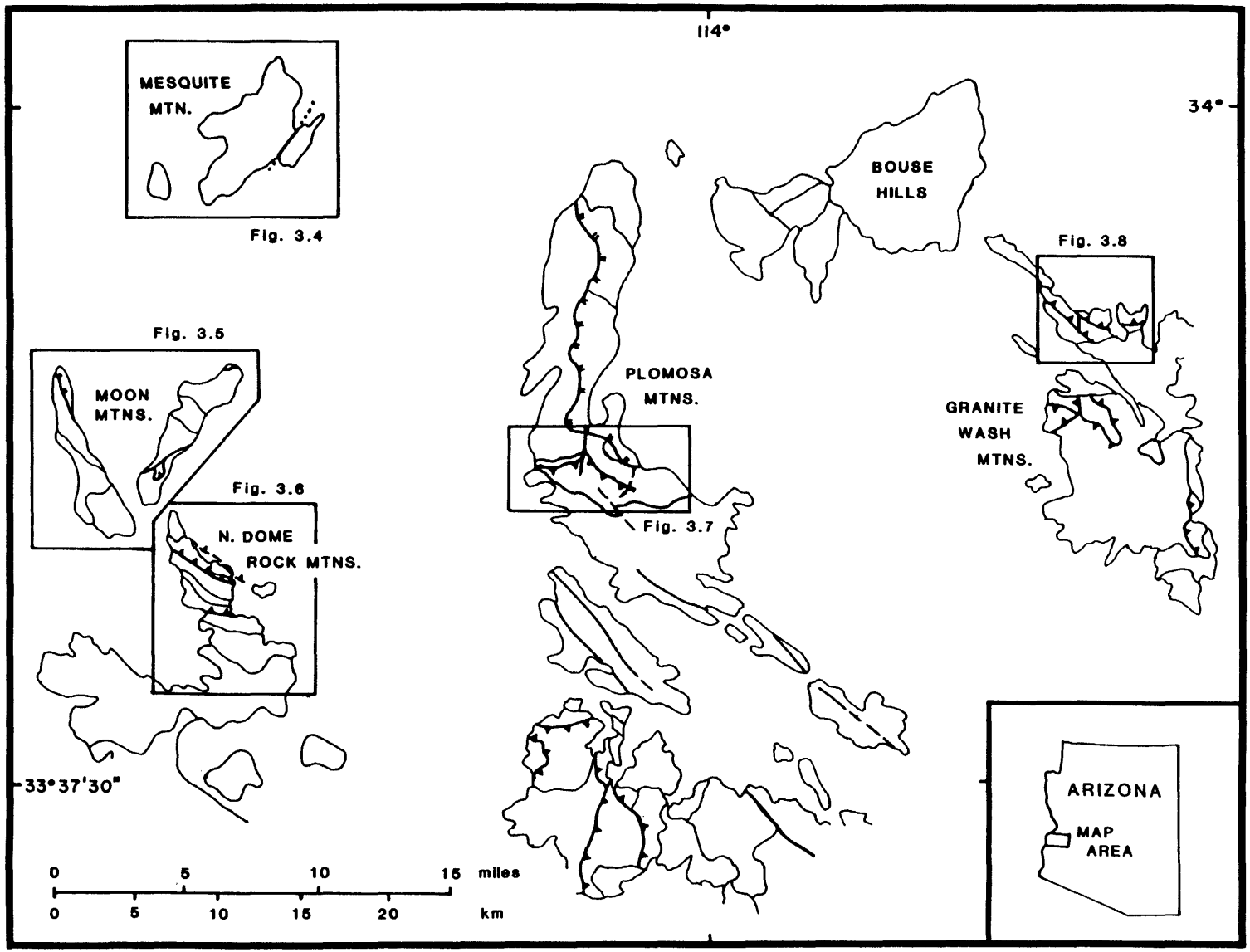
114°
34°
MESQUITE
MTN.
Fig. 3.4
BOUSE
HILLS
Fig. 3.8
Fig. 3.5
MOON
MTNS.
PLOMOSA
MTNS.
GRANITE
WASH
MTNS.
Fig. 3.6
N. DOME
ROCK MTNS.
Fig. 3.7
33°37'30"
0 5 10 15 miles
0 5 10 15 20 km
ARIZONA
MAP
AREA

Figure 3.3

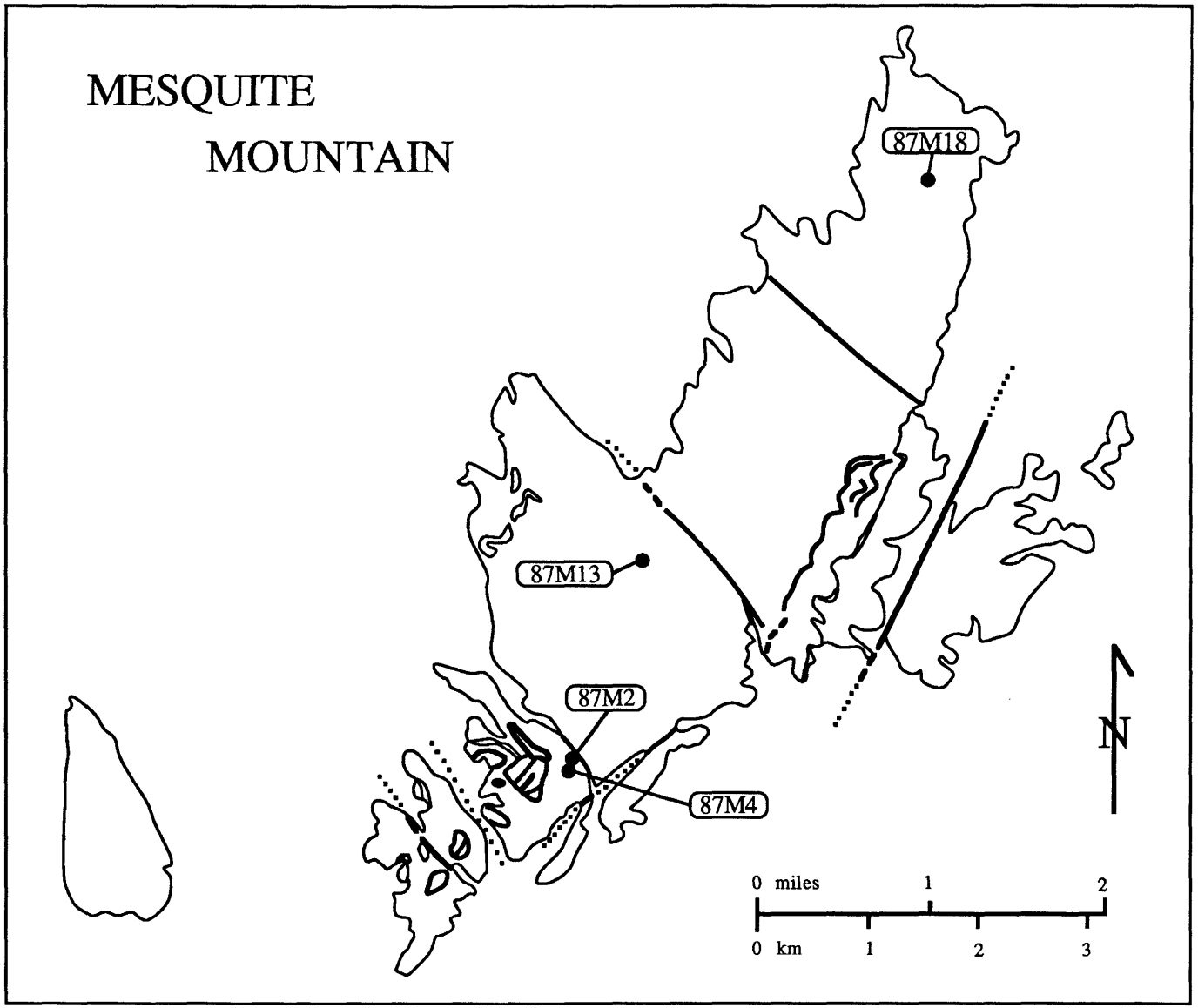

Figure 3.4

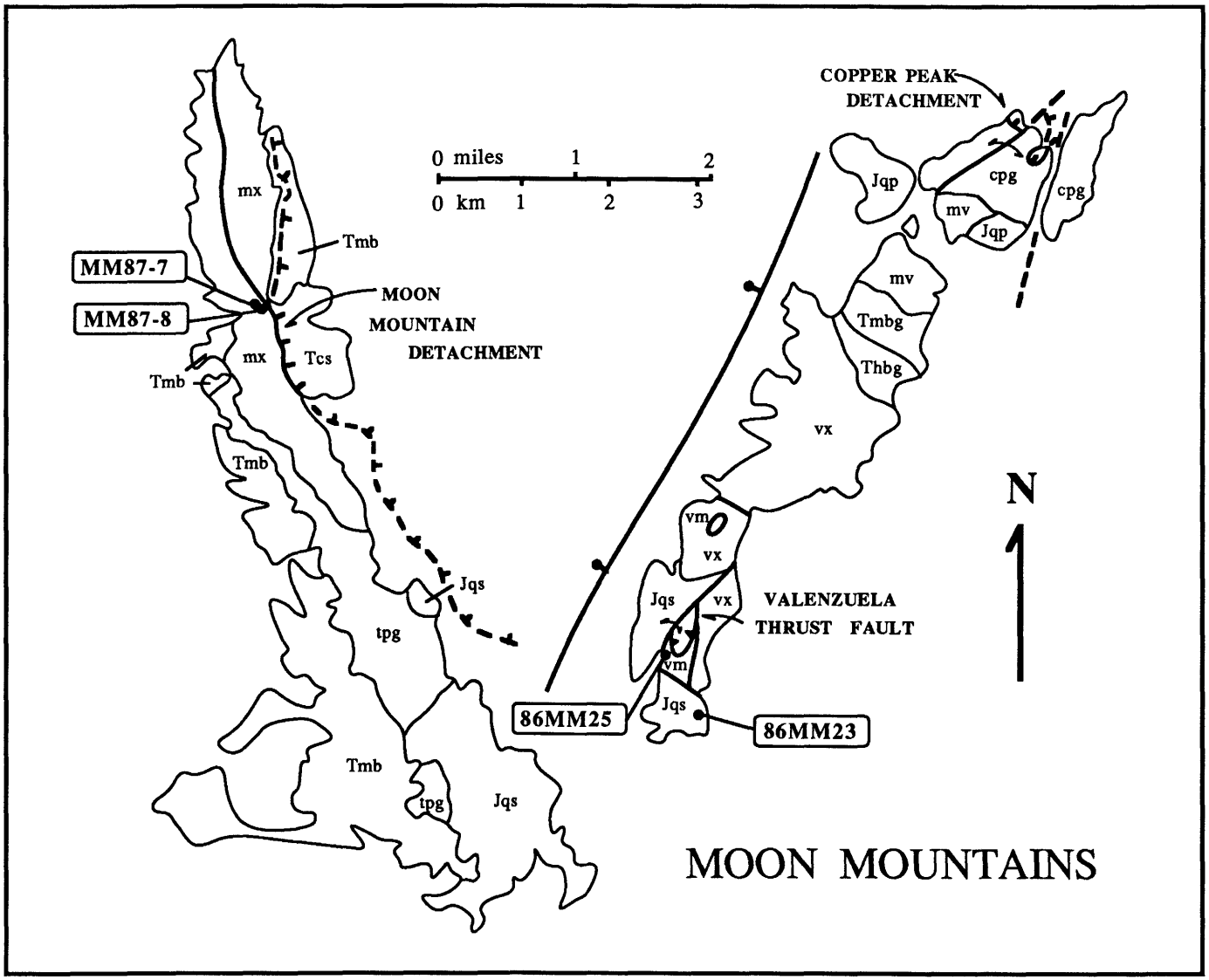
COPPER PEAK
DETACHMENT
0 miles 1 2
0 km 1 2 3
mx
Tmb
MM87-7
MM87-8
MOON
MOUNTAIN
DETACHMENT
mx
Tcs
Tmb
Tmb
Jqs
tpg
Tmb
tpg
Jqs
Jqp
cpg
cpg
mv
Jqp
mv
Tmbg
Thbg
vx
vm
vx
Jqs
vx
VALENZUELA
THRUST FAULT
vm
Jqs
86MM25
86MM23
N
MOON MOUNTAINS

Figure 3.5

BOYER'S GAP AREA, NORTHERN DOME ROCK MTNS.

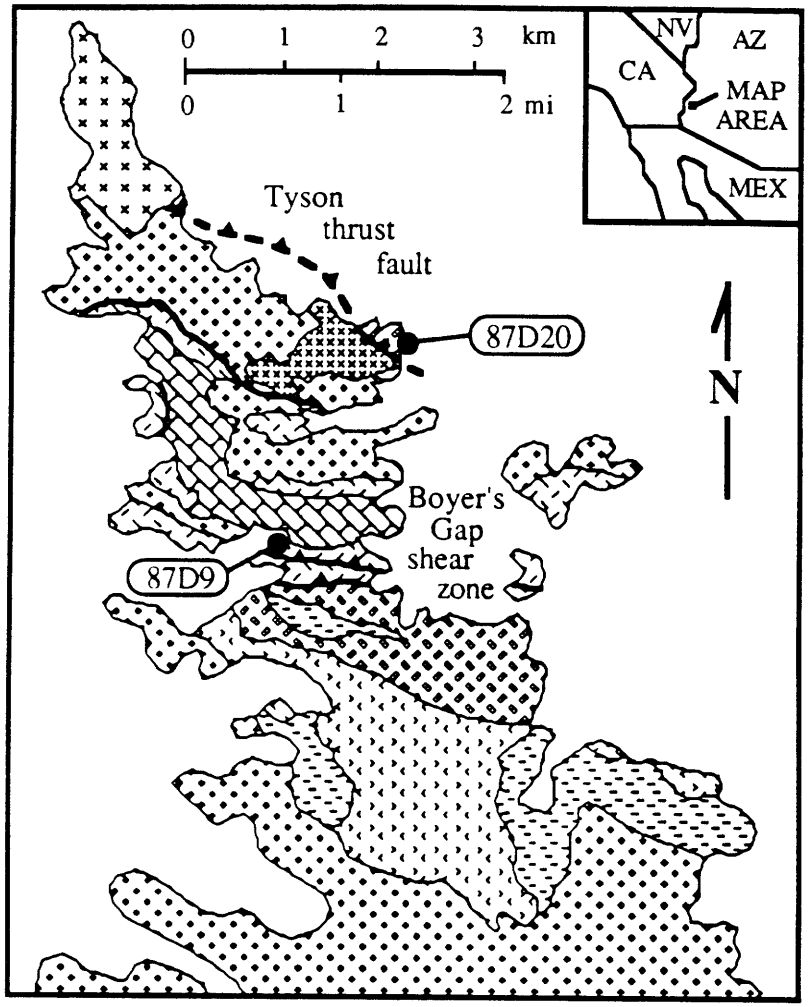

Tyson Wash granite

Jurassic(?) granite and granodiorite

Jurassic rhyodacite porphyry

Jurassic or Proterozoic augen gneiss

Mesozoic metavolcanic rocks

Lower Mesozoic sedimentary rocks

Paleozoic sedimentary rocks

Proterozoic granite

Figure 3.6

PLOMOSA PASS AREA, NORTHERN PLOMOSA MTNS.

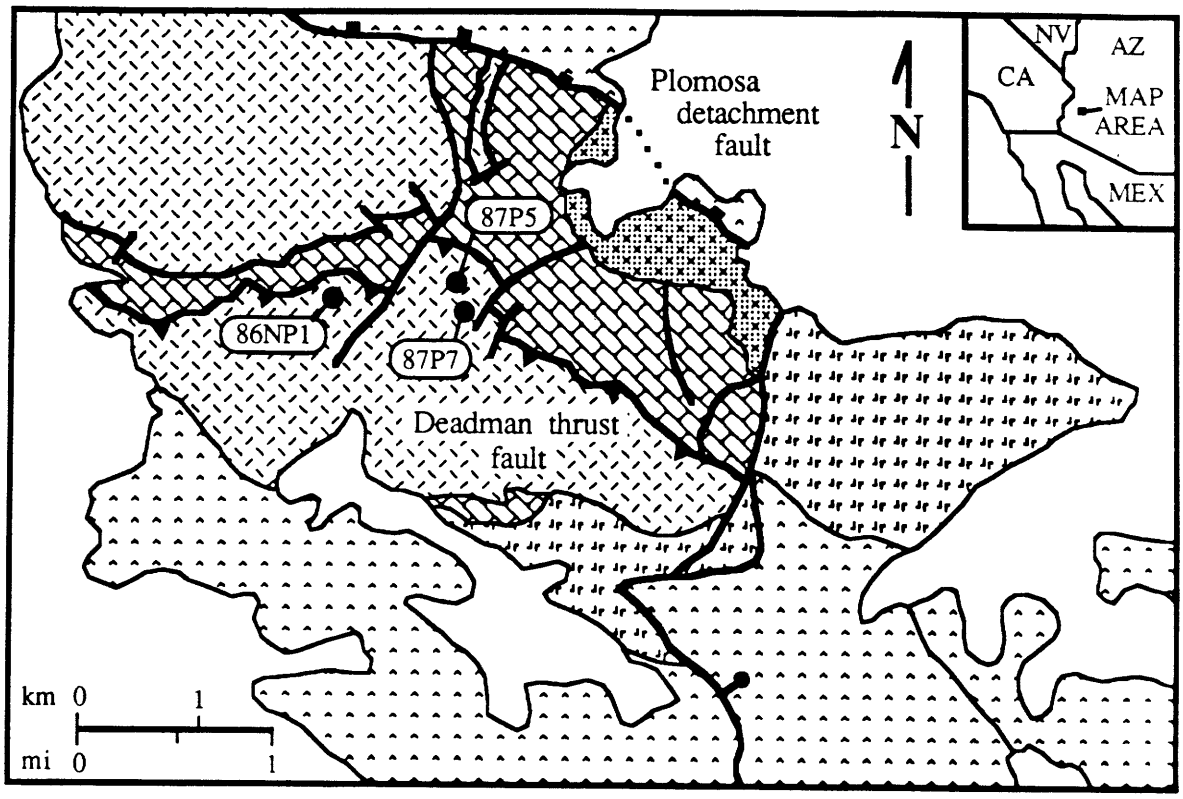

Tertiary volcanics and sediments

Paleozoic / Mesozoic metasediments

Cretaceous Mudersback granite

Proterozoic gneiss and granite

Southern Cross granite

Figure 3.7

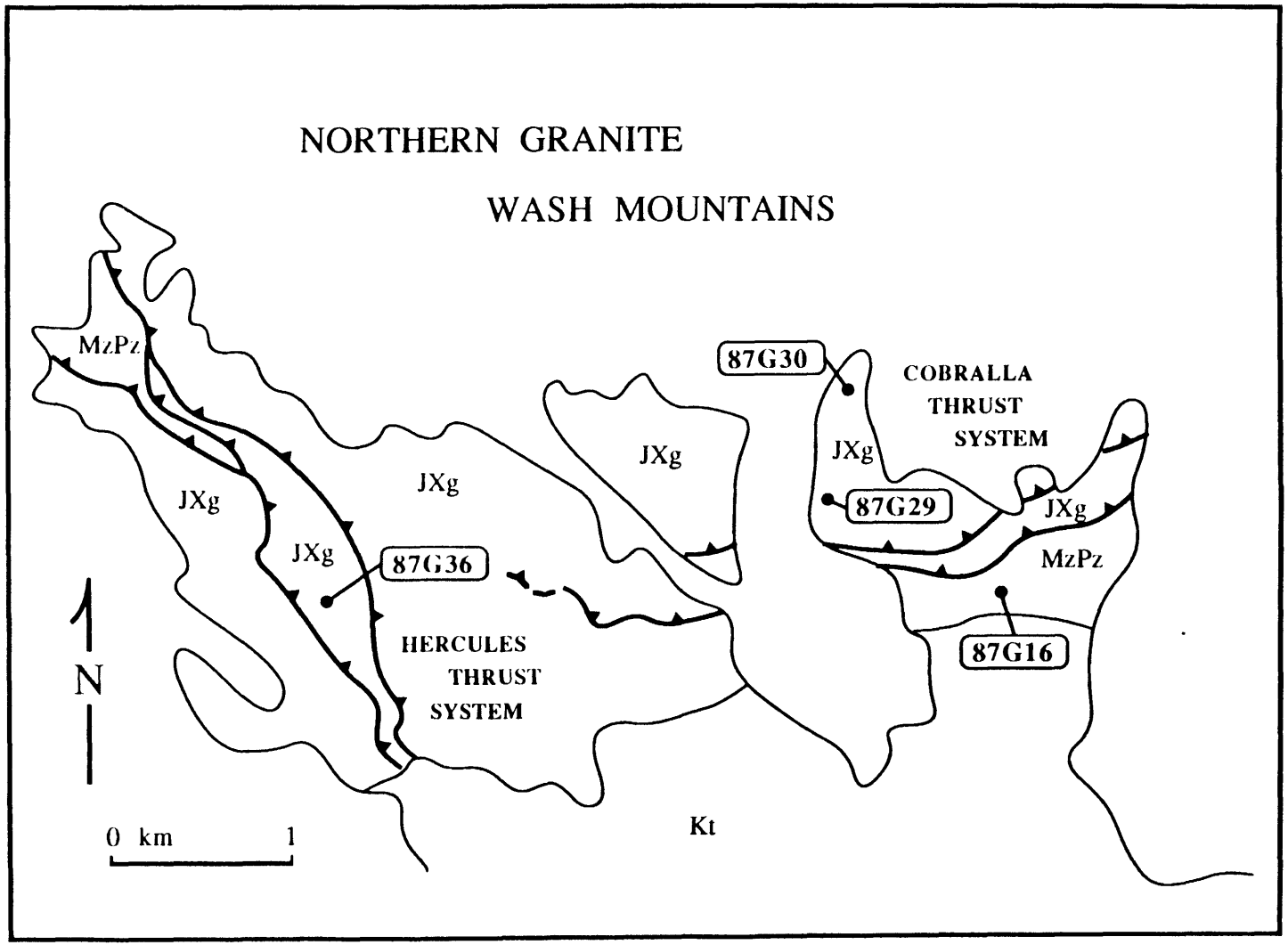
NORTHERN GRANITE
WASH MOUNTAINS
MzPz
JXg
JXg
JXg
JXg
87G36
87G30
87G29
87G16
COBRALLA
THRUST
SYSTEM
JXg
JXg
MzPz
HERCULES
THRUST
SYSTEM
Kt
N
0 km
1

Figure 3.8

Figure 3.9a

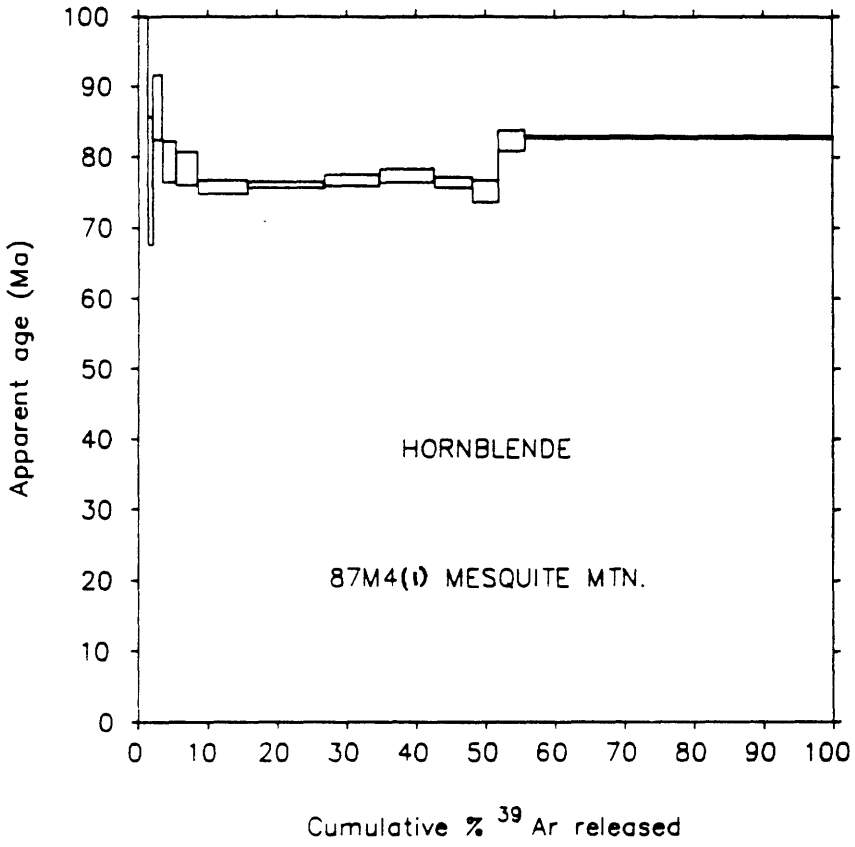
100
90
80
70
60
50
40
30
20
10
0
Apparent age (Ma)
HORNBLENDE
87M4(1) MESQUITE MTN.
0
10
20
30
40
50
60
70
80
90
100
Cumulative % 39 Ar released

Figure 3.9b

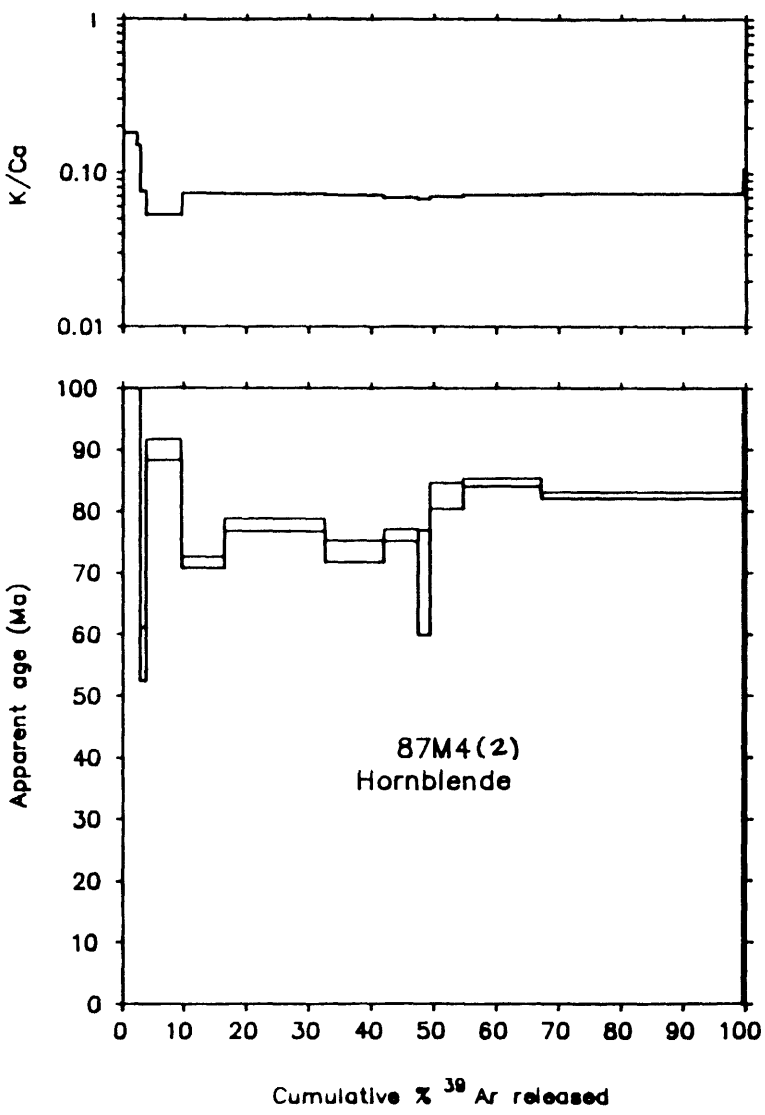

Figure 3.9c

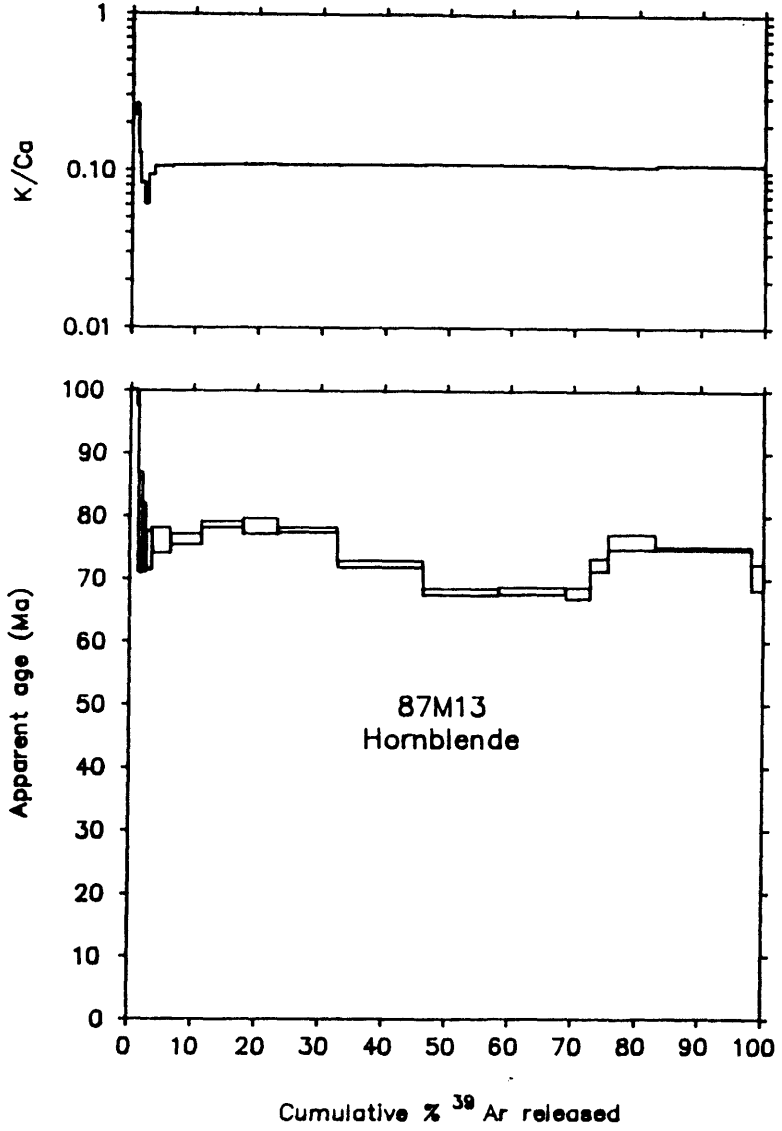

Figure 3.9e

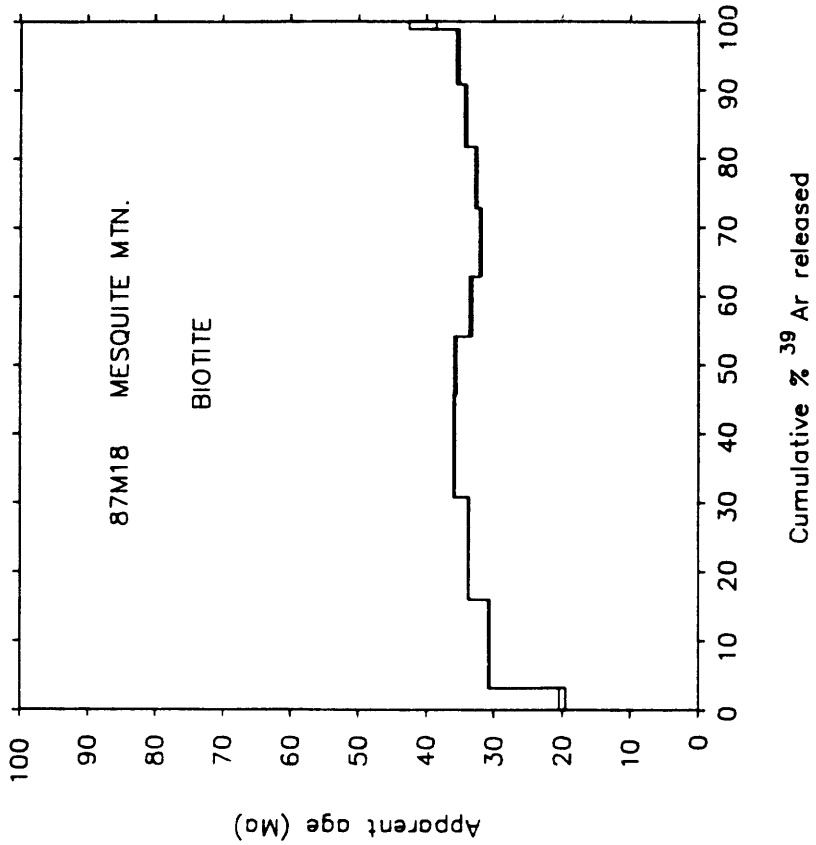

Figure 3.9d

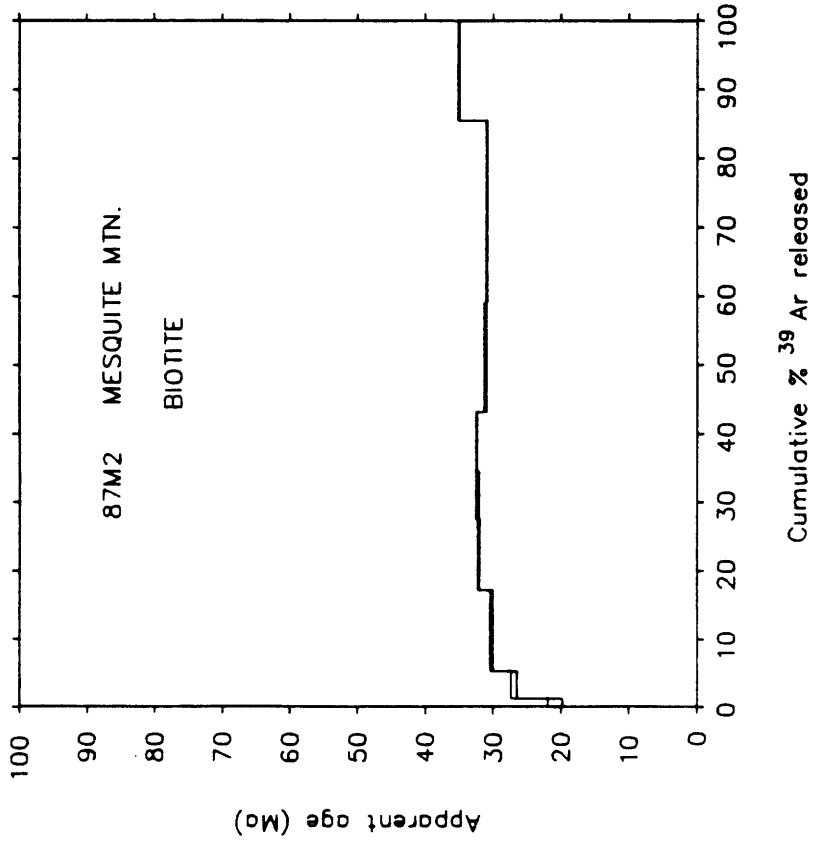

Figure 3.9f

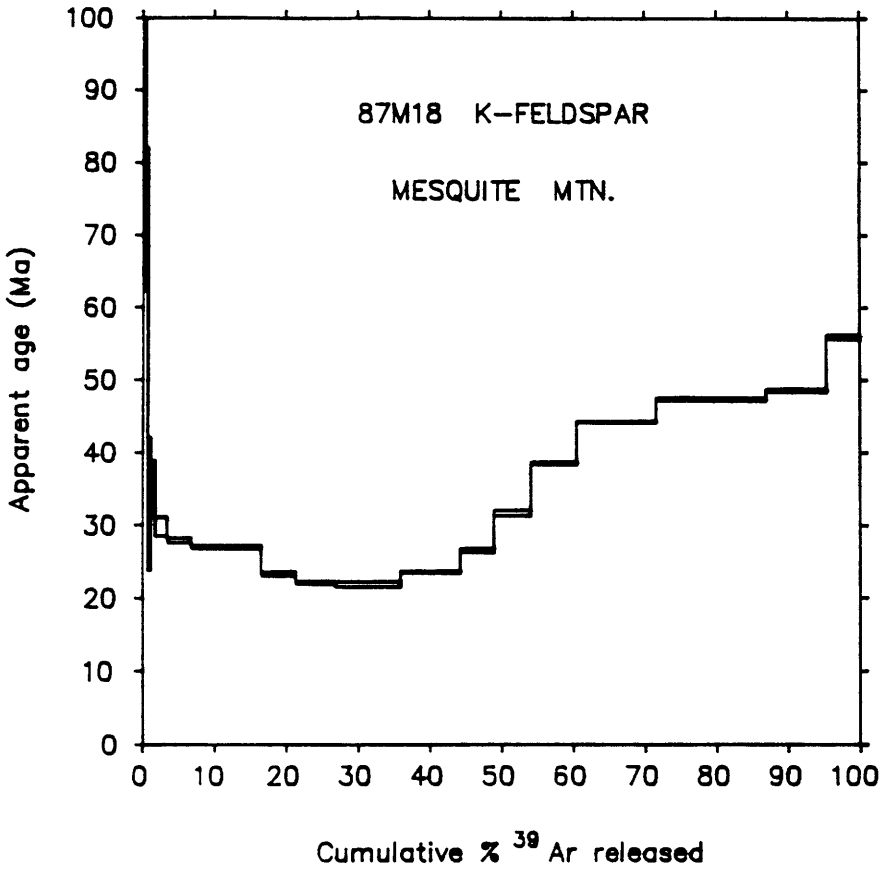
87M18 K-FELDSPAR
MESQUITE MTN.
Apparent age (Ma)
Cumulative % 39 Ar released
0
10
20
30
40
50
60
70
80
90
100

Figure 3.10a

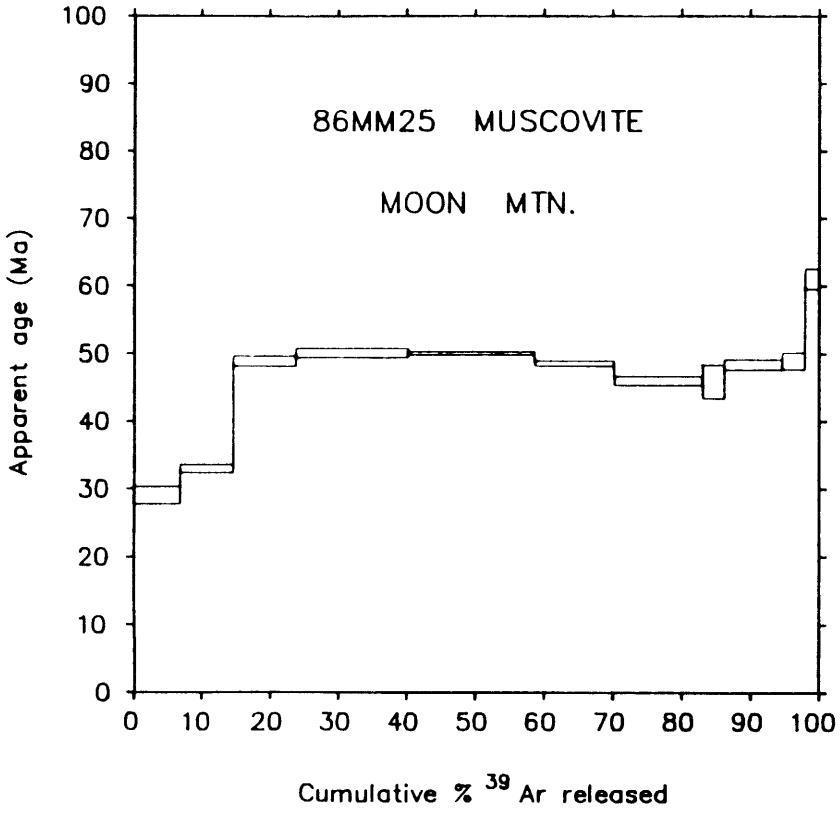

Figure 3.10b

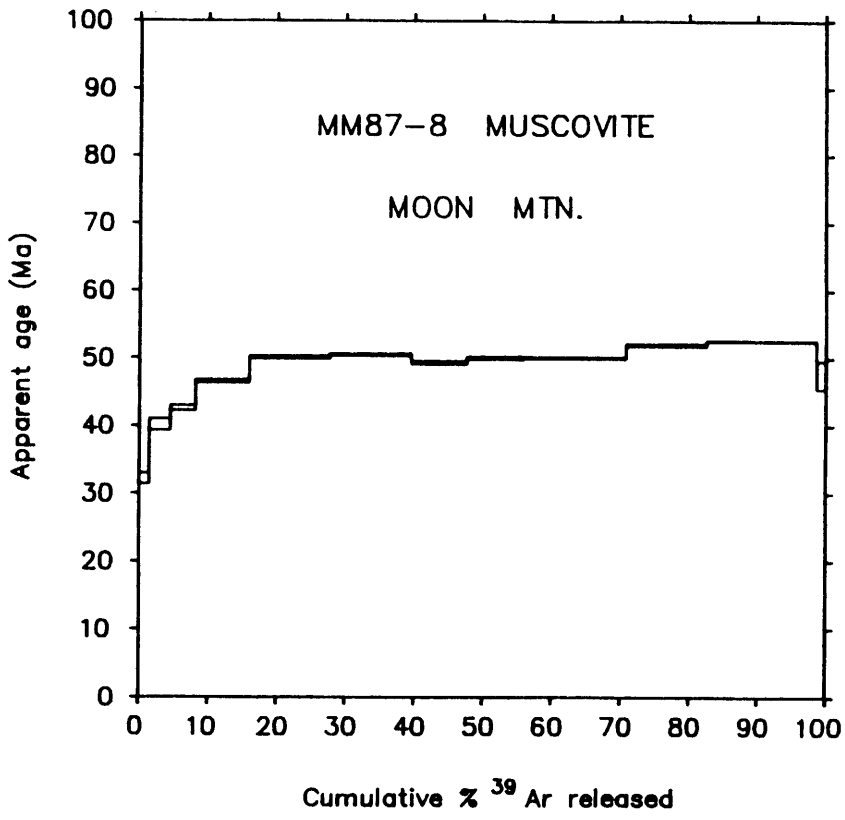

Figure 3.10c

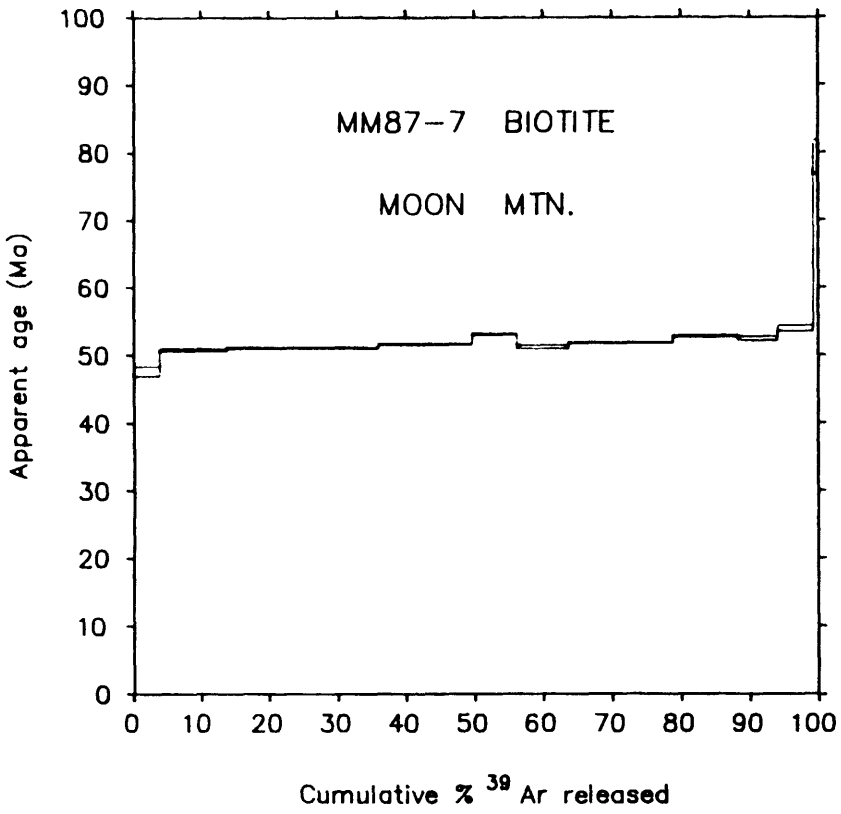

Figure 3.10d

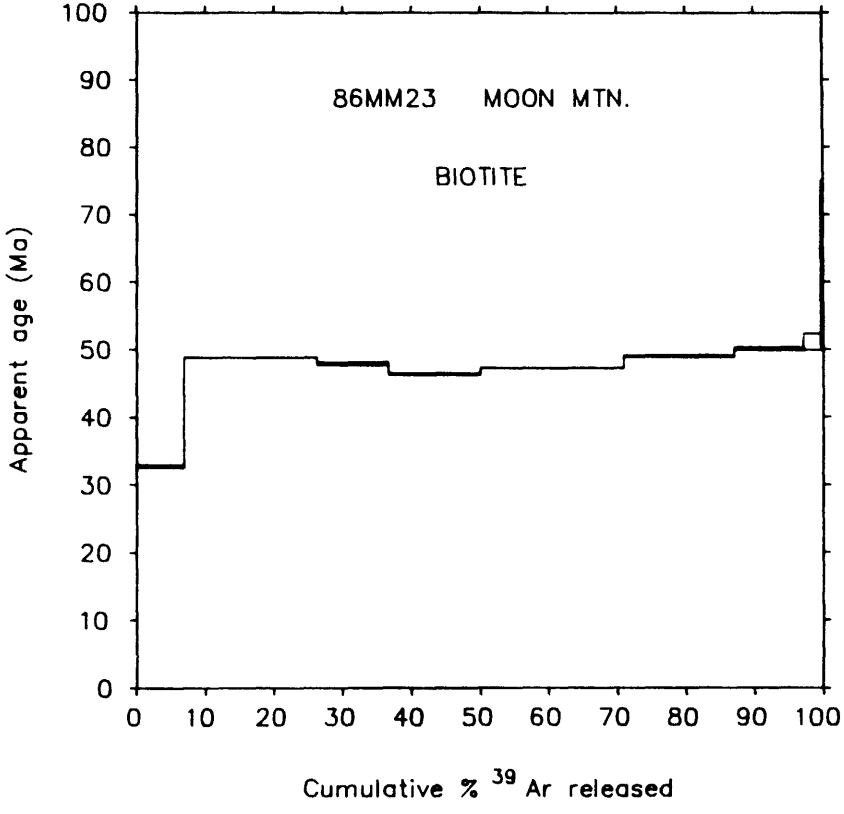

Figure 3.10e

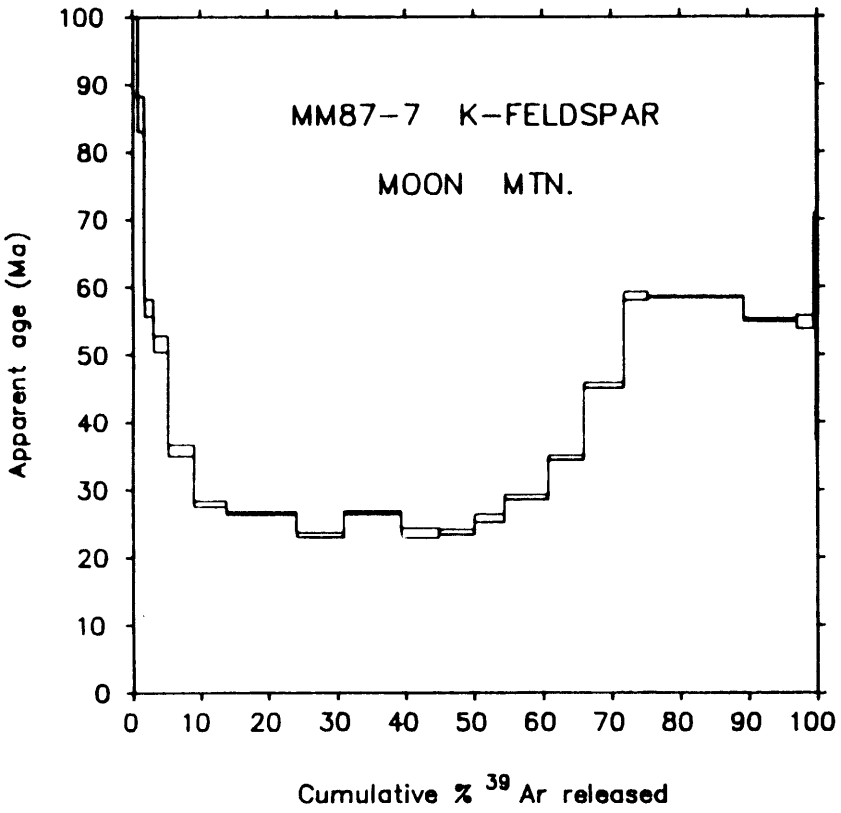

Figure 3.10f

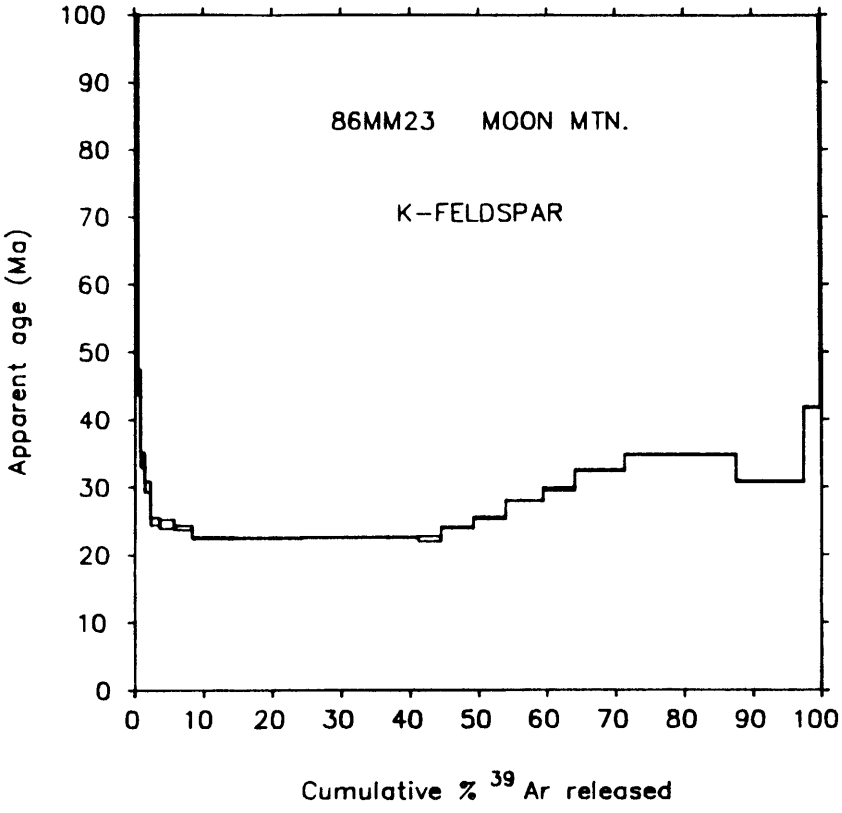

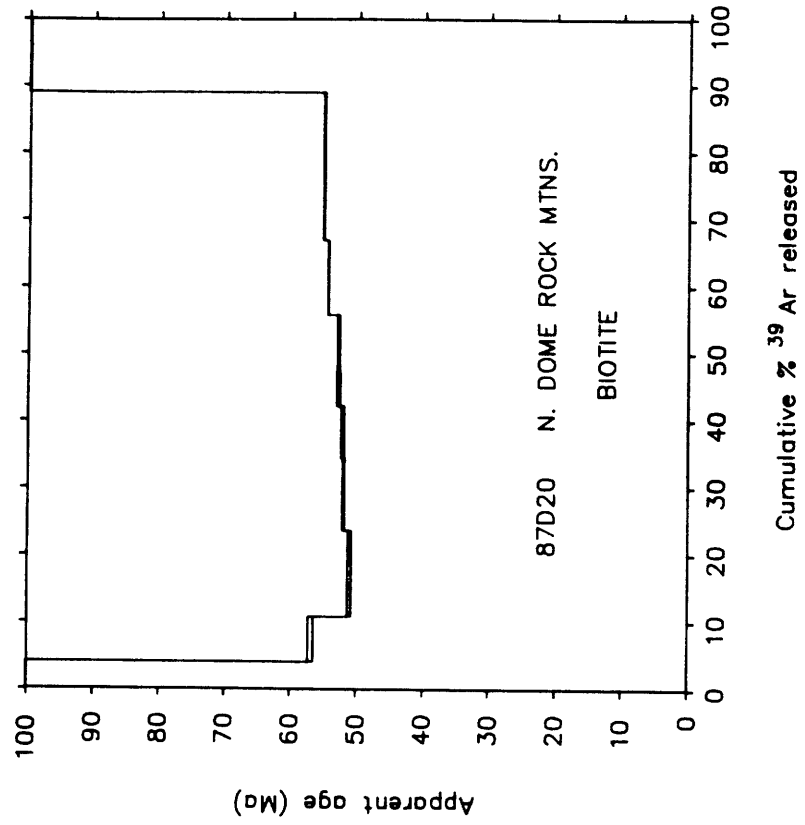

Figure 3.11b

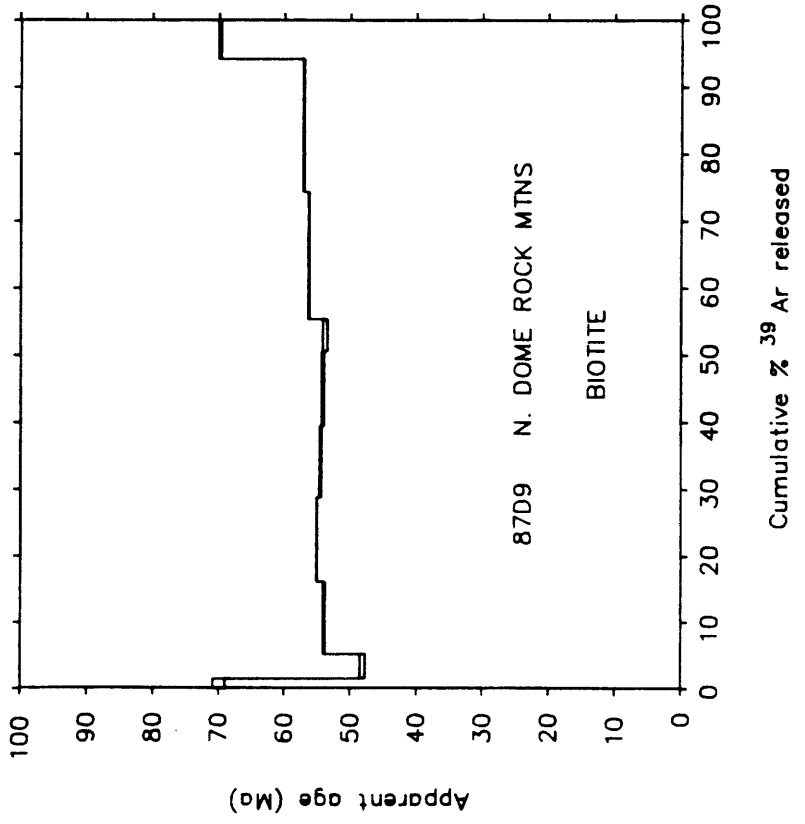

Figure 3.11a

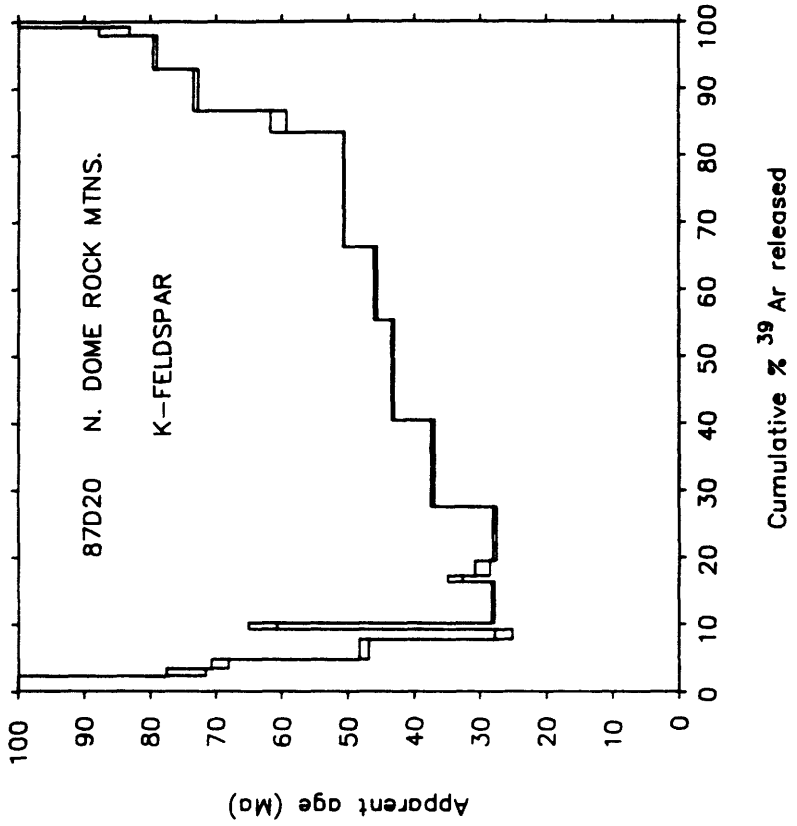

Figure 3.11d

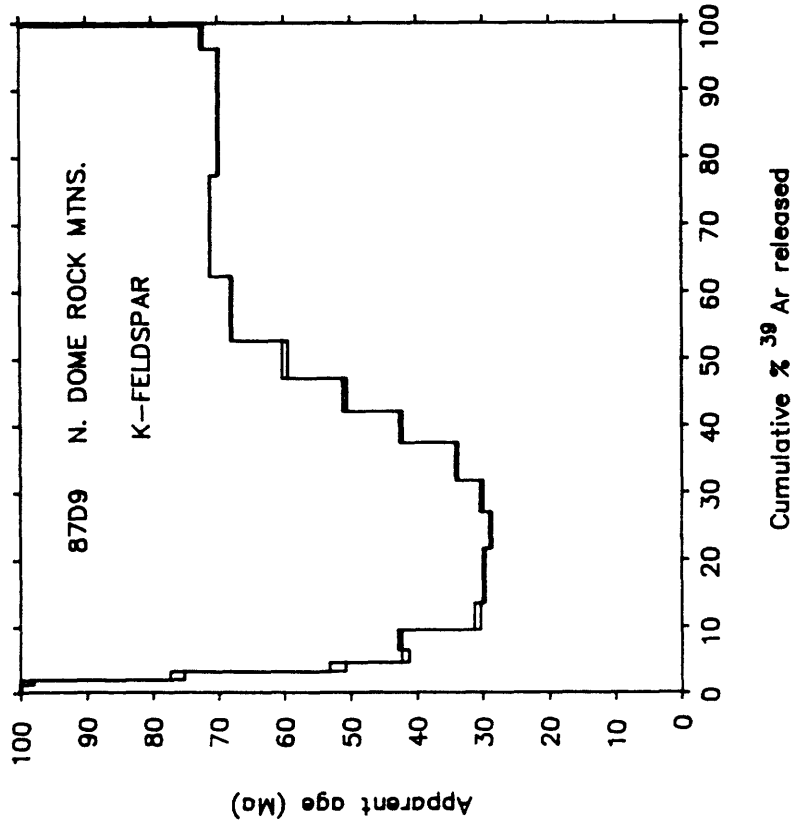

Figure 3.11c

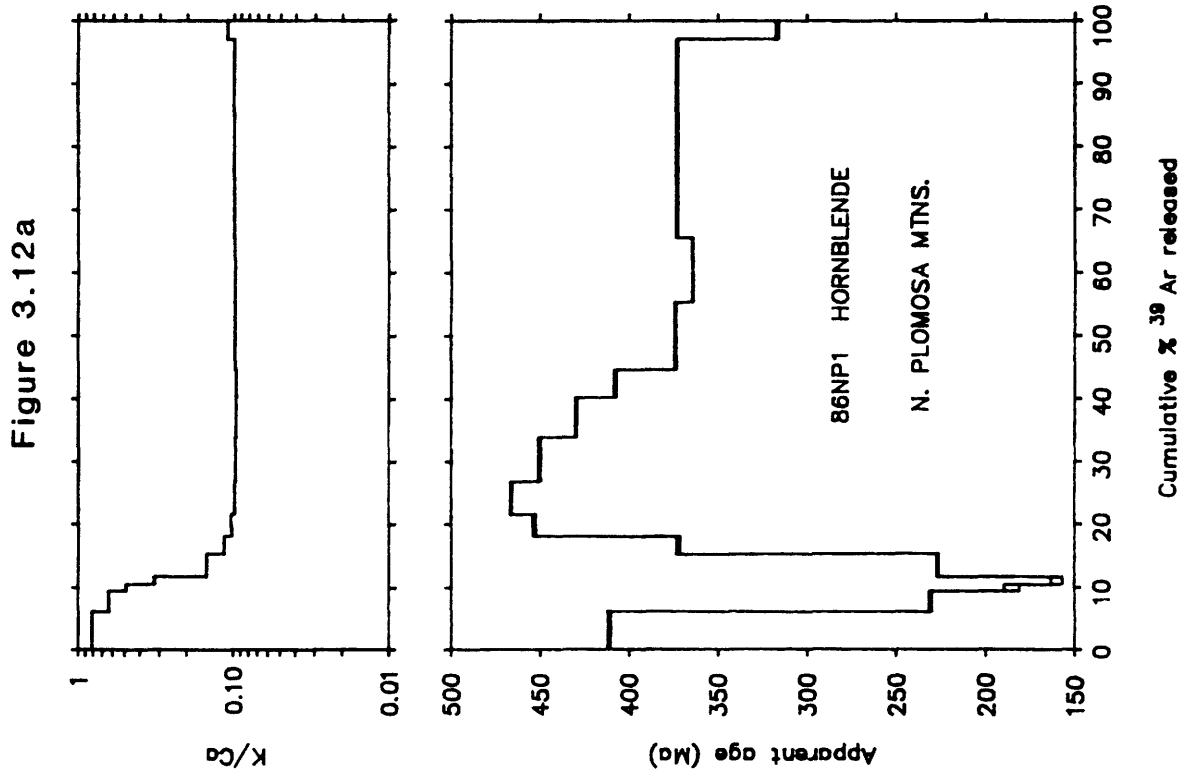
Figure 3.12a
K/Ca
1
0.10
0.01
Apparent age (Ma)
500
450
400
350
300
250
200
150
86NP1 HORNBLENDE
N. PLOMOSA MTNS.
0
10
20
30
40
50
60
70
80
90
100
Cumulative % 39 Ar released

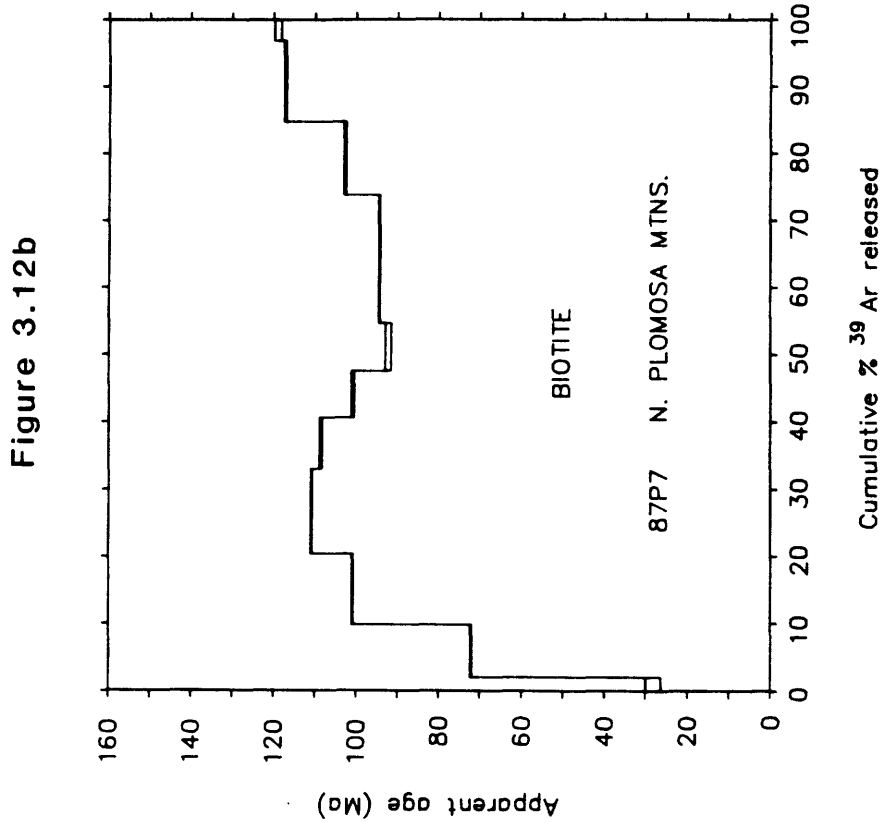
Figure 3.12b
Apparent age (Ma)
160
140
120
100
80
60
40
20
0
BIOTITE
87P7 N. PLOMOSA MTNS.
0
10
20
30
40
50
60
70
80
90
100
Cumulative % 39 Ar released

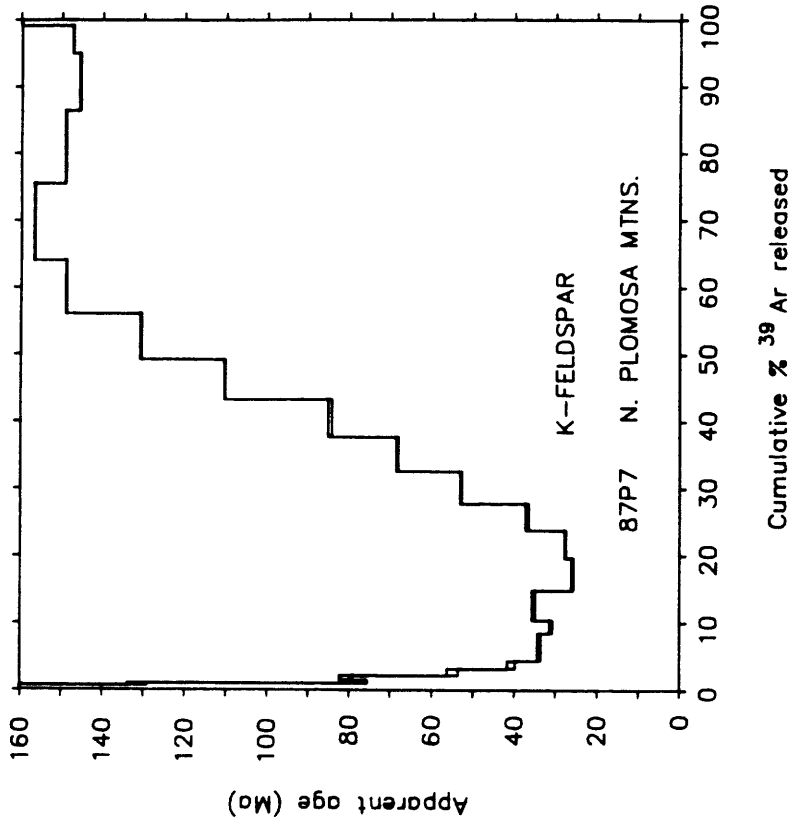

Figure 3.12d

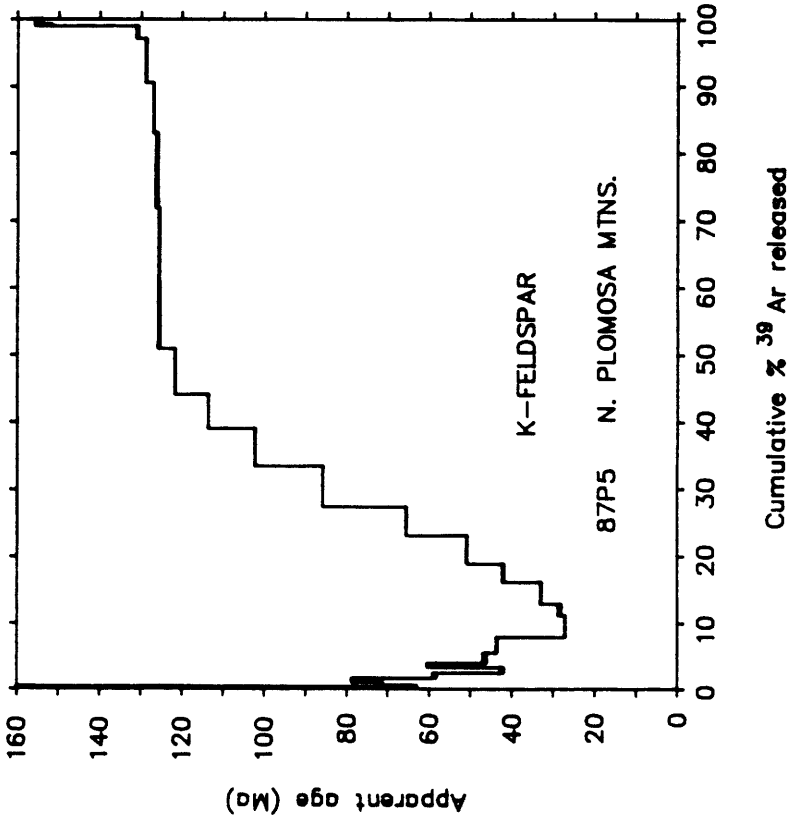

Figure 3.12c

Figure 3.13a

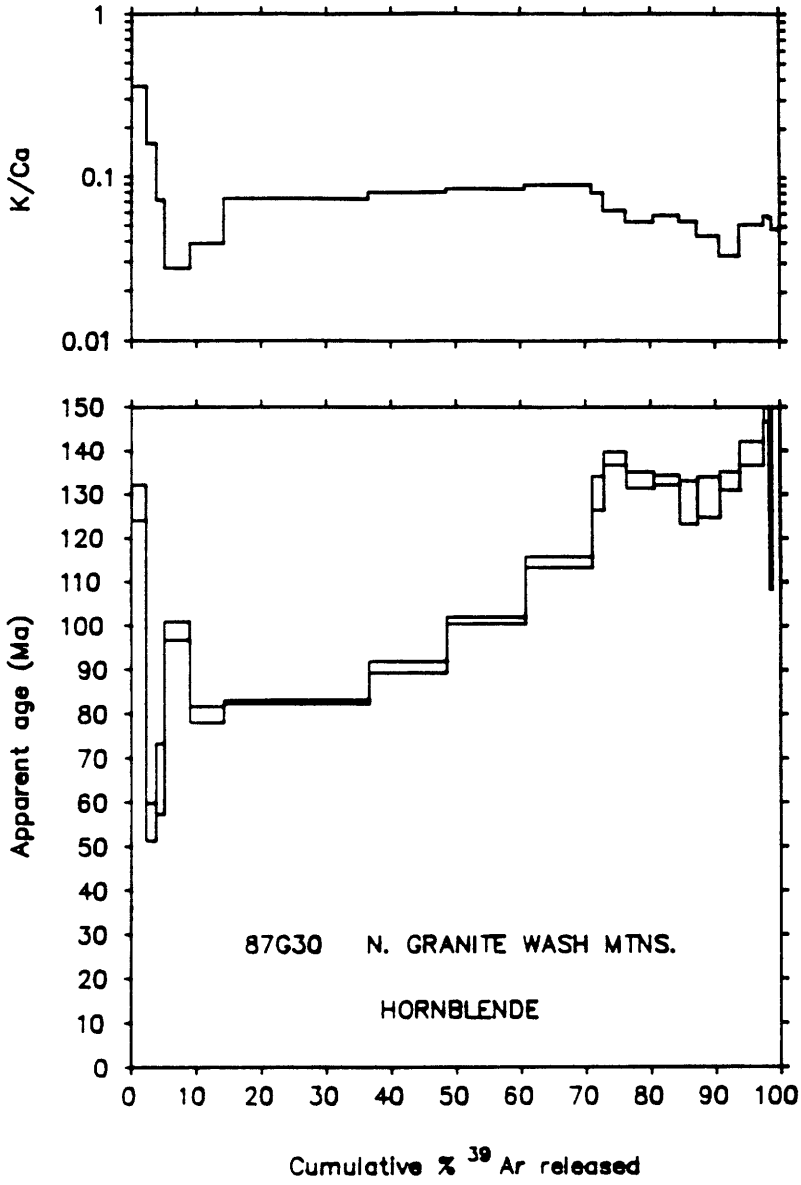
K/Ca
1
0.1
0.01
Apparent age (Ma)
150
140
130
120
110
100
90
80
70
60
50
40
30
20
10
0
0 10 20 30 40 50 60 70 80 90 100
87G30 N. GRANITE WASH MTNS.
HORNBLENDE
Cumulative % 39 Ar released

Figure 3.13b

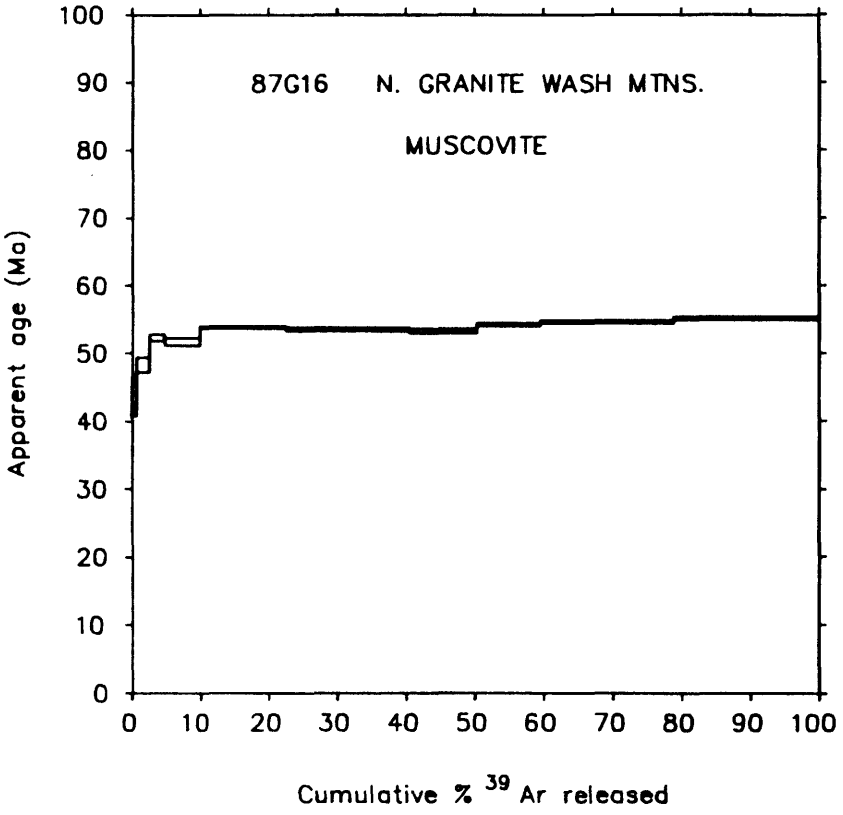

Figure 3.13c

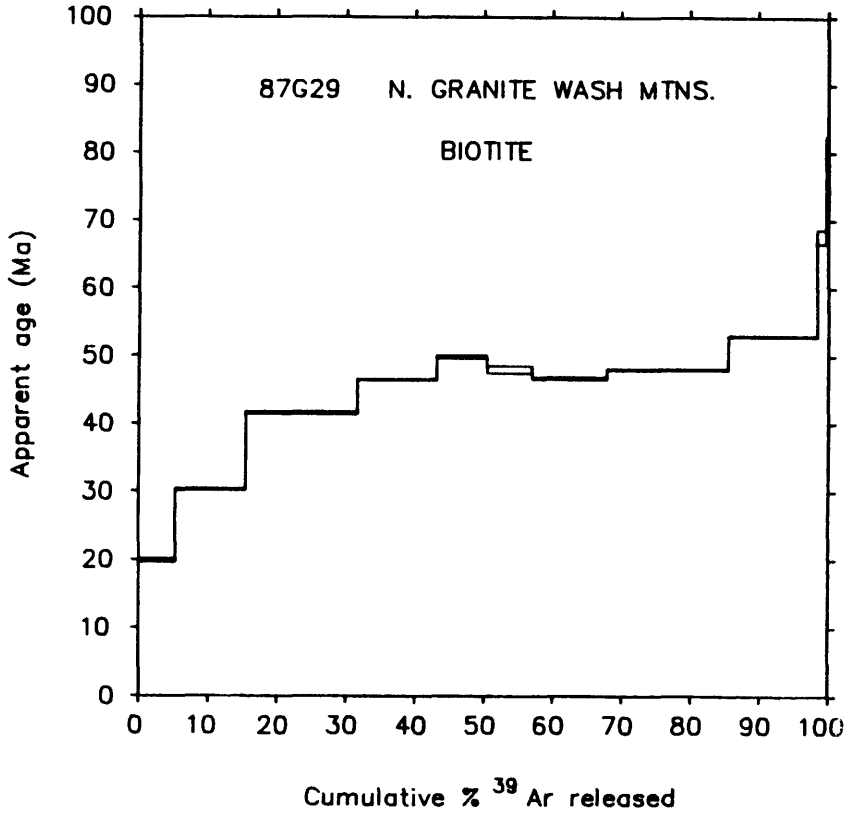

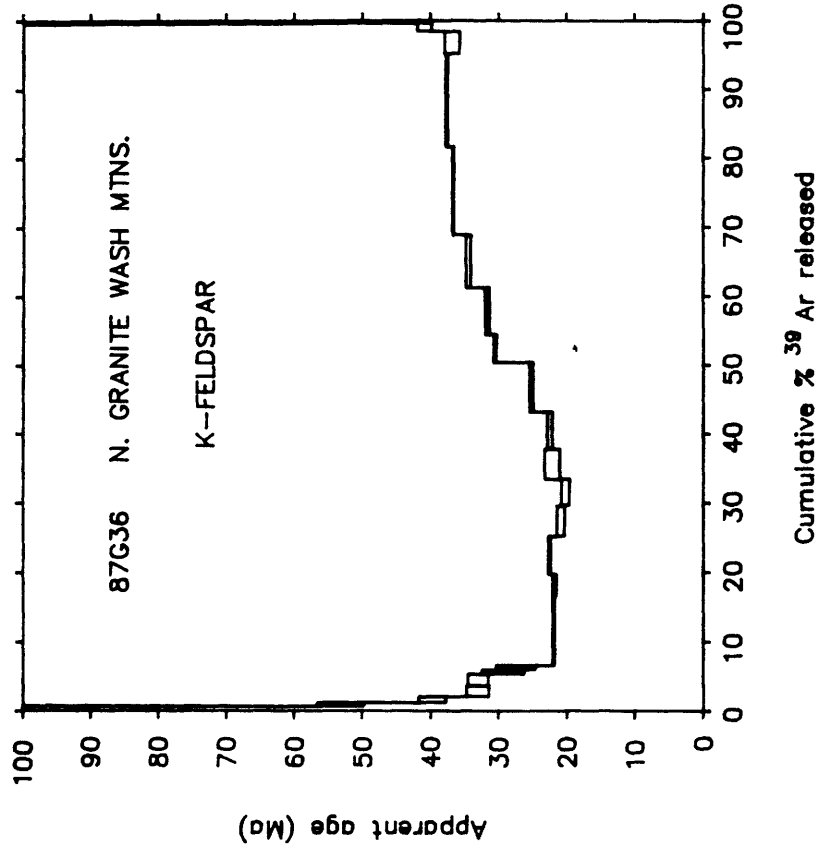

Figure 3.13e

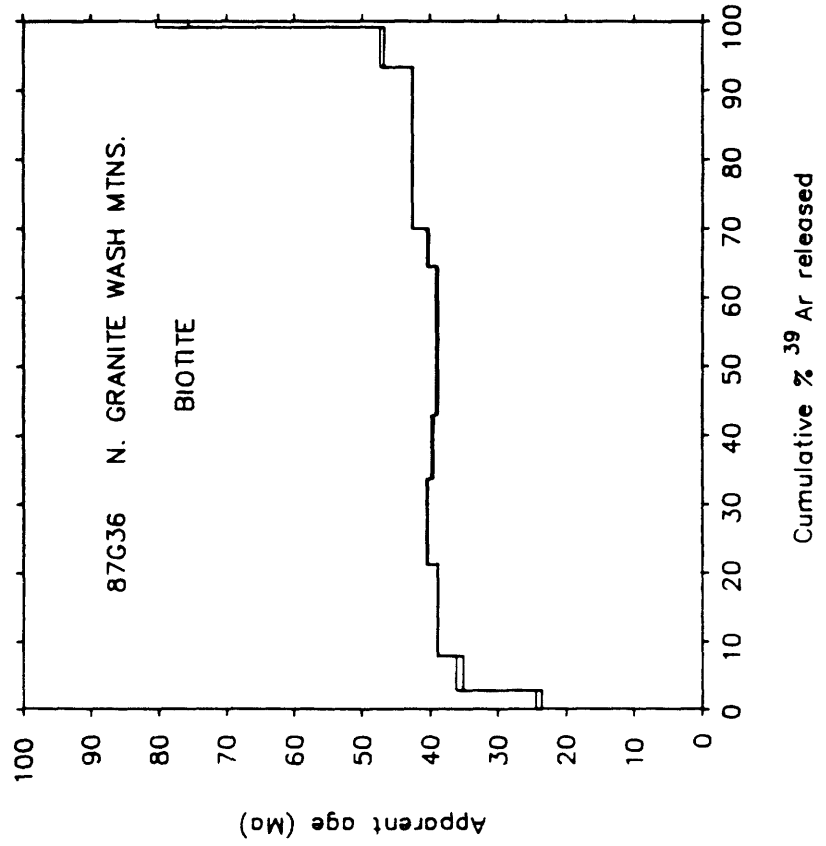

Figure 3.13d

Fig. 3.14a

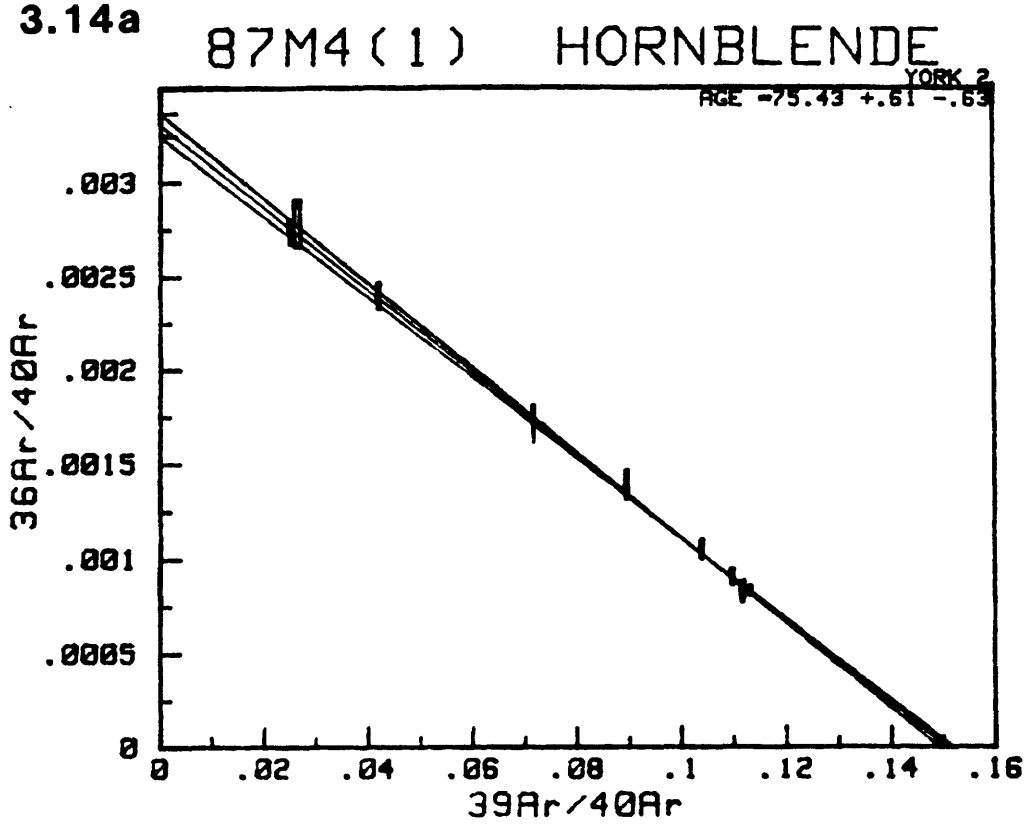

Fig. 3.14b

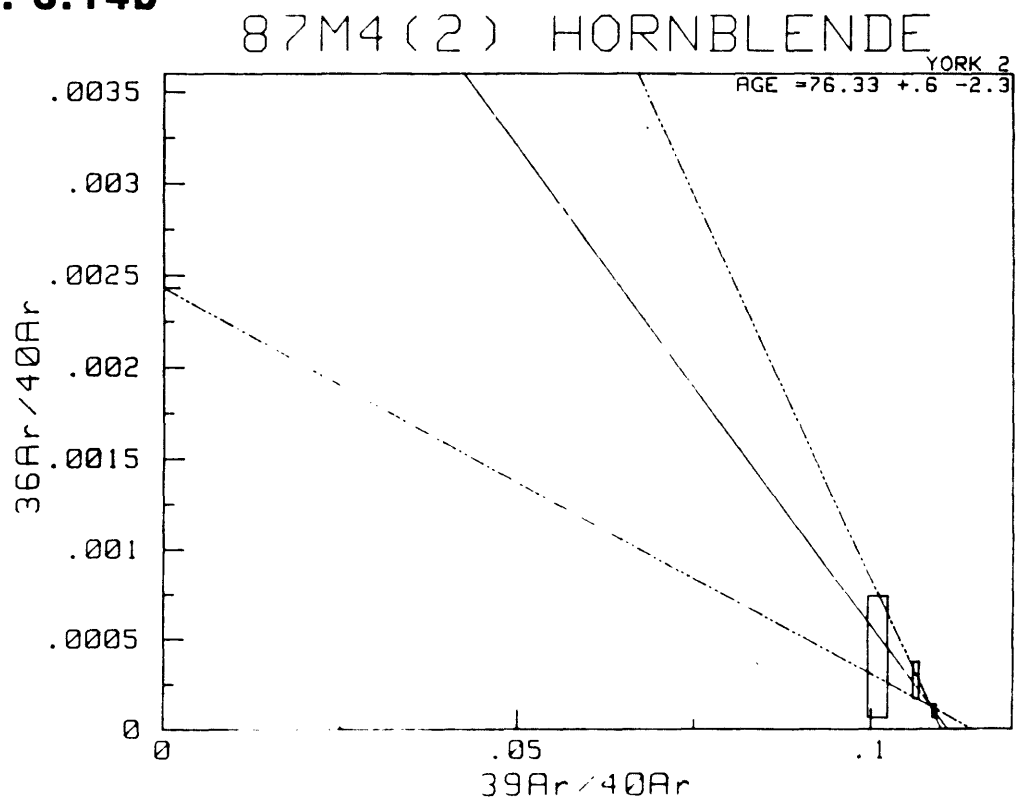

Fig. 3.14c

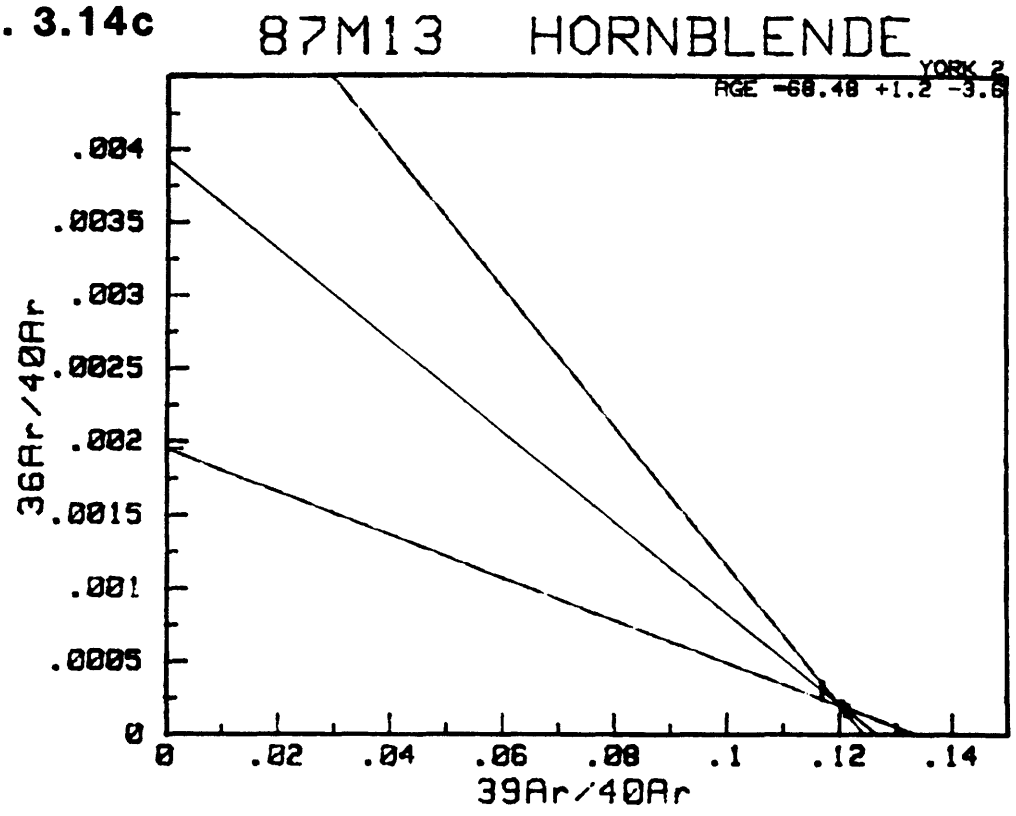

Fig. 3.14d

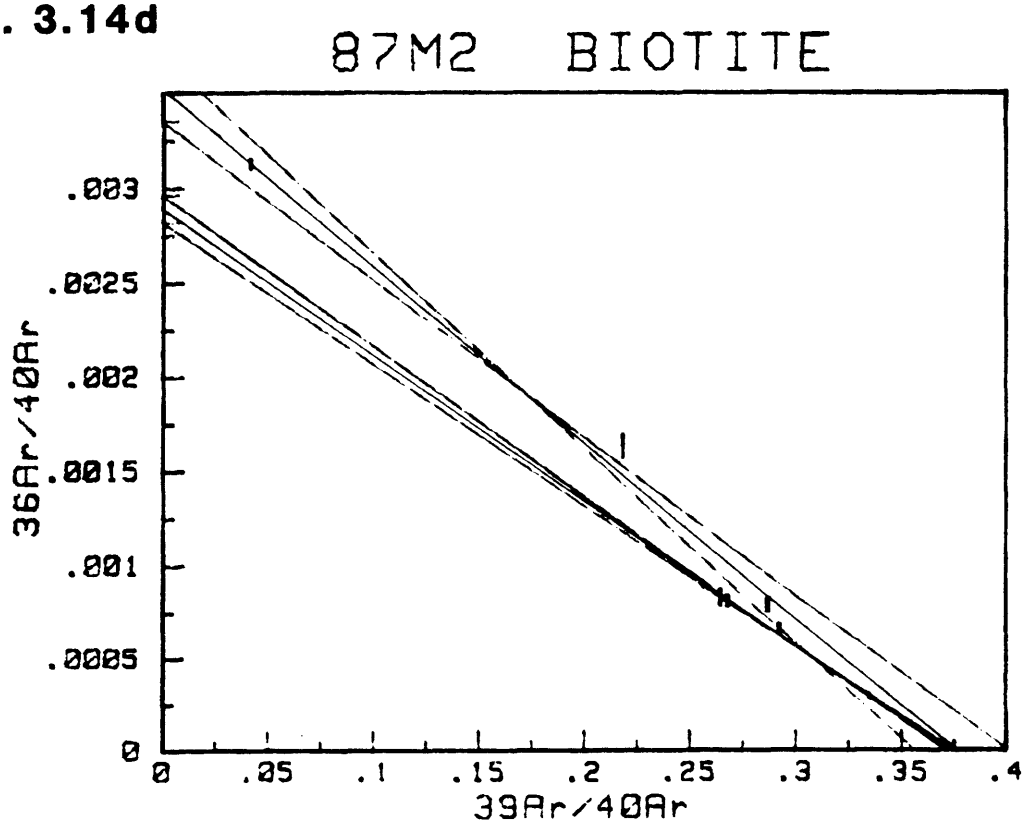

Fig. 3.14e

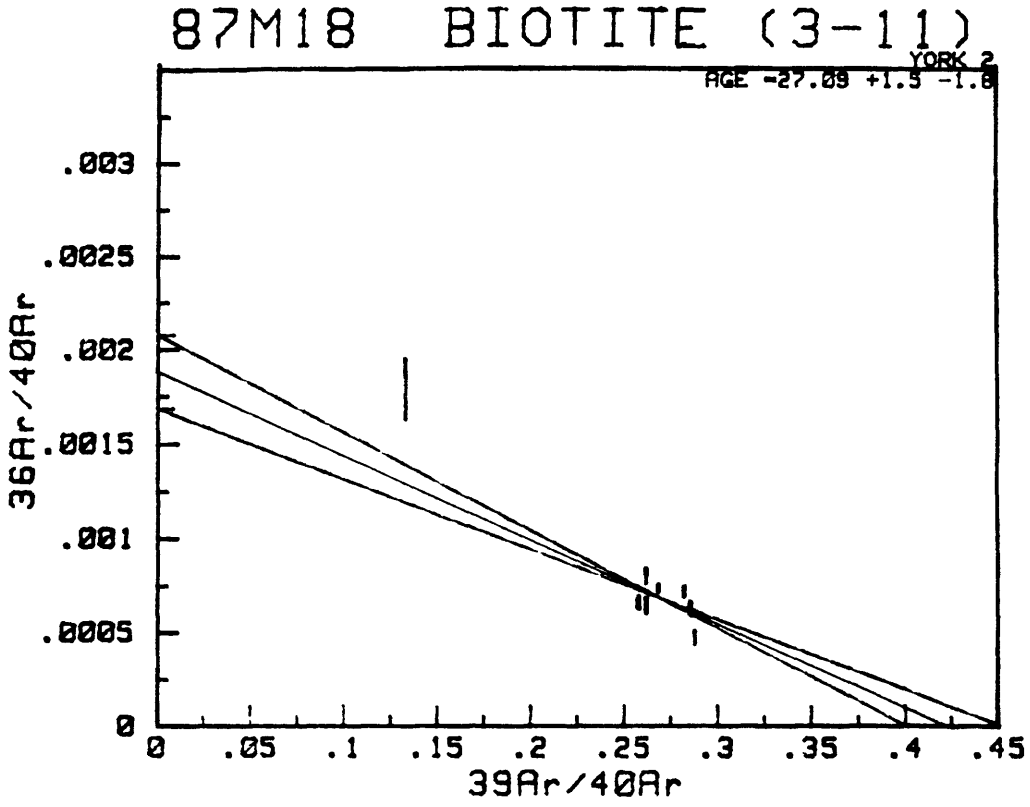

Fig. 3.15a

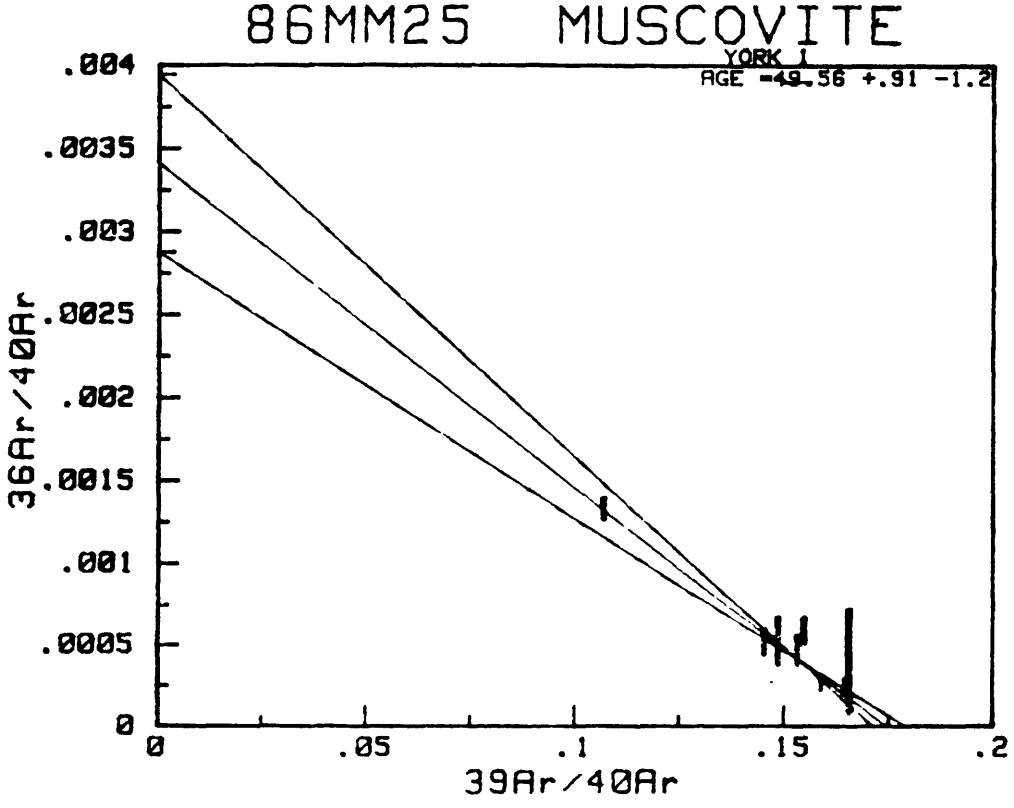

Fig. 3.15b

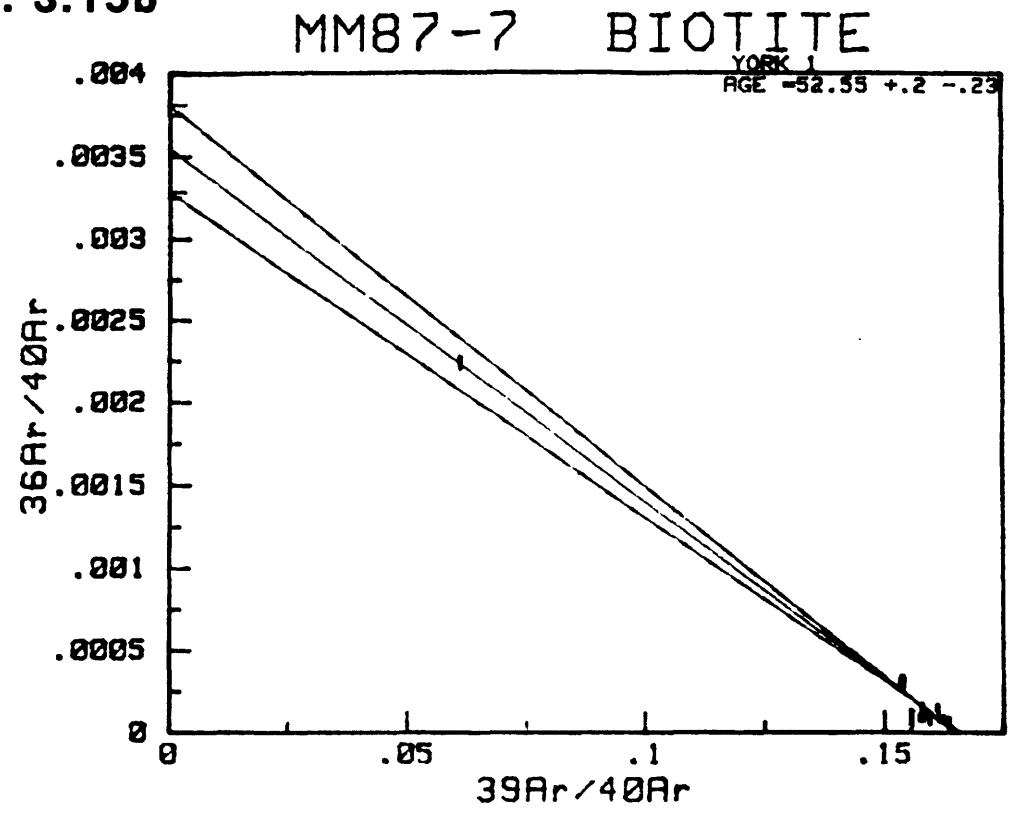

Fig. 3.15c

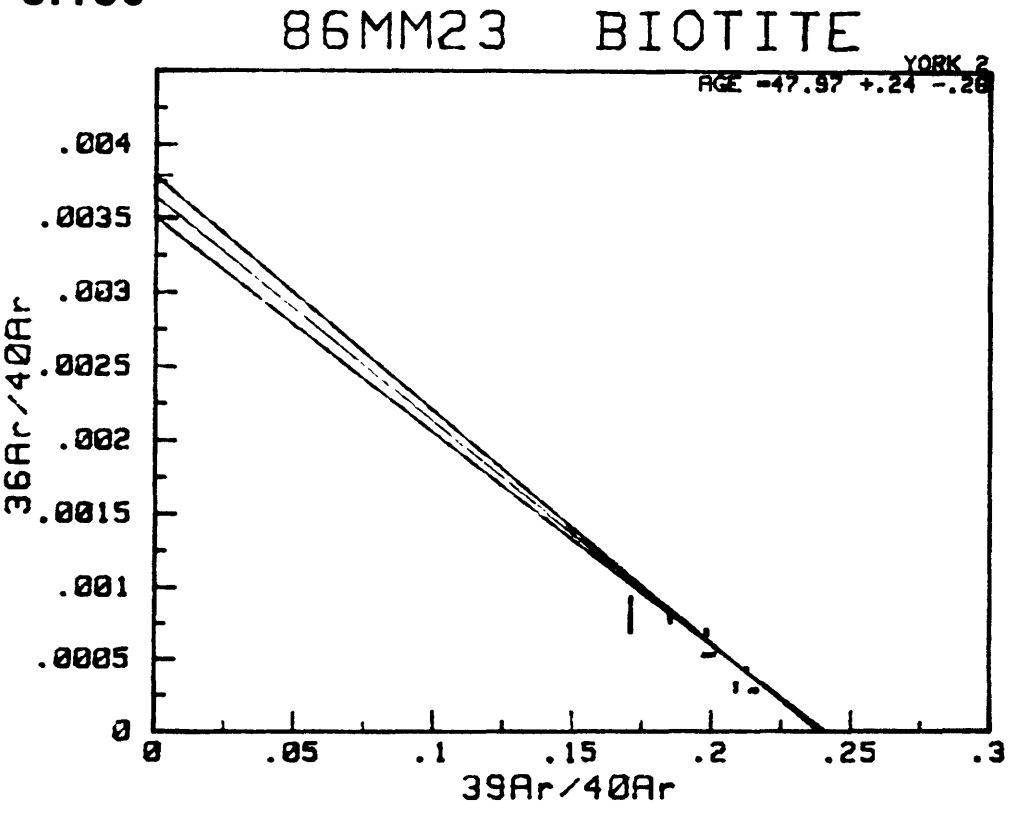

Fig. a

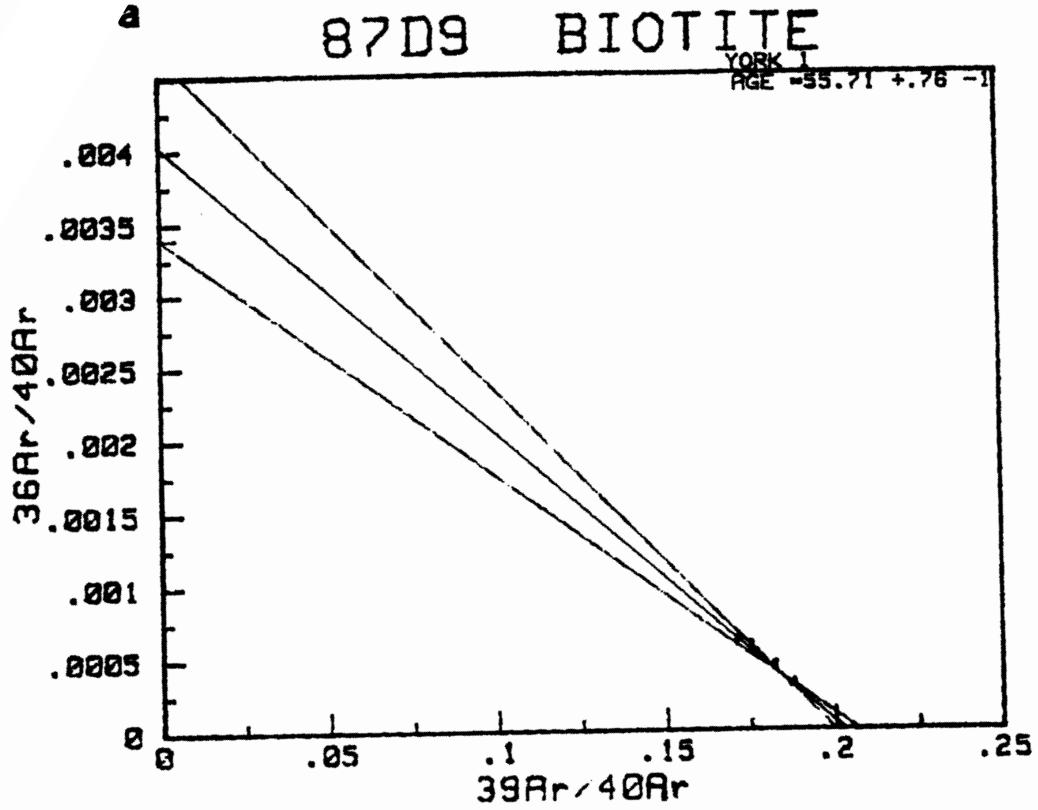

Fig. 3.16b

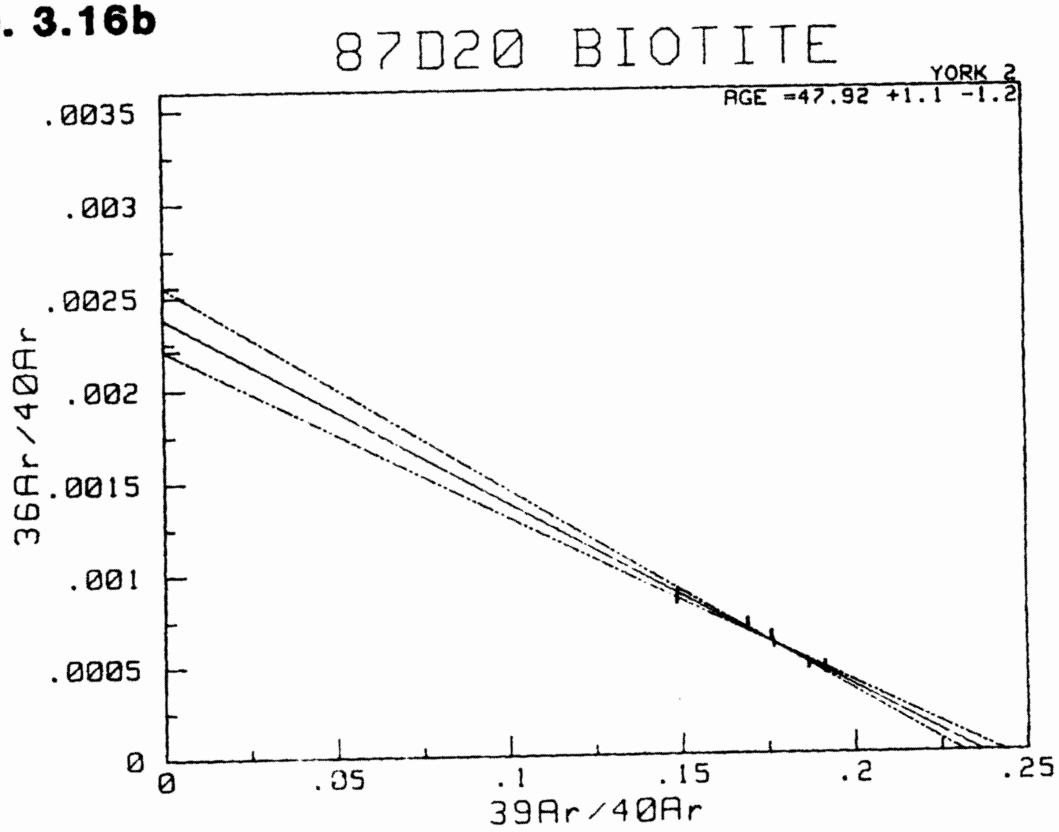

Fig. 3.16c

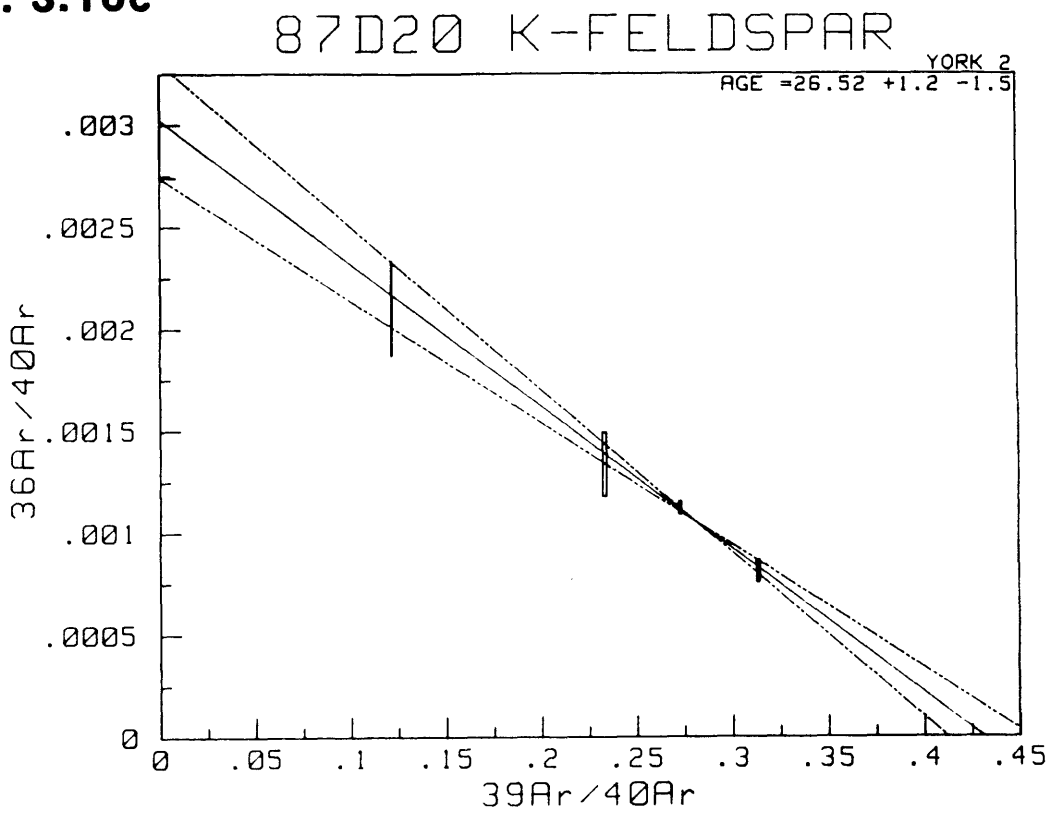

Fig. 3.17a

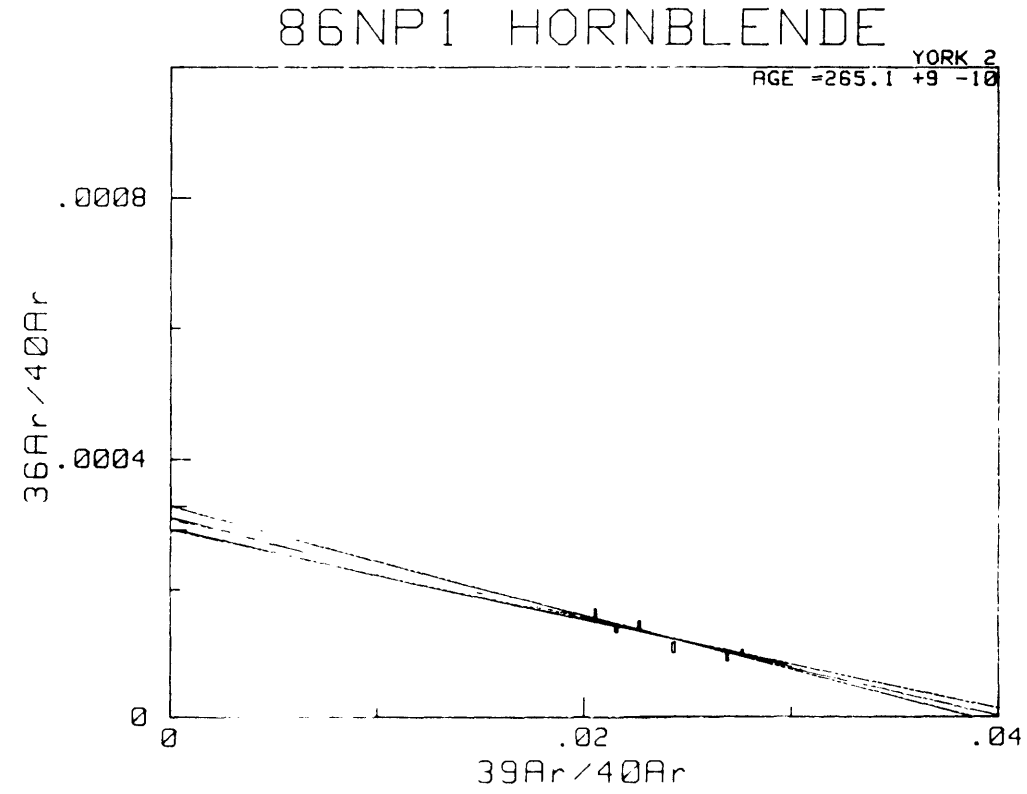

Fig. 3.17b

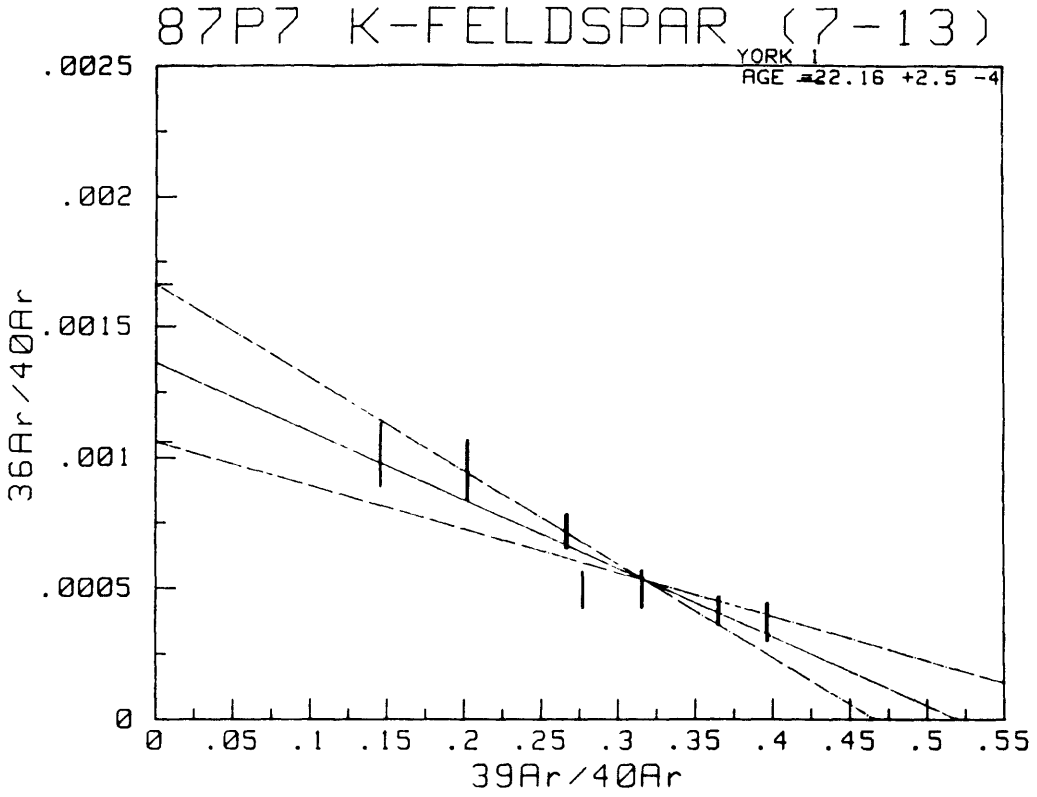

Fig. 3.18a

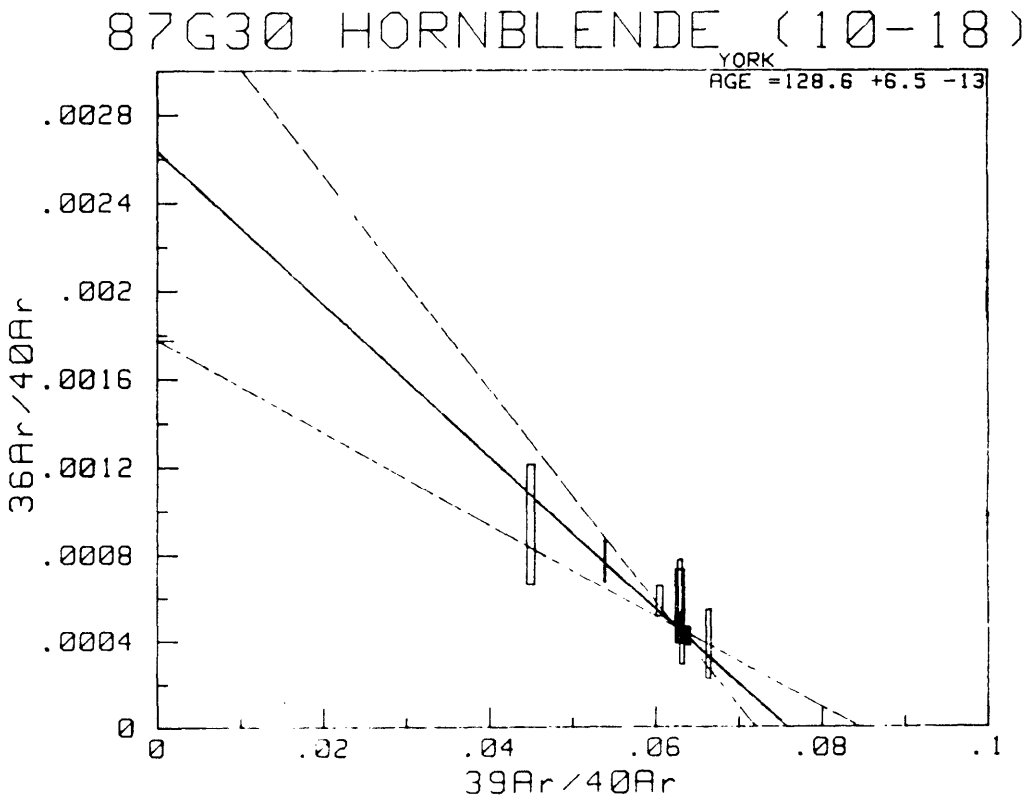

Fig. 3.18b

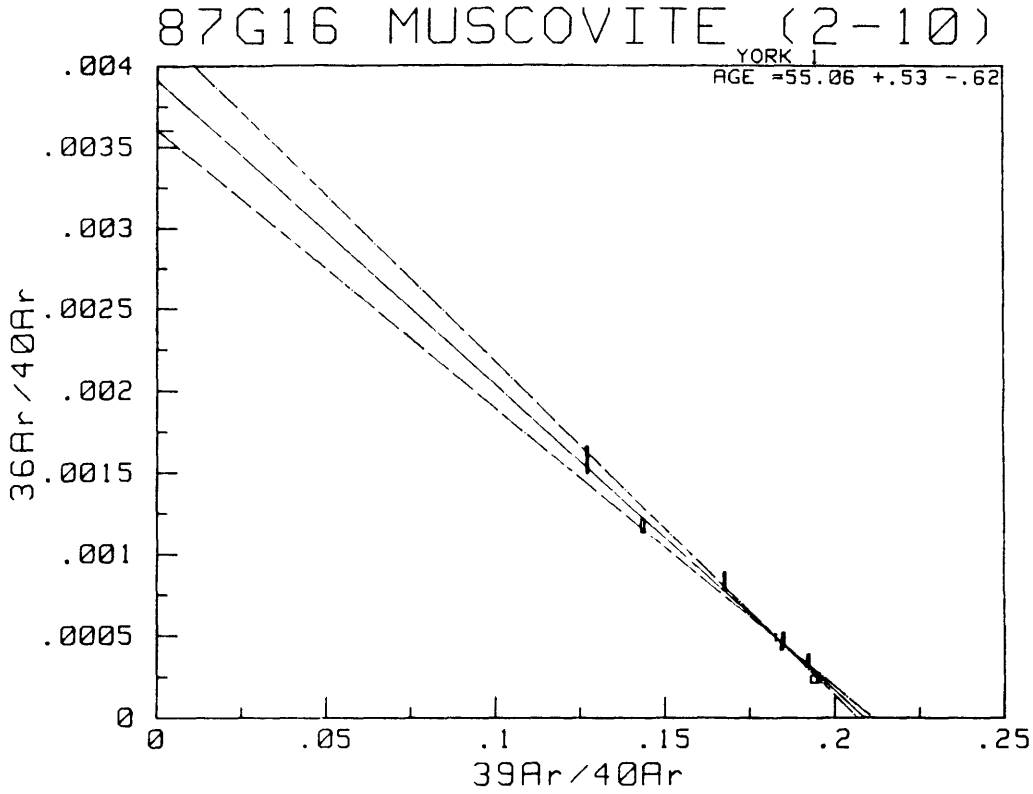

Fig. 3.18c

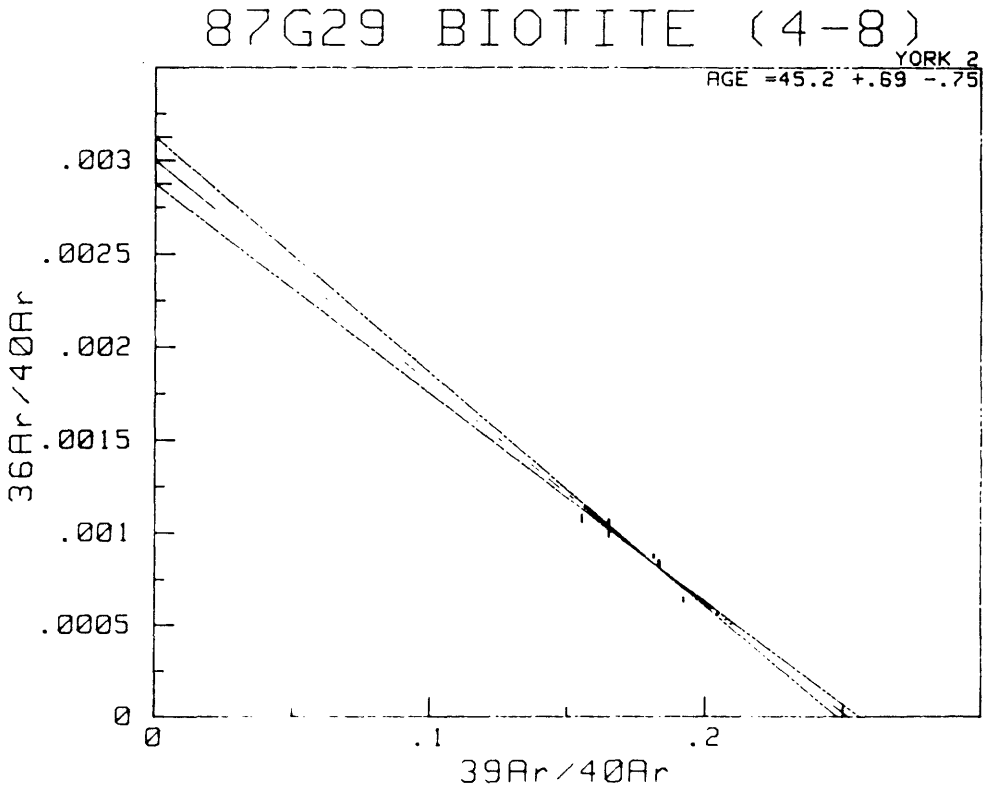

Fig. 3.18d

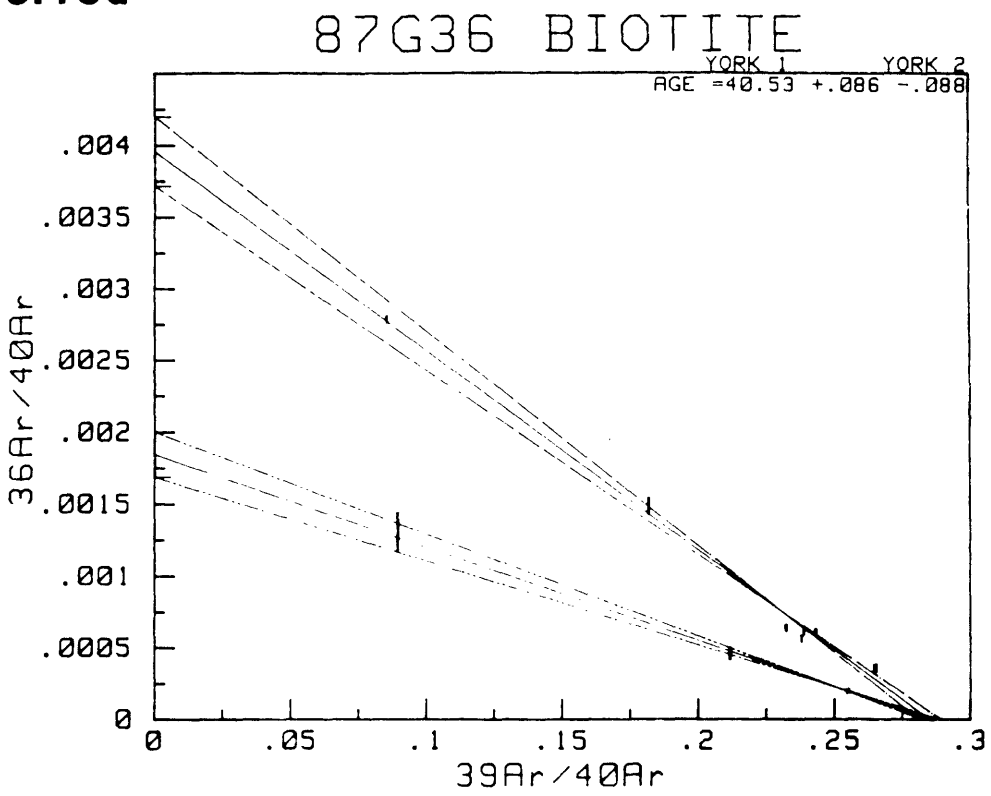

Fig. 3.18e

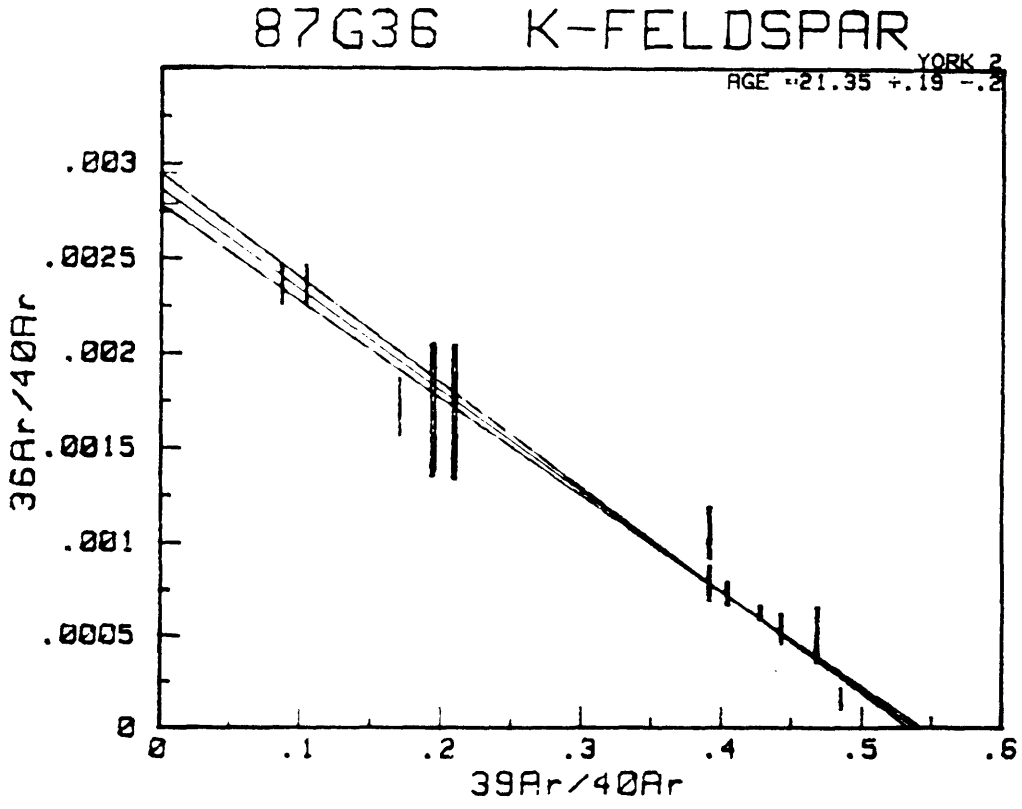

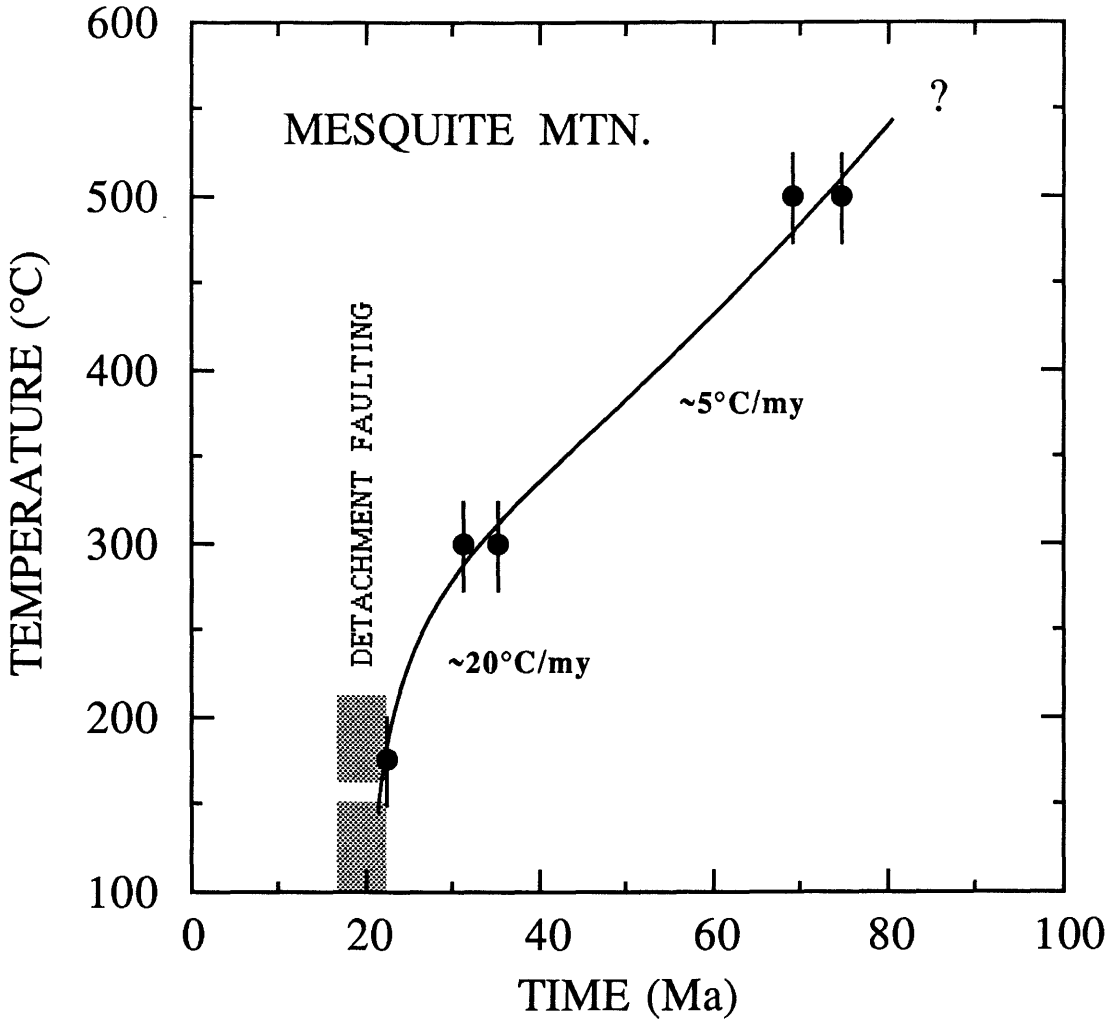
600
500
400
300
200
100
0
20
40
60
80
100
TEMPERATURE (°C)
TIME (Ma)
MESQUITE MTN.
?
DETACHMENT FAULTING
~5°C/my
~20°C/my

Figure 3.19

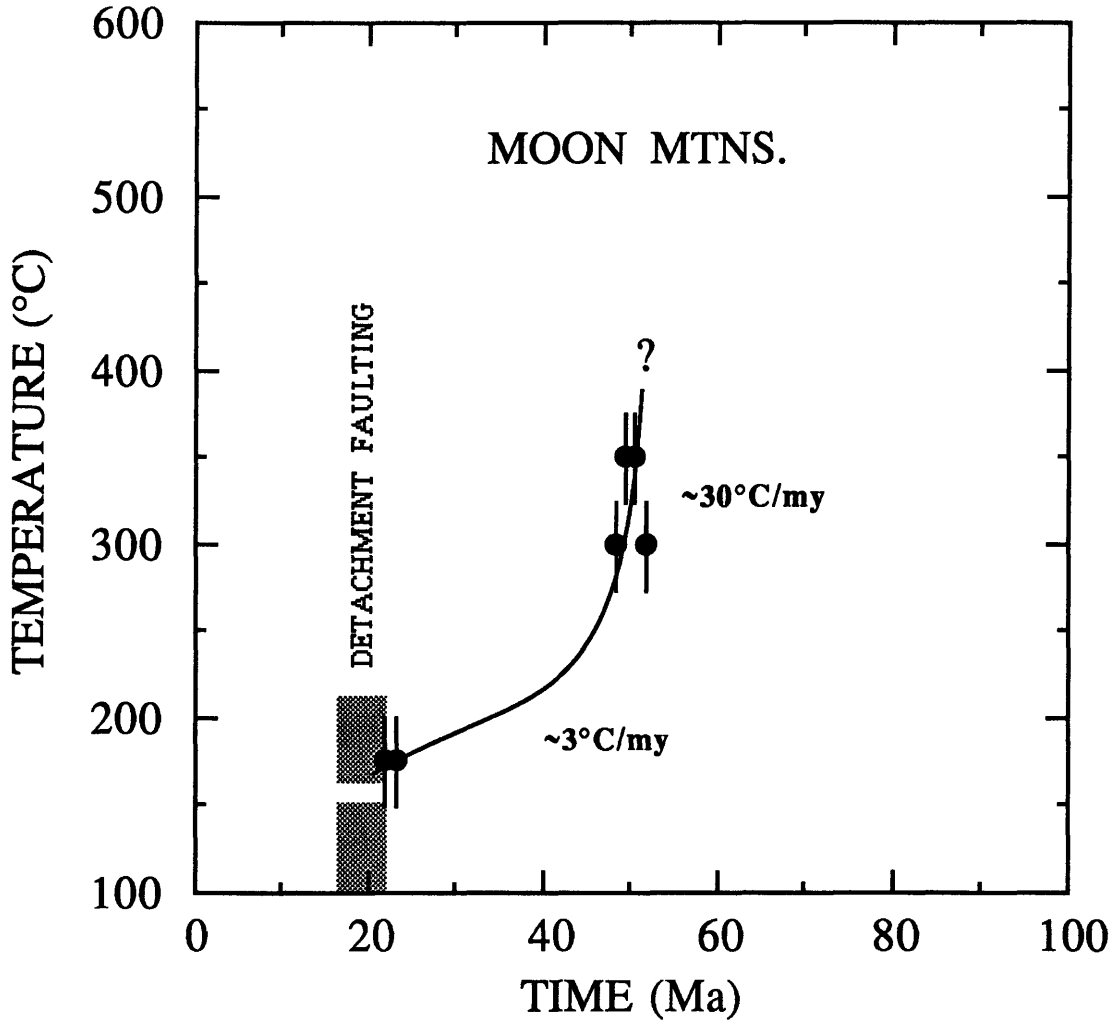
MOON MTNS.
TEMPERATURE (°C)
600
500
400
300
200
100
0
20
40
60
80
100
TIME (Ma)
DETACHMENT FAULTING
?
~30°C/my
~3°C/my

Figure 3.20

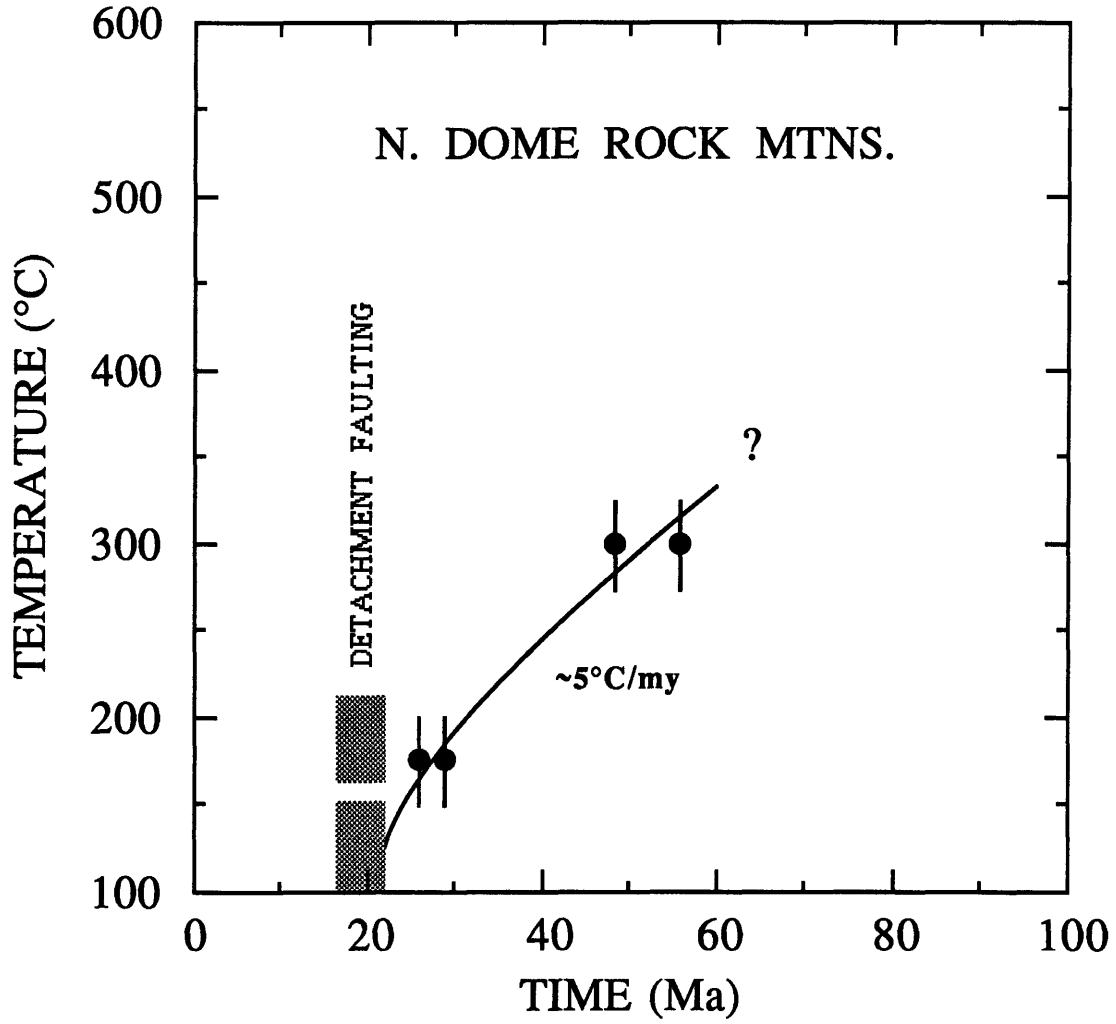
N. DOME ROCK MTNS.
TEMPERATURE (°C)
600
500
400
300
200
100
0
20
40
60
80
100
TIME (Ma)
DETACHMENT FAULTING
~5°C/my
?

Figure 3.21

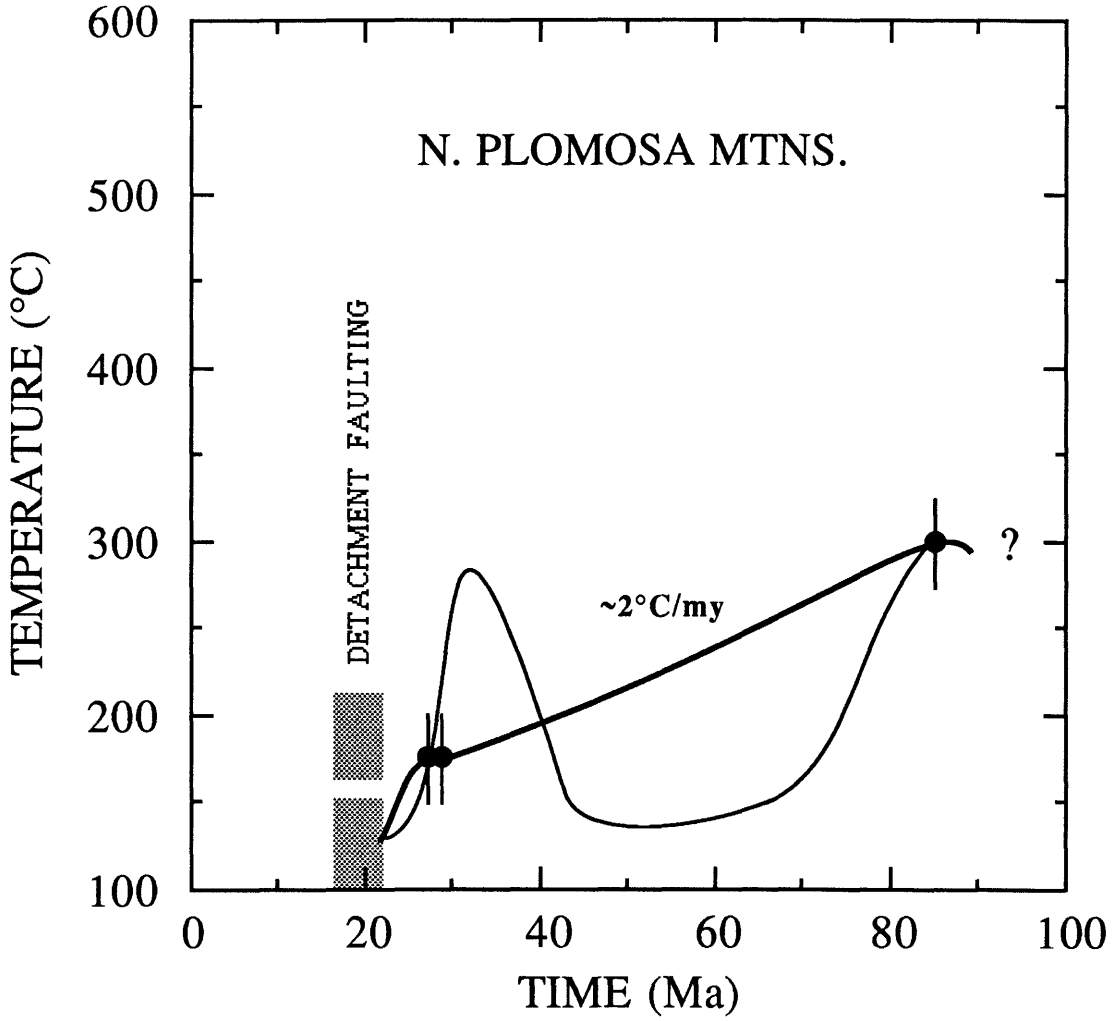
N. PLOMOSA MTNS.
TEMPERATURE (°C)
600
500
400
300
200
100
0
20
40
60
80
100
TIME (Ma)
DETACHMENT FAULTING
~2°C/my
?

Figure 3.22

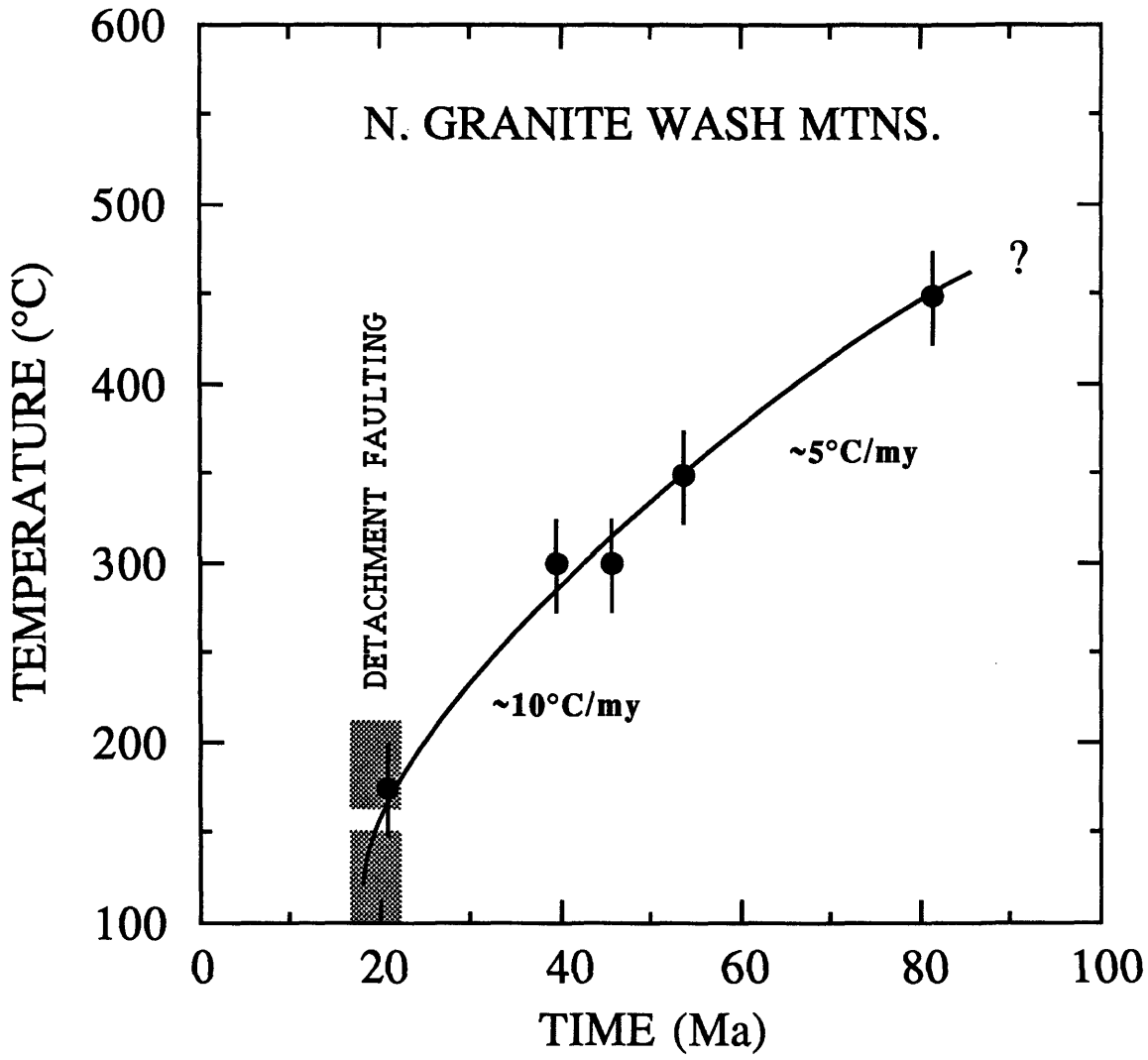
N. GRANITE WASH MTNS.
TEMPERATURE (°C)
600
500
400
300
200
100
0
20
40
60
80
100
TIME (Ma)
DETACHMENT FAULTING
~10°C/my
~5°C/my
?

Figure 3.23

CHAPTER 4

U-Pb GEOCHRONOLOGY OF MESOZOIC TO TERTIARY MAGMATISM IN WEST-CENTRAL ARIZONA: IMPLICATIONS FOR TECTONIC EVOLUTION OF THE MARIA FOLD AND THRUST BELT

James H. Knapp and J. Douglas Walker

ABSTRACT

Uranium-lead zircon ages of intrusive units from Mesquite Mountain and the Moon Mountains of the Colorado River Indian Reservation are representative of Jurassic through Tertiary magmatism in west-central Arizona, and help to clarify the nature and timing of major tectonic and magmatic events in the crustal evolution of this region. Megacrystic quartz syenite from the southern Moon Mountains yields a late Middle Jurassic age (160 ± 15 Ma) and defines the eastern limit of Jurassic plutonism at this latitude. The age of basement-involved thrusting in the Maria fold and thrust belt is constrained to post-date late Middle Jurassic time since this intrusive unit is carried in the hanging wall of the Valenzuela thrust system in the southern Moon Mountains. Garnet-bearing, granitic pegmatites are syn- to late-kinematic with the youngest movement on the Valenzuela thrust, and yield a lower intercept age of 71.1 ± 6.7 Ma, providing the first direct dating of the age of basement-involved thrusting in the Maria fold and thrust belt.

At Mesquite Mountain, a lower intercept age of 67.2 ± 1.4 Ma from a concordant, biotite-granite sill in the Mesquite Gneiss migmatite complex records the time of granitic injection associated with migmatization of these gneisses. We interpret *in situ* partial

melting and injection of the Mesquite Gneiss as a deep-seated response to Late Cretaceous crustal thickening in the Maria fold and thrust belt. Additional evidence for a widespread Late Cretaceous thermal event is seen in resetting of $^{40}Ar/^{39}Ar$ systematics for crystalline rocks of west-central Arizona. Early Tertiary time was marked by a distinct hiatus in magmatic activity, while the region underwent uplift and slow cooling. Magmatism resumed in late Oligocene to early Miocene time in association with crustal extension, as evidenced by widespread basaltic volcanism and granitic plutonism in western Arizona. A late- to post-kinematic, biotite granite from the footwall of the Copper Peak detachment fault in the northeastern Moon Mountains yields a U-Pb zircon lower intercept age of 20.8 ± 3.2 Ma. Timing constraints for development of the Whipple-Buckskin-Rawhide detachment system (~22-16 Ma) indicate that intrusive activity was synchronous with the early stages of extension.

Existing age constraints on deformation and syntectonic metamorphism in the Maria fold and thrust belt imply that Late Cretaceous (90?-70 Ma) tectonism here was broadly coeval with deformation in other areas of the Cordilleran thrust belt. Extensive involvement of crystalline rocks in Late Cretaceous thrusting in west-central Arizona may have been related to softening of the crust by magmatic activity, but on a local scale thrusting was not controlled by thermal anomalies. Much of the magmatism in the Maria fold and thrust belt appears to be syn- to post-kinematic, and may represent a response to crustal thickening. Development of basement-involved structures in the Maria fold and thrust belt was probably related to a number of factors, including changes in the direction and rate of relative plate motions during Cretaceous time.

The locus of large-magnitude, mid-Tertiary crustal extension in west-central Arizona was coincident with the Maria fold and thrust belt, suggesting a genetic link between extension and thickened crust. While thickened continental crust may have been a significant driving force for extension, other factors appear to have played a role. Oligocene magmatic activity occurred just prior to or during the earliest recognized stages of extension in the Whipple-Buckskin-Rawhide detachment system, and appears to mark a renewed thermal event distinct from that associated with the Late Cretaceous. In addition, extensional strain in the Whipple-Buckskin-Rawhide terrain was not accommodated along pre-existing thrust faults which could have acted as zones of preferential weakness. Such a feature might be explained by the oblique superposition of east-northeast - west-southwest extension across southeast-, south-, and north-vergent

structures of the Maria fold and thrust belt, and suggests that a fundamental change in relative plate motions along western North America was associated with extension.

INTRODUCTION

Magmatism in the Mojave-Sonora region of western Arizona and southeastern California constitutes part of a complex geologic history of the southwestern Cordillera of the United States. These igneous rocks range in age from Precambrian to Tertiary, and provide important controls on the structural and tectonic history of the area. Two major tectonic regimes are presently recognized in the Phanerozoic evolution of west-central Arizona. A Mesozoic compressional regime was characterized by thrusting, large-scale folding, greenschist to amphibolite facies metamorphism, and calc-alkaline magmatism within the Maria fold and thrust belt. Crystalline basement rocks were extensively involved in this deformation, unlike much of the remainder of the Mesozoic thrust belt in the North American Cordillera. An extensional regime characterized Cenozoic time in west-central Arizona, and involved large magnitudes of extension, basin formation, greenschist facies metamorphism, and bimodal magmatism in the regional Whipple-Buckskin-Rawhide detachment terrain.

The age and tectonic significance of the Maria fold and thrust belt has remained obscure due to the general lack of structural and geochronologic information for this area. Only in the past five to ten years has an understanding of this unique tectonic element in the western Cordillera of North America begun to emerge. The results of the present study represent some of the first U-Pb zircon geochronology to be conducted in the Maria fold and thrust belt, and place important constraints on the age and relative timing of deformation and magmatism in the region. In addition, results from the present study, in conjunction with regional relations, suggest that several factors may have been involved in the development of large-scale extension in the Whipple-Buckskin-Rawhide terrain and in the Basin and Range province in general.

MARIA FOLD AND THRUST BELT

The Maria fold and thrust belt (as first defined by Reynolds et al., 1986) extends some 250 km along an east-west trend from the Coxcomb Mountains in southeastern California to the Harquahala Mountains of west-central Arizona (Fig. 4.0). A number of features distinguish this segment of the thrust belt, including (1) a change in orientation from the characteristic north-south strike to an east-west trend, (2) episodes of thrusting

and large-scale folding which involved transport to the southeast, south, and north, (3) syn-tectonic metamorphism at upper greenschist to lower amphibolite facies, and (4) extensive involvement of the crystalline rocks in the deformation. Included within this deformational belt are all or parts of the Palen, McCoy, Big Maria, Little Maria, Riverside, Mesquite, Moon, Dome Rock, Buckskin, Plomosa, Granite Wash, Harcuvar, Harquahala, and Little Harquahala Mountains (Fig.4.0).

Within this belt of Mesozoic deformation, major thrust faults place Proterozoic and Mesozoic crystalline rocks over Mesozoic and Paleozoic strata, with evidence for multiple episodes of deformation. Reynolds et al. (1986) describe a set of large, southeast- to south-vergent folds and locally associated thrusts which are discordantly cut by thrusts that verge southwest, south, north, and northeast, and interleave Paleozoic and Mesozoic sedimentary rocks with crystalline rocks. The sense of vergence of these structures not only varies considerably within the Maria fold and thrust belt, but deviates significantly from the consistent eastward vergence which characterizes the North American Cordilleran thrust belt throughout much of its length.

The predominantly east-west strike of the Maria fold and thrust belt is perpendicular to the northerly trend of the Mesozoic thrust belt extending south from Canada. In the region of extensive Laramide deformation to the east in Colorado and New Mexico, structural trends strike generally north-south, and eastward vergence of large basement uplifts is inferred to have resulted from east-west convergence of the North American and Farallon plates in Late Cretaceous through early Tertiary time (Tweto, 1975).

Similarly, the Maria fold and thrust belt lies at an oblique orientation to the zone of Sevier-age and earlier deformation projecting southward from Utah and southern Nevada. The Sevier thrust belt, characterized by imbricate, east-vergent thrust sheets within Paleozoic and Mesozoic strata, displays the thin-skinned, décollement style of deformation typical of the thrust belt further along strike to the north in the U.S. and Canada, and to the south in Mexico. Work in recent years has extended the Sevier thrust belt from southern Nevada into the ranges of southeastern California in the Mojave region (Burchfiel and Davis, 1971, 1977; Miller et al., 1982). The southernmost known extent of this zone consists of a northeast-striking, southeast-vergent, basement-cored thrust nappe in the Old Woman Mountains of the central Mojave Desert (Miller et al., 1982).

The history of deformational events in the Maria fold and thrust belt is probably best understood in the eastern segment of this terrain in western Arizona. Reynolds et al. (1986) summarize the sequence of Mesozoic folding and thrusting in the Harquahala and Little Harquahala Mountains as follows. The earliest evidence for Mesozoic tectonism consists of coarse-grained conglomerates in the upper Mesozoic (McCoy Mountains Formation equivalent?) sedimentary rocks in these ranges. Deposition of this sequence is inferred to represent a Late Cretaceous tectonic disturbance, and was followed by formation of major southeast-facing folds with inferred southeast vergence. Southeast vergent thrusting may have accompanied this folding event, but has not been documented. Subsequently, large thrust sheets of Precambrian and Mesozoic crystalline rocks were emplaced discordantly across the earlier southeast-facing folds. A southward direction of transport was inferred for these thrust sheets based on (1) a north-trending mylonitic lineation along the thrust contacts with top-to-the-south sense of shear, and (2) an inferred original north dip of the thrusts based on the change from ductile fabrics along northern exposures of the thrusts to a more brittle cleavage along southern exposures. Formation of these structures and associated fabrics pre-dated intrusion of both the Granite Wash granodiorite in the western-most Little Harquahala Mountains, and the younger Tank Pass Granite to the north in the Granite Wash Mountains. These large granitic intrusions are generally undeformed, but the Tank Pass Granite was involved in a high-grade, fabric-forming event in the Harcuvar Mountains which resulted in migmatization associated with development of a gently-dipping foliation and northwest- to north-trending mineral lineation (Rehrig and Reynolds, 1980; Reynolds, 1982). Finally, a southwest dipping cleavage post-dates all of these fabrics, and has been interpreted as part of a late-stage, north-directed thrusting event (S. Richard, 1988; S. Reynolds, 1988, pers. comm.).

The age of deformational events within the Maria fold and thrust belt is not well-constrained. Most of the deformation is known to involve the Mesozoic McCoy Mountains Formation and its equivalents. This thick section (>7 km) of volcaniclastic and sedimentary rocks parallels the strike of the Maria fold and thrust belt in a west-northwest - east-southeast linear trough (Fig. 4.0). However, the age of these sedimentary rocks and the tectonic setting of the basin in which they accumulated remains controversial. Based on inferred interbedding of the basal McCoy Mountains Formation with underlying Jurassic volcanic rocks, and paleomagnetic data from the lower McCoy Mountains Formation, Harding et al. (1983), and Harding and Coney (1985) argued that the McCoy Mountains Formation was deposited and deformed in rapid succession prior

to late Middle to early Late Jurassic time. Subsequent revision of the Jurassic apparent polar wander path for North America (May and Butler, 1986) called into question the Jurassic age correlation made by Harding and Coney (1985). Other workers have proposed a post-mid-Cretaceous age for the McCoy Mountains Formation based on the presence of fossilized angiosperm wood in the upper part of the section (Pelka, 1973; Hamilton, 1982). Stone et al. (1987) argue convincingly for an early Late-Cretaceous age for at least the upper, fossil-bearing part of the McCoy Mountains Formation. An upper bound is placed on the major phases of south-vergent deformation in the Granite Wash and Little Harquahala Mountains by the Tank Pass Granite and Granite Wash Granodiorite (Reynolds et al., 1986).

WHIPPLE-BUCKSKIN-RAWHIDE EXTENSIONAL TERRAIN

Western Arizona was the site of major crustal extension during mid- to late-Tertiary time. Work in recent years has established this terrain as one of the most highly extended areas within the Basin and Range province of western North America, and mid-crustal crystalline rocks are exposed along a 200-km, northwest-trending zone through southeastern California and western Arizona in the Whipple-Buckskin-Rawhide detachment system. This zone of northeast-southwest-directed extension is situated along the northern edge of the Maria fold and thrust belt. The spatial relation of extension to areas which were previously thickened during Mesozoic to early Tertiary compression is well documented in the Basin and Range province; however, the cause of Tertiary extension is still a widely debated issue.

U-Pb ZIRCON GEOCHRONOLOGY

This paper presents results of U-Pb zircon analyses from four intrusive units within the Mesquite Mountain and Moon Mountains areas of the Colorado River Indian Reservation in west-central Arizona. Mesquite Mountain and the Moon Mountains are centrally located along the 250-km length of the Maria fold and thrust belt, and are positioned within the southern extent of the Whipple-Buckskin-Rawhide detachment terrain.

Two samples were collected from the Valenzuela thrust system in the southern Moon Mountains to better constrain the age of basement-involved deformation in the Maria fold and thrust belt. Megacrystic quartz syenite (sample MM87-16) is carried in the hanging wall of the Valenzuela thrust, and allows definition of a lower age limit for

movement on the Valenzuela thrust (Fig. 4.1). A series of garnet-bearing, granitic pegmatites (sample MM87-20) intrudes both the quartz syenite and surrounding crystalline rocks, and is interpreted to be syn- to late-kinematic with the youngest, north-directed phase of movement on the Valenzuela thrust (Fig. 4.1). These granitic dikes thus afford a means to directly date the age of most recent, thrust-related deformation in the Maria fold and thrust belt. Knapp (in prep.) gives a more thorough description of both the Valenzuela thrust system and of these intrusive rocks.

In the Mesquite Mountain area, outcrops consist primarily of a migmatitic gneiss complex which has experienced multiple phases of ductile deformation which post-date migmatization. A sample of a biotite granite sill (M87-15, Fig. 4.1) which is concordant with gneissic layering in the migmatitic gneiss was collected to assess the timing of injection associated with migmatization, and place a lower age constraint on the timing of ductile deformation at Mesquite Mountain. A more complete description of the Mesquite Gneiss and the fabrics and structures recorded at Mesquite Mountain is given in Knapp, in prep.

A sample of biotite granite (sample MM87-24) was collected from the Moon Mountains, in the footwall of the Copper Peak detachment fault. This small granite body intrudes a sequence of mylonitic metavolcanic rocks in the northern Moon Mountains, and is interpreted to be late- to post-kinematic with the development of mylonitic fabrics below the Copper Peak detachment fault. Dating of this unit was undertaken to establish an upper age limit for Tertiary ductile deformation in the footwall of the Copper Peak detachment.

ANALYTICAL TECHNIQUES

Bulk rock samples were crushed and hydraulically separated with facilities at Stanford University. Zircon and potassium feldspar separates were concentrated with standard heavy liquid and magnetic susceptibility techniques, and analyzed at the Isotope Geochemistry Laboratory at the University of Kansas. Dissolution of zircon fractions followed the methods of Krogh (1973) and Parrish (1987), and for potassium feldspar followed the methods of Coleman et al. (in press). Elemental separation was carried out with a modified HBr anion column chemistry for lead, and HCl (zircon) and HNO_3 (feldspar) column chemistries for uranium. Where appropriate, air abrasion was used following the methods of Krogh (1982). All samples were spiked with a mixed $^{205}Pb/^{235}U$ isotopic tracer. Mass fractionation corrections of 0.10%, as determined by

standard runs of NBS 981 (Common Lead) and NBS 982 (Equal Atom Lead), were applied to the Pb data. All analyses were carried out during 1988 when laboratory blank averaged 0.15 ng total lead and 0.02 ng uranium. Isotopic analyses were determined on a VG Sector multicollector thermal ionization mass spectrometer, and errors in $^{206}Pb/^{204}Pb$ were minimized by using a Daly multiplier. Decay constants used were $^{238}U=0.15513x10^{-9}$ yr^{-1} and $^{235}U=0.98485x10^{-9}$ yr^{-1} (Steiger and Jäger, 1977). Results for individual samples are plotted using regression models 1 and 2 of Ludwig (1983).

Common lead corrections were made using initial lead compositions determined from feldspar separates for each sample (Table 2). These compositions were used even though the zircon fractions show clear evidence for an inherited component. Although the actual common lead must be a mixture of lead incorporated from both magmatic and inherited zircon components, insignificant error is introduced by using the feldspar lead composition because of the relatively small amount of inheritance in these samples. Propagation of different initial lead compositions in reduction of lead data did not significantly change apparent ages of any of the fractions.

RESULTS

A summary of analytical data for the four igneous rock samples is given in Tables 1 and 2 for zircon and feldspar data, respectively. The U-Pb systematics are discussed below for each sample, and the interpretation of intercept ages is addressed, beginning with the Mesquite Mountain sample (M87-15) and proceeding with the Moon Mountains samples.

A total of four fractions were analyzed from sample M87-15 (Table 1, Fig. 4.2). Initial analysis of three bulk fractions gave a lower-intercept age of about 67 Ma, assuming a discordia between late Cretaceous magmatic zircon growth and Precambrian inheritance. Because of the relatively high uranium concentrations of these zircons (1,200-1,600 ppm), an additional fraction of the least discordant fraction was hand picked and air abraded to assess the possible role of lead loss. This abraded fraction was found to move along the regression line toward a more discordant composition, suggesting that lead loss is an unlikely explanation for the distribution of these data. The lower intercept age of 67.2 ± 1.4 Ma is thus interpreted as the crystallization age for this sample. The upper intercept age of 1490 ± 110 Ma is consistent with known ages of

Precambrian crystalline rocks in the Mojave-Sonora area (Silver, 1968; Wooden et al., 1988; Anderson, 1983), which are the most likely source of contaminant zircon.

Results for MM87-16, from the Moon Mountains (Fig. 4.1; Knapp, in prep.), are shown in Figure 4.3. Three bulk fractions were first analyzed and yielded very consistent ages, clustering between 160 and 164 Ma, despite the degree of deformation exhibited by the rock. To better constrain the potential effects of lead loss and inheritance in this sample, a second split of one of the initial fractions was air abraded. This sample moved away from the three bulk fractions toward a composition exhibiting more inheritance, but apparently no lead loss. A lower intercept age of 160 ± 15 Ma for regression of the four fractions together is interpreted as the crystallization age of this rock. The upper intercept age is unconstrained due to the clustering of points near the lower intercept. Mesozoic megacrystic granitic rocks of identical lithologic character to MM87-16 are documented in surrounding ranges (Dome Rock and Big Maria Mountains) with ages between 160 to 165 Ma (Tosdal, 1988; Silver, cited in Hamilton, 1982).

Sample MM87-20 had a very low zircon concentration, and a total of only 5 mg of zircon were recovered from about 120 kg of sample. Three populations of zircon grains were distinguished: clear, euhedral grains; yellow, euhedral to subhedral grains; and cloudy, stubby subhedral grains. A bulk sample of each of these fractions was analyzed, yielding a lower intercept age of 71.1 ± 6.7 Ma (with an essentially concordant fraction at the lower intercept) and a poorly-constrained, upper intercept age of 183 ± 52 Ma (Fig. 4.4). We interpret the lower intercept to be the crystallization age of the pegmatite. This conclusion must be qualified since the cloudy fraction, which is concordant within analytical error, has an extremely high uranium concentration. A correlation of lead loss with high uranium content in zircons has been observed and attributed to the effects of crystal lattice damage during radioactive decay. Significant lead loss is a possibility for this fraction, but is difficult to evaluate because both the inheritance and lead loss trends for these data are parallel to concordia. The cloudy fraction has a substantially different morphology and uranium and common lead concentration from the other two populations, possibly indicating a different time of crystallization. These features, combined with the concordant nature of the cloudy fraction, lead us to interpret the lower intercept as fairly representing the crystallization age. Significantly, the upper intercept age defined by the data seems to imply a Mesozoic rather than Precambrian inherited component (although inheritance of Mesozoic grains with minor Precambrian cores is likely).

Four size and magnetic fractions were analyzed from sample MM87-24 , and results are illustrated in Figure 4.5. Three bulk fractions yielded a lower intercept age of 22.5 ± 1 Ma (Model 1 of Ludwig, 1983). To better constrain the lower intercept, a fraction of the most concordant point was hand picked to be free of cores, leached in dilute HF acid, and analyzed. The resulting point plots closer to concordia but is still discordant, signifying that some inherited lead was retained. A lower intercept regressed through all four points yields a 20.8 ± 3.2 Ma age (Model 2 of Ludwig, 1983), which is interpreted to represent the crystallization age of the granite. The upper intercept age of 1480 ± 98 Ma is consistent with known ages of Precambrian basement rocks in west-central Arizona, and corresponds well with the results from sample M87-15.

DISCUSSION

The age of deformation within the Maria fold and thrust belt remains a critical unknown regarding the tectonic significance of this unique feature within the Cordillera of western North America. In addition, the nature and timing of magmatism with respect to deformation in this segment of the thrust belt will help to address the validity of various models which have been proposed to explain the region of basement-involvement in the thrusting of the southwestern United States. Finally, the spatial, temporal, and geometric relation of large-magnitude extension and associated magmatism in the Whipple-Buckskin-Rawhide detachment system with respect to the region of Mesozoic crustal thickening in the Maria fold and thrust belt affords insight into models concerning crustal extension in the southern Basin and Range province. The U-Pb ages obtained in this study place important timing constraints on deformation within the Maria fold and thrust belt and the relation of magmatism to deformation in the Whipple-Buckskin-Rawhide detachment system.

JURASSIC ARC MAGMATISM

The tectonic setting of Jurassic magmatism along the western edge of North America was related to development of a continental margin magmatic arc above a subducting oceanic plate in Mesozoic time (Burchfiel and Davis, 1975; Dickinson, 1981). Mid- to Late Jurassic intrusive rocks of the northern portion of the North American Cordillera are typically interpreted as products of arc magmatism above an east-dipping subduction zone (e.g., Dilles and Wright, 1988). In the Mojave-Sonora area of the southwestern Cordillera, Tosdal et al. (1988) point out that Jurassic rocks are the most

areally extensive Mesozoic rocks. This southern, northwest-trending segment of the magmatic arc was constructed along the truncated southwestern margin of the North American craton (Burchfiel and Davis, 1981). Middle and Late Jurassic plutonism in the Mojave Desert is broadly similar in chemistry and timing to that in the eastern Sierra Nevada to the north. (Stern et al., 1981).

The presence of Jurassic granitic rocks in the Moon Mountains marks the northeastern edge of the Jurassic magmatic arc at this latitude. Similar intrusive rocks of Jurassic age are known from the Big Maria (Hamilton, 1982), Dome Rock, and Trigo Mountains (Tosdal et al., 1988), and from southern Arizona (Tosdal et al., 1988), but are not present in areas to the east at the latitude of the Moon Mountains. These Jurassic intrusive rocks define a northwest-trending belt which continues both toward the north (southern Sierra Nevada) and the south (Sonoran batholith). In contrast, structures of the Maria fold and thrust belt trend roughly east-west, and show significant involvement of Jurassic intrusive rocks in southeastern California, but diverge from the main locus of Jurassic magmatism in the eastern end of the Maria fold and thrust belt. Thus, in a general sense, the locus of basement-involvement in the Maria fold and thrust belt trends obliquely across the Jurassic magmatic arc, and does not appear to be localized along the eastern edge of Jurassic arc magmatism.

AGE OF THRUSTING - MARIA FOLD AND THRUST BELT

The Valenzuela thrust system, exposed in the southern Moon Mountains, is a basement-involved structure of regional significance within the Maria fold and thrust belt (Knapp, in prep.). This thrust system carries crystalline gneisses and intrusive rocks (sample MM87-16) in the hanging wall above a sequence of deformed and metamorphosed lower Mesozoic supracrustal rocks. This structural juxtaposition is identical to that described for the Hercules thrust system in the Granite Wash and Little Harquahala Mountains (Reynolds et al., 1986). Deformation was apparently characterized by multiple periods of movement on the thrust system, with an earlier phase of south-directed folding and thrust emplacement followed by a north-vergent episode of movement. A well-defined metamorphic foliation and aligned mineral lineation, developed at amphibolite facies conditions, parallels the thrust surface and is interpreted to be syntectonic. The presence of sillimanite (after kyanite) in rocks of lower Mesozoic age in the footwall of the Valenzuela thrust, combined with the lack of evidence for amphibolite facies metamorphism of Tertiary age in western Arizona, demonstrates that this must be a Mesozoic metamorphic event.

A maximum age for development of the Valenzuela thrust system is provided by the late Middle Jurassic age on the megacrystic quartz syenite (sample MM87-16) which is carried in the hanging wall of the thrust. This age constraint is consistent with present interpretation of the pre-tectonic, upper McCoy Mountains Formation as early Late Cretaceous. The age of latest movement on the Valenzuela thrust system is constrained by syn- to late-kinematic, garnet-bearing, granitic dikes (sample MM87-20) which intrude the footwall gneisses of the Valenzuela thrust system. These granitic aplites and pegmatites cross cut the amphibolite facies metamorphic fabric within the crystalline rocks. In turn, the garnet-bearing granitic rocks contain this foliation, and show evidence of north-directed shear fabrics along shallowly north-dipping shear planes which appear synchronous with formation of the amphibolite facies foliation. Since no later fabrics or deformation are observed in association with the Valenzuela thrust, the north-directed period of thrusting is inferred to be the most recent movement on the thrust. Data presented in this study date the timing of this north-directed phase of thrusting as latest Late Cretaceous (71.1 ± 6.7 Ma), and represent the first direct dating of thrust events in the Maria fold and thrust belt.

It should be emphasized that north-directed movement on the Valenzuela thrust system, and in the Maria fold and thrust belt in general, represents the latest and perhaps only a minor phase of tectonic activity associated with thrusting in the region. In the Granite Wash, Harquahala, and Harcuvar Mountains in the eastern end of the Maria fold and thrust belt, thrust faults and thrust-related fabrics are discordantly cut by undeformed granitic plutons (Granite Wash Granodiorite and Tank Pass Granite) which yield Late Cretaceous and early Tertiary K-Ar and Ar-Ar ages, and have been interpreted as 80-70 Ma intrusions (Rehrig and Reynolds, 1980; and S. Richard, 1988, pers. comm.). The thrusts which are intruded by these granites are large, south-vergent structures (Reynolds et al., 1986), and probably represent the major phase of deformation in the Maria fold and thrust belt (S. Reynolds, pers. comm.). These timing relations imply that the major south-directed thrusting event in the Maria fold and thrust belt was early Late Cretaceous in age, and significantly earlier than the north-directed thrusting documented in the Moon Mountains.

Thrust-related deformation in the Maria fold and thrust belt was broadly coeval with deformation in the continuation of the Sevier belt through the Old Woman-Piute Mountains. Constraints on thrust deformation in the Old Woman Mountains come from late to post-tectonic granitic plutons which yield ages of 70-80 Ma (Miller et al., 1982).

Reconciliation of synchronous east-vergent thrusting in the thrust belt of southern Nevada and southeastern California with south-vergent thrusting in the Maria fold and thrust belt presents a problem of geometric and dynamic complexity which remains unresolved.

ANATECTIC RESPONSE TO CRUSTAL THICKENING

The Mesquite Gneiss migmatite complex from Mesquite Mountain was developed at amphibolite facies metamorphic conditions. Data from this study indicate that the age of migmatization and injection of the Mesquite Gneiss was latest Late Cretaceous. We interpret the cause of the partial melting and granitic injection to be crustal thickening associated with thrusting in the Maria fold and thrust belt. The age range of thrusting (90? to 70 Ma) is consistent with subsequent partial melting at deep crustal levels such as are exposed in the Mesquite Mountain area. In contrast, Proterozoic basement rocks from the Whipple Mountains, to the north, preserve intact Precambrian metamorphic assemblages and fabrics, suggesting that the northern limit of the effects of basement thrusting and partial melting lies between the Mesquite Mountain area and the Whipple Mountains.

The evolution of the crust in southern California and western Arizona has involved successive periods of magmatism and tectonism since Precambrian time. The signature of older crustal components in sequentially younger rocks is evident from various isotopic systems (see DePaolo and Wasserburg, 1979 or Farmer and DePaolo, 1983, Nd; Wooden et al., 1988; Pb), and typically involves a Precambrian isotopic inheritance in younger Phanerozoic magmatic rocks. In the samples for this study, evidence for this Precambrian inheritance is exhibited both in the presence of an inherited zircon component within the zircon population (present primarily as relict cores to zircon grains) and in common Pb data, reflecting contribution from a Precambrian crustal source.

In contrast, sample MM87-20, consisting of garnet-bearing, two-mica granite in pegmatite and aplite dikes, presents an apparently different inheritance signature. The highly evolved composition of these peraluminous granitic rocks in the Moon Mountains is similar to plutons of Late Cretaceous age which define a linear, discontinuous belt the length of the North American Cordillera (Miller and Bradfish, 1980). The origin of these granitic rocks has been interpreted as crustal anatexis in response to thrust-related thickening. A similar origin is inferred for the Moon Mountain dikes, and the Jurassic upper intercept age (183 ± 52 Ma) is suggestive that they were derived from a crustal

source area which contained a significant component of Mesozoic rock. The lower intercept age of 71.1 ± 6.7 Ma is interpreted as a crystallization age for these magmatic rocks, while the upper intercept age of 183 ± 52 Ma is suggestive of either (1) a crustal source area predominated by Mesozoic-age rocks, or (2) profound Pb loss experienced by the sample subsequent to crystallization. We prefer the former interpretation, based on consistency with regional relations, and speculate that the peraluminous granitic rocks resulted from dehydration and partial melting of a source area dominated by Jurassic rocks.

RELATION OF MAGMATISM TO DEFORMATION

The timing and spatial relationships between deformation, metamorphism, and magmatism within the Mesozoic thrust belt of the western North American Cordillera provide important insights into crustal processes in orogenic belts. Burchfiel and Davis (1975) proposed a model for Mesozoic deformation in the western North American Cordillera whereby intracratonal westward underthrusting along the western edge of North America resulted in large part from heating and softening of the crust through extensive arc magmatism. Consequently, they suggest that deformation was localized at the ductility transition from the relatively hot arc terrain in the west to the comparatively cool cratonal crust in the east. In contrast, other workers (Miller et al., 1982; Hoisch et al., 1988) have argued that deformation and accompanying metamorphism in the thrust belt largely preceded magmatic activity at mid- to upper-crustal levels. Hoisch (1985) concluded that synkinematic metamorphism in the Big Maria Mountains of southeastern California resulted from circulation of large volumes of hot fluids rather than conductive cooling from plutonism. Similarly, in the Old Woman Mountains, post-kinematic granitic plutons derived from crustal anatexis were emplaced after the thermal peak of metamorphism.

Recent studies in western Arizona (e.g. Reynolds et al., 1986) indicate that deformation and metamorphism in the basement-involved terrain of the Maria fold and thrust belt typically pre-dated intrusion of large volumes of granitic magma. A series of K-Ar radiometric age determinations for undeformed granitic rocks in the eastern end of the Maria fold and thrust belt yield Late Cretaceous to early Tertiary ages. The Tank Pass granite, from the Granite Wash and western Harcuvar Mountains, has yielded four K-Ar ages ranging from 44.1 to 55.0 Ma (Shafiqullah et al., 1980) while the Granite Wash granodiorite, which the Tank Pass granite intrudes, has yielded ages of 70.8 (Eberly and Stanley, 1978) and 66.5 ± 3.6 Ma (Shafiqullah et al., 1980). These ages have been

interpreted as minimum ages for the crystallization of these rocks, reflecting cooling of these intrusive bodies and their wall rocks following a regional metamorphic and intrusive event in Late Cretaceous time. These data and interpretations are consistent with the regional thermal history as deduced through Ar-Ar thermochronology (Knapp and Heizler, 1988 and in prep.), and clearly indicate a major, post-tectonic phase of granitic magmatism in Late Cretaceous time.

A similar history is documented for ranges in the eastern Mojave Desert of southeastern California. In the Old Woman Mountains, Miller et al. (1982) document intrusion of large volumes of granitic and granodioritic plutons which post-date thrusting and syntectonic metamorphism. Although locally deformed, these intrusive bodies consistently truncate thrust structures and are generally unaffected by deformation and metamorphism. Ages for these granitic rocks range between roughly 70-80 Ma, and place an upper limit on the time of thrusting in the Old Woman Mountains. In the Big Maria Mountains, directly adjacent to the Moon Mountains across the Colorado River, Late Cretaceous deformation and syntectonic metamorphism was largely amagmatic. Hamilton (1982) described garnetiferous pegmatites which he interpreted to be synkinematic with compressional deformation in the Big Maria Mountains, and Hoisch (1985) and Hoisch et al. (1988) documented amphibolite facies metamorphism of Late Cretaceous age in the Big Maria Mountains, which they attributed to circulation of enormous volumes (in excess of 16:1 water:rock ratios) of metamorphic fluids through the crust.

In contrast, John (1988) describes an extensive suite of deformed, Late Cretaceous granitic rocks in the Chemehuevi Mountains of southeastern California. This suite of metaluminous to peraluminous granitoids exhibits a well-developed, normal compositional zonation, ranging from early hornblende- and sphene-bearing, metaluminous members to muscovite-bearing, locally garnetiferous granite and granodiorite. John and Mukasa (1988) cite a Late Cretaceous age range for this plutonic suite based on U-Pb zircon geochronology. Discordant fractions define a chord with a lower intercept of ~90 Ma for the earliest phases, while these workers infer a Late Cretaceous age for the younger members. Upper intercept ages for all discordia yield Proterozoic ages, suggesting an inherited zircon population and crustal component for these rocks.

Based on fabric development within the Chemehuevi Mountains plutonic suite, John (1986, 1988) argues that mylonitization was synchronous with intrusion.

Developed in early phases of the complex are thick (>1.5 km), laterally continuous mylonitic zones, which are interpreted to have developed while the intrusives were still plastic. Younger portions of the suite are undeformed, and thereby bracket the timing of shear zone deformation in the Chemehuevi Mountains as Late Cretaceous. Northeast-directed shear is interpreted for a large, subhorizontal shear zone in the complex, and sinistral shear is indicated for a zone of steeply-dipping mylonites, continuous for about 12 km along strike. These mylonitic fabrics are interpreted as part of a regionally significant tectonic zone within the lower Colorado River region (John, 1988). John and Mukasa (1988) infer from these relations that the Chemehuevi Mountains plutonic complex records passage of the Late Cretaceous North American Cordillera fold and thrust belt into the active magmatic arc along the cratonal margin.

Both in the Mesquite Mountain area and in the Whipple Mountains to the north, extensive injection of granitic material occurred in Late Cretaceous time; however, Mesozoic structures have not been identified in these areas. At Mesquite Mountain, the intrusion of biotite granite, comprising up to 30-40 volume percent of the Mesquite Gneiss migmatite, is interpreted as the result of partial melting due to crustal thickening in the late Cretaceous. Significantly, no thrust structures are recognized in this area, despite evidence that temperatures were very high, in excess of 500°C in Late Cretaceous time. In the Whipple Mountains, Wright et al. (1986, 1987) document extensive intrusion of Late Cretaceous granites, yet no thrust-related structures have been identified, and crystalline rocks retain Proterozoic metamorphic assemblages and fabrics (Thomas et al., 1988; Davis et al., 1980; Podruski, 1979). Both of these areas are situated along the northern edge of the Maria fold and thrust belt, implying that Late Cretaceous, south-vergent thrusting actually occurred south of and further toward the edge of the craton from the locus of Late Cretaceous magmatism.

Coney and Reynolds (1977) provided an analysis of late Mesozoic to early Cenozoic magmatism in the southwestern United States, and on the basis of the age and distribution of these rocks, argued that the locus of arc magmatism swept first eastward then back westward across the continental margin in response to first shallowing and then steepening of the subducted oceanic slab. The general timing of the eastward passage of the arc through the area of western Arizona was between ~100 and 70 Ma, and generally contemporaneous with the age of basement involved thrusting in the Maria fold and thrust belt. The return passage of arc magmatism through western Arizona was very rapid, but

occurred roughly between 30 to 20 Ma, and was contemporaneous with the earliest manifestations of crustal extension in the region.

These examples serve to illustrate important features about the development of the Mesozoic deformational belt in the southwestern Cordillera of North America. Thrust deformation in the Maria fold and thrust belt was generally synchronous with arc magmatism in this segment of the thrust belt; however, arc magmatism appears to have outlasted thrusting, and the locus of thrusting does not appear to have been controlled locally by the influence of magmatism. Much of the magmatic activity in the Maria fold and thrust belt may have been the result of crustal thickening and partial melting of the lower crust in the production of granitic plutons.

IMPLICATIONS OF TERTIARY MAGMATISM

The Tertiary history of western Arizona is summarized by Spencer and Reynolds (in press), and was characterized by tectonic quiescence in early Tertiary time followed by renewed magmatism and crustal extension in mid-Tertiary time.

Early Tertiary time was a period of general tectonic and magmatic quiescence in west-central Arizona (Coney and Reynolds, 1977). A variety of features indicate that the area now occupied by the southern Basin and Range of western Arizona was a geomorphologic highland following thrusting and crustal thickening during Late Cretaceous time. While early Tertiary sedimentary deposits, with north- and east-directed paleocurrent indicators, are well documented from the adjacent Colorado Plateau (Young and McKee, 1978), strata of this age are unknown from west-central Arizona. The results of $^{40}Ar/^{39}Ar$ data indicate that rocks from the crystalline thrust nappes of the Maria fold and thrust belt experienced a period of slow cooling during early Tertiary time (Knapp and Heizler, in prep.). From these data we infer that denudation of the crustal welt produced by Late Cretaceous thrusting was dominated by erosion.

Constraints on the timing of deformation in the Whipple-Buckskin-Rawhide detachment system indicate that extension was largely of Miocene age in the lower Colorado River region. Age constraints for the timing of this deformation come largely from the Whipple Mountains of southeastern California and the adjacent Buckskin Mountains in western Arizona. The age of mylonitization in the lower plate gneisses of the Whipple detachment fault was determined on the basis of syn-kinematic tonalite dikes to be 26 ± 5 Ma (Wright et al., 1986; Davis, in press). In contrast, large tilts in the

hanging wall of the detachment on basalts dated at 18-19 Ma suggest that detachment faulting either outlasted or post-dated mylonitization of the footwall (Davis et al., 1980). Flat-lying basalt flows dated at 15-16 Ma provide an upper age limit for extension in this area.

A more complex timing of detachment faulting is documented for the Buckskin Mountains. Volcanic rocks near the base of tilted Tertiary strata in the hanging wall of the Buckskin detachment fault yield K-Ar ages on biotite of 21.8 Ma (Spencer and Reynolds, in press) in the Buckskin Mountains, and 23.0 Ma in the Artillery Mountains (Otton and Miller, cited in Spencer and Reynolds, in press). These ages suggest that tilting and basin formation in the detachment system began by earliest Miocene time. In the western-most Buckskin Mountains, the presence of flat-lying, 14-16 Ma-old basalts indicates detachment faulting had ceased in this area by this time. Basalts of this same age are steeply tilted in the Bill Williams Mountains to the north, suggesting that cessation of displacement on the detachment was a function of position along the fault.

Mid-Tertiary granitic magmatism in the Moon Mountains area appears to have been a mid- to upper-crustal phenomenon. While no quantitative geobarometric data for these rocks are currently available, Ar-Ar minimum apparent ages for potassium feldspar of 22.5-28 Ma indicate that the terrain in the lower plate of the Whipple-Buckskin-Rawhide detachment system in this area had been brought relatively near to the surface, such that even potassium feldspar had cooled through closure to Ar by the time of intrusion of this stock. Given the composition of this biotite granite (sample MM87-24) and the clear evidence for an inherited crustal component, it seems likely that lower structural levels remained at higher temperatures and were probably the locus of more extensive magmatism during the Tertiary event.

Mid-Tertiary magmatism is known also from the Whipple Mountains of southeastern California. Within the lower plate crystalline assemblage of the Whipple detachment terrain, a series of sheet-like biotite tonalite bodies yield a U-Pb zircon age of 26 ± 5 Ma (Wright et al, 1986). Based on field relations, these dikes are interpreted to be syn-kinematic with the age of major mylonitization in the lower plate of the Whipple detachment. Discordant fractions of this sample indicate an inherited zircon component which appears to be a mixture of 1.7 and 1.4 Ga zircons. In contrast to Late Cretaceous magmatism in the Whipple Mountains, where intrusive rocks exhibit relatively distinct, heterogeneous zircon sources, Tertiary magmatism appears to reflect homogenization of the source area for crustal contamination. A major body of post-kinematic,

clinopyroxene-biotite-hornblende diorite from the northwestern part of the Whipple Mountains yields a concordant U-Pb zircon age of 19 ± 2 Ma (Wright et al., 1986), similar in age to sample MM87-24 from the Moon Mountains area.

CRUSTAL Pb PROVINCES

Common Pb data for the Mesquite Mountain and Moon Mountains samples, determined from potassium feldspar separates, are summarized in Table 2. The Mojave-Sonora area has been identified as a region of distinctive common Pb signature (Wooden et al., 1986a, 1988). Mesozoic intrusive rocks from this area show an unusually wide range of initial $^{206}Pb/^{204}Pb$ values, implying significant variation in U/Pb ratios, and differentiation of U/Pb reservoirs sometime relatively late in the Proterozoic in the source area for these rocks. Such a wide and continuous variation of $^{206}Pb/^{204}Pb$ values is thought to be indicative of reworking of Precambrian continental crust (Doe and Zartman, 1979). In addition, these rocks define a linear trend on a plot of $^{207}Pb/^{204}Pb$ versus $^{206}Pb/^{204}Pb$ with a slope corresponding to an age of about 1.6 b.y. $^{208}Pb/^{204}Pb$ ratios for the Mesozoic intrusive rocks are relatively constant over the range of $^{206}Pb/^{204}Pb$ values at 39.2 ± 0.2. These isotopic signatures cover a variety of compositional types, and taken together indicate a source region which is very heterogeneous in both bulk composition and Pb isotopic composition, but with an average age of ~1.6 b.y.

Wooden et al. (1988) speculate that the area of western Arizona is the site of a crustal lead province boundary, separating a region of relatively higher $^{207}Pb/^{204}Pb$ initial ratios (with respect to initial $^{206}Pb/^{204}Pb$) in the Mojave Desert from a region with lower initial $^{207}Pb/^{204}Pb$ identified in southern Arizona. The exact location of this boundary is unclear due to the incompleteness of the data set, but is thought to trend north-south through western Arizona. Common Pb data from the Mesquite Mountain and Moon Mountains samples plot along the linear array in $^{207}Pb/^{204}Pb$ versus $^{206}Pb/^{204}Pb$ defined by pre-existing data from the eastern Mojave Desert, implying that the boundary between these provinces lies to the east of the Mesquite Mountain and Moon Mountains areas.

TECTONIC SYNTHESIS

Basement-involved thrusting and crustal thickening in the Maria fold and thrust belt was broadly coeval with arc magmatism associated with subduction of the Farallon Plate in Late Cretaceous time. Thrusting may have been active as early as 80-90 Ma (Reynolds et al., 1986), as evidenced by post-tectonic granitic plutons which intrude

thrust faults in the eastern segment of the Maria fold and thrust belt. Arc magmatism made an eastern sweep through the southwestern Cordillera of North America during Cretaceous time, and was probably at the longitude of present-day western Arizona during the Late Cretaceous (Coney and Reynolds, 1977). On a local scale, thrusting does not appear to have been controlled by thermal anomalies due to arc magmatism. Much of the magmatic activity in the Maria fold and thrust belt appears to be syn- to post-kinematic, and may represent a response to crustal thickening. Late Cretaceous migmatization of the Mesquite Gneiss at Mesquite Mountain suggests that injection and in situ partial melting occurred at deep crustal levels subsequent to much of the deformation in the Maria fold and thrust belt.

Additional evidence for the Late Cretaceous thermal event is preserved in the $^{40}Ar/^{39}Ar$ systematics for crystalline rocks of this terrain. Resetting of hornblende (T_c~500°C) occurred in several ranges in Late Cretaceous time (Knapp and Heizler, 1988, in prep.; Richard, 1988; Hoisch et al., 1988). Elevation of the crustal geotherm in western Arizona was probably related to both crustal thickening (e.g., Molnar et al., 1983) and passage of the migrating magmatic arc beneath the area of western Arizona during Late Cretaceous time (Coney and Reynolds, 1977).

The termination of deformation in the Maria fold and thrust belt, with an as yet poorly understood, north-directed phase of thrusting, occurred in latest Cretaceous time. Magmatism appears to have outlasted much of the deformation, but had ceased by early Tertiary time in western Arizona. Arc magmatism was still active in areas to the east (Coney and Reynolds, 1977; Reynolds et al., 1986), while the area of thickened crust in the Maria fold and thrust belt underwent erosional unroofing. Unlike examples from other compressional orogens (e.g., the Himalayas, Burchfiel et al., 1988) where crustal extension was synchronous and co-axial with compression, extensional features of Late Cretaceous and early Tertiary age are conspicuously absent in western Arizona. Instead, the region appears to have experienced relatively slow denudation, based on $^{40}Ar/^{39}Ar$ data which document slow cooling (5-10°C/m.y.) throughout early Tertiary time.

Several models have been proposed to explain the origin of Tertiary extension in the Basin and Range province of western North America. Atwater (1970) first proposed that extension was related to development of a transform plate boundary along the edge of the North American plate following subduction of the Farallon plate. Other workers have attributed extension in the Cordillera of the western United States to asthenospheric upwelling through a slab window resulting from subduction of the Pacific-Farallon

spreading ridge (Dickinson and Snyder, 1979: Dickinson, 1981). Sonder et al. (1987) appealed to gravitational collapse of weakened lithosphere that had been previously thickened during Mesozoic compressional tectonics, and related the temporal variation of extension directly to the temperature at the base of the crust at the end of crustal thickening.

A clear definition of the role that these various factors played in the evolution of the Basin and Range in general, and in the region of western Arizona in particular, remains unresolved. The results of this study imply that the crust of western Arizona was at elevated temperatures during the Late Cretaceous, through a combination of arc magmatism and thrust-burial of radioactive, upper-crustal rocks, yet did not experience syn-compressional extension as predicted by the model of Sonder et al. (1987). In contrast, the initiation of extension in early Miocene time appears to have been coincident with a renewed phase of arc magmatism in western Arizona during the westward retreat of the arc with foundering of the Farallon plate beneath North America (Coney and Reynolds, 1977; Dickinson, 1981). A renewed thermal event, distinct from that associated with the Late Cretaceous, is evidenced both by the inception of magmatism in western Arizona in the late Oligocene, and a cryptic signature of partially reset potassium feldspar ages in areas where Tertiary magmatism was not prevalent (see Knapp and Heizler, in prep.). In addition, the discordance of east-northeast/west-southwest extension with the southeast-, south-, and north- directed structures of the Maria fold and thrust belt suggest that extension occurred under a different regional stress. The discordance between Mesozoic shortening and Cenozoic extension directions in the region may have been strongly influenced by plate reorganization which occurred synchronously with the onset of extension at this latitude (Stock and Molnar, in press).

CONCLUSIONS

The results of this study place important new age constraints on the tectonic development of the Maria fold and thrust belt and on the relative timing of Tertiary extension and magmatism in the Whipple-Buckskin-Rawhide detachment terrain. Megacrystic quartz syenite from the southern Moon Mountains yields a late Middle Jurassic age of 160±15 Ma, and defines the northeastern limit of Jurassic plutonism at this latitude. Involvement of these rocks in the Valenzuela thrust fault of the Maria fold and thrust belt demonstrates a post-Middle Jurassic age for deformation, consistent with existing age constraints from the McCoy Mountains Formation.

Intrusion of garnet-bearing, granitic pegmatite dikes in the Moon Mountains was syn- to late-kinematic with the youngest, north-directed phase of movement on the Valenzuela thrust. These dikes yield a lower intercept age (3 fractions) of 71.1 ± 6.7 Ma, and constitute the first direct dating of thrusting in the Maria fold and thrust belt. Both the peraluminous composition and Jurassic (183±52 Ma) upper intercept age suggest these pegmatites were generated from partial melting of a Mesozoic crustal source area. At Mesquite Mountain, a lower intercept age (4 fractions) of 67.2±1.4 Ma from a concordant, biotite-granite sill in the Mesquite Gneiss migmatite complex records the time of injection associated with migmatization. We interpret injection and *in situ* partial melting of the Mesquite Gneiss as a deep-seated response to Late Cretaceous crustal thickening in the Maria fold and thrust belt. An upper intercept age of 1490±110 Ma for these data is consistent with known ages of Precambrian crystalline rocks from western Arizona. A latest Cretaceous age for migmatization of the Mesquite Gneiss demonstrates that subsequent development of mylonitic fabrics occurred during Tertiary time, and was related to crustal extension in the Whipple-Buckskin-Rawhide terrain.

Late- to post-kinematic biotite granite from the northeastern Moon Mountains yields an age of 20.8 ± 3.2 Ma, placing an upper age limit on ductile deformation in the footwall of the Copper Peak detachment fault, which is the southern exposed limit of the Whipple-Buckskin-Rawhide detachment terrain. Early Miocene granitic magmatism, with an inherited crustal component, indicates that heat was introduced to mid- and upper-crustal levels during the early stages of extension, and may have been causally related to extensional processes.

ACKNOWLEDGEMENTS

Appreciation is extended to the Tribal Council and Chuck Lamb of the Colorado River Indian Tribes for permission to collect geochronology samples on the Reservation. JHK would like to thank Elizabeth Miller and Jim Wright of Stanford University for use of rock crushing and Wilfly table facilities. Jim Wright and other members of the Stanford geology department provided valuable and timely advice on sample preparation. Assistance by Scott Ritterbush with sample collection and crushing of hundreds of kilograms of rock is gratefully acknowledged. This research was supported in part by the Student Research Fund at M.I.T. and B.C. Burchfiel's Schlumberger Chair in Geology at M.I.T.

REFERENCES

Anderson, J.L., 1983, Proterozoic anorogenic granite plutonism of North America, *in* Medaris, L.G., Jr., Byers, C.W., Mickelson, D.M., and Shanks, W.C., eds., Proterozoic Geology: Selected Papers From An International Proterozoic Symposium: Geol. Soc. Amer. Mem. 161, p. 133-154.

Armstrong, R.L., and Suppe, J., 1973, Potassium-Argon geochronometry of Mesozoic igneous rocks in Nevada, Utah, and southern California: Geological Society of America Bulletin, v. 84, p. 1375-1392.

Bishop, C.C., 1963, Geologic Map of California - Needles 2° Sheet, 1:250,000: Calif. Div. Mines Geol.

Burchfiel, B.C., and Davis, G.A., 1972, Structural framework and evolution of the southern part of the Cordilleran orogen, western United States: Amer. Jour. Sci., v. 272, p. 97-118.

Burchfiel, B.C., and Davis, G.A., 1975, Nature and controls of Cordilleran orogenesis, western United States: Extensions of an earlier synthesis: Amer. Jour. Sci., v. 275-A, p. 363-396.

Burchfiel, B.C., Hodges, K.V., Royden, L.H., Chen, Z., Deng, C., Liu, Y., 1988, Extension parallel to and contemporaneous with compression in the high Himalaya, southern Tibet [abs.]: Geol. Soc. Amer. Abstr. Progs., v. 20, no. 7, p. A321.

Carr, W.J., and Dickey, D.D., 1980, Geologic map of the Vidal, California, and Parker SW, California-Arizona, quadrangles: U.S. Geol. Survey Misc. Invest. Map, I-1125, 1:24,000.

Coleman, D.S., Walker, J.D., and Bickford, M.E., in press, Geochemical and tectonic significance of Mio-Pliocene volcanic rocks from the northwestern Panamint Mountains: Geol. Soc. Amer. Mem.

Coney, P.J., and Reynolds, S.J., 1977, Cordilleran Benioff zones: Nature, v. 270, p. 403-406.

Davis, G.A., and Lister, G.S., 1988, Detachment faulting in continental extension; Perspectives from the Southwestern U.S. Cordillera : Geol. Soc. Am. Special Paper 218, p. 133-159.

Davis, G.A., Anderson, J.L., Frost, E.G., and Shackelford, T.J., 1980, Mylonitization and detachment faulting in the Whipple-Buckskin-Rawhide Mountains terrane, southeastern California and western Arizona, *in* Crittenden, M.D., Jr., Coney, P.J., and Davis, G.H., eds., Cordilleran Metamorphic Core Complexes: Geol. Soc. Am. Mem. 153, p. 79-129.

Davis, G.A., in press, Rapid upward transport of mid-crustal mylonitic gneisses in the footwall of a Miocene detachment fault, Whipple Mountains, California.

Davis, G.H., 1980, Structural characteristics of metamorphic core complexes, southern Arizona, *in* Crittenden, M.D., Jr., Coney, P.J., and Davis, G.H., eds., Cordilleran Metamorphic Core Complexes: Geol. Soc. Am. Mem. 153, p. 35-77.

Depaolo, D.J., and Wasserburg, G.J., 1976, Nd isotopic variations and petrogenetic models: Geophys. Res. Letters, v. 3, p. 249-252.

Depaolo, D.J., and Wasserburg, G.J., 1979, Petrogenetic mixing models and Nd-Sr isotopic patterns: Geochim. Cosmochim. Acta, v. 43, p. 615-627.

Dickinson, W.R., 1981, Plate tectonic evolution of the southern Cordillera, in, Dickinson, W.R., and Payne, W.D., eds., Relations of Tectonics to Ore Deposits in the Southern Cordillera: Ariz. Geol. Soc. Digest, v. 14, p. 113-135.

Dilles, J.H., and Wright, J.E., 1988, The chronology of early Mesozoic arc magmatism in the Yerrington district of western Nevada and its regional implications: Geol. Soc. Amer. Bull., v. 100, p.644-652.

Doe, B.R., and Zartman, R.E., 1979, Plumbotectonics - I. The Phanerozoic, *in* Barnes, H., ed., Geochemistry of Hydrothermal Ore Deposits, 2nd ed.: New York, Wiley-Interscience, p. 22-70.

Eberly, L.D., and Stanley, T.B., Jr., 1978, Cenozoic stratigraphy and geologic history of southwestern Arizona: Geol. Soc. Amer. Bull., v. 89, p. 921-940.

Farmer, G.L., and DePaolo, D.J., 1983, Origin of Mesozoic and Tertiary granite in the western United States and implications for pre-Mesozoic crustal structure: 1. Nd and Sr isotopic studies in the geocline of the northern Great Basin: Journal of Geophysical Research, v. 88, p. 3379-3401.

Farmer, G.L., and DePaolo, D.J., 1984, Origin of Mesozoic and Tertiary granite in the western United States and implications for pre-Mesozoic crustal structure: 2. Nd and Sr isotopic studies of unmineralized and Cu- and Mo-mineralized granite in the Precambrian craton: Journal of Geophysical Research, v. 89, p. 10,141-10,160.

Hamilton, W., 1982, Structural evolution of the Big Maria Mountains, northeastern Riverside County, southeastern California, *in* Frost, E.G., and Martin, D.L., eds., Mesozoic-Cenozoic Tectonic Evolution of the Colorado River Region, California, Arizona, and Nevada: San Diego, California, Cordilleran Publishers, p. 1-27.

Hamilton, W., 1987, Mesozoic geology and tectonics of the Big Maria Mountains region, southeastern California, *in* Dickinson, W.R., and Klute, M.A., eds., Mesozoic Rocks of Southern Arizona and Adjacent Areas: Arizona Geological Society Digest, v. 18, p. 33-47.

Hamilton, W., 1987, Crustal extension in the Basin and Range Province, southwestern United States, *in* Coward, M.P., Dewey, J.F. and Hancock, P.L., Continental Extensional Tectonics: Geological Society of London Special Publication 28, p. 155-176.

Haxel, G.B., and Tosdal, R.M., 1986, Significance of the Orocopia Schist and Chocolate Mountains thrust in the late Mesozoic tectonic evolution of the southeastern California-southwestern Arizona region: Extended abstract, *in* Beatty,

B., and Wilkinson, P.A.K., eds., Frontiers In Geology and Ore Deposits of Arizona and the Southwest: Arizona Geological Society Digest, v. 16, p. 52-61.

Hopson, C.A., Mattinson, J.M., and Pessagno, E.A., Jr., 1981, Coast range ophiolite, western California, *in* Ernst, W.G., ed., The Geotectonic Development of California (Rubey Volume I): Englewood Cliffs, New Jersey, Prentice-Hall, p. 418-510.

Howard, K.A., and John, B.E., 1987, Crustal extension along a rooted system of imbricate low-angle faults: Colorado River extensional corridor, California and Arizona, *in* Coward, M.P., Dewey, J.F., and Hancock, P.L., eds., Continental Extensional Tectonics: Geological Society of London Special Publication 28, p. 299-311.

John, B.E., 1980, Reconnaissance study of Mesozoic plutonic rocks in the Mojave Desert region [abs.], *in* Howard, K.A., Carr, M.D., and Miller, D.M., Tectonic Framework of the Mojave and Sonoran Deserts, California and Arziona: U.S. Geol. Survey Open-File Report 81-503, p. 48-50.

John, B.E., 1982, Geologic framework of the Chemehuevi Mountains, southeastern California, *in* Frost, E.G., and Martin, D.L., eds., Mesozoic-Cenozoic Tectonic Evolution of the Colorado River Region, California, Arizona, and Nevada: San Diego, California, Cordilleran Publishers, p. 317-325.

John, B.E., 1986, Structural and intrusive history of the Chemehuevi Mountains area, southeastern California and western Arizona : Ph.D. dissertation, Santa Barbara, Univ. of California, 295 p.

John, B.E., 1987, Geometry and evolution of a mid-crustal extensional fault system, Chemehuevi Mountains, southeastern California, *in* Coward, M.P., Dewey, J.F., and Hancock, P.L., Continental Extensional Tectonics: Geological Society of London Special Publication 28, p. ?.

John, B.E., 1988, Structural reconstruction and zonation of a tilted mid-crustal magma chamber: The felsic Chemehuevi Mountains plutonic suite: Geology, v. 16, p. 613-617.

John, B.E., and Mukasa, S.B., 1988, Structural and geochronologic (U-Pb) evidence for the nature of Cretaceous plutonism and mylonitization in the Chemeheuvi Mountains core complex, southeastern California [abs.]: Geol. Soc. Amer. Abstr. Progs., v. 20, no. 7, p. A271-A272.

Knapp, J.H., and Heizler, M.T., 1988a, $^{40}Ar/^{39}Ar$ geochronology of crystalline thrust nappes of the Late Cretaceous Maria fold and thrust belt, west-central Arizona [abs.]: Geol. Soc. Amer. Abs. Progs., v. 20, no. 3, p. 173.

Knapp, J.H., and Heizler, M.T., 1988b, Tertiary thermal history of west-central Arizona: Implications for mechanisms of crustal extension [abs.]: Geol. Soc. Amer. Abs. Progs., v. 20, no. 7, p. A16-A17.

Knapp, J.H., and Heizler, M.T., in prep., Thermal history of crystalline thrust nappes of the Maria fold and thrust belt, west-central Arizona:

Knapp, J.H., in prep., Mid-Tertiary detachment tectonics at Mesquite Mountain, west-central Arizona:

Knapp, J.H., in prep., Mesozoic thrusting and Tertiary detachment faulting in the Moon Mountains, west-central Arizona:

Krogh, T.E., 1973, A low contamination method for hydrothermal decomposition of zircon and extraction of U and Pb for isotopic age determinations: Geochim. Cosmochim. Acta, v. 37, p. 485-494.

Krogh, T.E., 1982, Improved accuracy of U-Pb zircon ages by the creation of more concordant systems using air abrasion techniques: Geochim. Cosmochim. Acta, v. 46, p. 637-649.

Ludwig, K.R., 1983, Plotting and regression programs for isotope geochemists, for use with HP 86/87 microcomputers: U.S. Geol. Survey Open-File Report 83-849, 102 p.

May, S.R., and Butler, R.F., 1986, North American Jurassic apparent polar wander: Implications for plate motion, paleogeography, and Cordilleran tectonics: Jour. Geophys. Res., v. 91, p. 11,519-11,544.

Miller, C.F. and Bradfish, L.J., 1980, An inner Cordilleran belt of muscovite-bearing plutons: Geology, v. 8, p. 412-416.

Miller, C.F., Howard, K.A., and Hoisch, T.D., 1982, Mesozoic thrusting, metamorphism, and plutonism, Old Woman-Piute Range, southeastern California, *in* Frost, E.G., and Martin, D.L., eds., Mesozoic-Cenozoic Tectonic Evolution of the Colorado River Region, California, Arizona, and Nevada: San Diego, California, Cordilleran Publishers, p. 561-581.

Molnar, P., Chen, W., and Padovani, E., 1983, Calculated temperatures in overthrust terrains and possible combinations of heat sources responsible for the Tertiary granites in the Greater Himalaya: Jour. Geophys. Res., v. 88, p. 6415-6429.

Parrish, R.R., 1987, An improved micro-capsule for zircon dissolution in U-Pb geochronology: Chemical Geology, v. 66, p. 99-102.

Pindell, J., and Dewey, J.F., 1982, Permo-Triassic reconstruction of western Pangaea and the evolution of the Gulf of Mexico-Caribbean region: Tectonics, v. 1, p. 179-211.

Rehrig, W.A., and Reynolds, S.J., 1980, Geologic and geochronologic reconnaissance of a northwest-trending zone of metamorphic core complexes in southern and western Arizona, *in* Crittenden, M.D., Jr., Coney, P.J., and Davis, G.H., eds., Cordilleran Metamorphic Core Complexes: Geol. Soc. Am. Mem. 153, p. 131-157.

Reynolds, S.J., 1982, Multiple deformation in the Harcuvar and Harquahala Mountains, west-central Arizona, *in* Frost, E.G., and Martin, D.L., eds., Mesozoic-Cenozoic Tectonic Evolution of the Colorado River Region, California, Arizona, and Nevada: San Diego, California, Cordilleran Publishers, p. 137-142.

Reynolds, S.J., Florence, F.P., Welty, J.W., Roddy, M.S., Currier, D.A., Anderson, A.V., and Keith, S.B., 1986, Compilation of Radiometric Age Determinations in Arizona: Ariz. Bur. Geol. Min. Tech. Bull. 197, p. 258.

Reynolds, S.J., Spencer, J.E., Richard, S.M., and Laubach, S.E., 1986, Mesozoic structures in west-central Arizona, *in* Beatty, B., and Wilkinson, P.A.K., Frontiers In Geology and Ore Deposits of Arizona and the Southwest: Arizona Geological Society Digest 16, p. 35-51.

Shaffiqullah, M., Damon, P.E., Lynch, D.J., Reynolds, S.J., Rehrig, W.A., and Raymond, R.H., 1980, K-Ar geochronology and geologic history of southwestern Arizona and adjacent areas, *in* Jenny, J.P., and Stone, C., eds., Studies In Western Arizona: Ariz. Geol. Soc. Digest, v. 12, p. 201-260.

Silver, L.T., 1968, Precambrian batholiths of Arizona: Geol. Soc. Amer. Spec. Paper 121, p. 558-559.

Silver, L.T., and Anderson, T.H., 1974, Possible left-lateral early to middle Mesozoic disruption of the southwestern North American craton margin [abs.]: Geol. Soc. Amer. Abstr. Progs., v. 6, p. 955.

Spencer, J.E., and Reynolds, S.J., in press, Tertiary structure, stratigraphy and tectonics of the Buckskin Mountains, *in*, Spencer, J.E., and Reynolds, S.J., eds., Geology of the Buckskin Mountains: Arizona Bureau of Geology and Mineral Technology Bull. 198.

Steiger, R.H., and Jäger, E., 1977, Subsommission on geochronology: Convention on the use of decay constants in geo- and cosmochronology: Earth Plan. Sci. Letters, v. 1, p. 369-371.

Stern, T.W., Bateman, P.C., Morgan, B.A., Newell, M.F., and Peck, D.L., 1981, Isotopic U-Pb ages of zircon from the granitoids of the central Sierra Nevada, California: U.S. Geol. Survey Prof. Paper 185, 17 p.

Stock, J.M. and Molnar, P., in press, Uncertainties and implications of the Late Cretaceous and Tertiary position of North America relative to the Farallon, Kula, and Pacific plates, submitted to Tectonics.

Thomas, W.M., Clark, H.S., Young, E.D., Orell, S.E., and Anderson, J.L., 1988, Proterozoic high-grade metamorphism in the Colorado River region, Nevada, Arizona, and California, *in* Ernst, W.G., ed., Metamorphism and Crustal Evolution of the Western United States (Rubey Volume VII): Englewood Cliffs, New Jersey, Prentice-Hall, p. 526-537.

Tosdal, R.M., 1986, Mesozoic ductile deformations in the southern Dome Rock Mountains, northern Trigo Mountains, Trigo Peak and Livingston Hills, southwestern Arizona, and Mule Mountains, southeastern California, *in* Beatty, B., and Wilkinson, P.A.K., Frontiers In Geology and Ore Deposits of Arizona and the Southwest: Arizona Geological Society Digest 16, p. 62-71.

Tosdal, R.M., 1988, Mesozoic rock units along the late Cretaceous Mule Mountains thrust system, southeastern California and southwestern Arizona: Ph.D. dissertation, Santa Barbara, Univ. of California, 365 p.

Tosdal, R.M., Haxel, G.B., and Wright, J.E., in press, Jurassic geology of the Sonoran Desert region, southern Arizona, southeastern California, and northernmost Sonora: Construction of a continental-margin magmatic arc, *in* Jenny, J.P., and Reynolds, S.J., eds., Geologic evolution of Arizona: Ariz. Geol. Soc. Digest, v. 17.

Wooden, J.L., Stacey, J., Howard, K., and Miller, D., 1986, Crustal evolution in southeastern California--Constraints from Pb isotopic studies: Geol. Soc. Amer. Abs. Progs., v. 18, p. 200.

Wooden, J.L., Stacey, J.S., Howard, K.A., Doe, B.R., and Miller, D.M., 1988, Pb isotopic evidence for the formation of Proterozoic crust in the southwestern United States, *in* Ernst, W.G., ed., Metamorphism and Crustal Evolution of the Western United States (Rubey Volume VII): Englewood Cliffs, New Jersey, Prentice-Hall, p. 69-86.

Wright, J.E., Anderson, J.L., and Davis, G.A., 1986, Timing of plutonism, mylonitization, and decompression in a metamorphic core complex, Whipple Mountains, California [abs.]: Geol. Soc. Am. Abstr. Prog., v. 18, p. 201.

Wright, J.E., Howard, K.A., and Anderson, J.L., 1987, Isotopic systematics of zircons from late Cretaceous intrusive rocks, southeastern California: Implications for a vertically stratified crustal column [abs.]: Geol. Soc. Amer. Abstr. Progs., v. 19, no. 7, p. 898.

Yeats, K.J., 1985, Geology and structure of the northern Dome Rock Mountains, La Paz County, Arizona: M.S. thesis, Tucson, Univ. of Arizona, 123 p.

Young, R.A., and McKee, E.H., 1978, Early and middle Cenozoic drainage and erosion in west-central Arizona: Geol. Soc. Amer. Bull., v. 89, p. 1745-1750.

Young, R.A., 1982, Paleogeomorphologic evidence for the structural history of the Colorado Plateau margin in western Arizona, *in* Frost, E.G., and Martin, D.L., eds., Mesozoic-Cenozoic Tectonic Evolution of the Colorado River Region, California, Arizona, and Nevada: San Diego, California, Cordilleran Publishers, p. 29-39.

FIGURE CAPTIONS

Table 1: Summary of uranium (U) and lead (Pb) data for zircon fractions analyzed in this study. Fractions are grouped by sample, and magnetic and size characteristics are indicated for each fraction. Abraded fractions are noted with double dagger. Leached fraction is noted with double cross.

Table 2: Summary of common lead data for potassium feldspars from the four rock samples analyzed in this study. Values are consistent with initial lead compositions for Phanerozoic igneous rocks of the Mojave area.

Figure 4.0: Sketch map of the Maria fold and thrust belt in the southwestern U.S. Cordillera, showing mountain ranges of the Mojave-Sonora area referred to in text.

Figure 4.1: Geologic sketch map of the Mesquite Mountain and Moon Mountains areas on the Colorado River Indian Reservation, and sample localities for U-Pb zircon dating of this study.

Figure 4.2: Concordia diagram for sample M87-15 (4 fractions), which is a biotite granite sill from the Mesquite Gneiss migmatite at Mesquite Mountain. An air abraded fraction (aa) of the least discordant separate (-2, >200) moved up along the regression chord toward a more discordant composition, suggesting that lead loss is an unlikely problem with this sample. Lower intercept of 67.2 ± 1.4 Ma is interpreted as the crystallization age. The upper intercept of 1490 ± 110 Ma is consistent with known Proterozoic rocks from the region which probably served as source rocks.

Figure 4.3: Concordia diagram for sample MM87-16 (4 fractions), which is a quartz syenite from the hanging wall of the Valenzuela thrust system in the southeastern Moon Mountains. Note scale of concordia plot. One fraction (0, >200) is concordant within error at ~162 Ma. An air abraded fraction (aa) moved toward a composition exhibiting more inheritance, suggesting lead loss had not altered the systematics. The lower intercept of 160 ± 15 Ma is interpreted as the likely crystallization age of this sample.

Figure 4.4: Concordia diagram for sample MM87-20 (3 fractions), a garnet-bearing granitic pegmatite from the footwall of the Valenzuela thrust system in the southeastern Moon Mountains. All fractions plot close to concordia. The cloudy fraction is essentially concordant, and the lower intercept age of 71.1 ± 6.7 Ma is interpreted as the crystallization age. The upper intercept age (183 ± 52 Ma) is thought to reflect a source area with a significant Mesozoic-age component.

Figure 4.5: Concordia diagram for sample MM87-24 (4 fractions), which consists of a late- to post-mylonitic, biotite-bearing granite from the footwall of the Copper Peak detachment fault, northeastern Moon Mountains. The lower intercept from regression of all four points is 20.8 ± 3.2 Ma, and is interpreted as the crystallization age for this sample.

TABLE 1
U-Pb ZIRCON DATA

sample	fraction	weight (mg)	U (ppm)	$^{206}Pb^*$ (ppm)	measured ratios† 206/204	207/206	208/206	radiogenic ratios§ $^{206*}/^{238}$	$^{207*}/^{235}$	$^{207*}/^{206*}$	isotopic ages+ $^{206*}/^{238}$	$^{207*}/^{235}$	$^{207*}/^{206*}$
M87-15	nm(-2) <200	3.222	1283.33	13.68	1828	0.062405	0.034111	0.01241	0.09325	0.054498	79.5	90.5	391.4 ± 3
M87-15	nm(-2) >200	5.722	1215.98	11.62	5051	0.052983	0.015952	0.01112	0.07687	0.050133	71.3	75.2	201.4 ± 2
M87-15	nm(-2) >200††	0.188	1014.04	10.64	882	0.070829	0.065916	0.01221	0.09168	0.054462	78.2	89.1	386.7 ± 66
M87-15	nm(-1) <200	5.821	1595.39	17.63	8696	0.057878	0.018144	0.01286	0.09976	0.056265	82.4	96.6	462.9 ± 2
MM87-16	nm(-1) <200	5.316	958.85	21.05	2045	0.056995	0.228625	0.02556	0.17574	0.049874	162.7	164.4	189.2 ± 4
MM87-16	nm(0) <200	6.102	923.57	19.98	1946	0.057386	0.238220	0.02518	0.17324	0.049898	160.3	162.2	190.5 ± 4
MM87-16	nm(0) >200	4.390	868.19	19.02	1000	0.064069	0.246177	0.02550	0.17387	0.049445	162.3	162.8	168.9 ± 6
MM87-16	nm(0) >200††	3.597	904.50	20.83	1679	0.059470	0.245677	0.02587	0.18097	0.050736	164.6	168.9	229.1 ± 5
MM87-20	<240 yel	0.393	1180.54	20.67	833	0.066576	0.215362	0.02038	0.13756	0.048944	130.1	130.9	144.2 ± 6
MM87-20	<240 clr	0.405	1011.64	18.94	1284	0.061032	0.222801	0.02179	0.14914	0.049634	139.0	141.2	176.5 ± 4
MM87-20	<240 cld	0.739	3648.69	35.17	565	0.073848	0.118708	0.01122	0.07331	0.047770	71.9	72.4	73.0 ± 8
MM87-24	nm(-1) <240	4.040	727.73	4.87	1111	0.085543	0.168901	0.00779	0.07826	0.072823	50.1	76.5	1009.1 ± 3
MM87-24	nm(-1) >240	6.330	653.31	6.12	1536	0.088896	0.152800	0.01091	0.12002	0.079817	69.9	115.1	1192.6 ± 2
MM87-24	nm(0) <240	6.800	816.30	3.97	803	0.082882	0.211829	0.00567	0.05083	0.065045	36.4	50.3	775.6 ± 4
MM87-24	nm(0) >240++	0.167	705.93	2.81	136	0.167792	0.424711	0.00464	0.04032	0.063013	29.8	40.1	700.1 ± 33

nm = non-magnetic; (#) = side tilt on Frantz magnetic separator at 1.5 a; 200, 240 refer to size fraction in mesh units

* radiogenic isotope

† measured ratios uncorrected for blank and non-radiogenic Pb

§ radiogenic ratios corrected for blank, non-radiogenic Pb, and spike in the case of samples analyzed with $^{205}Pb/^{235}U$ tracer; U corrected for blank

+ ages in Ma; decay constants used were ^{238}U=0.15513 E-9 yr^{-1}, ^{235}U=0.98485 E-9 yr^{-1} (Steiger and Jäger, 1977)

†† fraction air abraded, after technique of Krogh, 1982

++ fraction leached with cold, dilute HF and HNO_3 mixture for 30 min.

TABLE 2
K-feldspar Common-Pb Data

sample	weight (mg)	U (ppb)	Pb§ (ppm)	atomic ratios† 206/204	207/204	208/204
M87-15	311.1	52.1	14.5	18.74	15.63	38.9
MM87-16	546.6	286	20.5	19.26	15.67	39.7
MM87-20	443.4	674	53.2	19.95	15.75	40.2
MM87-24	468.1	110	21.3	18.90	15.67	39.3

§ total lead values
† corrected for mass fractionation factor

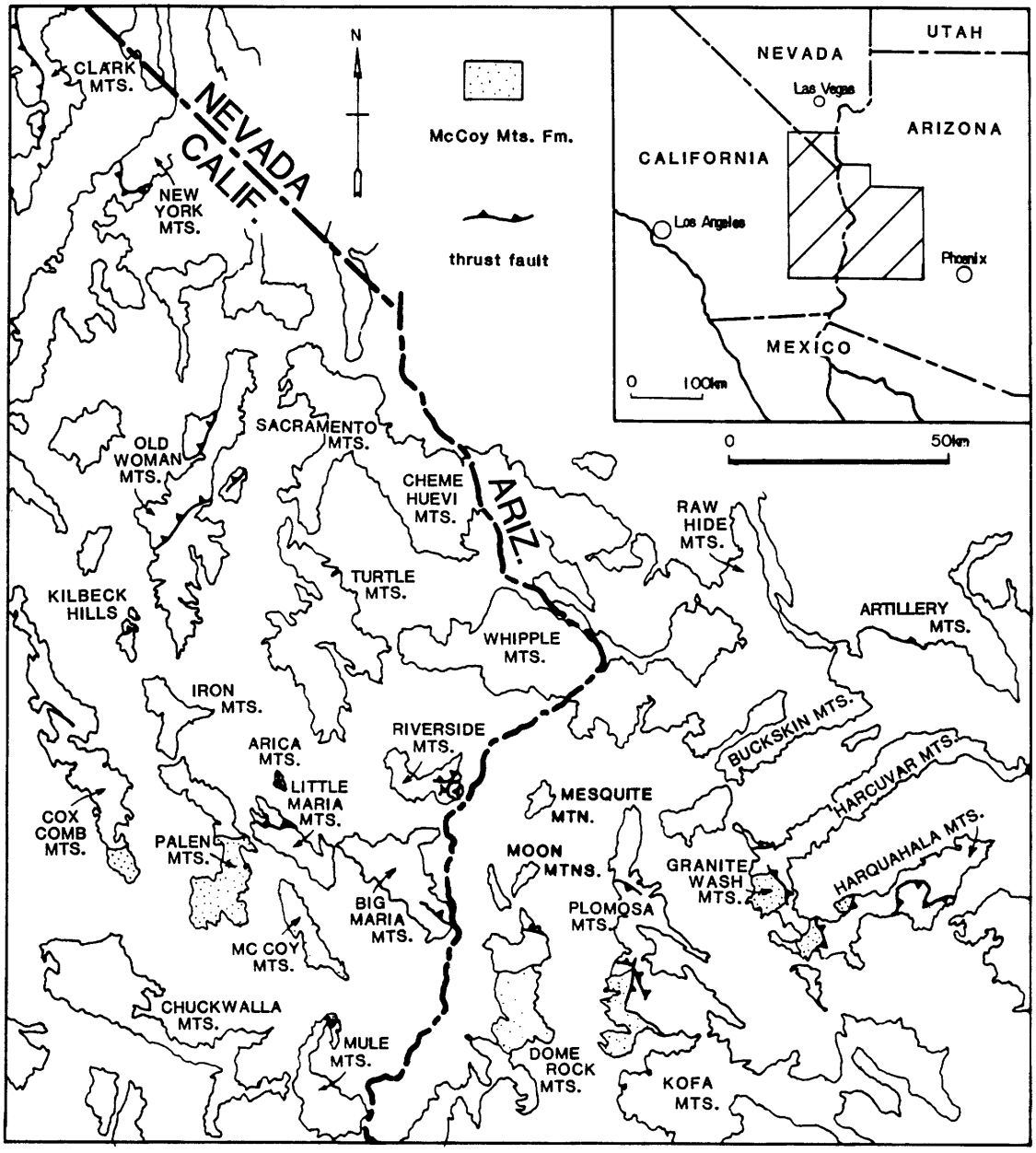
N
McCoy Mts. Fm.
thrust fault
NEVADA
CALIF.
ARIZ.
CLARK MTS.
NEW YORK MTS.
OLD WOMAN MTS.
SACRAMENTO MTS.
CHEME HUEVI MTS.
TURTLE MTS.
KILBECK HILLS
WHIPPLE MTS.
IRON MTS.
ARICA MTS.
LITTLE MARIA MTS.
RIVERSIDE MTS.
COX COMB MTS.
PALEN MTS.
BIG MARIA MTS.
MC COY MTS.
CHUCKWALLA MTS.
MULE MTS.
DOME ROCK MTS.
KOFA MTS.
MESQUITE MTN.
MOON MTNS.
PLOMOSA MTS.
RAW HIDE MTS.
ARTILLERY MTS.
BUCKSKIN MTS.
HARCUVAR MTS.
HARQUAHALA MTS.
GRANITE WASH MTS.
UTAH
NEVADA
Las Vegas
ARIZONA
CALIFORNIA
Los Angeles
Phoenix
MEXICO
0 100km
0 50km

Figure 4.0

MOUNTAINS OF THE COLORADO RIVER INDIAN RESERVATION,
WEST-CENTRAL ARIZONA

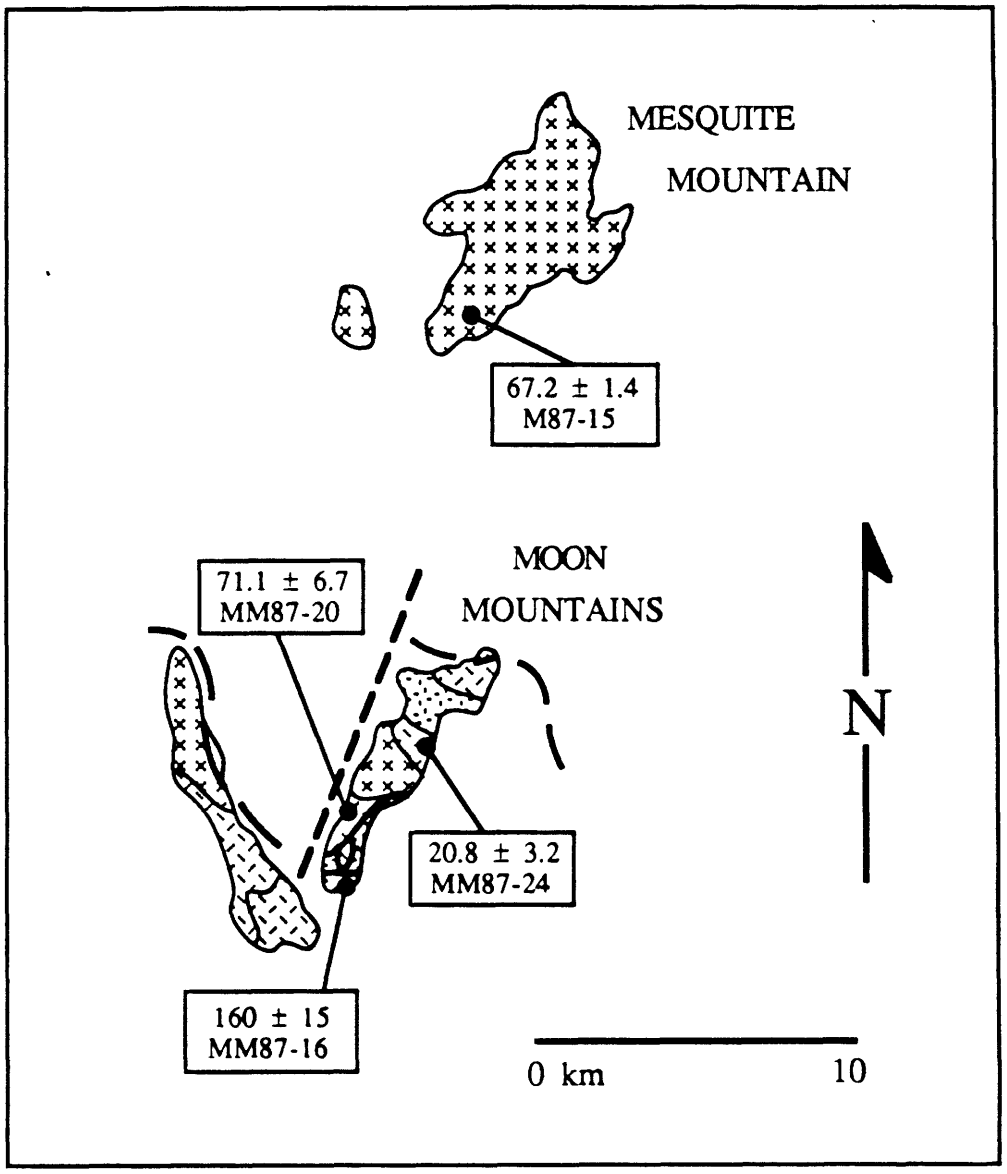

Figure 4.1

Figure 4.2

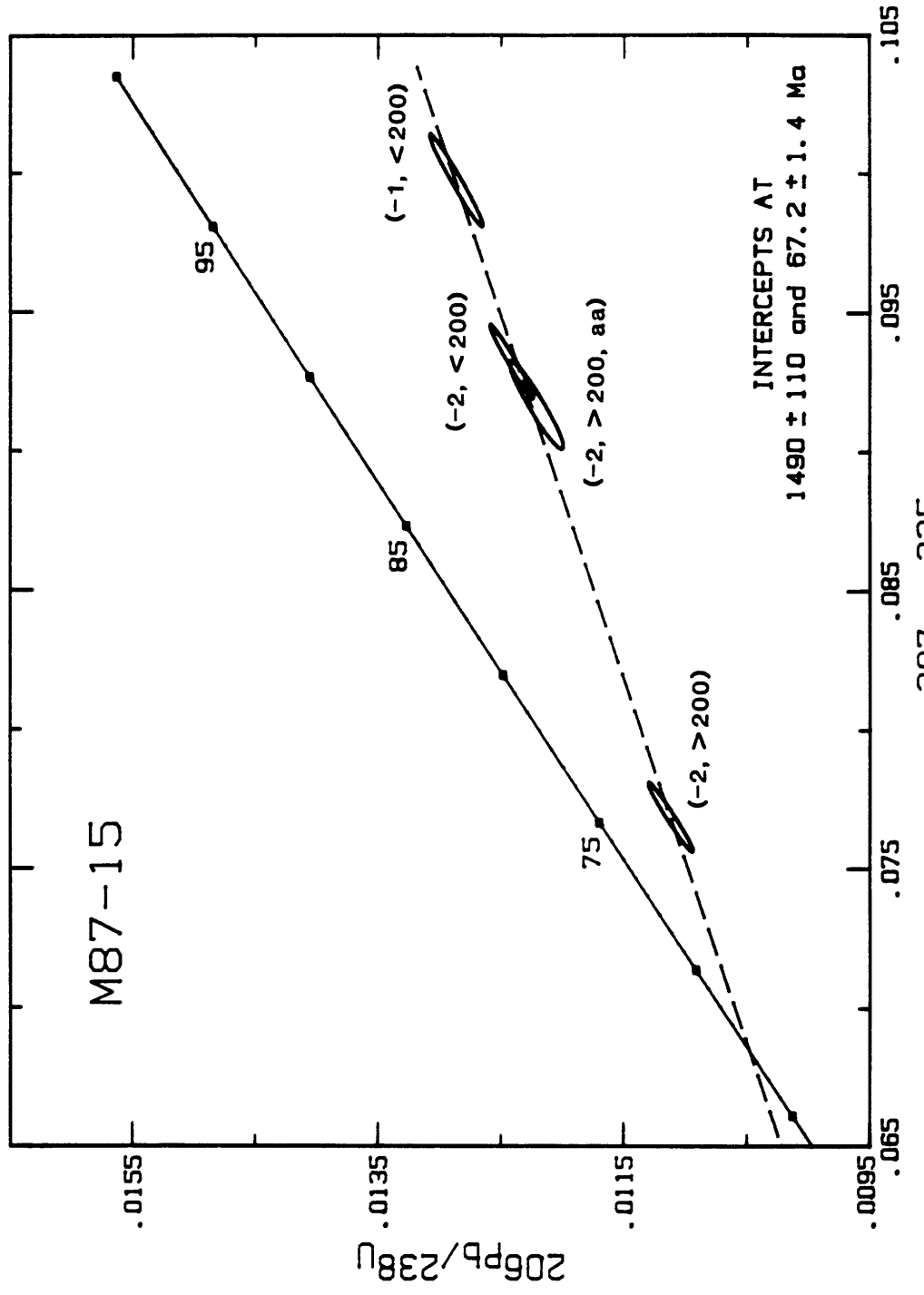
M87-15
95
85
75
(-1, <200)
(-2, <200)
(-2, >200, aa)
(-2, >200)
INTERCEPTS AT
1490 ± 110 and 67.2 ± 1.4 Ma
.0155
.0135
.0115
.0095
.065
.075
.085
.095
.105
206Pb/238U
207Pb/235U

Figure 4.3

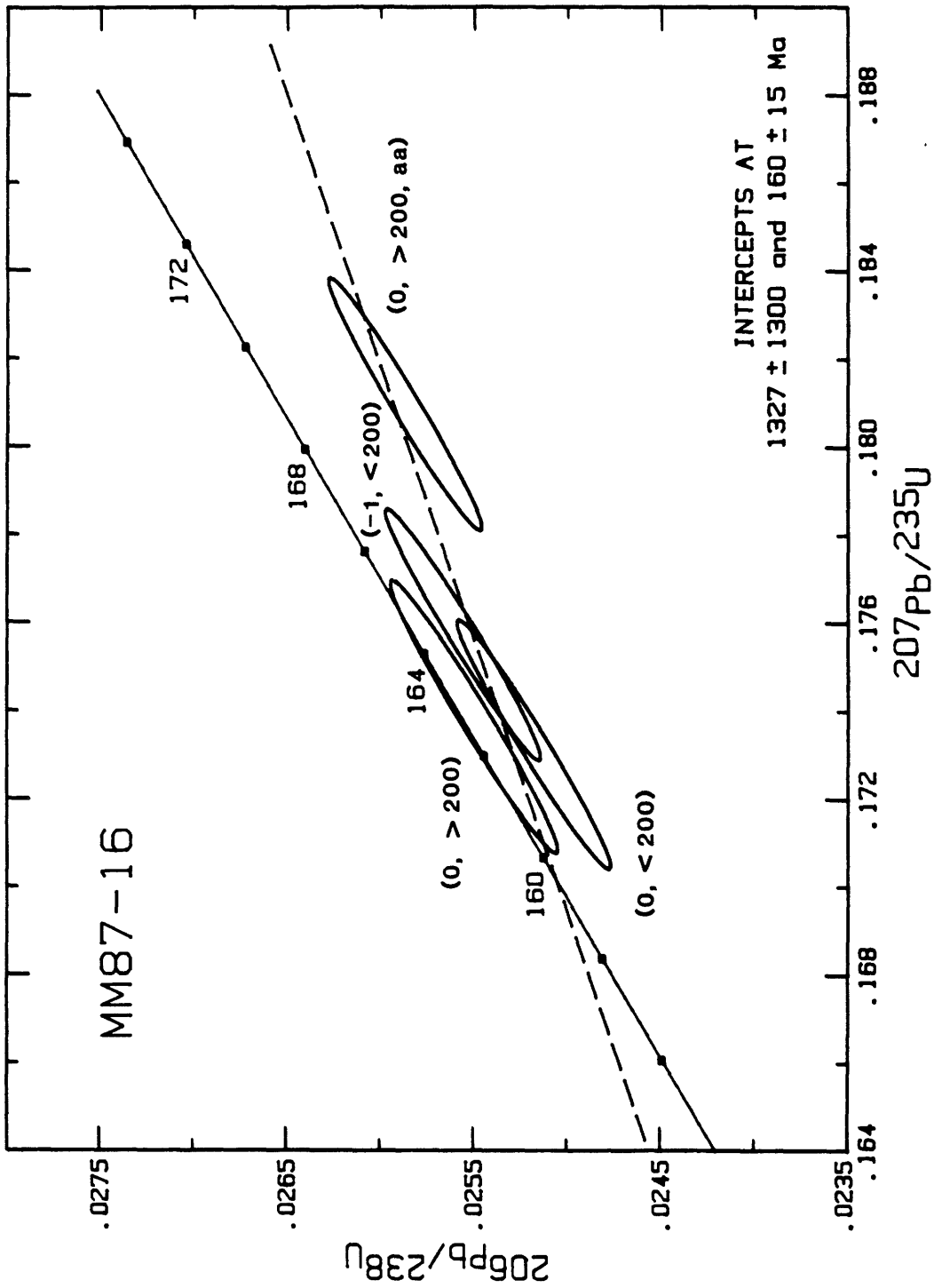
MM87-16
INTERCEPTS AT
1327 ± 1300 and 160 ± 15 Ma
172
168
164
160
(0, > 200, aa)
(-1, < 200)
(0, > 200)
(0, < 200)
.0275
.0265
.0255
.0245
.0235
.164
.168
.172
.176
.180
.184
.188
$^{206}Pb/^{238}U$
$^{207}Pb/^{235}U$

Figure 4.4

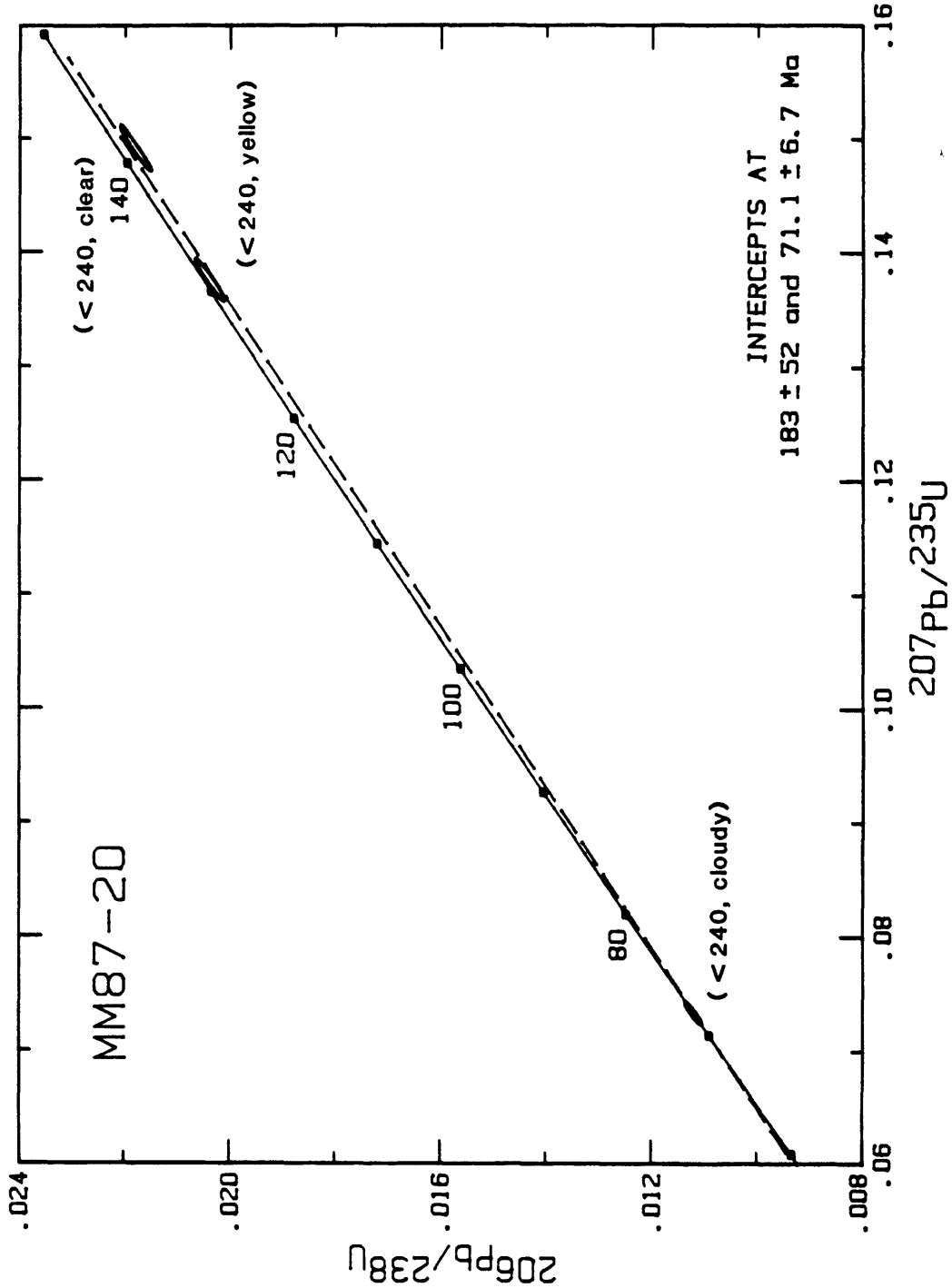
MM87-20
(< 240, clear)
(< 240, yellow)
(< 240, cloudy)
140
120
100
80
INTERCEPTS AT
183 ± 52 and 71.1 ± 6.7 Ma
.024
.020
.016
.012
.008
.06
.08
.10
.12
.14
.16
206Pb/238U
207Pb/235U

Figure 4.5

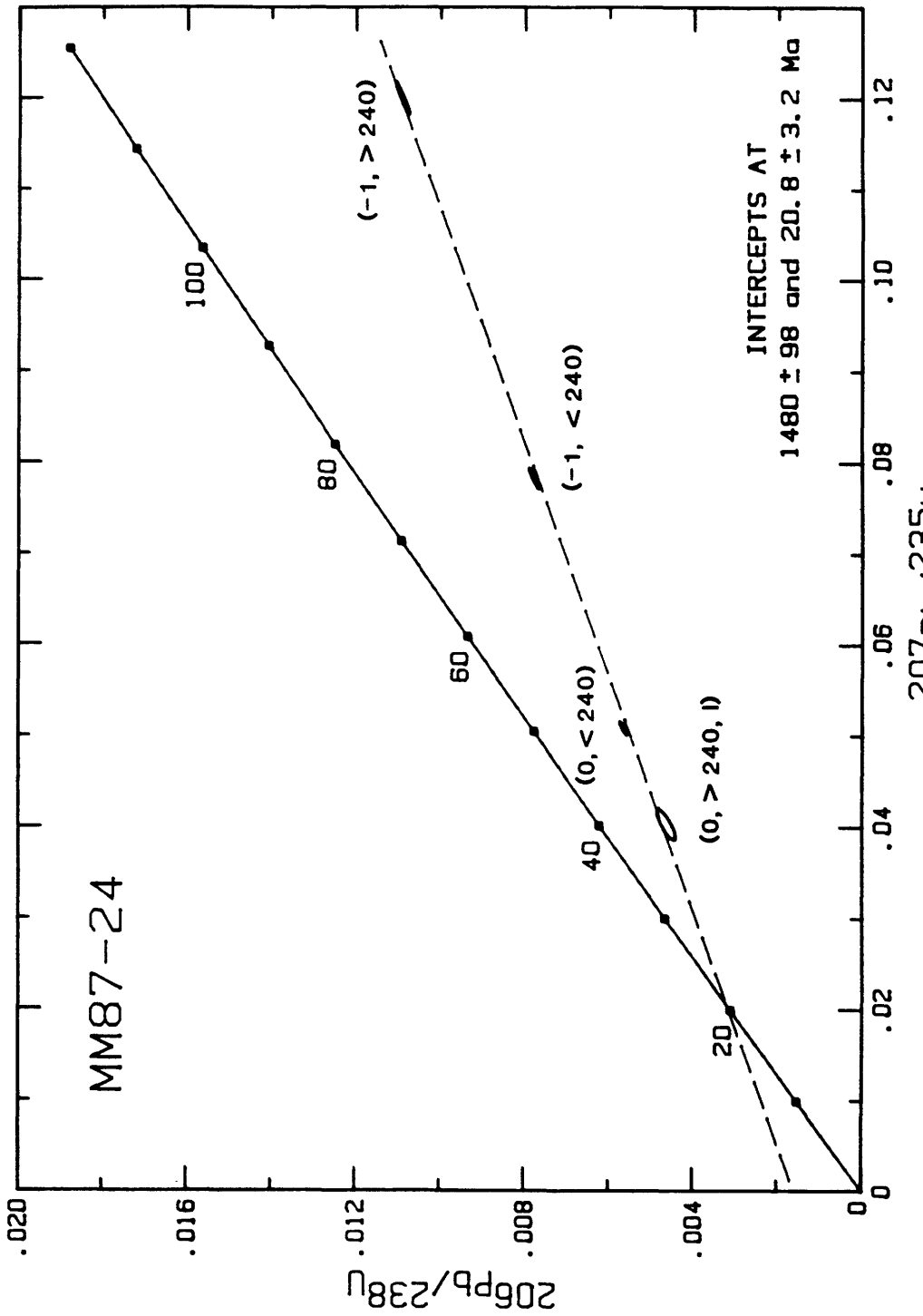
MM87-24
INTERCEPTS AT
1480 ± 98 and 20.8 ± 3.2 Ma
(-1, > 240)
(-1, < 240)
(0, < 240)
(0, > 240, I)
20
40
60
80
100
.020
.016
.012
.008
.004
0
.02
.04
.06
.08
.10
.12
206Pb/238U
207Pb/235U

GEOLOGIC MAP OF MESQUITE MTN. COLORADO RIVER INDIAN RESERVATION LA PAZ CO., ARIZONA

JAMES H. KNAPP

1988

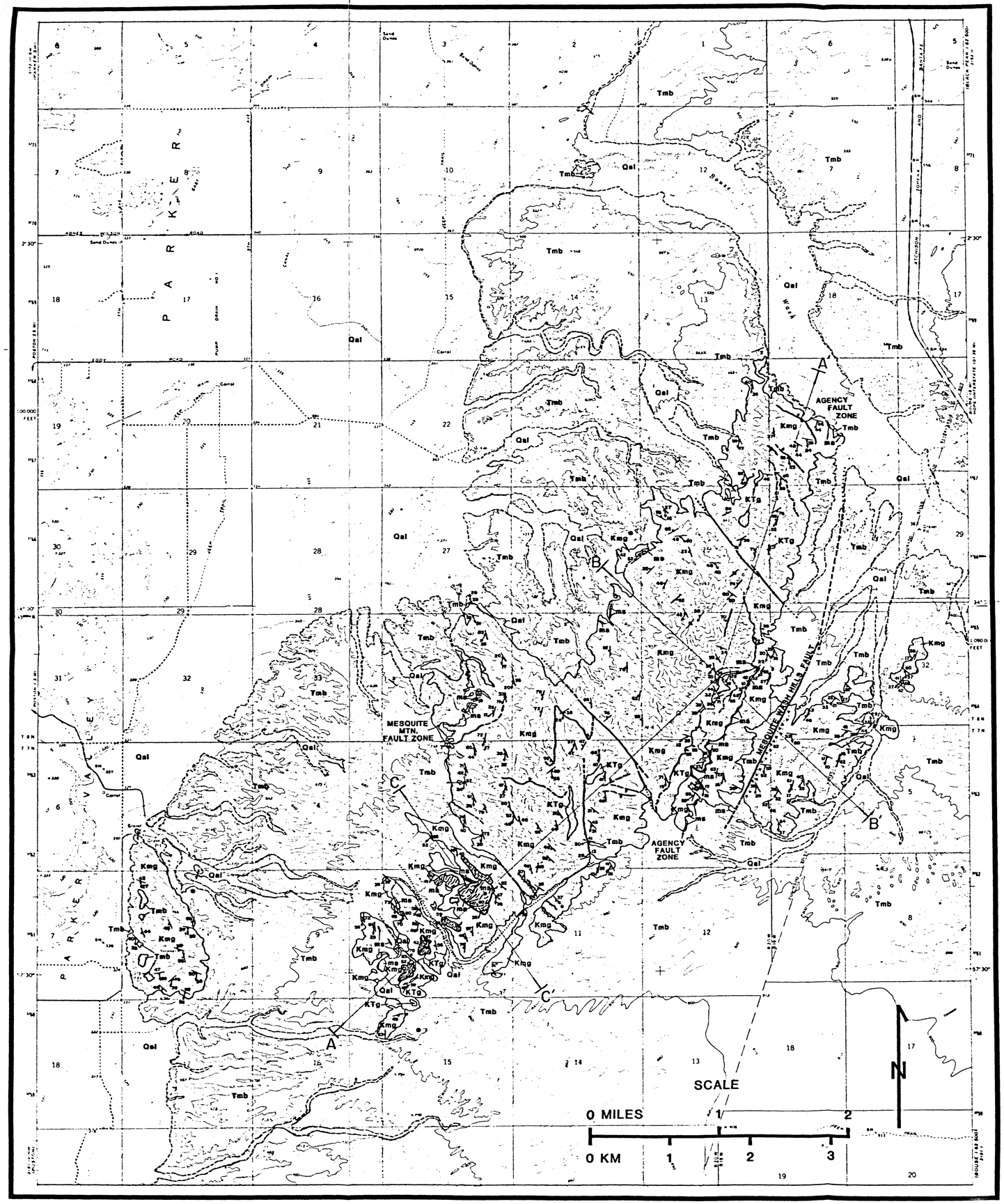

ROCK UNITS

CENOZOIC — MESOZOIC — PALEOZOIC

QUATERNARY

- Qal — ALLUVIUM, UNDIVIDED

TERTIARY

- Tmb — MIOCENE BOUSE FM.
- BASIC TO INTERMEDIATE DIKES

CRETACEOUS

- KTg — BIOTITE GRANITE
- Kmg — MESQUITE GNEISS (PRE-CAMBRIAN PROTOLITH)

TRIASSIC(?)

- ms — PALEOZOIC AND MESOZOIC METASEDIMENTARY ROCKS

1:24,000 TOPO BASE MAPS

PARKER SE

MOON MTN. NE

U.S. GEOLOGICAL SURVEY

MAP SYMBOLS

CONTACTS

- LITHOLOGIC CONTACT – DEFINITE, APPROXIMATE, CONCEALED
- FAULT CONTACT – DEFINITE, APPROXIMATE, CONCEALED; ARROW INDICATES DIP

ATTITUDES

- BEDDING – INCLINED (WITH DIP), HORIZONTAL
- FOLIATION – INCLINED (WITH DIP), HORIZONTAL, VERTICAL
- MYLONITIC LINEATION (WITH PLUNGE)

PATTERNS

- ZONE OF INTENSE MYLONITIZATION
- ZONE OF BRECCIATION

PLATE 1-1

PLATE 1-2

GEOLOGIC CROSS SECTIONS OF MESQUITE MTN.

JAMES H. KNAPP

1988

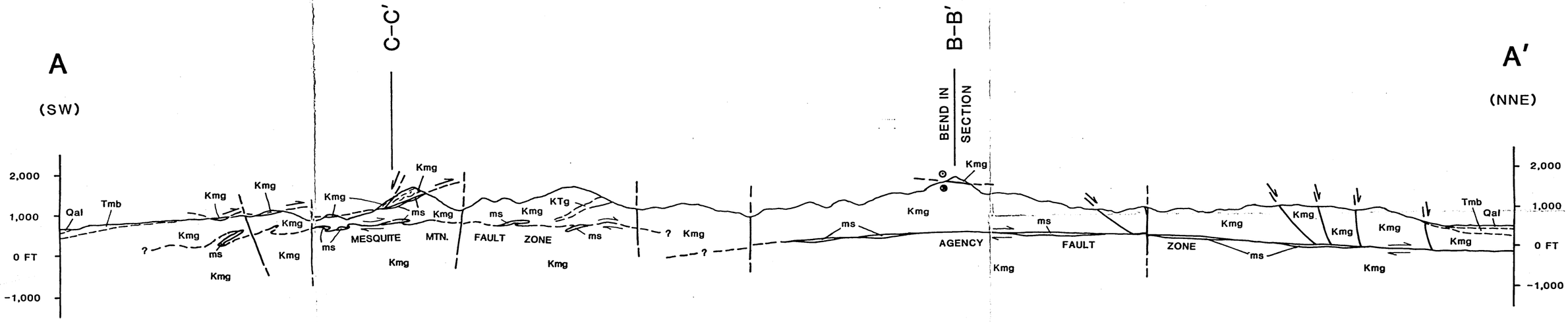

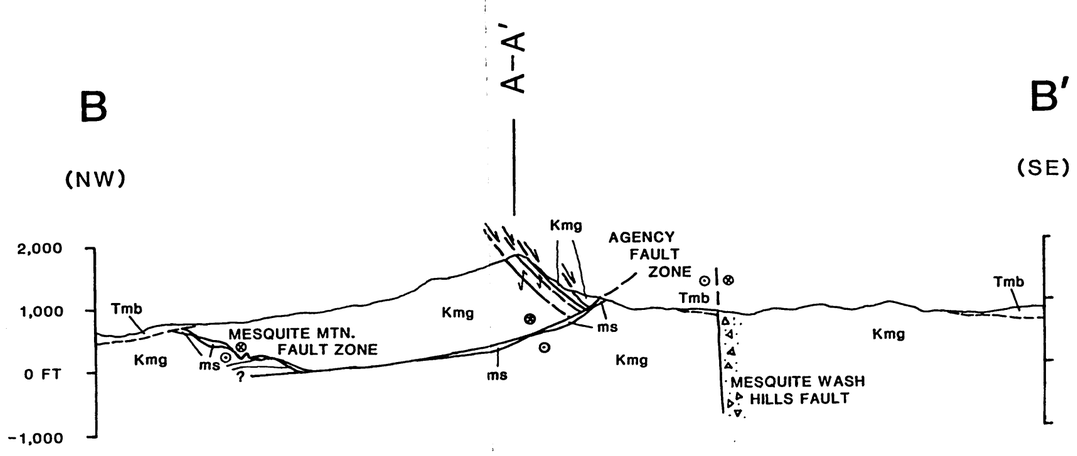

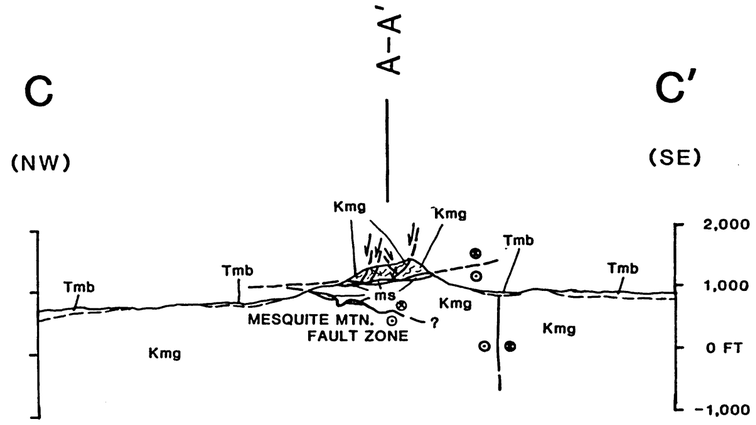

SCALE 1:24,000

NO VERTICAL EXAGGERATION

Knapp
1988
Ph.D.
EAPS
V.2

GEOLOGIC MAP OF THE MOON MTNS. COLORADO RIVER INDIAN RESERVATION LA PAZ CO., ARIZONA

JAMES H. KNAPP

1988

STATE OF CALIFORNIA
COLORADO RIVER BOUNDARY COMMISSION

MOON MTN. QUADRANGLE
ARIZONA—YUMA CO.
7.5 MINUTE SERIES (TOPOGRAPHIC)

UNITED STATES
DEPARTMENT OF THE INTERIOR
GEOLOGICAL SURVEY

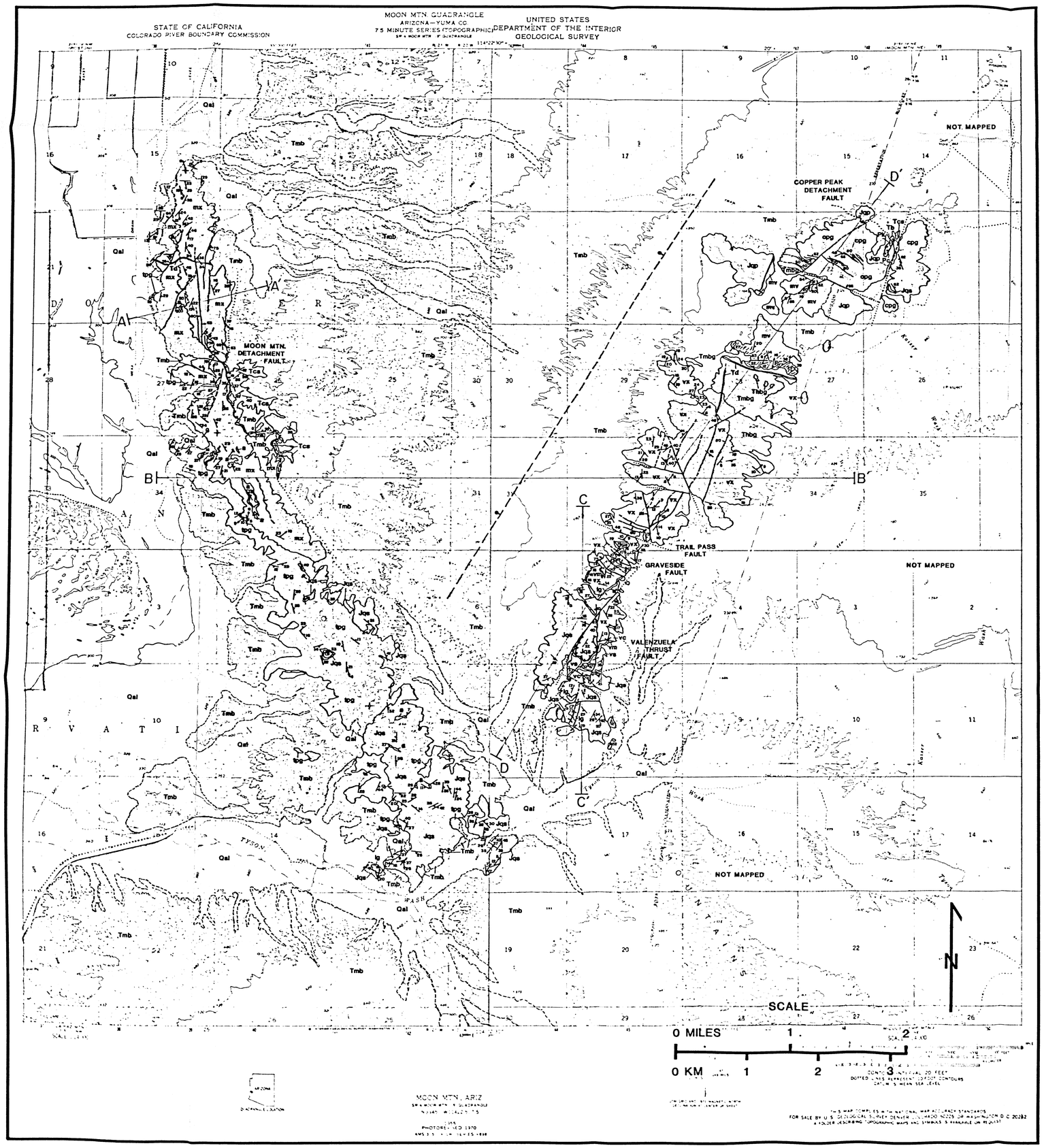

ROCK UNITS

SEDIMENTARY AND VOLCANIC UNITS

CENOZOIC

QUATERNARY

- Qal — ALLUVIUM

TERTIARY

- Tmb — MIOCENE BOUSE FM.
- Tb — BASALT
- Tcs — CONGLOMERATE AND SANDSTONE

CRETACEOUS(?)

MESOZOIC

JURASSIC

- Jqp — QUARTZ PORPHYRY
- mv — MOJAVE PAINT BASIN METAVOLCANIC ROCKS

TRIASSIC(?)

VALENZUELA METASEDIMENTARY SEQUENCE

- vm — MICACEOUS MARBLE
- vs — INTERBEDDED SCHIST AND QUARTZITE
- vq — THINLY BEDDED QUARTZITE
- vc — CALC-SILICATE

PRE-CAMBRIAN y PALEOZOIC

PERMIAN

- Pk — CHERTY MARBLE (KAIBAB?)
- Pc — QUARTZITE (COCONINO?)

PLUTONIC AND METAMORPHIC UNITS

- Td — BASIC TO INTERMEDIATE DIKES
- Thbg — HORNBLENDE BIOTITE GRANITE
- Tmbg — BIOTITE-GRANITE
- cpg — COPPER PEAK GRANITE
- tpg — TYSON PEAK GRANITE
- lg — LEUCOGRANITE
- Jqs — MEGACRYSTIC QUARTZ SYENITE

- vx — VALEN CRYSTALLINE ASSEMBLAGE
- mx / a — MOON MTN. CRYSTALLINE ASSEMBLAGE

MAP SYMBOLS

CONTACTS

- LITHOLOGIC CONTACT – DEFINITE, APPROXIMATE, CONCEALED
- FAULT CONTACT – DEFINITE, APPROXIMATE, CONCEALED; ARROW INDICATES DIP

FAULT ORNAMENTATION

- THRUST FAULT; TEETH ON UPPER PLATE
- LOW-ANGLE NORMAL FAULT; TICK MARKS ON UPPER PLATE

ATTITUDES

- BEDDING – INCLINED (WITH DIP), HORIZONTAL
- FOLIATION – INCLINED (WITH DIP), HORIZONTAL, VERTICAL
- LINEATION (WITH PLUNGE)
- DIKE ORIENTATION (WITH DIP)

1:24,000 TOPO BASE MAPS

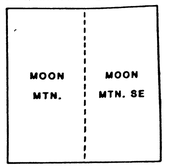

U.S. GEOLOGICAL SURVEY

PLATE 2-1

PLATE 2-2

GEOLOGIC CROSS SECTIONS OF THE MOON MTNS.

JAMES H. KNAPP

1988

SCALE 1:24,000

NO VERTICAL EXAGGERATION

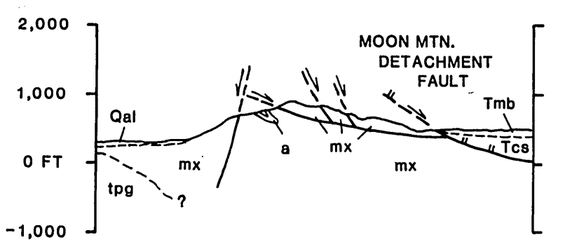

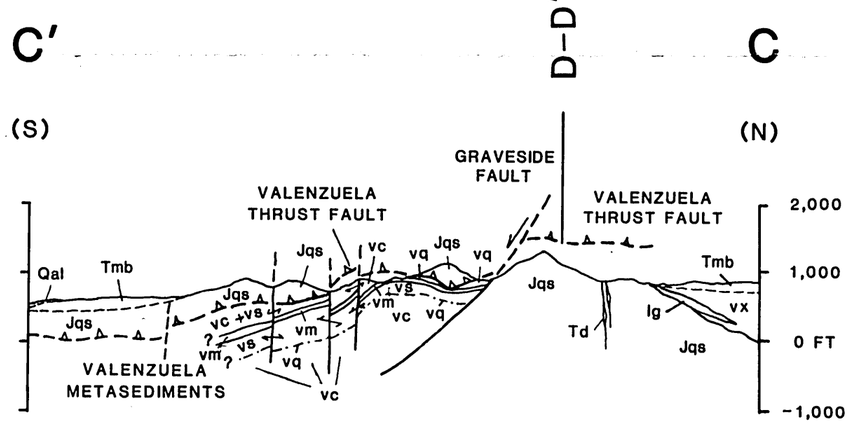

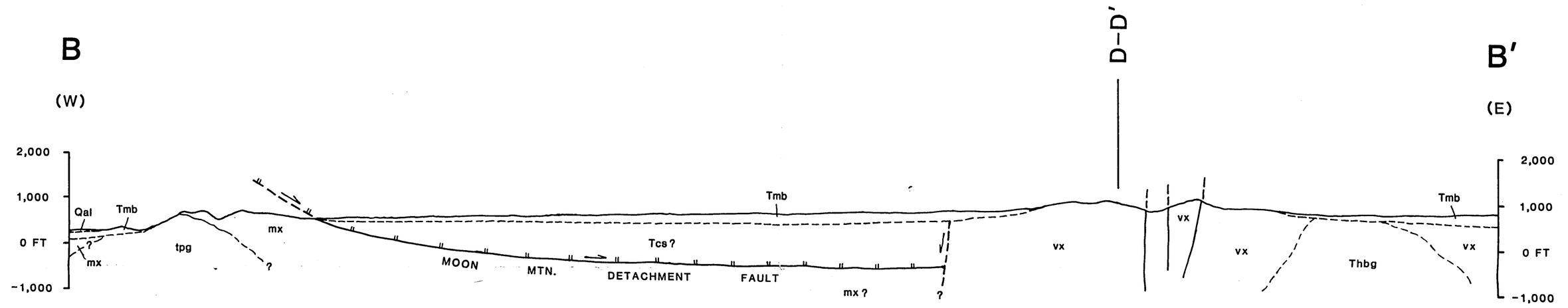

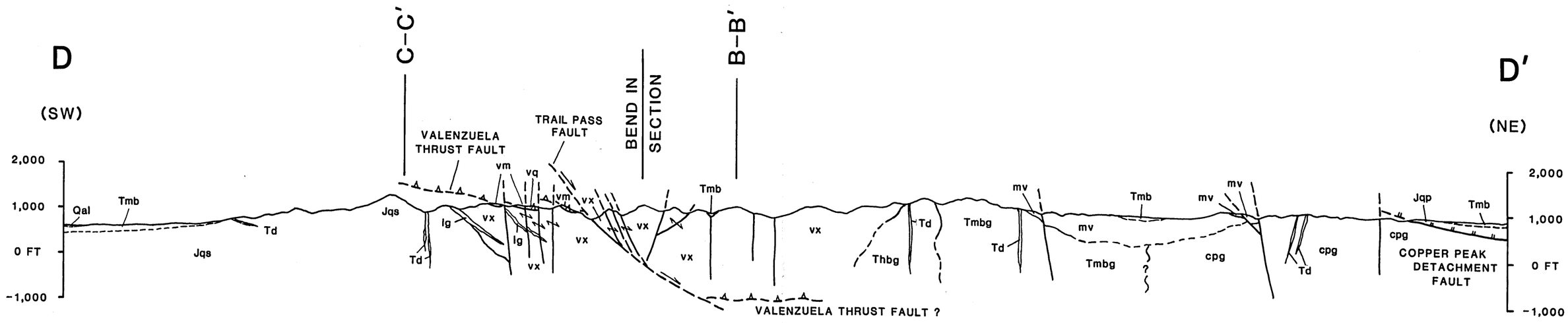

GEOLOGY OF THE VALENZUELA AREA, MOON MTNS., ARIZONA

J.H. KNAPP

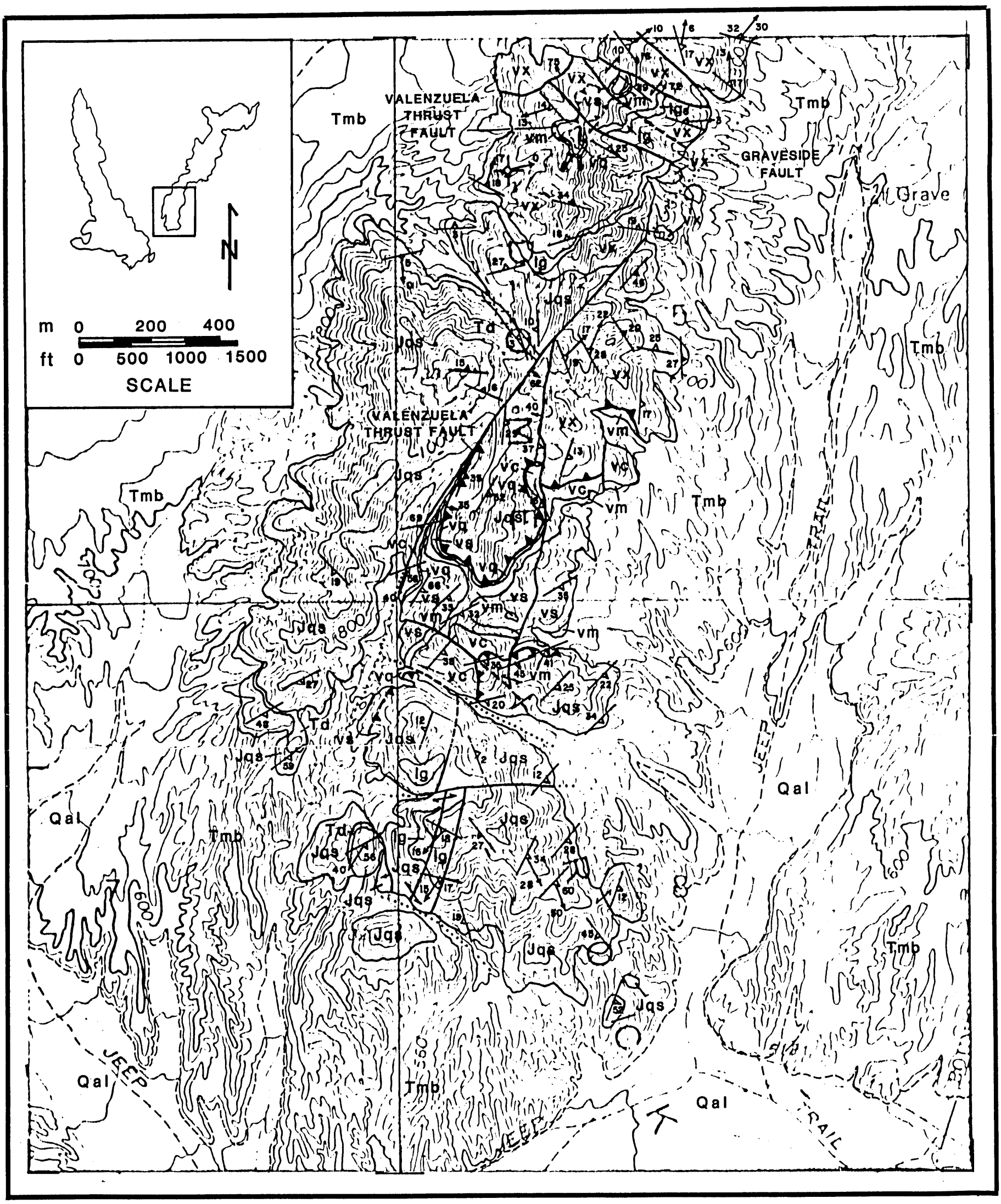

PLATE 2-3